

MECHANISMS OF *GNAO1*-ASSOCIATED NEUROLOGICAL DISORDERS

By

Huijie Feng

A DISSERTATION

Submitted to
Michigan State University
in partial fulfillment of the requirements
for the degree of

Pharmacology and Toxicology—Doctor of Philosophy

2019

ABSTRACT

MECHANISMS OF *GNAO1*-ASSOCIATED NEUROLOGICAL DISORDERS

By

Huijie Feng

Tremendous advances in the genetics of neurodevelopmental disorders have markedly improved the understanding of disease mechanisms. This project will focus on understanding the mechanisms of *GNAO1* encephalopathies, a devastating but complex disorder, which exhibit multiple neurological symptoms. These include developmental delay and variable components of early onset epilepsy and/or hyperkinetic movement disorders (MDs). These symptoms are associated with mutations in the *GNAO1* gene, which encodes the $G\alpha_o$ protein. *GNAO1* mutation-associated neurological disorders include neurodevelopmental delay with involuntary movements (NEDIM, OMIM#617493) and early infantile epileptic encephalopathy (EIEE17, OMIM#615473). The number of identified patients and mutant alleles for EIEE17 or NEDIM is increasing rapidly.

$G\alpha_o$ is the most abundant membrane protein in the mammalian central nervous system. It couples to multiple G protein-coupled receptors (GPCRs) including GABA_B, α_2 adrenergic, D₂ dopamine, and adenosine A₁ receptors; all are associated with both MDs and epilepsy. In addition, GPCRs are readily targetable by agonists and antagonists. This provides the possibility of treating *GNAO1*-associated neurological disorders.

This project revealed a fundamental mechanistic distinction among these *GNAO1*

mutations: Loss-of-function (LOF) *GNAO1* alleles are associated with epilepsy, while gain-of-function (GOF) *GNAO1* alleles are associated primarily with MDs. However, this simple model is insufficient to explain all clinical observations. To explore this correlation, we have created mouse models carrying two of the most common human *GNAO1* mutant alleles (G203R and R209H). They largely share the human pathophysiology; the G203R mouse model exhibits both MD and enhanced seizure propensity, while the R209H mutant results in MD alone, as seen in children with those mutations. Using these models, we can further explore mechanisms that lead to distinct patterns in human *GNAO1* encephalopathies. To explore electrophysiological alterations in the *Gnao1* G203R mutant mouse model, I performed patch clamp studies on cerebellar Purkinje cells. The results show a decreased frequency of both miniature inhibitory postsynaptic currents (mIPSCs) and spontaneous inhibitory postsynaptic currents (sIPSCs), suggesting a reduced presynaptic GABA release.

This study provides a molecular and physiological understanding of different *GNAO1* alleles *in vitro*, and identifies key candidate alleles for further analysis in *in vivo* mouse models and in human *GNAO1*-associated neurological disorders. Furthermore, our study may serve as a prototype for other correlations between reported monogenic mutations and human neurological disorders.

ACKNOWLEDGEMENTS

I would like to thank my mentor Dr. Richard R. Neubig. I consider myself fortunate to have had this opportunity to work with him. Through Dr. Neubig's mentorship I have become not just a better scientist but also a better writer and presenter. I appreciate Rick's constant attention to details and his enthusiasm in pushing my project forward. His suggestions have been invaluable to the results presented in this dissertation. I also would like to thank him for his encouragement and trust for me to freely explore and decide what I deem the best in science and in my career development. This helps me to become an independent thinker and researcher.

I also highly value the mentorship of Dr. Yukun Yuan, who has unique and extensive experience and knowledge in doing patch clamp recordings. I deeply appreciate his generous sharing of his research equipment and his help in troubleshooting failed experiments. My other committee members have also played an important role in guiding the development of the work presented in this dissertation. I would like to thank Dr. Colleen Hegg, Dr. James Galligan and Dr. Charles Lee Cox for their insights and suggestions during every committee meeting I had. Their questions and perspectives have helped me assess my experimental results from alternative viewpoints and have enhanced the work presented here. I would also like to thank any clinical knowledge and detailed explanations regarding movement disorders and epilepsy given by Dr. Christos Sidiropoulos and Dr. Florian Kagerer.

Within the Neubig lab, I would like to thank Jeff Leipprandt who managed with all my orders and animal subjects. In addition, I would also like to thank former research associate Dr. Benita Sjögren, who patiently helped me through my first year in the lab and whose detailed lab records provided me invaluable resources when in need. I am thankful for our Masters student Cassie Larrivee, who helped with a majority of behavioral experiments. I also would like to express my gratitude to the current members of the laboratory. Dr. Erika Lisabeth, Behirda Karaj, Dr. Vincent Shaw, Sean Misek, Yajing Ji, and Zhe Zhang have been great friends and colleagues during my time in the lab. I also value the assistance of our undergraduate student, Nils Wellhausen, who has been important to my ability to conduct this research.

I would like to thank the MSU Transgenic Core headed by Dr. Elena Demireva and Dr. Huirong Xie. Their work provided me with animal subjects to work with. I also would like to thank Dr. Thomas Dexheimer from the Assay Development and Drug Repurposing Core, who gave me valuable suggestions for my experiments.

I would like to thank the Department of Pharmacology and Toxicology. Dr. Anne Dorrance offered mentorship and support during my time as a graduate student at MSU. In addition, I would like to thank the department office staff for their patience and assistance with administrative issues during my completion of the department's academic requirements.

The research presented in this dissertation would not have been possible without the

funding received from numerous sources. I would like to express my thanks to the Bow Foundation, whose grants supported my research, and to American Epilepsy Society (AES), for the pre-doctoral fellowship that supplied my stipend for a year. I would also like to thank the Neuroscience Program for providing me with a teaching assistantship and the Department of Pharmacology & Toxicology for a dissertation completion fellowship. I have also received financial support from the AES, Society of Neurosciences (SfN) and MSU Council of Graduate Students to attend scientific meetings.

A heartfelt thanks also goes to all the *GNAO1* patients and families. Their support is a big driving force of the advancement of this project. I sincerely hope this project will benefit the development of new therapeutics for treating the *GNAO1*-encephalopathies.

I reserve special thanks for my friends and family. I owe them a great deal of credit for my success.

TABLE OF CONTENTS

LIST OF TABLES.....	xi
LIST OF FIGURES.....	xiii
KEY TO ABBREVIATIONS.....	xviii
CHAPTER 1: AN OVERVIEW OF <i>GNAO1</i>-ASSOCIATED NEUROLOGICAL DISORDERS	1
1.1 Abstract.....	2
1.2 Introduction.....	2
1.3 $G\alpha_o$ (<i>GNAO1</i>) mechanisms.....	5
1.4 The clinical spectrum of <i>GNAO1</i> mutation-associated movement disorders.....	7
1.4.1 <i>GNAO1</i> encephalopathy displays a variety of neurological symptoms.....	7
1.4.2 Movement disorders related to <i>GNAO1</i> encephalopathy show limited response to pharmacological treatments.....	9
1.5 Potential pathogenic mechanisms of <i>GNAO1</i> -associated movement disorders...	13
1.5.1 Role of cAMP regulation in movement disorders.....	14
1.5.1.1 <i>GNAL</i>	17
1.5.1.2 <i>GNB1</i>	18
1.5.1.3 <i>ADCY5</i>	19
1.5.1.4 <i>PDE10A</i>	21
1.5.1.5 Summary of cAMP regulation in movement control.....	22
1.5.2 Role of neurotransmitter release and synaptic vesicle fusion in movement disorders.....	23
1.5.2.1 <i>SYT1</i>	25
1.5.2.2 <i>PRRT2</i>	26
1.5.2.3 <i>SNAP25</i>	27
1.5.2.4 <i>KCNMA1</i>	28
1.5.2.5 <i>CACNA1A</i>	29
1.5.2.6 <i>CACNA1B</i>	30
1.5.2.7 <i>GPR88</i>	31
1.5.2.8 Summary of neurotransmitter release and synaptic vesicle fusion in movement control.....	32
1.6 Developmental defects may also contribute to movement disorders.....	32
1.7 Conclusion.....	34
1.8 Organization of the thesis.....	35
APPENDIX.....	37
REFERENCES.....	46

CHAPTER 2: MOVEMENT DISORDER IN <i>GNAO1</i> ENCEPHALOPATHY ASSOCIATED WITH GAIN-OF-FUNCTION MUTATIONS	66
2.1 Abstract.....	67
2.2 Introduction.....	68
2.3 Materials and Methods.....	70
2.3.1 Materials.....	70
2.3.2 DNA constructs and mutagenesis.....	70
2.3.3 Cell culture and transfections.....	71
2.3.4 SDS-PAGE and Western blot.....	72
2.3.5 cAMP measurements.....	73
2.3.6 Data analysis and statistics.....	73
2.4 Results.....	74
2.4.1 Most pathogenic <i>GNAO1</i> mutations cause reduced $G\alpha_o$ protein expression.....	74
2.4.2 Validation of an in vitro assay to assess function of <i>GNAO1</i> mutations.....	76
2.4.3 Nine <i>GNAO1</i> mutations result in loss- (LOF) or partial loss-of-function (PLOF).....	77
2.4.4 Six <i>GNAO1</i> mutations result in gain-of-function (GOF) or normal function (NF).....	80
2.4.5 Clinical correlation with biochemical behavior of mutant <i>GNAO1</i> alleles.....	86
2.4.6 Location of mutations linked to <i>GNAO1</i> encephalopathies in the $G\alpha_o$ protein.....	87
2.5 Discussion.....	88
APPENDICES.....	93
APPENDIX A: SUPPLEMENTAL DATA.....	94
APPENDIX B: VALIDATION OF THE GENOTYPE-PHENOTYPE CORRELATION OF <i>GNAO1</i> -ASSOCIATED NEUROLOGICAL DISORDERS.....	103
REFERENCES.....	112

CHAPTER 3: BEHAVIORAL ASSESSMENT OF MOUSE MODELS WITH <i>GNAO1</i>-ASSOCIATED MOVEMENT DISORDER AND EPILEPSY	119
3.1 Abstract.....	120
3.2 Introduction.....	121
3.3 Materials and Methods.....	126
3.3.1 Animals.....	126
3.3.2 Generation of <i>Gnao1</i> mutant mice.....	126
3.3.2.1 Generation of <i>Gnao1</i> ^{+/<i>G203R</i>} mouse model.....	126
3.3.2.2 Generation of <i>Gnao1</i> ^{+/<i>R209H</i>} mouse model.....	130
3.3.3 Genotyping and Breeding.....	132
3.3.3.1 Genotyping <i>Gnao1</i> ^{+/<i>G203R</i>} mice.....	132
3.3.3.2 Genotyping <i>Gnao1</i> ^{+/<i>R209H</i>} mice.....	133
3.3.4 Behavioral Studies.....	134

3.3.4.1 Open Field	134
3.3.4.2 RotaRod.....	135
3.3.4.3 Grip Strength.....	135
3.3.4.4 DigiGait	136
3.3.5 PTZ Kindling Susceptibility	137
3.3.6 Data Analysis.....	137
3.4 Results	138
3.4.1 The growth patterns of the three newly developed <i>Gnao1</i> mutant mouse models (G203R, R209H and ΔT191F197)	138
3.4.1.1 <i>Gnao1</i> ^{+G203R} mice showed normal viability and growth.....	138
3.4.1.2 <i>Gnao1</i> ^{+R209H} mice have expected frequency and normal viability	138
3.4.1.3 <i>Gnao1</i> ^{+ΔT191F197} mice developed spontaneous seizures at P7 and died before P16	139
3.4.2 Behavioral assessment of mutant <i>Gnao1</i> mouse models (G184S, G203R, R209H and KO) for movement patterns	141
3.4.2.1 Female <i>Gnao1</i> ^{+G184S} and male <i>Gnao1</i> ^{+G203R} mice show similar movement abnormalities and gait disturbances	141
3.4.2.2 <i>Gnao1</i> ^{+R209H} mouse model exhibits unique hyperactive behavior in the open field arena but no abnormal motor coordination in other behavior tests and minor disturbance in gait analysis.....	149
3.4.2.3 Previously described <i>Gnao1</i> ^{+/-} mouse model did not show any abnormalities in the behavioral test battery	152
3.4.3 PTZ kindling study of G203R and R209H mice.....	155
3.4.3.1 Male <i>Gnao1</i> ^{+G203R} mice are sensitized to PTZ kindling.....	155
3.4.3.2 R209H mutant mice are not hypersensitive to PTZ kindling.....	157
3.5 Discussion.....	158
APPENDIX.....	165
REFERENCES.....	183

CHAPTER 4: MICE WITH *GNAO1*-ASSOCIATED MOVEMENT DISORDER EXHIBIT REDUCED INHIBITORY SYNAPTIC INPUT TO CEREBELLAR PURKINJE CELLS.....

.....	193
4.1 Abstract.....	194
4.2 Introduction	195
4.3 Materials and Methods.....	198
4.3.1 Tissue preparation and solutions	198
4.3.2 Electrophysiological recording	199
4.3.3 Pharmacology	201
4.3.4 SDS Page and Western Blots.....	201
4.3.5 Statistical Analysis	203
4.4 Results	204
4.4.1 Presynaptic GABA release is suppressed in the cerebellar Purkinje cells of	

<i>Gnao1</i> ^{+G203R} mice	205
4.4.2 $G\alpha_o$ blockers can reverse the enhanced inhibition of mIPSC frequency in G203R mice	207
4.4.3 Presynaptic glutamate release is not affected by the G203R mutation in $G\alpha_o$ protein	211
4.4.4 Effects of G-protein coupled GABA _B receptors on AP-independent GABA release onto Purkinje cells	213
4.4.5 Effects of G-protein coupled α_{2A} adrenergic receptors on AP-dependent GABA release onto Purkinje cells	215
4.4.6 α_{2A} adrenergic receptor-induced inhibition of sIPSC frequency depends on activation of voltage-gated calcium channels	217
4.4.7 G203R mice exhibit decreased $G\alpha_o$ protein expression but no change in G β levels	221
4.5 Discussion	223
APPENDIX	230
REFERENCES	236

CHAPTER 5: CONCLUSION AND FUTURE DIRECTIONS	244
5.1 General conclusion	243
5.2 Testing the functional changes of a growing variety of <i>GNAO1</i> mutations	248
5.2.1 Do <i>GNAO1</i> mutations affect G_o 's inhibition of high-voltage gated calcium channels (N- type & P/Q- type calcium channels)?	248
5.2.2 Do <i>GNAO1</i> mutations affect G_o 's activation of G protein-regulated inward rectifying potassium (GIRK) channels?	251
5.2.3 How do <i>GNAO1</i> mutations affect G protein-regulated neurite outgrowth? ..	252
5.3 Comparison between R209H and G203R mouse models	254
5.3.1 Do G203R and R209H mouse models exhibit delayed development?	255
5.3.2 How does the G203R mutation in $G\alpha_o$ lead to epileptogenesis?	258
5.3.3 How do G203R and R209H mice differ in movement disorder phenotypes?	260
5.3.4 How is sex involved in abnormalities of the <i>Gnao1</i> mutant mice?	262
5.4 Development of a high-throughput assay for drug repurposing or drug development	267
5.5 Impact of work in this thesis on the field	270
APPENDIX	272
REFERENCES	281

LIST OF TABLES

Table 1.1 Most Common <i>GNAO1</i> Mutant Alleles Associated With Movement Disorders	8
Table 1.2 Drugs showing beneficial effects to control involuntary movements of <i>GNAO1</i> encephalopathy patients.....	9
Table 1.3 Patients responding positively to deep brain stimulation (DBS).....	12
Table S1.1 A complete summary of clinical information regarding <i>GNAO1</i> patients	38
Table 2.1 Functional data for loss-of-function (LOF) and partial loss-of-function (PLOF) mutants.....	79
Table 2.2 Functional data for normal and gain-of-function (GOF) mutants.....	82
Table 2.3 Correlation between cAMP inhibition and clinical diagnosis.....	83
Table S2.1 Primer sequences for mutagenesis to create <i>GNAO1</i> mutants.....	95
Table S2.2 All non-functioning <i>GNAO1</i> mutations tested with <i>GNAS</i> KO cells.....	110
Table S2.3 All functioning <i>GNAO1</i> mutations tested with <i>GNAS</i> KO cells.....	110
Table S2.4 Genotype-phenotype correlation of the newly reported <i>GNAO1</i> mutations	111
Table 3.1 The status of <i>Gnao1</i> mutant mice.....	125
Table 3.2 Location, sequence and genotyping of gRNA targets in the <i>Gnao1</i> locus. ..	128
Table 3.3 Location and sequence of gRNA and ssODN template for CRISPR-Cas targeting <i>Gnao1</i> locus; primers and genotyping method for <i>Gnao1</i> ^{+/<i>R209H</i>} mice.....	131
Table 3.4 Phenotypes of <i>Gnao1</i> mutant mice	160

Table S3.1 Gait analysis parameters of male <i>Gnao1</i> G203R mutant mice	173
Table S3.2 Gait analysis parameters of female <i>Gnao1</i> G203R mutant mice	174
Table S3.3 Gait analysis parameters of male <i>Gnao1</i> G184S mutant mice	175
Table S3.4 Gait analysis parameters of female <i>Gnao1</i> G184S mutant mice	176
Table S3.5 Gait analysis parameters of male <i>Gnao1</i> R209H mutant mice	177
Table S3.6 Gait analysis parameters of female <i>Gnao1</i> R209H mutant mice	178
Table S3.7 Gait analysis parameters of male <i>Gnao1</i> KO mutant mice	179
Table S3.8 Gait analysis parameters of female <i>Gnao1</i> KO mutant mice	180
Table S3.9 Benchling off-target list for <i>Gnao1</i> G203R gRNA	181
Table 5.1 Comparison of clinical patterns of G203R and R209H patients	254

LIST OF FIGURES

Figure 1.1 Summary of reported cases of <i>GNAO1</i> encephalopathy	5
Figure 1.2 Genes regulating the cAMP pathway are related to movement disorders	16
Figure 1.3 Pathogenic mutations in genes that regulate neurotransmitter release	25
Figure S1.1 Correlation between seizure frequency and a severe EEG/MRI result.....	44
Figure 2.1 Location and protein expression levels of human <i>GNAO1</i> mutations related to epileptic encephalopathy.	75
Figure 2.2 Effect on α_2A AR-mediated cAMP inhibition by <i>GNAO1</i> mutants.....	78
Figure S2.1 Alignment of the human and mouse $G\alpha_o$ protein sequences.....	97
Figure S2.2 Validation of the Lance Ultra cAMP assay with transient transfection of α_{2A} adrenergic receptor (α_{2A} AR) and Pertussis toxin (PTX)-insensitive $G\alpha_o$	98
Figure S2.3 Assessment of dominant-negative effect of complete LOF mutants G40R, N270H, D174G, T191_F197del, L199P, and F275S.....	99
Figure S2.4 Paired t-test analysis of LogEC ₅₀ values for normal and GOF mutants....	101
Figure S2.5 Mapping of mutations on the structure of $G\alpha_o$ -GDP bound to RGS16.....	102
Figure S2.6 Comparison of validation of the Lance Ultra cAMP assay between HEK293T and <i>GNAS</i> KO HEK293 cells with transient transfection of α_{2A} adrenergic receptor (α_{2A} R) and Pertussis toxin (PTX)-insensitive $G\alpha_o$	107
Figure S2.7 <i>GNAO1</i> mutations' functionalities correlate to their protein expression patterns.....	108
Figure S2.8 <i>GNAO1</i> mutations' functionalities correlate to their protein expression patterns (assays done by Nils Wellhausen with a different group of mutations from those	

in Figure S2.7).	109
Figure 3.1 Development of <i>Gnao1</i> ^{+G203R} mouse model.	127
Figure 3.2 Targeting of the mouse <i>Gnao1</i> locus.	131
Figure 3.3 The timeline for utilizing animals in this study.	134
Figure 3.4 <i>Gnao1</i> ^{+ΔT191F197} mice developed spontaneous seizures at P7 and died before P16.	140
Figure 3.5 Female <i>Gnao1</i> ^{+G184S} mice and male <i>Gnao1</i> ^{+G203R} mice show reduced time on RotaRod and reduced grip strength.	143
Figure 3.6 G184S mutant mice showed reduced activities in Open Field Test but G203R mutants do not.	145
Figure 3.7 DigiGait Imaging System reveals sex-specific gait abnormalities in <i>Gnao1</i> ^{+G184S} mice and <i>Gnao1</i> ^{+G203R} mice.	148
Figure 3.8 <i>Gnao1</i> ^{+R209H} mice show significant hyperactivity and reduced time in center in the open field arena.	150
Figure 3.9. Male and female <i>Gnao1</i> ^{+R209H} mice shows gait abnormalities in different tests on the DigiGait imaging system.	151
Figure 3.10 Male and female <i>Gnao1</i> ^{+/-} mice do not show any abnormalities in the behavioral tests including open field, Rotarod, and grip strength.	154
Figure 3.11 DigiGait Imaging System reveals the decreased stride length in male <i>Gnao1</i> ^{+/-} mice.	155
Figure 3.12 <i>Gnao1</i> ^{+G203R} male mice have an enhanced Pentylentetrazol (PTZ) Kindling response.	157
Figure 3.13 <i>Gnao1</i> ^{+R209H} mice do not have an enhanced pentylentetrazol (PTZ) kindling response.	158

Figure S3.1 RotaRod test was conducted with 5 training sessions and 1 test session over two consecutive days.....	166
Figure S3.2 Time spent at the center in the Open Field Test.....	167
Figure S3.3 RotaRod learning curve was collected in 10 consecutive tests with a 5-min break between each test.	168
Figure S3.4 False discovery rate (FDR) calculation probed of significantly different parameters from the DigiGait data in <i>Gnao1</i> ^{+/^{G184S} mice.....}	169
Figure S3.5 False discovery rate (FDR) calculation probed of significantly different parameters from the DigiGait data in <i>Gnao1</i> ^{+/^{G203R} mice.....}	170
Figure S3.6 False discovery rate (FDR) calculation probed of significantly different parameters from the DigiGait data in <i>Gnao1</i> ^{+/^{R209H} mice.}	171
Figure S3.7 False discovery rate (FDR) calculation probed of significantly different parameters from the DigiGait data in <i>Gnao1</i> ^{+/-} mice.	172
Figure 4.1 Cerebellar Purkinje cells in brain slices from 4-6 week-old G203R mice display reduced GABAergic spontaneous synaptic currents (sIPSCs) and reduced miniature synaptic currents (mIPSCs).	206
Figure 4.2 The frequencies of mIPSCs were sensitive to NEM, an inhibitor of $G\alpha_{i/o}$ proteins.....	209
Figure 4.3 A selective inhibitor of $G_{i/o}$, pertussis toxin (PTX), increased the frequency of mIPSCs in G203R but not WT mice.	210
Figure 4.4 G203R mutant slices show no difference in either spontaneous excitatory postsynaptic currents (sEPSCs) or miniature excitatory postsynaptic currents (mIPSCs).	212
Figure 4.5 Activating GABAB receptor with baclofen reduces mIPSC frequency but not amplitude. PTX incubation eliminates baclofen-induced inhibition of mIPSC frequency in WT and G203R mice.	214
Figure 4.6 The frequency of sIPSCs is modulated by α_{2A} R receptors.....	216

Figure 4.7 Cadmium-block of extracellular calcium influx suppresses the frequency of sIPSCs in both WT and G203R mice.	219
Figure 4.8 Cadmium-block of extracellular calcium influx does not affect the frequency and the amplitude of mIPSCs in both WT and G203R mice.	220
Figure 4.9 G203R mice showed a significant decrease in $G\alpha_o$ protein expression.	222
Figure 4.10 G203R mice did not show any significant changes in $G\beta$ expression in the brain.	223
Figure 4.11 Models of $GABA_B$ R and α_{2A} R mediated inhibition of GABA release.	225
Figure 4.12 $G\beta\gamma$ may play a major role in the regulation of IPSCs.	227
Figure 4.13 <i>GNAO1</i> mutations may have region specific effects, which cause an imbalance between excitatory and inhibitory neurotransmitters.	229
Figure S4.1 Despite the hypothesis that α_{2A} receptor antagonist yohimbine (10 μ M) could reverse the inhibition of sIPSC frequency induced by UK14, 304, the application of yohimbine further reduced the sIPSC frequency with the application of UK14, 304.	231
Figure S4.2 Baclofen does not affect either frequency or amplitude of sIPSCs, and UK14,304 does not affect mIPSC frequency or amplitude.	232
Figure S4.3 Heterozygous G184S (GOF) mice also showed a low $G\alpha_o$ protein expression level.	233
Figure S4.4 Female <i>Gnao1</i> ^{+G184S} mice showed reduced sIPSC frequency in hippocampal pyramidal cells, cortical layer II/IV pyramidal cells but not in cerebellar Purkinje cells.	234
Figure S4.5 Brain $G\alpha_o$ expression does not change in R209H mice's brain lysates.	235
Figure S5.1 α_{2A} R activates $G\alpha_o$, which inhibits N-type calcium channels in G1A1 cells. GOF mutation G184S enhance the inhibition of calcium currents.	273
Figure S5.2 Both G1A1 and SH-SY5Y cells are good candidates to study mutant $G\alpha_o$'s	

effects on N-type calcium channels with Fluo-4-NW dye in a Hamamatsu μ CELL plate reader.274

Figure S5.3 Neurite outgrowth in rat pheochromocytoma cells (PC12) can be induced by 50 ng/mL Nerve Growth Factor (NGF) in normal growth medium with reduced serum.275

Figure S5.4 Neurite outgrowth can be induced by 10 μ M retinoid acid (RA) in normal growth medium with reduced serum (30% FBS) in human neuroblastoma cells (SH-SY5Y).276

Figure S5.5 Representative traces of modulations in calcium oscillations with different ion concentration in mixed cortical cultures from a WT mouse.277

Figure S5.6 High-throughput assessment of neural excitability in cortical cultures.278

Figure S5.7 Nissl staining compares gross morphological changes in cerebellum from *Gnao1*^{+/^{G184S} and *Gnao1*^{+/^{+ mice at age 8 weeks old.279}}}

KEY TO ABBREVIATIONS

AC	Adenylyl cyclases
ACSF	Artificial cerebral spinal fluid
ADHD	Attention Deficit Hyperactivity Disorder
ANOVA	Analysis of variance
AP	Action potential
APV	2-Amino-5-phosphonopentanoic acid
BRET	Bioluminescence resonance energy transfer
DMEM	Dulbecco's modified Eagle's medium
CNQX	6-Cyano-7-nitroquinoxaline-2,3-dione
DOR	Delta opioid receptor
CREB	cAMP-response element binding protein
CRISPR	Clustered regularly interspaced short palindromic repeats
EA2	Episodic ataxia type 2
EIEE17	Early infantile epileptic encephalopathy 17
FBS	Fetal bovine serum
FDR	False discovery rate
FFT	Fast Fourier Transform

GABA	γ -Aminobutyric acid
GDD	Developmental delay
GIRK	G-protein activated inward rectifying potassium channels
GOF	Gain-of-function
GPCR	G protein coupled receptor
HD	Huntington's Disease
ID	Intellectual disability
KO	Knock-out
LID	L-DOPA-induced dyskinesia
LOF	Loss-of-function
MD	Movement disorder
M-D	Myoclonus-dystonia syndrome
ME	Mercaptoethanol
mEPSC	Miniature excitatory postsynaptic current
mIPSC	Miniature inhibitory postsynaptic current
MOR	Mu opioid receptor
NAc	Nucleus accumbens
NEDIM	Neurodevelopmental disorder with involuntary movement

NEM	N-Ethylmaleimide
NF	Normal-functioning
NGF	Nerve Growth Factor
PD	Parkinson's Disease
PDE	Phosphodiesterase
PI3-K	Phosphatidyl-inositol-4,5-bisphosphate 3-kinase
PLOF	Partial-loss-of-function
PNKD3	Paroxysmal nonkinesigenic dyskinesia 3
PRRT2	Proline-rich transmembrane protein 2
PTX	Pertussis toxin
PTZ	Pentylentetrazol
RNP	Ribonucleoprotein
sEPSC	Spontaneous excitatory postsynaptic current
sIPSC	Spontaneous inhibitory postsynaptic current
SNAP25	Synaptosomal associated protein-25
ssODN	Single-stranded oligo DNA nucleotides
SV	Synaptic vesicles
TH	Tyrosine hydroxylase

TTX

Tetrodotoxin

WT

Wildtype

CHAPTER 1: AN OVERVIEW OF *GNAO1*-ASSOCIATED NEUROLOGICAL DISORDERS

Modified from Feng, H., Khalil, S., Neubig, R. R., & Sidiropoulos, C. (2018). A mechanistic review on *GNAO1*-associated movement disorder. *Neurobiology of disease*, 116, 131-141. DOI: <https://doi.org/10.1016/j.nbd.2018.05.005>.

With permission from the Elsevier. All rights reserved.

1.1 Abstract

Mutations in the *GNAO1* gene cause a complex constellation of neurological disorders including epilepsy, developmental delay, and movement disorders. *GNAO1* encodes $G\alpha_o$, the α subunit of G_o , a member of the $G_{i/o}$ family of heterotrimeric G protein signal transducers. G_o is the most abundant membrane protein in the mammalian central nervous system and plays major roles in synaptic neurotransmission and neurodevelopment. *GNAO1* mutations were first reported in early infantile epileptic encephalopathy 17 (EIEE17), but are also associated with a more common syndrome termed neurodevelopmental disorder with involuntary movements (NEDIM). Here we review a mechanistic model in which loss-of-function (LOF) *GNAO1* alleles cause epilepsy and gain-of-function (GOF) alleles are primarily associated with movement disorders. We also develop a signaling framework related to cyclic AMP (cAMP), synaptic vesicle release, and neural development and discuss gene mutations perturbing those mechanisms in a range of genetic movement disorders. Finally, we analyze clinical reports of patients carrying *GNAO1* mutations with respect to their symptom onset and discuss pharmacological/surgical treatments in the context of our mechanistic model.

1.2 Introduction

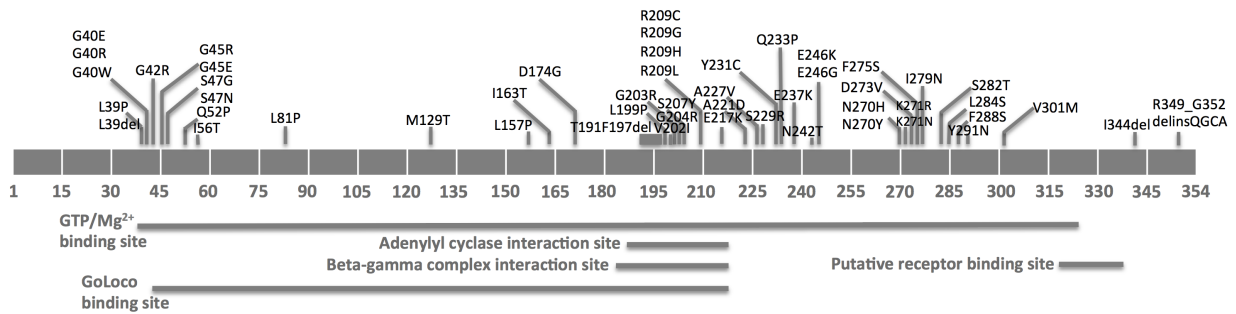
Mutations in *GNAO1* were first reported in patients with Ohtahara syndrome and early infantile epileptic encephalopathy 17 (EIEE17, OMIM 61547) (Nakamura et al.,

2013). More recently, a syndrome of neurodevelopmental disorder with involuntary movements without epileptic seizures (NEDIM, OMIM 617493) has been defined, expanding the phenotypic spectrum of *GNAO1* mutation-associated neurological disorders (Ananth et al., 2016; Zhu et al., 2015). Currently, there have been published reports on 81 patients representing 36 different *GNAO1* mutations (23 missense, 1 in-frame deletion and 1 splicing site mutation, see Figure 1.1) (Ananth et al., 2016; Arya, Spaeth, Gilbert, Leach, & Holland, 2017; Blumkin et al., 2018; Bruun et al., 2018; Carecchio et al., 2019; Danti et al., 2017; R. Dhamija, Mink, Shah, & Goodkin, 2016; Dietel, 2016; Epi, 2016; Epi et al., 2013; Euro, Epilepsy Phenome/Genome, & Epi, 2014; Farwell et al., 2015; Gawlinski et al., 2016; Gerald et al., 2018; Helbig et al., 2016; Honey et al., 2018; Kelly et al., 2019; Koy et al., 2018; Kulkarni, Tang, Bhardwaj, Bernes, & Grebe, 2016; Law et al., 2015; Malaquias et al., 2019; Marce-Grau et al., 2016; Menke et al., 2016; Nakamura et al., 2013; Okumura et al., 2018; Saitsu et al., 2016; Sakamoto et al., 2017; Schirinzi et al., 2019; Schorling et al., 2017; Takezawa et al., 2018; Talvik et al., 2015; Ueda, Serajee, & Huq, 2016; Waak et al., 2018; Xiong et al., 2018; Yilmaz et al., 2016).

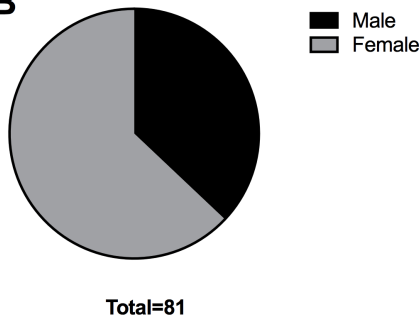
Although recent reviews on monogenic complex hyperkinetic disorders recognized *GNAO1* mutations as pathogenic (Carecchio & Mencacci, 2017; Mencacci & Carecchio, 2016), our review focuses on a mechanistic analysis illustrating the shared pathways of pathogenic mutations across multiple movement disorder-associated genes. It is

important to consider the mechanisms that underlie the *GNAO1*-associated movement disorders to rationalize the clinical heterogeneity resulting from different mutations in *GNAO1*, as well as the implications for therapeutic choices. We (H.F. and R.R.N.) recently demonstrated that *GNAO1* mutations associated with movement disorders result in a gain-of-function (GOF) biochemical behavior related to control of cAMP levels, while epilepsy-associated mutations cause loss-of-function (LOF) behavior (Feng et al., 2017). This is consistent with other single-gene epilepsy and movement disorders, which also share causal genes (Batty, Fenrich, & Fouad, 2017; Szczepanik et al., 2015). Focusing on movement disorders, there is a clear functional connection between *GNAO1* and other “movement disorder genes” related to two molecular mechanisms. Both the cAMP pathway (*GNAL*, *GNB1*, *ADCY5*, *PDE10A*) and regulation of synaptic vesicle fusion and neurotransmitter release (*GNB1*, *CACNA1A*, *CACNA1B*, *KCNMA1*, *SYT1*, *SNAP25*, and *PRRT2*) have been implicated. In this review, we attempt to develop models of these systems and explore how they may connect pathophysiology with clinical patterns and therapeutic responses.

A



B



C

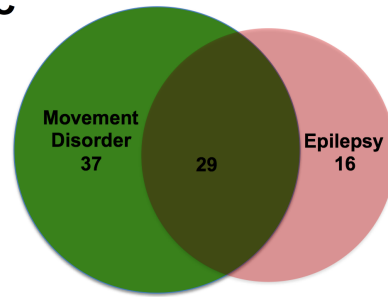


Figure 1.1 Summary of reported cases of *GNAO1* encephalopathy

(A) Locations of reported mutations on the $G\alpha_o$ amino acid sequence. The splicing site mutations are not included here. (B) Sex distribution among the 48 patients reported. (C) Distribution of movement disorders and/or epilepsy symptoms in *GNAO1* encephalopathy patients (Green = movement disorder only; Red = epilepsy only; Orange = both phenotypes).

1.3 $G\alpha_o$ (*GNAO1*) mechanisms

GNAO1 encodes the α -subunit of a heterotrimeric guanine nucleotide-binding protein ($G\alpha_o$), which is the most abundant membrane protein in the mammalian central nervous system, constituting approximately 1% of total brain membrane protein. $G\alpha_o$ localizes ubiquitously throughout the brain with relatively high expression in hippocampus,

striatum and cerebellum (Worley, Baraban, Van Dop, Neer, & Snyder, 1986). It couples to a variety of important G protein coupled receptors (GPCRs) including GABA_B, α_2 adrenergic, adenosine A₁ (A₁R), and dopamine D₂ (D₂R) receptors. These play key roles in regulating neurotransmitter release, movement, and neural development.

There are multiple downstream signaling targets of G_o, as well as of the other members of the G_{i/o} family. These include: inhibition of adenylyl cyclases (ACs) which decreases cAMP production, inhibition of N-type (Ca_v2.2) and P/Q type calcium channels (Ca_v2.1) (Colecraft, Brody, & Yue, 2001; McDavid & Currie, 2006), and direct inhibition of neurotransmitter vesicle release by the binding of G $\beta\gamma$ released from active G α_o to inhibit syntaxin 1A and SNAP25 (Zamponi & Currie, 2013). Both G α_o and G $\beta\gamma$ subunits also bind to G protein-coupled inward rectifying potassium (GIRK) channels to stimulate channel opening (Luscher & Slesinger, 2010). GIRK channels are well-recognized as playing a role in seizure disorders (Mayfield, Blednov, & Harris, 2015; Signorini, Liao, Duncan, Jan, & Stoffel, 1997; Torrecilla et al., 2002).

Many of these targets of G_o (both G α_o and G $\beta\gamma$) signaling are also implicated in movement disorders. Mutations in *ADCY5* (which encodes adenylyl cyclase type 5) have been reported in patients with dyskinesia and dystonia (Meijer, Miravite, Kopell, & Lubarr, 2017; Mencacci, Erro, et al., 2015; Shaw, Hisama, Friedman, & Bird, 1993). Mutations in *CACNA1A* (encoding Cav2.1) cause episodic ataxia type 2 (EA2) (Sintas et al., 2017; Wan et al., 2011). In the G protein family, mutations in both *GNAL* (Dufke et al., 2014;

Kumar et al., 2014; Putzel et al., 2016) and *GNB1* (Lohmann et al., 2017; Steinrucke et al., 2016) are also associated with dystonic syndromes. The former encodes $G\alpha_{\text{olf}}$ which mediates dopamine $D_{1/5}$ receptor stimulation of AC and the latter encodes $G\beta_1$ which mediates many actions of $G_{i/o}$.

1.4 The clinical spectrum of *GNAO1* mutation-associated movement disorders

1.4.1 *GNAO1* encephalopathy displays a variety of neurological symptoms

To understand the molecular mechanisms underlying *GNAO1* disorders, it is important to consider the substantial clinical heterogeneity which includes both early-onset epileptic encephalopathy (Nakamura et al., 2013) and patients with complex movement disorders with or without epilepsy (Ananth et al., 2016; Kulkarni et al., 2016; Menke et al., 2016; Saitsu et al., 2016; Sakamoto et al., 2017; Zhu et al., 2015). Recently, we reported a biochemical analysis of 15 different *GNAO1* mutant alleles (Feng et al., 2017), which revealed that LOF mutations are associated with epileptic seizures while mutations that result in GOF for inhibition of cAMP as well as mutations that show largely normal function in this assay (p.R209 mutations) are mainly associated with movement disorders (Feng et al., 2017).

The two most common manifestations of patients with *GNAO1* mutations (Table S1.1 and Figure S1), regardless of their clinical pattern or biochemical phenotype, are hypotonia (68%) and developmental delay (78%, Table S1.1). Choreoathetotic movements (44%) and dystonia (32%) are the next most common findings (Table S1.1).

Approximately 28% of patients had intellectual disability.

While many individuals have abnormal EEG or MRI findings (Table S1.1), less than half of patients with *GNAO1* mutations (50%) showed markedly abnormal EEGs and that was primarily in epilepsy patients with LOF mutations. Approximately 64% of the reported patients showed significant MRI findings and these were distributed across both epilepsy and movement disorder patients (Table S1.1). This heterogeneity in both clinical pattern and effect on brain structure/function suggests a role for both neurodevelopmental alterations and functional signaling perturbations. The latter seems more prominent in patients with the GOF mutants who show less evidence for brain structural abnormalities as well as having some therapeutic responses to drug treatment (see below).

Table 1.1 Most Common *GNAO1* Mutant Alleles Associated With Movement Disorders

<i>GNAO1</i> alleles	No. of patients	Frequency of occurring							
		Epileptic seizures	Hypotonia	Chorea/athetosis	Dystonia	Myoclonus	Ballismus	Dyskinesia	Stereotypies
p. R209H/L/G/C	12	25%	83%	67%	33%	8%	8%	25%	8%
p. E246K	9	22%	89%	63%	56%	0	50%	25%	0
p. G203R	7	100%	14%	43%	29%	0	0	0	0
p. E237K	2	0	100%	100%	100%	50%	50%	50%	0

Table 1.2 Drugs showing beneficial effects to control involuntary movements of *GNAO1* encephalopathy patients

Drug Positive Response	<i>GNAO1</i> Mutations	Sex	Inheritance	Age of onset	Symptoms		Ref
					Epileptic seizures	Movement Disorders	
Tetrabenazine	p.E246G	F	<i>de novo</i>	6 mo	+	+	Danti et al., 2017
	p.S47G	M	<i>de novo</i>	5 mo	+	+	Danti et al., 2017
	p.R209H	M	<i>de novo</i>	10 mo		+	Dhamija, 2016
	p.E237K	M	<i>de novo</i>	4 mo		+	This report
	p.E237K	M	<i>de novo</i>	3 mo		+	Waak et al., 2017
	p.E246K	F	<i>de novo</i>	4 y		+	Ananth et al., 2016
	p.E246K	F	<i>de novo</i>	6 mo		+	Ananth et al., 2016
	p.E246K	M	<i>de novo</i>	14 y		+	Ananth et al., 2016
	p.E246K	F	<i>de novo</i>	3 mo		+	Waak et al., 2017
Levetiracetam	p.G45R	M	<i>de novo</i>	NA	+	+	Ueda, 2016
	p.E237K	M	<i>de novo</i>	4 mo		+	This report
Topiramate	p.R209C	F	<i>de novo</i>	11 mo		+	Saitsu et al., 2016; Sakamoto et al., 2017
Trihexyphenidyl	p.R209H	M	<i>de novo</i>	10 mo		+	Dhamija, 2016

1.4.2 Movement disorders related to *GNAO1* encephalopathy show limited response to pharmacological treatments

There are three mutation hotspots (G203, R209 and E246) in *GNAO1* that prominently result in movement disorders (Table 1.1) (Ananth et al., 2016; Arya et al., 2017; Danti et al., 2017; R. Dhamija et al., 2016; Honey et al., 2018; Kulkarni et al., 2016; Menke et al., 2016; Nakamura et al., 2013; Saitsu et al., 2016; Sakamoto et al., 2017; Waak et al., 2018; Xiong et al., 2018; Zhu et al., 2015). All show GOF or normal function (NF) phenotypes in the *in vitro* cAMP regulation assay (Feng et al., 2017). This

correlation raises the possibility of rationalized drug selection in treating diseases related to *GNAO1* mutations. $G\alpha_o$ -coupled-receptor antagonists should reduce signaling in movement disorder patients by decreasing the signal from hyperactive GOF *GNAO1* mutants. $G\alpha_o$ -coupled-receptor agonists might be beneficial in epilepsy. In both cases, however, the receptors mediating the abnormal function would need to be identified.

The NF mutant alleles (in p.R209) raise questions about the simple GOF/LOF model despite the fact that those patients show clear clinical movement disorder pathology. Moreover, the G203R mutation results in a modest GOF biochemical effect (Feng et al., 2017) but causes both movement disorder and frequent seizures – though the latter are reasonably easily controlled (Table S1.1). These mutations show that there is more to learn about the genotype-phenotype correlation. A key question will be whether another downstream signal (e.g. calcium and potassium channel regulation) may better correlate with clinical patterns.

Among patients with movement disorders, tetrabenazine is the most effective drug (Table 1.2) (Ananth et al., 2016; Danti et al., 2017). This is not surprising given that tetrabenazine's actions on VMAT2 will deplete multiple amine neurotransmitters (dopamine, norepinephrine, and serotonin). This should result in a wide-spread reduction of G_o signaling through, for example, α_{2A} adrenergic receptors, D_2/D_4 receptors, and 5-HT₁ receptors.

Responses were also reported to trihexyphenidyl, topiramate, and levetiracetam

(Table 1.2). Trihexyphenidyl is described as a selective muscarinic M1 receptor antagonist, but it binds to all five muscarinic receptors subtypes with similar affinity (Dorje et al., 1991). The M4 muscarinic receptor subtype is second most potently inhibited by trihexyphenidyl. That receptor is $G_{i/o}$ coupled and strongly implicated in striatal function (Ztaou et al., 2016). This may be a therapeutic target worth serious consideration. Interestingly, the patient with the p.R209H mutation who responded to trihexyphenidyl also responded to tetrabenazine (R. Dhamija et al., 2016). Topiramate was very effective in suppressing chorea in a patient carrying a p.R209C mutation (Table 1.2) (Sakamoto et al., 2017). Levetiracetam also showed effectiveness in two patients. Neither of these latter two drugs is known to affect G protein coupled receptors. However, levetiracetam partly works by binding to its high-affinity binding site on a synaptic vesicle protein to inhibit neurotransmitter release globally (Grimminger et al., 2013; Ohno & Tokudome, 2017), which would explain its multi-functionality in suppressing both epilepsy and movement disorders. While multiple therapies have shown some efficacy in controlling involuntary movements, no drug seems to be able to mitigate developmental delay.

Table 1.3 Patients responding positively to deep brain stimulation (DBS)

<i>GNAO1</i> Mutation	Sex	Inheritance	Age of onset	Symptoms		DBS Positive Response	Ref
				Epileptic seizures	Movement Disorders		
p.E246G	F	<i>de novo</i>	6 mo	+	+	Y	Danti et al., 2017
p.E237K	M	<i>de novo</i>	3 mo		+	Y	Waak et al., 2017
p.E246K	F	<i>de novo</i>	3 mo		+	Y	Waak et al., 2017
p.R209H	M	<i>de novo</i>	18 mo		+	Y	Kulkarni et al., 2016
p.R209H	M	<i>de novo</i>	2 y		+	Y	Kulkarni et al., 2016
p.R209C	F	<i>de novo</i>	6 mo	+	+	Y	Waak et al., 2017
p,R209L	M	<i>de novo</i>	2 y		+	Y	Honey et al., 2018
p.Q233P	F	<i>de novo</i>	13 mo		+	Y	Yilmaz et al., 2016

In contrast to the modest efficacy of drug treatment, in seven cases where DBS was performed, patients all responded well and involuntary movements were suppressed (Table 1.3) (Danti et al., 2017; Honey et al., 2018; Kulkarni et al., 2016; Waak et al., 2017; Yilmaz et al., 2016). Consequently, DBS targeting the globus pallidus pars interna (GPi), appears to be the most effective treatment for *GNAO1* related movement disorders, at least in medication refractory cases. There are no reports to assess the effectiveness of DBS in other brain regions such as the subthalamic nucleus. DBS may be effective due to its general effects in modulating aberrant synchronization in the basal ganglia-thalamo-cortical loops (McIntyre & Anderson, 2016). There is no information yet on long-term-sustained efficacy however. Furthermore, there may be a publication bias

towards patients who responded well and DBS can have a prominent placebo effect, as seen for patients with Parkinson's disease (de la Fuente-Fernandez, 2004; Mercado et al., 2006).

Seizures in patients with *GNAO1* mutations can be controlled to some degree by multiple anti-epileptic drugs (AEDs) (Danti et al., 2017). However, no drug has been shown to be particularly effective (Table S1.1).

1.5 Potential pathogenic mechanisms of *GNAO1*-associated movement disorders

The possible etiological bases of *GNAO1*-associated movement disorder may be explained by examination of *GNAO1* signaling. Inhibition of cAMP is a canonical pathway of G_o , which may be mediated by $G\alpha_o$ itself or by the released $G\beta\gamma$ (Dortch-Carnes & Potter, 2003; Gill & Hammes, 2007). Mutations in *ADCY5* (which encodes an AC protein that synthesizes cAMP) also result in movement abnormalities in human patients. Dysregulation of cAMP signaling leads to brain malfunction (Borlikova & Endo, 2009; Guan et al., 2011). Therefore disturbances of cAMP levels could disrupt a finely tuned neurodevelopmental system.

A second theoretical basis of *GNAO1*-associated movement disorder relates to G_o 's role in regulating neurotransmitter release. A close relationship has been proposed among neurotransmitter levels, brain morphology and behavioral experience (Goldstein, 2006). Deficiency of key neurotransmitters like catecholamines (dopamine, epinephrine and norepinephrine) and serotonin are widely studied in movement disorders or seizures

(Mercimek-Mahmutoglu et al., 2015). G_o 's presynaptic role in regulating neurotransmitter release suggests another potential mechanism in the etiology of movement disorders.

A third possibility, from a developmental view, could be alterations of neuronal maturation, which needs to occur at appropriate stages of neurological development. Therefore children with developmental defects would exhibit abnormal behaviors. It is striking that most patients with *GNAO1*-associated movement disorders also suffer from severe developmental delay. Morphologically, MRI scans may show global atrophy and delayed myelination. Overall, genetic causes are responsible for about 40% of the developmental delay cases, including developmental delay/intellectual disability (GDD/ID) (Miclea, Peca, Cuzmici, & Pop, 2015). Control of cAMP levels and neurotransmitter release clearly could affect ongoing neural functions as well as neurological development. By this concept, *GNAO1*-associated movement disorders could result from perturbations of either of these processes (Leung & Wong, 2017). Clearly, the former would be more amenable to the therapeutic intervention than the latter.

1.5.1 Role of cAMP regulation in movement disorders

The second messenger cAMP modulates a broad spectrum of cellular functions including gene expression, metabolism, exocytosis, and neuronal development. cAMP is synthesized from ATP by the AC enzymes upon activation by G-protein coupled receptors (GPCRs). An increase of cAMP levels activates protein kinase A (PKA), which

phosphorylates other kinases, transcription factors, and ion channels. cAMP can also activate the Rap guanine nucleotide exchange factor Epac, which has important functions in neural plasticity (Schmidt, Dekker, & Maarsingh, 2013; Tong et al., 2017). cAMP formation is negatively regulated by phosphodiesterases (PDEs) or $G_{i/o}$ family coupled GPCRs such as these associated with *GNAO1*. There are many isoforms of ACs and PDEs in specific brain regions, consistent with the need to maintain a delicate a balance of cAMP levels for a normally functioning nervous system. cAMP signaling in the brain is known to mediate neuronal excitability and synaptic plasticity, which further regulates learning and memory, and motor function (Bollen & Prickaerts, 2012; Kandel, 2012; Pierre, Eschenhagen, Geisslinger, & Scholich, 2009). Also, dibutyryl-cAMP, an analog of cAMP, promotes axon regeneration and the recovery of motor function by inhibiting the RhoA signaling pathway (Jeon et al., 2012). The importance of cAMP in pro-regenerative action makes it a potential therapeutic target for enhancing nerve repair (Yu, Wang, Wu, & Yi, 2017).

In this section, we will focus on the role that cAMP plays in movement disorders. There are many movement disorder-related genes that directly regulate cAMP levels in the brain (D'Angelo et al., 2017; Padovan-Neto & West, 2017). Figure 1.2 provides a schematic overview of the genes discussed including the type of mutations (LOF or GOF) seen. However, see the text below for details, as not all results in the literature are clear-cut. Based on functional studies associated with those genes, both up- and down-

regulation of cAMP production may contribute to the pathophysiology of movement disorders. Here we provide a hypothetical model of the role of cAMP regulation in movement disorders (Figure 1.2).

Unfortunately, however, there is not a simple, completely coherent model of the relationship between predicted changes in cAMP concentration and the presence of movement disorders. It is clear that perturbations in cAMP mechanisms are pathological. Potential explanations for this complexity are described below after consideration of each gene in detail.

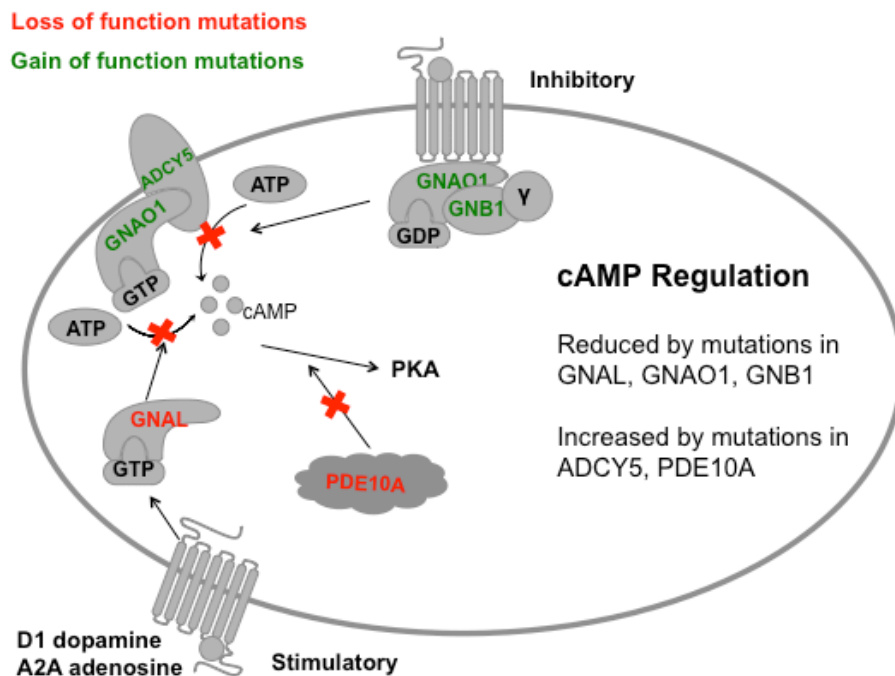


Figure 1.2 Genes regulating the cAMP pathway are related to movement disorders GPCRs activate G_α (encoded by *GNAO1*), which may either inhibit or stimulate cAMP production depending on the AC subtype present. G_β₁ (encoded by *GNB1*) forms a complex with G_γ and this G_{βγ} complex, typically released from G_o or G_i-family G proteins, can also inhibit or stimulate cAMP production. Activation of G_o (encoded by *GNAL*) stimulates cAMP. Phosphodiesterase 10A (encoded by the *PDE10A* gene) hydrolyzes

Figure 1.2 (cont'd) cAMP to the monophosphate. Both gain-of-function (GOF) mutations in *GNAO1* and loss-of-function (LOF) mutations in *GNAL* likely result in a decrease of cAMP. LOF mutant alleles in *PDE10A* and GOF mutations in *ADCY5* increase cAMP.

1.5.1.1 *GNAL*

GNAL encodes the alpha subunit of the guanine nucleotide-binding protein G_{olf} . It belongs to the G_s family and can be activated by odorant receptors in the olfactory epithelium. It is also strongly expressed in the striatum. G_s family and $G_{i/o}$ family proteins have opposite functional effects on AC. Once activated by G_s -coupled GPCRs, G_{olf} activates AC enzymes to produce cAMP. In the striatum, G_{olf} couples to D1 dopamine (D_1R) and A_{2A} adenosine (A_2AR) receptors to activate type 5 adenylyl cyclase (AC5), which is encoded by the *ADCY5* gene (Mercimek-Mahmutoglu et al., 2015).

GNAL mutations account for about 1% of all cases of focal or segmental dystonia (Kumar et al., 2014). These include autosomal dominant, partial LOF mutations in *GNAL* (Dos Santos et al., 2016; Masuho et al., 2016). As GOF mutations in *GNAO1* and LOF mutations in *GNAL* result in a similar functional change in cAMP production, it seems logical that they may share similar mechanisms leading to dystonic/choreo-athetoid disorders. Other previous functional studies of mutant *GNAL* also revealed deficiencies in AC activation after D_1R stimulation (Fuchs et al., 2013; Kumar et al., 2014). Typically, patients with heterozygous *GNAL* mutations exhibit an adult-onset focal cervical, laryngeal, and/or segmental dystonia (Masuho et al., 2016). Animal studies also support

the idea that LOF mutations in *GNAL* with a reduction in striatal cAMP lead to movement disorders. A heterozygous mouse model *Gnal*^{+/-} was reported with abnormal postures and movements compared to WT mice after treatment with the muscarinic agonist oxotremorine (Pelosi, Menardy, Popa, Girault, & Herve, 2017) (Zwart, Reed, Clarke, & Sher, 2016) (Pelosi et al., 2017; Zwart et al., 2016). Note that oxotremorine-induced movement disorders in *Gnal*^{+/-} mice can be replicated with infusion of oxotremorine into the striatum but not cerebellum (Pelosi et al., 2017), which indicates the crucial role of cAMP signaling in striatal projection neurons and the potential role of muscarinic receptors in modulating the motor movement.

1.5.1.2 *GNB1*

The *GNB1* gene encodes the G protein β subunit $G\beta_1$. In G protein signaling, $G\alpha$ binds with $G\beta\gamma$ and GDP in its inactive state. Upon activation, $G\alpha$ binds to GTP and the $G\alpha$ -GTP and $G\beta\gamma$ separate, both carrying out downstream signaling.

Recently, *de novo* mutations in *GNB1* have been identified using whole-exome sequencing in patients with severe neurodevelopmental disability, hypotonia, and seizures (Lohmann et al., 2017; Petrovski et al., 2016). The symptoms in *GNB1* patients share characteristics with *GNAO1* encephalopathy patients. Moreover, patients with *GNB1* mutations also display early onset of movement abnormalities similar to patients with *GNAO1* mutations (Petrovski et al., 2016).

However, the functional change of the known *GNB1* mutations is unclear due a

variety of assays used by different groups. Lohmann et al defines their mutant *GNB1* as LOF by using real-time bioluminescence resonance energy transfer (BRET) assays to assess Gβγ's ability to couple to D₁R (Lohmann et al., 2017). However, other groups describe *GNB1* mutations as having a GOF effect due to enhancement of downstream signaling pathways (Petrovski et al., 2016; Yoda et al., 2015). One unified functional assay such as Gβγ-regulated inhibition of cAMP production or of N-type calcium channels should be performed on all *GNB1* mutants to clarify definitions of LOF or GOF. Whether mutations in *GNAO1* affect Gβγ function or not remains unknown, but the fact that non-functioning Ca_v2.1 and Ca_v2.2 result in similar movement disorders (see below) suggests a hypothesis that Gβγ inhibition of calcium channels may be enhanced by GOF mutations in *GNAO1* as well as GOF mutations in *GNB1* itself.

1.5.1.3 *ADCY5*

Mutations in the *ADCY5* gene, which encodes AC5 also cause early onset persistent or paroxysmal choreic, myoclonic, and/or dystonic movements as well as alternating hemiplegia of childhood (Carapito et al., 2015; Friedman et al., 2016; Mencacci, Erro, et al., 2015; Westenberger et al., 2017). Patients carrying *ADCY5* mutations display mixed hyperkinetic movements including dystonia, facial myokymia, chorea, myoclonus and tremor (D. H. Chen et al., 2015). In addition to abnormal movements, axial hypotonia with paroxysmal exacerbations is also associated with *ADCY5* mutations (D. H. Chen et al., 2015). Delayed milestones and axial hypotonia seem to be almost universal features

in infants with *ADCY5* mutations (Carecchio et al., 2017). This is very similar to patients with *GNAO1* mutations (Table S1.1).

One functional study measuring β -adrenergic agonist-stimulated intracellular cAMP shows that two *de novo* mutations (c.1252C>T, p.R418W and c.2176G>A, p.A726T) in *ADCY5* are gain-of-function (GOF) mutations (Y. Z. Chen et al., 2014). More functional studies need to be done in assessing other mutations in *ADCY5* to define a clear genotype-phenotype correlation. A GOF mutation in *ADCY5* should increase cAMP levels contrasting with expected effects of *GNAL* and *GNAO1* mutations.

AC5 is highly expressed in striatum and nucleus accumbens (NAc). The striatum and NAc are part of the dopaminergic system that is activated in response to stress (Carapito et al., 2015). Chen et al reported that *Adcy5*-null mice developed a movement disorder, which can be worsened by stress (D. H. Chen et al., 2015). In addition, L-DOPA-induced dyskinesia (LID) is profoundly reduced in AC5 knockout mice and suppression of AC5 in the dorsal striatum is sufficient to attenuate LID (Park et al., 2014). Since G_o inhibits AC, this is consistent with the fact that knockout AC5 animals show impaired movements (Iwamoto et al., 2003). However, it remains unclear why GOF mutations in *ADCY5* lead to hyperkinetic movements in humans. These studies confirm the importance of regulation of cAMP in the development of movement disorders and suggest that inappropriate changes in either direction may be detrimental.

1.5.1.4 *PDE10A*

PDE10A (encoded by *PDE10A* gene) participates in signal transduction by regulating the levels of intracellular cyclic nucleotides. *PDE10A* is localized in dendritic spines proximally to postsynaptic sites in striatal medium spiny neurons (Xie et al., 2006). It hydrolyzes both cAMP and cGMP to nucleoside 5' monophosphate (Russwurm, Koesling, & Russwurm, 2015). However, *PDE10A* is the major cellular mechanism for degradation for cAMP but has only modest activity for cGMP in the striatum (Russwurm et al., 2015). Recently, LOF mutations in *PDE10A* are found in infancy-onset hyperkinetic movement disorders and childhood-onset chorea (Diggle et al., 2016; Mencacci et al., 2016). Loss of striatal *PDE10A* associates with movement disorders like Huntington's and Parkinson's disease (Ahmad et al., 2014; Giorgi et al., 2011). *Pde10a* knockout mice also show abnormalities in movements (Siuciak et al., 2008). LOF mutations in *PDE10A* increase cAMP concentration, which seems contradictory to GOF mutations in *GNAO1*. However, *PDE10A* levels differ in different striatum regions in an animal model of dystonia. *PDE10A* is increased in the globus pallidus but decreased in the entopeduncular nucleus/substantia nigra in a DYT1 model (D'Angelo et al., 2017), which lead to opposite regulation on cAMP concentration. This result further suggests the balance of cAMP concentration is more important in regulating neuronal functions than shifting either way.

1.5.1.5 Summary of cAMP regulation in movement control

cAMP has complex effects on neurotransmission. It can enhance neurotransmission through multiple actions on Ca^{++} concentration or on synaptic vesicle release and trafficking (Neher, 2006). It also strongly modulates synaptic plasticity – generally increasing neurotransmission (Nestler, Alreja, & Aghajanian, 1999), which may involve the cAMP-response element binding protein (CREB) or Epac (Eagle, Gajewski, & Robison, 2016; Tong et al., 2017). cAMP is also important in serotonin-mediated enhancement of synaptic transmission where it modulates hyperpolarization-activated cation channels (I_h channels), which underlie repetitive neuronal firing (Beaumont & Zucker, 2000).

In addition to these relatively acute actions of cAMP on neurotransmission, it also plays key roles in neurodevelopment. cAMP activates neurite outgrowth and facilitates axonal guidance (Akiyama, Fukuda, Tojima, Nikolaev, & Kamiguchi, 2016; Inda et al., 2017). It is possible that gene mutations that elevate cAMP production (i.e. LOF mutations in *PDE10A*, GOF mutations in *ADCY5*) increase neurite outgrowth and may result in enhanced or disordered synapse formation. This may increase excitatory neurotransmission and neuron hyperexcitability. It is clear, however, that genetic mutations which lead to decreased cAMP production (i.e. LOF mutations in *GNAL* and GOF mutations in *GNAO1*) also result in movement disorders. Indeed for some movement-disorder-associated genes (i.e. *GNB1*), both LOF and GOF functions and

effects have been reported (Lohmann et al., 2017; Petrovski et al., 2016).

There are several possible explanations for this highly complex picture. First, *in vitro* studies used to characterize GOF/LOF behavior of mutant alleles differ between labs so the concept of GOF or LOF may not directly correlate with *in vivo* cAMP production. Second, some actions may be mediated in different neuron populations or different brain regions. Finally, keeping an appropriate balance of cAMP levels may be the critical underlying element for normal movement performance. So either an increase or a decrease in cAMP could result in the observed movement disorders.

1.5.2 Role of neurotransmitter release and synaptic vesicle fusion in movement disorders

In addition to the control of cAMP production, regulation of neurotransmitter release is also strongly implicated in movement disorders, epilepsy, and neurodevelopmental delays (Figure 1.3). Mutations in genes for a number of proteins directly involved in synaptic vesicle fusion (e.g. *SYT1*, *SNAP25*, and *PRRT2*) have been identified. Presynaptic calcium influx is another driving factor for neurotransmitter release and most CNS synapses rely on Ca_v2.1 (*CACNA1A*) or Ca_v2.2 (*CACNA1B*) calcium channels for synaptic transmission. Mutations in both of these channel genes are associated with movement disorders.

Further tightening the connection among these various genes related to movement disorder, Gα_o activation drives Gβγ release, which mediates direct inhibition of vesicle

release (Zurawski et al., 2017) as well as indirect inhibition by suppression of voltage-gated calcium channels (i.e. $Ca_v2.1$ and $Ca_v2.2$ encoded by *CACNA1A* and *CACNA1B*) (Agler et al., 2005; McDavid & Currie, 2006). These mechanisms generate a relatively consistent model in which reductions in neurotransmitter release associate with movement disorder. GOF mutations in both *GNAO1* and *GNB1* would result in increased activity of $G\alpha_o$ and $G\beta\gamma$, which would suppress both calcium channel activity and the synaptic vesicle release machinery (Figure 1.3). LOF mutations in the genes encoding calcium channels (*CACNA1A* and *CACNA1B*) and three proteins involved in vesicle release (*SYT1*, *SNAP25*, and *PRRT2*) also are involved in movement abnormalities.

It is well-established that calcium influx through Ca_v channels triggers synaptic vesicle fusion via synaptotagmin (Sudhof, 2012). Indeed presynaptic calcium channels form a complex with synaptotagmin and other proteins in the vesicle release machinery such as syntaxin 1 and SNAP-25 (Leveque et al., 1994; Simms & Zamponi, 2014). Also, $G\beta\gamma$ released from activated G_o ($G\alpha_o/G\beta\gamma$) competes with synaptotagmin-1 for binding to SNARE proteins to modulate vesicle fusion (Zurawski et al., 2017), providing a tight network of mutant proteins controlling neurotransmitter vesicle release where suppressed synaptic vesicle release is associated with human movement disorders.

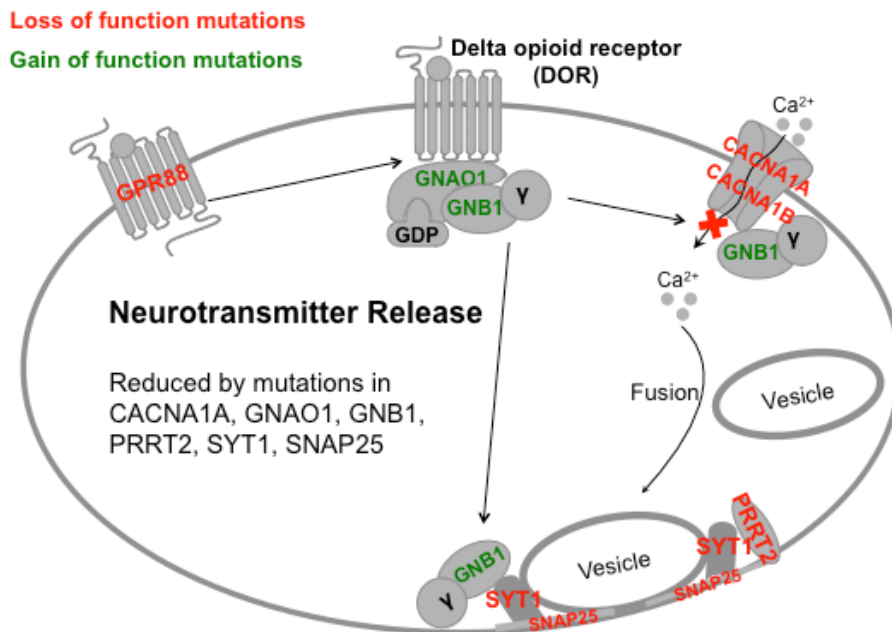


Figure 1.3 Pathogenic mutations in genes that regulate neurotransmitter release

Activation of $G\alpha_o$ by multiple GPCRs (including *GPR88*) inhibits voltage gated calcium channels (*CACNA1A* and *CACNA1B*). Calcium influx promotes synaptotagmin-1 (encoded by *SYT1*) and SNAP25 (encoded by *SNAP25* gene) anchoring the vesicle to the membrane in preparation for exocytosis. Reduced functions in *CACNA1A*, *CACNA1B*, *GPR88*, *SYT1* and *SNAP25* or increased function of *GNAO1*, *GNB1* and *KCNMA1* all reduce synaptic neurotransmitter releases.

1.5.2.1 *SYT1*

Synaptotagmin-1 (encoded by *SYT1*) is a calcium-binding synaptic vesicle protein required for both exocytosis and endocytosis. Tucker et al., 2004 investigated the effect of synaptotagmin-1 on membrane fusion mediated by the SNARE protein complex SNAP25, syntaxin and synaptobrevin. In the presence of calcium, the cytoplasmic domain of synaptotagmin-1 strongly stimulates membrane fusion (Figure 1.3).

Stimulation of fusion is abolished by disrupting the calcium-binding activity of synaptotagmin-1 (Rickman & Davletov, 2003). Thus, synaptotagmin-1 and SNAREs are likely to represent the minimal protein unit for calcium-triggered exocytosis (Tucker, Weber, & Chapman, 2004).

The study of *STY1*'s relation to movement disorders is limited. Only one patient has been reported so far. A trio analysis of whole-exome sequences identified a *de novo* *SYT1* missense variant (I368T) in a case of human neurodevelopmental disorder associated with hypotonia and hyperkinetic movements without seizures (Baker et al., 2015). Functional studies showed that this mutation slows evoked synaptic vesicle (SV) fusion and also affects SV retrieval from the plasma membrane during endocytosis (Baker et al., 2015). It is therefore a LOF mutation. Interestingly, an equivalent *STY1* mutation in *Drosophila* also resulted in a reduction in evoked neurotransmitter release (Paddock et al., 2011).

1.5.2.2 *PRRT2*

Proline-rich transmembrane protein 2 (*PRRT2*) is encoded by the *PRRT2* gene. Heterozygous mutations in *PRRT2* lead to epilepsy, kinesigenic dyskinesia, and migraine. *PRRT2* is enriched in presynaptic terminals. It regulates synapse number and release of SV. Most of pathogenic mutations in *PRRT2* lead to impaired *PRRT2* protein expression, which could result in impairment of neurotransmitter release (Weston, 2017). Moreover, *PRRT2* protein interacts with the synaptic protein SNAP25 and

synaptotagmin-1 (H. Y. Lee et al., 2012; Weston, 2017). Prrt2 expression is high in mouse cerebral cortex, hippocampus, and cerebellum (W. J. Chen et al., 2011).

Chen et al identified 3 heterozygous truncating mutations in *PRRT2* gene from eight unrelated Han Chinese families with episodic kinesigenic dyskinesia-1 (2011). Independently, Wang et al identified one insertion and one nonsense mutation from 27 members of two families with autosomal dominant paroxysmal kinesigenic dyskinesias (Wang et al., 2011). Two patients in each family also developed an infantile convulsion and choreoathetosis syndrome (Wang et al., 2011). Law et al reported a common *PRRT2* mutation in a case series of 16 patients with familial paroxysmal kinesigenic dyskinesia (Law et al., 2016). Heron et al identified heterozygous mutations in *PRRT2* from separate families with familial infantile seizures-2 and with familial infantile convulsions with paroxysmal choreoathetosis (Heron et al., 2012), suggesting that mutations in *PRRT2* are pathogenic for both epilepsy and movement disorders.

1.5.2.3 SNAP25

Synaptosomal associated protein-25 (SNAP25 encoded by *SNAP25*) is a component of the SNARE complex, which is essential to synaptic vesicle exocytosis. It also negatively modulates neuronal voltage-gated calcium channels by directly interacting with calcium channel subunits. The *SNAP25* gene is associated Attention Deficit Hyperactivity Disorder (ADHD), schizophrenia, and bipolar disorder (Antonucci et al., 2016; Corradini, Verderio, Sala, Wilson, & Matteoli, 2009). In 2013, whole exome

sequencing identified a novel *de novo* mutation p.F48V (c.142G>T) in *SNAP25* from a 15y old female with severe static encephalopathy, intellectual disability and generalized epilepsy (Rohena et al., 2013). *SNAP25* also plays a major role in neuronal survival. Neuronal cultures from *Snap-25* knockout mice show degenerated dendrites and ultimately neuronal death (Delgado-Martinez, Nehring, & Sorensen, 2007).

The relationship between *SNAP25* and G_o has been well-studied. *SNAP25* is a key downstream target of $G\beta\gamma$ subunits. $G\beta\gamma$ binds to the extreme C terminus of *SNAP25* to inhibit vesicle release in response to $G_{i/o}$ -coupled receptors activation (Zurawski, Rodriguez, Hyde, Alford, & Hamm, 2016).

1.5.2.4 *KCNMA1*

KCNMA1 encodes the pore-forming subunit of calcium-activated potassium channels (BK channels), which are in close proximity with voltage-gated calcium channels in neurons. Membrane depolarization activates calcium channels and increases calcium entry, which activates BK channels to help terminate the action potential, to produce after hyperpolarization, and to block calcium channels (U. S. Lee & Cui, 2010). Both GOF and LOF mutations of *KCNMA1* were reported in patients with paroxysmal nonkinesigenic dyskinesia 3 (PNKD3), with or without generalized epilepsy. This highlights the sensitivity of developing brain to both increased and decreased BK channel activities. Similar to *GNAO1*-associated movement disorders, developmental delay is also commonly associated with PNKD3 patients (Tabarki, AlMajhad, AlHashem,

Shaheen, & Alkuraya, 2016; Yesil et al., 2018; Zhang, Tian, Gao, Jiang, & Wu, 2015).

GOF mutants of *GNAO1* may work to regulate the function of BK channels both positively and negatively. G_o activates the production of phosphatidylinositol-4,5-bisphosphate 3-kinase (PI3-K), which in turn activates BK channels (Patel, 2004; Shanley, O'Malley, Irving, Ashford, & Harvey, 2002). However, the $G\beta\gamma$ subunit dissociated from $G\alpha_o$ inhibits voltage-gated calcium channels (illustrated in 3.2.5 and 3.2.6), which would reduce intracellular calcium concentrations preventing the activation of BK channels (Castillo et al., 2015). Therefore, it is difficult to pinpoint the relationship between GOF mutations in *GNAO1* and mutations in *KCNMA1*.

1.5.2.5 CACNA1A

CACNA1A encodes the P/Q type voltage gated calcium channel α_1 subunit ($Ca_v2.1$). Similar to N-type calcium channels ($Ca_v2.2$), activation of P/Q type calcium channels promotes neurotransmitter release. Moreover, influx of calcium through P/Q-type channels is responsible for activating expression of syntaxin-1A, a presynaptic protein that mediates vesicle docking (Sutton, McRory, Guthrie, Murphy, & Snutch, 1999).

LOF mutations in *CACNA1A* also cause episodic ataxia type 2 (EA2), an autosomal dominant neurological disease (Guida et al., 2001; Jen, Yue, Karrim, Nelson, & Baloh, 1998; Sintas et al., 2017; Wan et al., 2011) and familial hemiplegic migraine type 1 (Garza-Lopez et al., 2012; Mullner, Broos, van den Maagdenberg, & Striessnig, 2004). There is evidence of a dominant negative effect of EA2 mutants in the *CACNA1A* gene

(Gao et al., 2012; Jeng, Chen, Chen, & Tang, 2006; Jouvenceau et al., 2001). Haploinsufficiency is also pathologic (Guida et al., 2001; Wan et al., 2011).

The *leaner* mutation in mice affects the P/Q-type calcium channels Ca_v2.1 subunits, causing a reduction in calcium currents, predominantly in cerebellar Purkinje cells (Alonso et al., 2008). Homozygous *leaner* mice show severe, progressive cerebellar ataxia from postnatal day 10 (Alonso et al., 2008). Age-dependent impairment in motor and cognitive tasks is also observed in heterozygous *leaner* mice (Alonso et al., 2008). In addition, silencing of P/Q-type calcium channels in Purkinje neurons of adult mouse leads to a phenotype similar to episodic ataxia type 2 (EA2) (Salvi et al., 2014). Thus P/Q-type calcium channels play an important role control of movement as well as in neurodevelopment.

1.5.2.6 CACNA1B

A disruptive missense mutation p.R1389H (c.4166G>A) in the *CACNA1B* gene, encoding neuronal voltage-gated N-type calcium channels (Ca_v2.2), was identified in a new familial myoclonus-dystonia (M-D) syndrome (J. L. Groen et al., 2015). Five affected family members were identified in a 16-member family across 3 generations (J. Groen, van Rootselaar, van der Salm, Bloem, & Tijssen, 2011). But a genome-wide study in a large European multicentric M-D cohort failed to detect the mutation in the 146 probands with familial M-D (Mencacci, R'Bibo, et al., 2015). Therefore, a causal association between the *CACNA1B* mutation p.R1389H (c.4166G>A) and movement disorder is still

under debate. However, a recent study linked LOF mutations in *CACNA1B* to the onset of neurodevelopmental disorder with seizures and nonepileptic hyperkinetic movements (NEDNEH; OMIM# 618497), which provides evidence for the role of Ca_v2.2 in human neurodevelopment (Gorman et al., 2019).

1.5.2.7 GPR88

GPR88 (encoded by *GPR88* gene) is an orphan G-protein coupled receptor (GPCR) in the rhodopsin-like receptor family. It is widely expressed in the striatum, caudate nucleus, putamen, nucleus accumbens, and olfactory tubercle, but is not detected in the cerebellum (Massart, Guilloux, Mignon, Sokoloff, & Diaz, 2009). Its CNS expression is particularly robust in the striatum, paralleling that of the dopamine D2 receptor (Mizushima et al., 2000). Striatal GPR88 is enriched in both D1 and D2 expressing medium spiny neurons (Jin et al., 2014) and it is emerging as a key player in the pathophysiology of several neurological diseases. Agonists of GPR88 were developed as potential treatment for CNS disorders such as schizophrenia (Bi et al., 2015).

One case of GPR88-associated chorea has been reported in human patients. Alkufri et al reported a deleterious mutation p.C291X in GPR88 associated with chorea, speech delay and learning disabilities (Alkufri, Shaag, Abu-Libdeh, & Elpeleg, 2016). Homozygous *Gpr88* knockout mice displayed reduced striatal dependent behaviors such as rearing, grooming, and burying (Meirsmann et al., 2016). Mechanistic studies in striatal medium spiny neurons demonstrated increased glutamatergic responses and reduced

GABAergic inhibition in the absence of GPR88 which results in enhanced neuronal firing *in vivo* (Quintana et al., 2012). Studies also showed enhanced function of $G_{i/o}$ -coupled delta and mu opioid (DOR and MOR) in striatal membranes in Gpr88 knockout mice, suggesting a functional antagonism between GPR88 and other $G_{i/o}$ -coupled receptor activities (Figure 1.3) (Meirsman et al., 2016). The increasing interest in GPR88 may result in the design of treatments for this orphan disease, considering its unique location.

1.5.2.8 Summary of neurotransmitter release and synaptic vesicle fusion in movement control

The disruption of neurotransmitter release leads to a broad spectrum of movement impairments including chorea, ataxia and dystonia but also results in neurodevelopmental abnormalities and epilepsy. Apart from the relatively constrained expression of GPR88 in striatum, the rest of the proteins mentioned above are ubiquitously expressed throughout the brain. Therefore, it is relatively hard to determine which brain regions are involved in the pathogenesis of the related movement disorders. Hence, clear delineation of the neural mechanisms and relevant pathways remains challenging. The fact that *GNAO1* is involved in the regulation of many of the proteins encoded by the above-mentioned genes makes G_o -coupled receptors a possible therapeutic target in developing treatments for patients carrying these mutations.

1.6 Developmental defects may also contribute to movement disorders

In addition to ongoing alterations in cAMP signaling and neurotransmitter release

mechanisms, it is likely that developmental abnormality that results in disordered synaptic or neural pathway organization could contribute to the observed movement disorders. It is estimated that genetic factors are responsible for up to 40% of developmental disabilities (Miclea et al., 2015). Such changes in neural development and organization could contribute to the observation that developmental delay and epilepsy are often seen with the gene mutations discussed in this review. However, the development effects and the physiological effects may not be mutually exclusive.

cAMP signaling affects many developmental processes including facilitation of neuronal cell differentiation and maturation (Lepski, Jannes, Nikkhah, & Bischofberger, 2013; Sharma, Hansen, & Notter, 1990), induction of axon growth (Corredor et al., 2012), control of guidance cue (Forbes, Thompson, Yuan, & Goodhill, 2012), and enhancement of synaptic connections (Lessmann & Heumann, 1997). This could explain why most patients carrying the GOF mutations in *GNAO1*, which would be expected to suppress cAMP levels, exhibit severe developmental delay.

Similarly, synaptic release mechanisms are implicated in both developmental abnormalities and movement disorders. Specifically, the individual carrying the LOF mutation in *SYT1* with hypotonia and hyperkinetic movements discussed above also exhibited severe motor delay and profound cognitive impairment (Baker et al., 2015). Clearly, therapeutic approaches to modulate ongoing cAMP signaling or synaptic neurotransmitter release will be more tractable than attempting to alter developmental

abnormalities that may have already occurred by the time that the disorder is recognized.

1.7 Conclusion

A full understanding of the exact etiology of *GNAO1*-related movement disorders remains elusive, however, the mechanistic clustering of *GNAO1* and other movement disorder-related genes in the pathways for control of cAMP and neurotransmitter release strongly suggest a role for those mechanisms. For synaptic vesicle release, it appears that loss of function is the primary alteration observed. In contrast, for cAMP control, the picture is more confusing with mutations predicted to cause either increases or decreases being implicated. Clearly more needs to be learned about the specific brain regions, neuron types, and receptors that control *GNAO1* signaling in these disorders. This may be facilitated by the development of new animal models beyond the two *GNAO1* mutants already reported (Jiang & Bajpayee, 2009; Jiang et al., 1998; Kehrl et al., 2014). In particular, it is surprising that *Gnao1*^{+/-} mice, which have relatively normal behaviors, do not mimic patients with heterozygous LOF *GNAO1* mutations who exhibit severe epileptic encephalopathy. Animal knock-in models carrying the specific *GNAO1* mutant alleles that are found in human epilepsy and movement disorders may also help clarify this conundrum.

In addition to the mechanistic analysis, our review of the clinical literature also has implications for therapeutics. Since GOF mutations in *GNAO1* cause movement disorders (Feng et al., 2017), it is not surprising that tetrabenazine has proven to be the

most effective drug in controlling patient's chorea (Table 1.3) (Ananth et al., 2016; Danti et al., 2017; R. M. Dhamija, J, W.; Shah, B, B.; Goodkin, H, P., 2016; Waak et al., 2017). The broad depletion of multiple monoamines such as dopamine, serotonin, norepinephrine, and histamines from nerve terminals suggests that many receptors may be involved. A better understanding of the associated upstream GPCRs that are driving the enhanced signaling through G_o may permit the use of more selective agonists or antagonists against these receptors to alleviate symptoms with fewer side effects in *GNAO1* associated movement disorders.

1.8 Organization of the thesis

This dissertation shows a genotype-phenotype correlation model of the *GNAO1*-associated neurological disorders and how this model helps further mechanistic study of the *GNAO1*-related neurological disorders. The organization of this thesis is as follows. Chapter 1 gives a broad review of *GNAO1* encephalopathies and provides analysis of the pathophysiological mechanisms. The appendix includes a review of each case of reported human patients carrying *GNAO1* mutations. Chapter 2 introduces the genotype-phenotype correlation model based on *in vitro* biochemical functional analysis. The appendices verify and expand this model with newly reported *GNAO1* mutations. Chapter 3 provides a detailed behavioral description on the animal models carrying the human mutations G203R, R209H and T191F197del respectively. These three animal models are compared with the previously reported mouse model carrying a GOF *Gnao1*

mutant G184S and the *Gnao1* KO mice. The appendix includes all the raw data collected from the behavioral experiments. Chapter 4 explores the electrophysiological mechanisms of the cerebellar Purkinje cells of the G203R mutant mice. The appendix expands the analysis to other mouse models mentioned in Chapter 3. Chapter 5 summarizes and analyzes all the experimental data collected from Chapter 2 to Chapter 4. In addition, this chapter speculates on the future directions and the significance of this project. This chapter also shows preliminary results of experiments that have not been developed maturely in the appendix. These results may help the future efforts of optimizing assays for further testing of *GNAO1* mutations and for drug development or repurposing.

APPENDIX

APPENDIX

SUPPLEMENTAL DATA

Table S1.1 A complete summary of clinical information regarding *GNAO1* patients

No.	GNAO1 Mutations	Sex	Inheritance	Age of onset	Reported involvement										
					Seizures	Hypotonia	Chorea/athetosis	Dystonia	Myoclonus	Ballismus	Dyskinesia	Stereotypies	Developmental Delay	Intellectual Disability	Other
1	p.G40R c.118G>A	F	de novo	birth	+	+							+		
2	p.G40R c.118G>A	F	de novo	3 y	+							+		+	microcephaly
3	p.G40R c.118G>A	M	de novo	birth	+	+									
4	p.G40R c.118G>A	M	de novo	2.5 mo	+	+								+	ataxia
5	p.G40V c.118G>T	F	de novo	5 wk	+	+								+	
6	p.G40E c.119G>A	M	de novo	15 hr	+	+								+	
7	p.G40E c.119G>A	F	de novo	2 hr	+	+			+					+	
8	p.G45E c.134G>A	F	de novo	infancy	+	+							+		PEHO Syndrome; Accompanying mutation HESX1 (A9T)
9	p.G45R c.133G>C	M	de novo	NA	+	+	+						+		cerebellar ataxia, accompanying with ATP2B3 (T113M)
10	p.D174G c.521A>G	F	de novo, somatic mosaic	29 d	+										Ohtahara syndrome
11	p.T191_F197del c.572_592del	F	de novo	14 d	+				+						Ohtahara syndrome
12	p.R349_C352del insQGCA c.1046_1055del1 0ms10	F	de novo	6 mo	+	+							+	+	oromotor apraxia
13	p.L199P c.596T>C	F	de novo	3 mo	+	+					+		+		tetraparesis
14	p.A227V c.880C>T	F	de novo	2 mo	+	+	+					+			acquired microcephaly
15	p.Y231C c.692 A>G	F	de novo	2.5 mo	+							+	+		Ohtahara syndrome
16	p.Y231C c.692A>G	M	de novo	5 d	+	+							+	+	
17	p.E246G c.737A>G	F	de novo	6 mo	+	+			+						lower limb spasticity
18	p.N270H c.808A>G	F	de novo	3 mo	+	+								+	
19	p.D273V c.818A>T	F	de novo	2 d	+	+							+	+	
20	p.D273V c.818A>T	F	de novo	2 d	+	+			+				+		
21	p.F275S c.824T>C	F	de novo	3 d	+	+								+	
22	p.I279N c.836T>A	M	de novo	9 d	+								+		
23	p.I279N c.836T>A	F	de novo	4 d	+										Ohtahara syndrome
24	p.I279N c.836T>A	M	de novo	1 h	+	+	+						+	+	
25	p.Y291N c.871T>A	F	de novo	2 mo	+	+							+	+	
26	p.S47G c.139A>G	M	de novo	5 mo	+	+			+				+	+	
27	p.I56T c.167T>C	F	de novo	4 y	+									+	
28	p.G203R c.607G>A	F	de novo	7 mo	+		+						+		
29	p.G203R c.607G>A	F	de novo	7 d	+		+						+		
30	p.G203R c.607G>A	F	de novo	9 d	+								+		bradycardia
31	p.G203R c.607G>A	M	de novo	1 mo	+		+						+		
32	p.G203R c.607G>A	F	de novo	3 mo	+			+					+	+	
33	p.G203R c.607G>A	F	de novo	birth	+	+			+				+	+	
34	p.G203R c.607G>A	F	de novo	birth	+				+					+	
35	p.G203R c.607G>A	F	de novo	birth	+	+	+	+	+	+			+		
36	p.G203R c.607G>A	M	de novo	12 d	+	+		+		+			+		
37	p.G204R c.610G>C	M	de novo	24 mo	+	+	+	+		+	+		+		tachycardia, hyperthermia, sweating
38	p.G42R c.124G>C	F	de novo	NA		+	+						+		frequent arching of the back
39	p.S207Y c.620C>A	M	de novo	infancy		+		+					+		

Table S1.1 (cont'd)

No.	EEG Findings	Severe EEG	Brain MRI	Severe MRI
1	a disorganized background with frequent multi-focal high-amplitude sharp and spike wave discharges, no definite burst-suppression patterns	++	normal	
2	burst suppression at onset; slow background multifocal spike waves	++	mild ventricular enlargement; thin corpus callosum	+
3	discontinuous background, bilateral temporal sharp waves	++	bilateral increased signal in frontal and peritrigonal white matter in T1	+
4	3 y: slow spike and wave, multifocal spikes	++	4 mo: mildly prominent bifrontal subarachnoid spaces	+
5	9 mo: right temporal seizures, focal spikes, focal slowing	++	4 mo: bilateral mesial temporal sclerosis, diffuse parenchymal atrophy, delayed myelination	++
6	2 mo: hypsarhythmia; 14 y: generalized onset of tonic seizures and epileptic spasms, generalized slowing	++	2 y: status posttemporal lobectomy; left cerebral atrophy	++
7	9 d: multifocal spikes; 14 y: focal spikes and waves, absence of normal awake and sleep features	++	15 mo: nonspecific signal increase in globi pallidi, normal myelination	++
8	NA		cerebral and cerebellar atrophy	++
9	NA		NA	
10	burst suppression at 2 mo; hypsarhythmia at 3 mo; diffuse spike-and-slow-wave complex at 1 yr 7 mo; sharp waves at frontal lobe at 3 yr 9 mo	++	delayed myelination and thin corpus callosum at 10 mo	++
11	suppression-burst pattern at 2 week; hypsarhythmia at 4 mo	++	normal at 3 mo	
12	7 y: sleep-activated posterior temporal and occipital spikes		normal	
13	background slowing, multifocal high-voltage sharp waves and spike and slow-wave complexes	++	delayed myelination and thin corpus callosum	++
14	hypsarhythmia and multifocal with ictal	++	progressive cerebral atrophy, thin corpus callosum at 10 mo	++
15	modified burst-suppression at 3 mo; hypsarhythmia in awake burst-suppression pattern in sleep at 7 mo; slowing of background activity with multifocal interictal epileptiform discharge at 9 mo	++	delayed myelination, short and thin corpus callosum and hippocampus	++
16	Neonatal: multifocal epileptiform sharp waves; 20 mo: frequent bioccipital spikes	++	2 y: prominent subarachnoid spaces	+
17	normal		mild loss of volume (atrophy) in generalized distribution	+
18	hypsarhythmia and slow background	++	minimal atrophy	+
19	Abnormal epileptiform activity	++	normal	
20	normal at first; later unknown		normal at first; later unknown	
21	burst-suppression pattern, hypsarhythmia, later slow background with multifocal discharges	++	delayed myelination and thinning of white matter	++
22	multifocal modified hypsarhythmia, burst-suppression in sleep, high-voltage midline central discharges during spasms, generalized decrement with low voltage fast activity	++	moderate-severe progressive global atrophy with delayed myelination, thin corpus callosum	++
23	burst-suppression pattern at 4 d; multifocal sharp waves at 1 yr, 4 mo; burst-suppression pattern at 5 yr, 6 mo	++	normal at 1 mo; cerebral atrophy at 5 yr 6 mo	++
24	Neonatal: multifocal sharp waves with high-amplitude bursts (not burst suppression); 8 mo: modified hypsarhythmia	++	2.5 y: moderate to progressive atrophy with delayed myelination	++
25	1 y: multifocal spikes, focal seizures; 3 y: intermittent posterior slowing	++	normal	
26	right frontotemporal spikes	+	ventricular enlargement; thin and dysmorphic corpus callosum; mild hypoplasia of caudate	++
27	left frontotemporal spikes	+	left frontal lesion (diffuse astrocytoma WHO grade 2); low-lying cerebellar tonsils	++
28	diffuse irregular spike-and-slow-wave complex at 5 yr	++	delayed myelination at 1 yr, 3 mo; reduced cerebral white matter, thin corpus callosum at 4 yr, 8 mo	++
29	slow-wave bursts, migrating focal epileptiform discharges	++	progressive cerebral atrophy with delayed myelination at 14 mo	++
30	delta and theta activity and rare multi-regional, bi-hemispheric epileptic activity	+	mild atrophy	+
31	multifocal and diffuse discharges, along with generalized-onset seizures	++	progressive diffuse cerebral atrophy and volume loss in cerebellum	++
32	background slowing		atrophy, thin corpus callosum (2 y)	+
33	multifocal sharp waves, left temporal seizure pattern	++	mild atrophy (10 mo)	+
34	hypsarhythmia	++	NA	NA
35	multifocal paroxysmal activities in both temporal hemispheres	++	thin corpus callosum	+
36	NA		hypomyelination and atrophy	+
37	NA		14 y: bilateral hyperintensities of the thalamus on T2	+
38	NA		NA	
39	15 mo: slow posterior dominant rhythm		1 y: generalized thinning of corpus callosum, relative paucity of deep white matter	++

Table S1.1 (cont'd)

No.	Drug Trialed	Drug Positive Response	DBS	DBS Positive Response	Study	PMID or DOI
1	NA	NA	N	N	Law et al 2015	26485252
2	multiple AEDs, ketogenic diet, vagus nerve stimulation	NA	N	N	Danti et al 2017	28357411
3	NA	NA	N	N	Bruun et al 2017	28817111
4	NA	NA	N	N	Kelly et al 2019	30682224
5	NA	NA	N	N	Kelly et al 2019	30682224
6	NA	NA	N	N	Kelly et al 2019	30682224
7	NA	NA	N	N	Kelly et al 2019	30682224
8	NA	NA	N	N	Gawlinski et al 2016	27343026
9	pyridoxine, phenobarbital, levetiracetam, topiramate, vigabatrin, ACTH, zonisamide, clobazam	ACTH, levetiracetam, clobazam, zonisamide	N	N	Ueda et al 2015	DOI: 10.1055/s-0036-1597627
10	NA	NA	N	N	Nakamura et al 2013	23993195
11	NA	NA	N	N	Nakamura et al 2013	23993195
12	NA	NA	N	N	Kelly et al 2019	30682224
13	ketogenic diet	NA	N	N	Marce-Grau A et al 2016	27072799
14	prednisone, valproic acid, clonazepam	prednisone	N	N	Saito et al 2015	25966631
15	phenobarbitone, vigabatrin, lamotrigine	N	N	N	Talvik et al 2015	DOI: 10.1177/2329048X15583717
16	NA	NA	N	NA	Kelly et al 2019	30682224
17	NA	tetrabenazine	Y	Y	Danti et al 2017	28357411
18	NA	NA	N	N	EuroEPINOMICS-RES Consortium 2014	25262651
19	NA	NA	N	N	Kelly et al 2019	30682224
20	lamotrigine, valproic acid, trihexyphenidyl and melatonin	seizures and dyskinesic movements well-controlled	N	N	Schirinzi et al 2018	30642806
21	NA	NA	N	N	EuroEPINOMICS-RES Consortium 2014	25262651
22	valproate, ketogenic diet, pyridoxal-5-phosphate, vigabatrin, levetiracetam, phenobarbitone, prednisolone	NA	N	N	Epi4k 2016	27476654
23	NA	NA	N	N	Nakamura et al 2013	23993195
24	NA	NA	N	NA	Kelly et al 2019	30682224
25	NA	NA	N	NA	Kelly et al 2019	30682224
26	NA	tetrabenazine, well-controlled on AED	N	N	Danti et al 2017	28357411
27	NA	well-controlled on AED	N	N	Danti et al 2017	28357411
28	NA	NA	N	N	Nakamura et al 2013	23993195
29	phenobarbital	phenobarbital	N	N	Saito et al 2015	25966631
30	lamotrigine, zonisamide	controlled epileptic activity but not involuntary movements	N	N	Dietel et al 2016	DOI: 10.1055/s-0036-1583625
31	NA	NA	N	N	Arya et al 2017	28202424
32	Vit B6, sulthiame, levetiracetam, L-DOPA	N	N	N	Schorling et al 2017	28628939
33	Vit B6, phenobarbital, levetiracetam, topiramate, valproic acid, vigabatrin, oxcarbazepine, phenytoin, clobazam, lacosamide, ketogenic diet, gabapentin, trihexyphenidyl, baclofen, benzodiazepines	lamotrigine and zonisamide controlled epileptic activity, benzodiazepines reduced paroxysmal dystonias	N	N	Schorling et al 2017	28628939
34	NA	topiramate, vigabatrin	N	N	Xiong et al 2018	29429466
35	phenobarbital, carbamazepine, benzodiazepines, topiramate, clonazepam	topiramate, clonazepam	N	N	Schirinzi et al 2018	30642806
36	tetrabenazine, lorazepam, baclofen and phenobarbital	phenobarbital	N	N	Schirinzi et al 2018	30642806
37	NA	tetrabenazine	Evaluated	N	Koy et al 2018	30103967
38	NA	NA	N	N	Zhu et al 2014	25590979
39	NA	NA	N	NA	Kelly et al 2019	30682224

Table S1.1 (cont'd)

No.	GNAO1 Mutations	Sex	Inheritance	Age of onset	Reported involvement										
					Seizures	Hypotonia	Chorea/athetosis	Dystonia	Myoclonus	Ballismus	Dyskinesia	Stereotypies	Developmental Delay	Intellectual Disability	Other
40	p.R209H c.626G>A	M	de novo	1 y		+		+	+				+		
41	p.R209H c.626G>A	M	de novo	18 mo		+	+						+		
42	p.R209H c.626G>A	M	de novo	2 y			+						+		excessive movements
43	p.R209H c.626G>A	M	de novo	10 mo		+	+	+					+		
44	p.R209H c.626G>A	M	de novo	3 y		+	+			+			+		tachycardia
45	p.R209H c.626G>A	F	de novo	6 mo		+		+					+	+	ataxia
46	p.R209H c.626G>A	M	de novo	6 mo		+	+	+					+		dysarthria
47	p.R209L c.626G>T	M	de novo	birth		+		+	+				+		
48	p.R209G c.625C>G	F	de novo	3 y 10 mo		+	+						+		
49	p.R209C c.625C>T	F	de novo	11 mo		+	+						+		quadriplegia
50	p.R209C c.625C>T	M	de novo	birth	+	+							+	+	excessive movements; microcephaly
51	p.R209C c.625C>T	M	de novo	7 mo	+							+	+	+	
52	p.R209C c.625C>T	F	de novo	6 mo	+	+	+	+		+	+		+		
53	p.R209C c.625C>T	F	de novo	6 mo		+	+	+					+	+	gait ataxia
54	p.R209C c.625C>T	F	de novo	6 mo		+							+	+	
55	p.R209C c.625C>T	F	de novo	birth			+	+		+	+		+		
56	p.R209C c.625C>T	F	de novo	neonate			+	+			+		+		
57	p.R209C c.625C>T	M	de novo	infant	+	+	+	+		+			+		
58	p. C215Y c. 644G>A	M	de novo	12 yr				+	+						
59	p.A221D c.662C>A	F	de novo	9 mo		+		+					+	+	
60	p.Q233P c.698A>C	F	de novo	13 mo		+	+					+	+		
61#	p.E237K c.709G>A	M	de novo	4 mo		+	+	+	+				+		
62	p.E237K c.709G>A	M	de novo	3 mo		+	+	+		+	+		+		peripheral spasticity
63	p.E237K c.709G>A	F	de novo	6 mo		+					+		+		
64	p.E237K c.709G>A	F	de novo	6 mo		+	+				+		+		
65	p.E237K c.709G>A	M	de novo	neonate		+		+					+		
66	p.E237K c.709G>A	M	de novo	neonate		+					+		+		
67	p.E246K c.736G>A	F	de novo	4 mo		+	+	+					+	+	
68	p.E246K c.736G>A	M	de novo	4 y		+	+			+			+		
69	p.E246K c.736G>A	F	de novo	4 y		+	+			+			+		
70	p.E246K c.736G>A	F	de novo	6 mo		+	+			+			+		tachycardia, hypertension
71	p.E246K c.736G>A	M	de novo	14 y		+	+						+		
72*	p.E246K c.736G>A	M	de novo	11 mo		+		+					+	+	
73*	p.E246K c.736G>A	F	de novo	3 mo	+			+					+	+	
74	p.E246K c.736G>A	F	de novo	3 mo		+		+		+	+		+	+	
75	p.E246K c.736G>A	F	de novo	13 mo		+	+	+		+			+	+	
76	p.E246K c.736G>A	F	de novo	4 yr			+	+		+				+	
77	p.E246K c.736G>A	F	de novo	30 mo							+			+	
78	p.L284S c.851T>C	F	de novo	11 d	+	+							+		microcephaly
79	p.1344del c.1030_1032delA TT	F	de novo	12 mo	+	+	+	+					+	+	single seizure at 4 yr
80	c.723+1G>T	F	de novo	3 y		+	+	+			+		+		tachycardia, hyperthermia, sweating
81	c.723+1G>A	F	de novo	4 mo	+	+	+				+		+	+	microcephaly

Table S1.1 (cont'd)

No.	EEG Findings	Severe EEG	Brain MRI	Severe MRI
40	normal		normal	
41	no irregularities other than diffuse slowing		normal	
42	no irregularities other than diffuse slowing		normal	
43	NA		normal	
44	NA		global atrophy at 15 yr	++
45	normal		13 mo: frontal lobe volume loss	++
46	NA		normal	
47	normal		normal	
48	NA		normal at 13 mo	
49	diffused low activities	+	progressive cerebral and cerebellar atrophy, brainstem atrophy, thin corpus callosum	++
50	low background activities	+	ventricular enlargement; thin corpus callosum; mild hypoplasia of caudate; hypoplasia of inferior vermis	++
51	bilateral centrotemporal spikes	+	normal	
52	normal		normal	
53	diffuse slow activity	+	posterior left periventricular hypersignal	+
54	15 mo: slow posterior dominant rhythm	+	1 y: generalized thinning of corpus callosum, relative paucity of deep white matter	++
55	normal		temporal atrophy, ventricular enlargement and mild temporal hypomyelination	++
56	NA		Cortical (prominent frontally) subcortical atrophy. Bilateral hypointense signals of globus pallidus on SWI and T2* MRI sequences	++
57	NA		Cortical (prominent frontally) subcortical atrophy. Bilateral hypointense signals of globus pallidus on SWI and T2* MRI	++
58	NA		normal	
59	11 y: normal; 15 y: abnormal during sleep, frequent sharp waves		normal	
60	NA		NA	
61#	NA		NA	
62	NA		progressive global atrophy (8 y, 12 y)	++
63	NA		NA	
64	NA		13 mo: mild hyperintensity in the occipital white matter	+
65	NA		Small medio- putaminal atrophy	+
66	NA		normal	
67	normal at 12 yr		normal at 4 and 12 yr	
68	NA		normal at 12 mo	
69	NA		global atrophy at 5.5 yr	++
70	NA		global atrophy and T2 hypointensity in globus pallidi at 9 yr	++
71	NA		T2 hypointensity in globus pallidi at 14 yr	+
72*	normal		normal	
73*	right-sided polyspike-wave formations	++	atrophy of right hippocampus	+
74	NA		progressive global atrophy (1y, 5y, 8y)	++
75	NA		NA	
76	NA		mild diffuse cortical atrophy	+
77	NA		slight hyperintensity of the left pars triangularis	
78	suppression-burst pattern	++	diffuse cerebral atrophy	++
79	normal		normal	
80	NA		8 yr: cerebral atrophy	++
81	NA		ventricular enlargement and dilated subarachnoid spaces; moderate cortical atrophy; dysmorphic corpus callosum; mild hypoplasia of caudate nuclei	++

Table S1.1 (cont'd)

No.	Drug Trialed	Drug Positive Response	DBS	DBS Positive Response	Study	PMID or DOI
40	NA	NA	NA	NA	Menke et al 2016	27625011
41	clonazepam, valproic acid	N	Y	Y	Kulkarni et al 2015	26060304
42	clonidine, clonazepam	N	Y	Y	Kulkarni et al 2015	26060304
43	clonazepam, tetrabenazine, trihexyphenidyl	tetrabenazine, trihexyphenidyl	Evaluated	NA	Dhamija et al 2016	DOI: 10.1002/mdc3.12344
44	dexmedetomidine, opioids, benzodiazepam, vecuronium, risperidone	risperidone	N	N	Ananth et al 2016	27068059
45	NA	NA	N	N	Kelly et al 2019	30682224
46	L-DOPA	N	N	N	Blumkin et al 2018	29801190
47	NA	NA	NA	NA	Menke et al 2016	27625011
48	clonidine, valproic acid, clonazepam, bethanechol, lorazepam, trihexyphenidyl, dexmedetomidine, propofol, midazolam	N	N	N	Ananth et al 2016	27068059
49	diazepam, midazolam, clonazepam, phenobarbital, bromazepam, haloperidol, tiapride, eperisone, topiramate	topiramate	N	N	Saito et al 2016, Sakamoto et al 2017	25966631; 27916449
50	NA	well-controlled on AED	N	N	Danti 2017	28357411
51	NA	well-controlled on AED	N	N	Danti 2017	28357411
52	carbamazepine, acetazolamide, oxcarbazepine	carbamazepine, acetazolamide, oxcarbazepine controlled epileptic activity	Y	Y	Waak et al 2018	28668776
53	levodopa, clonazepam, trihexyphenidyl	N	N	N	Malaquias et al 2019	31190250
54	NA	NA	N	N	Kelly et al 2019	30682224
55	haloperidol, midazolam, propofol, phenytoin, baclofen, clonazepam, levodopa, tetrabenazine, clonidine, phenobarbital, lorazepam, curare	NA	N	N	Schirinzi et al 2018	30642806
56	NA	N	Y	Y	Koy et al 2018	30103967
57	NA	tetrabenazine	Y	Y	Koy et al 2018	30103967
58	trihexyphenidyl, clonazepam	trihexyphenidyl, clonazepam	N	N	Carecchio et al 2019	31216378
59	NA	NA	N	N	Kelly et al 2019	30682224
60	midazolam, fentanyl, pimozide, clonazepam, haloperidol, carbamazepine, acetazolamide, diazepam, ketogenic diet	midazolam, fentanyl, pimozide	Y	Y	Yilmaz et al 2016	27278281
61#	levetiracetam, clonazepam, tetrabenazine, resperidone	levetiracetam, tetrabenazine	N	N	Feng et al. 2018	29758257
62	baclofen, phenobarbitone, tetrabenazine	incomplete response to tetrabenazine	Y	Y	Waak et al 2018	28668776
63	NA	NA	N	N	Okumura et al 2018	29935962
64	NA	NA	N	N	Schirinzi et al 2018	30642806
65	NA	N	Y	Y	Koy et al 2018	30103967
66	NA	N	N	N	Koy et al 2018	30103967
67	NA	NA	N	N	Saito et al 2015	25966631
68	N	N	N	N	Ananth et al 2016	27068059
69	clonazepam, clonidine, trazodone, midazolam, risperidone, tetrabenazine	tetrabenazine	N	N	Ananth et al 2016	27068059
70	clonazepam, clobazam, topiramate, levetiracetam, valproic acid, clonidine, baclofen, tetrabenazine, haloperidol, diazepam, pentobarbital, propofol, versed, fentanyl, dexmedetomidine	baclofen, clobazam, tetrabenazine, haloperidol, diazepam	N	N	Ananth et al 2016	27068059
71	oxcarbazepine, clonazepam, risperidone, diazepam, tetrabenazine	diazepam, tetrabenazine	N	N	Ananth et al 2016	27068059
72*	L-DOPA	N	N	N	Schorling et al 2017	28628939
73*	levetiracetam	NA	N	N	Schorling et al 2017	28628939
74	haloperidol, baclofen, tetrabenazine, phenobarbital	tetrabenazine, phenobarbital	Y	Y	Waak et al 2018	28668776
75	Trihexy-phenidyl, nitrazepam, clonazepam, tetrabenazine, baclofen, L-DOPA, lev-etracetam, phenobarbital	NA	Y	Y	Carecchio et al 2019	31076915
76	Flunitrazepam, baclofen, trihexyphenidyl, tetrabenazine, pimozide	NA	Y	Y	Carecchio et al 2019	31076915
77	NA	NA	N	N	Takezawa et al 2018	29761117
78	phenobarbital, clobazam, valproic acid, pyridoxine, levetiracetam, fosphenytoin, valproate, clobazam, zonisamide, rufinamide, high dose prednisone, ACTH, IVIG, ketogenic diet	N	N	N	Gerald et al 2017	https://doi.org/10.1016/j.spen.2017.08.008
79	NA	NA	N	N	Kelly et al 2019	30682224
80	NA	N	Y	Y	Koy et al 2018	30103967
81	NA	well-controlled on AED	N	N	Danti et al 2017	28357411

* Patients are siblings

Patient was presented to our clinic

Newly reported cases after Feng et al 2018 was publish

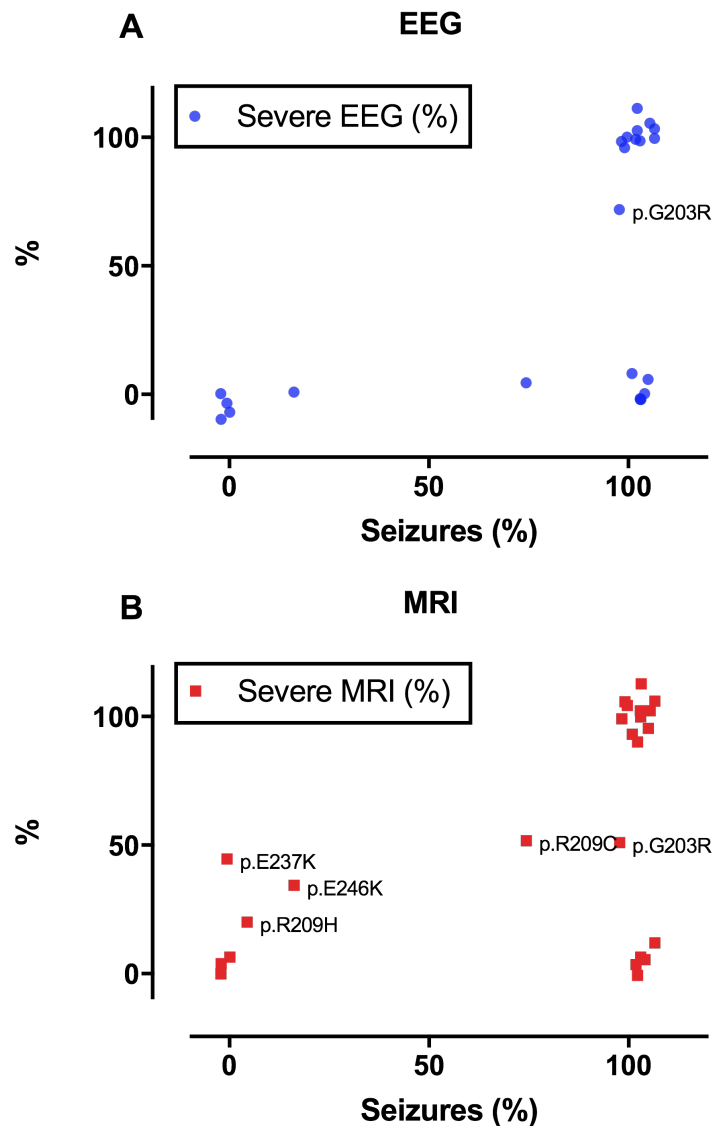


Figure S1.1 Correlation between seizure frequency and a severe EEG/MRI result

Clinical descriptions of EEG and MRI results were classified by one of the authors (C.S.) as normal or not reported (), mild (+), or severe (++). The correlation of EEG and MRI findings with either presence or absence of seizures or mutation status are illustrated here and listed in Table S1.1. (A) Over 50% of patients with a seizure disorder (most carrying LOF mutants) exhibit severe EEG. Also, patients carrying the GOF mutation G203R frequently displayed seizure symptoms and severe EEG readings. (B) Patients carrying the GOF mutations G203R and R209C showed occurrence of seizures, and almost half also showed serious abnormalities in MRI. However, less than 50% of the

Figure S1.1 (cont'd) patients carrying GOF mutation E237K, E246K, or R209H showed seizure activity, while almost 50% of them showed a severe MRI results. All values have been shifted slightly (jitter with SD=5) to avoid overlap. Many patients with singleton LOF mutations fell at 100% Seizures and 100% Severe MRI or EEG. The jitter was added to better demonstrate how many different mutations result in patterns that fall in each region of the graph.

REFERENCES

REFERENCES

- Agler, H. L., Evans, J., Tay, L. H., Anderson, M. J., Colecraft, H. M., & Yue, D. T. (2005). G protein-gated inhibitory module of N-type (ca(v)2.2) ca²⁺ channels. *Neuron*, 46(6), 891-904. doi:10.1016/j.neuron.2005.05.011
- Ahmad, R., Bourgeois, S., Postnov, A., Schmidt, M. E., Bormans, G., Van Laere, K., & Vandenberghe, W. (2014). PET imaging shows loss of striatal PDE10A in patients with Huntington disease. *Neurology*, 82(3), 279-281. doi:10.1212/WNL.0000000000000037
- Akiyama, H., Fukuda, T., Tojima, T., Nikolaev, V. O., & Kamiguchi, H. (2016). Cyclic Nucleotide Control of Microtubule Dynamics for Axon Guidance. *J Neurosci*, 36(20), 5636-5649. doi:10.1523/JNEUROSCI.3596-15.2016
- Alkufri, F., Shaag, A., Abu-Libdeh, B., & Elpeleg, O. (2016). Deleterious mutation in GPR88 is associated with chorea, speech delay, and learning disabilities. *Neurol Genet*, 2(3), e64. doi:10.1212/NXG.0000000000000064
- Alonso, I., Marques, J. M., Sousa, N., Sequeiros, J., Olsson, I. A., & Silveira, I. (2008). Motor and cognitive deficits in the heterozygous leaner mouse, a Cav2.1 voltage-gated Ca²⁺ channel mutant. *Neurobiol Aging*, 29(11), 1733-1743. doi:10.1016/j.neurobiolaging.2007.04.005
- Ananth, A. L., Robichaux-Viehoever, A., Kim, Y. M., Hanson-Kahn, A., Cox, R., Enns, G. M., . . . Bernstein, J. A. (2016). Clinical Course of Six Children With GNAO1 Mutations Causing a Severe and Distinctive Movement Disorder. *Pediatr Neurol*, 59, 81-84. doi:10.1016/j.pediatrneurol.2016.02.018
- Antonucci, F., Corradini, I., Fossati, G., Tomasoni, R., Menna, E., & Matteoli, M. (2016). SNAP-25, a Known Presynaptic Protein with Emerging Postsynaptic Functions. *Front Synaptic Neurosci*, 8, 7. doi:10.3389/fnsyn.2016.00007
- Arya, R., Spaeth, C., Gilbert, D. L., Leach, J. L., & Holland, K. D. (2017). GNAO1-associated epileptic encephalopathy and movement disorders: c.607G>A variant represents a probable mutation hotspot with a distinct phenotype. *Epileptic Disord*, 19(1), 67-75. doi:10.1684/epd.2017.0888

- Baker, K., Gordon, S. L., Grozeva, D., van Kogelenberg, M., Roberts, N. Y., Pike, M., . . . Raymond, F. L. (2015). Identification of a human synaptotagmin-1 mutation that perturbs synaptic vesicle cycling. *J Clin Invest*, *125*(4), 1670-1678. doi:10.1172/JCI79765
- Batty, N. J., Fenrich, K. K., & Fouad, K. (2017). The role of cAMP and its downstream targets in neurite growth in the adult nervous system. *Neurosci Lett*, *652*, 56-63. doi:10.1016/j.neulet.2016.12.033
- Beaumont, V., & Zucker, R. S. (2000). Enhancement of synaptic transmission by cyclic AMP modulation of presynaptic Ih channels. *Nat Neurosci*, *3*(2), 133-141. doi:10.1038/72072
- Bi, Y., Dzierba, C. D., Fink, C., Garcia, Y., Green, M., Han, J., . . . Macor, J. E. (2015). The discovery of potent agonists for GPR88, an orphan GPCR, for the potential treatment of CNS disorders. *Bioorg Med Chem Lett*, *25*(7), 1443-1447. doi:10.1016/j.bmcl.2015.02.038
- Blumkin, L., Lerman-Sagie, T., Westenberger, A., Ben-Pazi, H., Zerem, A., Yosovich, K., & Lev, D. (2018). Multiple Causes of Pediatric Early Onset Chorea-Clinical and Genetic Approach. *Neuropediatrics*, *49*(4), 246-255. doi:10.1055/s-0038-1645884
- Bollen, E., & Prickaerts, J. (2012). Phosphodiesterases in neurodegenerative disorders. *IUBMB Life*, *64*(12), 965-970. doi:10.1002/iub.1104
- Borlikova, G., & Endo, S. (2009). Inducible cAMP early repressor (ICER) and brain functions. *Mol Neurobiol*, *40*(1), 73-86. doi:10.1007/s12035-009-8072-1
- Bruun, T. U. J., DesRoches, C. L., Wilson, D., Chau, V., Nakagawa, T., Yamasaki, M., . . . Mercimek-Andrews, S. (2018). Prospective cohort study for identification of underlying genetic causes in neonatal encephalopathy using whole-exome sequencing. *Genet Med*, *20*(5), 486-494. doi:10.1038/gim.2017.129
- Carapito, R., Paul, N., Untrau, M., Le Gentil, M., Ott, L., Alsaleh, G., . . . Bahram, S. (2015). A de novo ADCY5 mutation causes early-onset autosomal dominant chorea and dystonia. *Mov Disord*, *30*(3), 423-427. doi:10.1002/mds.26115
- Carecchio, M., Invernizzi, F., Gonzalez-Latapi, P., Panteghini, C., Zorzi, G., Romito, L., . . . Nardocci, N. (2019). Frequency and phenotypic spectrum of KMT2B dystonia in childhood: A single-center cohort study. *Mov Disord*.

doi:10.1002/mds.27771

Carecchio, M., & Mencacci, N. E. (2017). Emerging Monogenic Complex Hyperkinetic Disorders. *Curr Neurol Neurosci Rep*, 17(12), 97. doi:10.1007/s11910-017-0806-2

Carecchio, M., Mencacci, N. E., Iodice, A., Pons, R., Panteghini, C., Zorzi, G., . . . Nardocci, N. (2017). ADCY5-related movement disorders: Frequency, disease course and phenotypic variability in a cohort of paediatric patients. *Parkinsonism Relat Disord*, 41, 37-43. doi:10.1016/j.parkreldis.2017.05.004

Castillo, K., Contreras, G. F., Pupo, A., Torres, Y. P., Neely, A., Gonzalez, C., & Latorre, R. (2015). Molecular mechanism underlying beta1 regulation in voltage- and calcium-activated potassium (BK) channels. *Proc Natl Acad Sci U S A*, 112(15), 4809-4814. doi:10.1073/pnas.1504378112

Chen, D. H., Meneret, A., Friedman, J. R., Korvatska, O., Gad, A., Bonkowski, E. S., . . . Raskind, W. H. (2015). ADCY5-related dyskinesia: Broader spectrum and genotype-phenotype correlations. *Neurology*, 85(23), 2026-2035. doi:10.1212/WNL.0000000000002058

Chen, W. J., Lin, Y., Xiong, Z. Q., Wei, W., Ni, W., Tan, G. H., . . . Wu, Z. Y. (2011). Exome sequencing identifies truncating mutations in PRRT2 that cause paroxysmal kinesigenic dyskinesia. *Nat Genet*, 43(12), 1252-1255. doi:10.1038/ng.1008

Chen, Y. Z., Friedman, J. R., Chen, D. H., Chan, G. C., Bloss, C. S., Hisama, F. M., . . . Torkamani, A. (2014). Gain-of-function ADCY5 mutations in familial dyskinesia with facial myokymia. *Ann Neurol*, 75(4), 542-549. doi:10.1002/ana.24119

Colecraft, H. M., Brody, D. L., & Yue, D. T. (2001). G-protein inhibition of N- and P/Q-type calcium channels: distinctive elementary mechanisms and their functional impact. *J Neurosci*, 21(4), 1137-1147.

Corradini, I., Verderio, C., Sala, M., Wilson, M. C., & Matteoli, M. (2009). SNAP-25 in neuropsychiatric disorders. *Ann N Y Acad Sci*, 1152, 93-99. doi:10.1111/j.1749-6632.2008.03995.x

Corredor, R. G., Trakhtenberg, E. F., Pita-Thomas, W., Jin, X., Hu, Y., & Goldberg, J. L. (2012). Soluble adenylyl cyclase activity is necessary for retinal ganglion cell

- survival and axon growth. *J Neurosci*, 32(22), 7734-7744. doi:10.1523/JNEUROSCI.5288-11.2012
- D'Angelo, V., Castelli, V., Giorgi, M., Cardarelli, S., Saverioni, I., Palumbo, F., . . . Sancesario, G. (2017). Phosphodiesterase-10A Inverse Changes in Striatopallidal and Striatoentopeduncular Pathways of a Transgenic Mouse Model of DYT1 Dystonia. *J Neurosci*, 37(8), 2112-2124. doi:10.1523/JNEUROSCI.3207-15.2016
- Danti, F. R., Galosi, S., Romani, M., Montomoli, M., Carss, K. J., Raymond, F. L., . . . Guerrini, R. (2017). GNAO1 encephalopathy: Broadening the phenotype and evaluating treatment and outcome. *Neurol Genet*, 3(2), e143. doi:10.1212/NXG.000000000000143
- de la Fuente-Fernandez, R. (2004). Uncovering the hidden placebo effect in deep-brain stimulation for Parkinson's disease. *Parkinsonism Relat Disord*, 10(3), 125-127. doi:10.1016/j.parkreldis.2003.10.003
- Delgado-Martinez, I., Nehring, R. B., & Sorensen, J. B. (2007). Differential abilities of SNAP-25 homologs to support neuronal function. *J Neurosci*, 27(35), 9380-9391. doi:10.1523/JNEUROSCI.5092-06.2007
- Dhamija, R., Mink, J. W., Shah, B. B., & Goodkin, H. P. (2016). GNAO1-Associated Movement Disorder. *Mov Disord Clin Pract*, 3(6), 615-617. doi:10.1002/mdc3.12344
- Dhamija, R. M., J, W.; Shah, B, B.; Goodkin, H, P. (2016). GNAO1-Associated Movement Disorder. *Movement Disorders Clinical Practice*, 3(6), 615-617. doi:10.1002/mdc3.12344
- Dietel, T. (2016). Genotype and phenotype in GNAO1-Mutation – Case report of an unusual course of a childhood epilepsy. In G. S. T. B. Haack , I. Cordes , R. Trollmann , T. Bast (Ed.), (Vol. 47, pp. P01-17). Neuropediatrics: Thieme.
- Diggle, C. P., Sukoff Rizzo, S. J., Popiolek, M., Hinttala, R., Schulke, J. P., Kurian, M. A., . . . Brandon, N. J. (2016). Biallelic Mutations in PDE10A Lead to Loss of Striatal PDE10A and a Hyperkinetic Movement Disorder with Onset in Infancy. *Am J Hum Genet*, 98(4), 735-743. doi:10.1016/j.ajhg.2016.03.015
- Dorje, F., Wess, J., Lambrecht, G., Tacke, R., Mutschler, E., & Brann, M. R. (1991). Antagonist binding profiles of five cloned human muscarinic receptor subtypes. *J*

Pharmacol Exp Ther, 256(2), 727-733.

- Dortch-Carnes, J., & Potter, D. E. (2003). Delta-opioid agonist-stimulated inositol phosphate formation in isolated, rabbit iris-ciliary bodies: role of G(i/o) proteins and Gbetagamma-subunits. *Exp Eye Res*, 77(6), 647-652.
- Dos Santos, C. O., Masuho, I., da Silva-Junior, F. P., Barbosa, E. R., Silva, S. M., Borges, V., . . . de Carvalho Aguiar, P. (2016). Screening of GNAL variants in Brazilian patients with isolated dystonia reveals a novel mutation with partial loss of function. *J Neurol*, 263(4), 665-668. doi:10.1007/s00415-016-8026-2
- Dufke, C., Sturm, M., Schroeder, C., Moll, S., Ott, T., Riess, O., . . . Grundmann, K. (2014). Screening of mutations in GNAL in sporadic dystonia patients. *Mov Disord*, 29(9), 1193-1196. doi:10.1002/mds.25794
- Eagle, A. L., Gajewski, P. A., & Robison, A. J. (2016). Role of hippocampal activity-induced transcription in memory consolidation. *Rev Neurosci*, 27(6), 559-573. doi:10.1515/revneuro-2016-0010
- Epi, K. C. (2016). De Novo Mutations in SLC1A2 and CACNA1A Are Important Causes of Epileptic Encephalopathies. *Am J Hum Genet*, 99(2), 287-298. doi:10.1016/j.ajhg.2016.06.003
- Epi, K. C., Epilepsy Phenome/Genome, P., Allen, A. S., Berkovic, S. F., Cossette, P., Delanty, N., . . . Winawer, M. R. (2013). De novo mutations in epileptic encephalopathies. *Nature*, 501(7466), 217-221. doi:10.1038/nature12439
- Euro, E.-R. E. S. C., Epilepsy Phenome/Genome, P., & Epi, K. C. (2014). De novo mutations in synaptic transmission genes including DNMT1 cause epileptic encephalopathies. *Am J Hum Genet*, 95(4), 360-370. doi:10.1016/j.ajhg.2014.08.013
- Farwell, K. D., Shahmirzadi, L., El-Khechen, D., Powis, Z., Chao, E. C., Tippin Davis, B., . . . Tang, S. (2015). Enhanced utility of family-centered diagnostic exome sequencing with inheritance model-based analysis: results from 500 unselected families with undiagnosed genetic conditions. *Genet Med*, 17(7), 578-586. doi:10.1038/gim.2014.154
- Feng, H., Sjogren, B., Karaj, B., Shaw, V., Gezer, A., & Neubig, R. R. (2017). Movement disorder in GNAO1 encephalopathy associated with gain-of-function mutations.

Neurology, 89(8), 762-770. doi:10.1212/WNL.0000000000004262

Forbes, E. M., Thompson, A. W., Yuan, J., & Goodhill, G. J. (2012). Calcium and cAMP levels interact to determine attraction versus repulsion in axon guidance. *Neuron*, 74(3), 490-503. doi:10.1016/j.neuron.2012.02.035

Friedman, J. R., Meneret, A., Chen, D. H., Trouillard, O., Vidailhet, M., Raskind, W. H., & Roze, E. (2016). ADCY5 mutation carriers display pleiotropic paroxysmal day and nighttime dyskinesias. *Mov Disord*, 31(1), 147-148. doi:10.1002/mds.26494

Fuchs, T., Saunders-Pullman, R., Masuho, I., Luciano, M. S., Raymond, D., Factor, S., . . . Ozelius, L. J. (2013). Mutations in GNAL cause primary torsion dystonia. *Nat Genet*, 45(1), 88-92. doi:10.1038/ng.2496

Gao, Z., Todorov, B., Barrett, C. F., van Dorp, S., Ferrari, M. D., van den Maagdenberg, A. M., . . . Hoebeek, F. E. (2012). Cerebellar ataxia by enhanced Ca(V)2.1 currents is alleviated by Ca²⁺-dependent K⁺-channel activators in Cacna1a(S218L) mutant mice. *J Neurosci*, 32(44), 15533-15546. doi:10.1523/JNEUROSCI.2454-12.2012

Garza-Lopez, E., Sandoval, A., Gonzalez-Ramirez, R., Gandini, M. A., Van den Maagdenberg, A., De Waard, M., & Felix, R. (2012). Familial hemiplegic migraine type 1 mutations W1684R and V1696I alter G protein-mediated regulation of Ca(V)2.1 voltage-gated calcium channels. *Biochim Biophys Acta*, 1822(8), 1238-1246. doi:10.1016/j.bbadis.2012.04.008

Gawlinski, P., Posmyk, R., Gambin, T., Sielicka, D., Chorazy, M., Nowakowska, B., . . . Wiszniewski, W. (2016). PEHO Syndrome May Represent Phenotypic Expansion at the Severe End of the Early-Onset Encephalopathies. *Pediatr Neurol*, 60, 83-87. doi:10.1016/j.pediatrneurol.2016.03.011

Gerald, B., Ramsey, K., Belnap, N., Szelinger, S., Siniard, A. L., Balak, C., . . . Narayanan, V. (2018). Neonatal epileptic encephalopathy caused by de novo GNAO1 mutation misdiagnosed as atypical Rett syndrome: Cautions in interpretation of genomic test results. *Semin Pediatr Neurol*, 26, 28-32. doi:10.1016/j.spn.2017.08.008

Gill, A., & Hammes, S. R. (2007). G beta gamma signaling reduces intracellular cAMP to promote meiotic progression in mouse oocytes. *Steroids*, 72(2), 117-123. doi:10.1016/j.steroids.2006.11.006

- Giorgi, M., Melchiorri, G., Nuccetelli, V., D'Angelo, V., Martorana, A., Sorge, R., . . . Sancesario, G. (2011). PDE10A and PDE10A-dependent cAMP catabolism are dysregulated oppositely in striatum and nucleus accumbens after lesion of midbrain dopamine neurons in rat: a key step in parkinsonism physiopathology. *Neurobiol Dis*, *43*(1), 293-303. doi:10.1016/j.nbd.2011.04.006
- Goldstein, L. B. (2006). Neurotransmitters and motor activity: effects on functional recovery after brain injury. *NeuroRx*, *3*(4), 451-457. doi:10.1016/j.nurx.2006.07.010
- Gorman, K. M., Meyer, E., Grozeva, D., Spinelli, E., McTague, A., Sanchis-Juan, A., . . . Kurian, M. A. (2019). Bi-allelic Loss-of-Function CACNA1B Mutations in Progressive Epilepsy-Dyskinesia. *Am J Hum Genet*, *104*(5), 948-956. doi:10.1016/j.ajhg.2019.03.005
- Grimminger, T., Pernhorst, K., Surges, R., Niehusmann, P., Priebe, L., von Lehe, M., . . . Becker, A. J. (2013). Levetiracetam resistance: Synaptic signatures & corresponding promoter SNPs in epileptic hippocampi. *Neurobiol Dis*, *60*, 115-125. doi:10.1016/j.nbd.2013.08.015
- Groen, J., van Rootselaar, A. F., van der Salm, S. M., Bloem, B. R., & Tijssen, M. (2011). A new familial syndrome with dystonia and lower limb action myoclonus. *Mov Disord*, *26*(5), 896-900. doi:10.1002/mds.23557
- Groen, J. L., Andrade, A., Ritz, K., Jalalzadeh, H., Haagmans, M., Bradley, T. E., . . . Tijssen, M. A. (2015). CACNA1B mutation is linked to unique myoclonus-dystonia syndrome. *Hum Mol Genet*, *24*(4), 987-993. doi:10.1093/hmg/ddu513
- Guan, J. S., Su, S. C., Gao, J., Joseph, N., Xie, Z., Zhou, Y., . . . Tsai, L. H. (2011). Cdk5 is required for memory function and hippocampal plasticity via the cAMP signaling pathway. *PLoS One*, *6*(9), e25735. doi:10.1371/journal.pone.0025735
- Guida, S., Trettel, F., Pagnutti, S., Mantuano, E., Tottene, A., Veneziano, L., . . . Pietrobon, D. (2001). Complete loss of P/Q calcium channel activity caused by a CACNA1A missense mutation carried by patients with episodic ataxia type 2. *Am J Hum Genet*, *68*(3), 759-764.
- Helbig, K. L., Farwell Hagman, K. D., Shinde, D. N., Mroske, C., Powis, Z., Li, S., . . . Helbig, I. (2016). Diagnostic exome sequencing provides a molecular diagnosis for a significant proportion of patients with epilepsy. *Genet Med*, *18*(9), 898-905.

doi:10.1038/gim.2015.186

- Heron, S. E., Grinton, B. E., Kivity, S., Afawi, Z., Zuberi, S. M., Hughes, J. N., . . . Dibbens, L. M. (2012). PRRT2 mutations cause benign familial infantile epilepsy and infantile convulsions with choreoathetosis syndrome. *Am J Hum Genet*, *90*(1), 152-160. doi:10.1016/j.ajhg.2011.12.003
- Honey, C. M., Malhotra, A. K., Tarailo-Graovac, M., van Karnebeek, C. D. M., Horvath, G., & Sulistyanto, A. (2018). GNAO1 Mutation-Induced Pediatric Dystonic Storm Rescue With Pallidal Deep Brain Stimulation. *J Child Neurol*, *33*(6), 413-416. doi:10.1177/0883073818756134
- Inda, C., Bonfiglio, J. J., Dos Santos Claro, P. A., Senin, S. A., Armando, N. G., Deussing, J. M., & Silberstein, S. (2017). cAMP-dependent cell differentiation triggered by activated CRHR1 in hippocampal neuronal cells. *Sci Rep*, *7*(1), 1944. doi:10.1038/s41598-017-02021-7
- Iwamoto, T., Okumura, S., Iwatsubo, K., Kawabe, J., Ohtsu, K., Sakai, I., . . . Ishikawa, Y. (2003). Motor dysfunction in type 5 adenylyl cyclase-null mice. *J Biol Chem*, *278*(19), 16936-16940. doi:10.1074/jbc.C300075200
- Jen, J. C., Yue, Q., Karrim, J., Nelson, S. F., & Baloh, R. W. (1998). Spinocerebellar ataxia type 6 with positional vertigo and acetazolamide responsive episodic ataxia. *J Neurol Neurosurg Psychiatry*, *65*(4), 565-568.
- Jeng, C. J., Chen, Y. T., Chen, Y. W., & Tang, C. Y. (2006). Dominant-negative effects of human P/Q-type Ca²⁺ channel mutations associated with episodic ataxia type 2. *Am J Physiol Cell Physiol*, *290*(4), C1209-1220. doi:10.1152/ajpcell.00247.2005
- Jeon, C. Y., Moon, M. Y., Kim, J. H., Kim, H. J., Kim, J. G., Li, Y., . . . Park, J. B. (2012). Control of neurite outgrowth by RhoA inactivation. *J Neurochem*, *120*(5), 684-698. doi:10.1111/j.1471-4159.2011.07564.x
- Jiang, M., & Bajpayee, N. S. (2009). Molecular mechanisms of go signaling. *Neurosignals*, *17*(1), 23-41. doi:10.1159/000186688
- Jiang, M., Gold, M. S., Boulay, G., Spicher, K., Peyton, M., Brabet, P., . . . Birnbaumer, L. (1998). Multiple neurological abnormalities in mice deficient in the G protein Go. *Proc Natl Acad Sci U S A*, *95*(6), 3269-3274. doi:10.1073/pnas.95.6.3269

- Jin, C., Decker, A. M., Huang, X. P., Gilmour, B. P., Blough, B. E., Roth, B. L., . . . Zhang, X. P. (2014). Synthesis, pharmacological characterization, and structure-activity relationship studies of small molecular agonists for the orphan GPR88 receptor. *ACS Chem Neurosci*, *5*(7), 576-587. doi:10.1021/cn500082p
- Jouveneau, A., Eunson, L. H., Spauschus, A., Ramesh, V., Zuberi, S. M., Kullmann, D. M., & Hanna, M. G. (2001). Human epilepsy associated with dysfunction of the brain P/Q-type calcium channel. *Lancet*, *358*(9284), 801-807. doi:10.1016/S0140-6736(01)05971-2
- Kandel, E. R. (2012). The molecular biology of memory: cAMP, PKA, CRE, CREB-1, CREB-2, and CPEB. *Mol Brain*, *5*, 14. doi:10.1186/1756-6606-5-14
- Kehrl, J. M., Sahaya, K., Dalton, H. M., Charbeneau, R. A., Kohut, K. T., Gilbert, K., . . . Neubig, R. R. (2014). Gain-of-function mutation in Gnao1: a murine model of epileptiform encephalopathy (EIEE17)? *Mamm Genome*, *25*(5-6), 202-210. doi:10.1007/s00335-014-9509-z
- Kelly, M., Park, M., Mihalek, I., Rochtus, A., Gramm, M., Perez-Palma, E., . . . Poduri, A. (2019). Spectrum of neurodevelopmental disease associated with the GNAO1 guanosine triphosphate-binding region. *Epilepsia*, *60*(3), 406-418. doi:10.1111/epi.14653
- Koy, A., Cirak, S., Gonzalez, V., Becker, K., Roujeau, T., Milesi, C., . . . Cif, L. (2018). Deep brain stimulation is effective in pediatric patients with GNAO1 associated severe hyperkinesia. *J Neurol Sci*, *391*, 31-39. doi:10.1016/j.jns.2018.05.018
- Kulkarni, N., Tang, S., Bhardwaj, R., Bernes, S., & Grebe, T. A. (2016). Progressive Movement Disorder in Brothers Carrying a GNAO1 Mutation Responsive to Deep Brain Stimulation. *J Child Neurol*, *31*(2), 211-214. doi:10.1177/0883073815587945
- Kumar, K. R., Lohmann, K., Masuho, I., Miyamoto, R., Ferbert, A., Lohnau, T., . . . Schmidt, A. (2014). Mutations in GNAL: a novel cause of craniocervical dystonia. *JAMA Neurol*, *71*(4), 490-494. doi:10.1001/jamaneurol.2013.4677
- Law, C. Y., Chang, S. T., Cho, S. Y., Yau, E. K., Ng, G. S., Fong, N. C., & Lam, C. W. (2015). Clinical whole-exome sequencing reveals a novel missense pathogenic variant of GNAO1 in a patient with infantile-onset epilepsy. *Clin Chim Acta*, *451*(Pt B), 292-296. doi:10.1016/j.cca.2015.10.011

- Law, C. Y., Yeung, W. L., Cheung, Y. F., Chan, H. F., Fung, E., Hui, J., . . . Lam, C. W. (2016). A common PRRT2 mutation in familial paroxysmal kinesigenic dyskinesia in Hong Kong: a case series of 16 patients. *Hong Kong Med J*, 22(6), 619-622. doi:10.12809/hkmj154579
- Lee, H. Y., Huang, Y., Bruneau, N., Roll, P., Roberson, E. D., Hermann, M., . . . Ptacek, L. J. (2012). Mutations in the gene PRRT2 cause paroxysmal kinesigenic dyskinesia with infantile convulsions. *Cell Rep*, 1(1), 2-12. doi:10.1016/j.celrep.2011.11.001
- Lee, U. S., & Cui, J. (2010). BK channel activation: structural and functional insights. *Trends Neurosci*, 33(9), 415-423. doi:10.1016/j.tins.2010.06.004
- Lepski, G., Jannes, C. E., Nikkhah, G., & Bischofberger, J. (2013). cAMP promotes the differentiation of neural progenitor cells in vitro via modulation of voltage-gated calcium channels. *Front Cell Neurosci*, 7, 155. doi:10.3389/fncel.2013.00155
- Lessmann, V., & Heumann, R. (1997). Cyclic AMP endogenously enhances synaptic strength of developing glutamatergic synapses in serum-free microcultures of rat hippocampal neurons. *Brain Res*, 763(1), 111-122.
- Leung, C. C. Y., & Wong, Y. H. (2017). Role of G Protein-Coupled Receptors in the Regulation of Structural Plasticity and Cognitive Function. *Molecules*, 22(7). doi:10.3390/molecules22071239
- Leveque, C., el Far, O., Martin-Moutot, N., Sato, K., Kato, R., Takahashi, M., & Seagar, M. J. (1994). Purification of the N-type calcium channel associated with syntaxin and synaptotagmin. A complex implicated in synaptic vesicle exocytosis. *J Biol Chem*, 269(9), 6306-6312.
- Lohmann, K., Masuho, I., Patil, D. N., Baumann, H., Hebert, E., Steinrucke, S., . . . Martemyanov, K. A. (2017). Novel GNB1 mutations disrupt assembly and function of G protein heterotrimers and cause global developmental delay in humans. *Hum Mol Genet*, 26(6), 1078-1086. doi:10.1093/hmg/ddx018
- Luscher, C., & Slesinger, P. A. (2010). Emerging roles for G protein-gated inwardly rectifying potassium (GIRK) channels in health and disease. *Nat Rev Neurosci*, 11(5), 301-315. doi:10.1038/nrn2834
- Malaquias, M. J., Fineza, I., Loureiro, L., Cardoso, L., Alonso, I., & Magalhaes, M. (2019).

- GNAO1 mutation presenting as dyskinetic cerebral palsy. *Neurol Sci*. doi:10.1007/s10072-019-03964-7
- Marce-Grau, A., Dalton, J., Lopez-Pison, J., Garcia-Jimenez, M. C., Monge-Galindo, L., Cuenca-Leon, E., . . . Macaya, A. (2016). GNAO1 encephalopathy: further delineation of a severe neurodevelopmental syndrome affecting females. *Orphanet J Rare Dis*, 11, 38. doi:10.1186/s13023-016-0416-0
- Massart, R., Guilloux, J. P., Mignon, V., Sokoloff, P., & Diaz, J. (2009). Striatal GPR88 expression is confined to the whole projection neuron population and is regulated by dopaminergic and glutamatergic afferents. *Eur J Neurosci*, 30(3), 397-414. doi:10.1111/j.1460-9568.2009.06842.x
- Masuh, I., Fang, M., Geng, C., Zhang, J., Jiang, H., Ozgul, R. K., . . . Kruer, M. C. (2016). Homozygous GNAL mutation associated with familial childhood-onset generalized dystonia. *Neurol Genet*, 2(3), e78. doi:10.1212/NXG.0000000000000078
- Mayfield, J., Blednov, Y. A., & Harris, R. A. (2015). Behavioral and Genetic Evidence for GIRK Channels in the CNS: Role in Physiology, Pathophysiology, and Drug Addiction. *Int Rev Neurobiol*, 123, 279-313. doi:10.1016/bs.irm.2015.05.016
- McDavid, S., & Currie, K. P. (2006). G-proteins modulate cumulative inactivation of N-type (Cav2.2) calcium channels. *J Neurosci*, 26(51), 13373-13383. doi:10.1523/JNEUROSCI.3332-06.2006
- McIntyre, C. C., & Anderson, R. W. (2016). Deep brain stimulation mechanisms: the control of network activity via neurochemistry modulation. *J Neurochem*, 139 Suppl 1, 338-345. doi:10.1111/jnc.13649
- Meijer, I. A., Miravite, J., Kopell, B. H., & Lubarr, N. (2017). Deep Brain Stimulation in an Additional Patient With ADCY5-Related Movement Disorder. *J Child Neurol*, 32(4), 438-439. doi:10.1177/0883073816681353
- Meersman, A. C., Le Merrer, J., Pellissier, L. P., Diaz, J., Clesse, D., Kieffer, B. L., & Becker, J. A. (2016). Mice Lacking GPR88 Show Motor Deficit, Improved Spatial Learning, and Low Anxiety Reversed by Delta Opioid Antagonist. *Biol Psychiatry*, 79(11), 917-927. doi:10.1016/j.biopsych.2015.05.020
- Mencacci, N. E., & Carecchio, M. (2016). Recent advances in genetics of chorea. *Curr*

Opin Neurol, 29(4), 486-495. doi:10.1097/WCO.0000000000000352

- Mencacci, N. E., Erro, R., Wiethoff, S., Hersheson, J., Ryten, M., Balint, B., . . . Bhatia, K. P. (2015). ADCY5 mutations are another cause of benign hereditary chorea. *Neurology*, 85(1), 80-88. doi:10.1212/WNL.0000000000001720
- Mencacci, N. E., Kamsteeg, E. J., Nakashima, K., R'Bibo, L., Lynch, D. S., Balint, B., . . . Bhatia, K. P. (2016). De Novo Mutations in PDE10A Cause Childhood-Onset Chorea with Bilateral Striatal Lesions. *Am J Hum Genet*, 98(4), 763-771. doi:10.1016/j.ajhg.2016.02.015
- Mencacci, N. E., R'Bibo, L., Bandres-Ciga, S., Carecchio, M., Zorzi, G., Nardocci, N., . . . Wood, N. W. (2015). The CACNA1B R1389H variant is not associated with myoclonus-dystonia in a large European multicentric cohort. *Hum Mol Genet*, 24(18), 5326-5329. doi:10.1093/hmg/ddv255
- Menke, L. A., Engelen, M., Alders, M., Odekerken, V. J., Baas, F., & Cobben, J. M. (2016). Recurrent GNAO1 Mutations Associated With Developmental Delay and a Movement Disorder. *J Child Neurol*, 31(14), 1598-1601. doi:10.1177/0883073816666474
- Mercado, R., Constantoyannis, C., Mandat, T., Kumar, A., Schulzer, M., Stoessl, A. J., & Honey, C. R. (2006). Expectation and the placebo effect in Parkinson's disease patients with subthalamic nucleus deep brain stimulation. *Mov Disord*, 21(9), 1457-1461. doi:10.1002/mds.20935
- Mercimek-Mahmutoglu, S., Sidky, S., Hyland, K., Patel, J., Donner, E. J., Logan, W., . . . Kyriakopoulou, L. (2015). Prevalence of inherited neurotransmitter disorders in patients with movement disorders and epilepsy: a retrospective cohort study. *Orphanet J Rare Dis*, 10, 12. doi:10.1186/s13023-015-0234-9
- Miclea, D., Peca, L., Cuzmici, Z., & Pop, I. V. (2015). Genetic testing in patients with global developmental delay / intellectual disabilities. A review. *Clujul Med*, 88(3), 288-292. doi:10.15386/cjmed-461
- Mizushima, K., Miyamoto, Y., Tsukahara, F., Hirai, M., Sakaki, Y., & Ito, T. (2000). A novel G-protein-coupled receptor gene expressed in striatum. *Genomics*, 69(3), 314-321. doi:10.1006/geno.2000.6340
- Mullner, C., Broos, L. A., van den Maagdenberg, A. M., & Striessnig, J. (2004). Familial

- hemiplegic migraine type 1 mutations K1336E, W1684R, and V1696I alter Cav2.1 Ca²⁺ channel gating: evidence for beta-subunit isoform-specific effects. *J Biol Chem*, 279(50), 51844-51850. doi:10.1074/jbc.M408756200
- Nakamura, K., Kodera, H., Akita, T., Shiina, M., Kato, M., Hoshino, H., . . . Saitsu, H. (2013). De Novo mutations in GNAO1, encoding a Gα_o subunit of heterotrimeric G proteins, cause epileptic encephalopathy. *Am J Hum Genet*, 93(3), 496-505. doi:10.1016/j.ajhg.2013.07.014
- Neher, E. (2006). A comparison between exocytic control mechanisms in adrenal chromaffin cells and a glutamatergic synapse. *Pflugers Arch*, 453(3), 261-268. doi:10.1007/s00424-006-0143-9
- Nestler, E. J., Alreja, M., & Aghajanian, G. K. (1999). Molecular control of locus coeruleus neurotransmission. *Biol Psychiatry*, 46(9), 1131-1139.
- Ohno, Y., & Tokudome, K. (2017). Therapeutic Role of Synaptic Vesicle Glycoprotein 2A (SV2A) in Modulating Epileptogenesis. *CNS Neurol Disord Drug Targets*, 16(4), 463-471. doi:10.2174/1871527316666170404115027
- Okumura, A., Maruyama, K., Shibata, M., Kurahashi, H., Ishii, A., Numoto, S., . . . Kojima, S. (2018). A patient with a GNAO1 mutation with decreased spontaneous movements, hypotonia, and dystonic features. *Brain Dev*, 40(10), 926-930. doi:10.1016/j.braindev.2018.06.005
- Paddock, B. E., Wang, Z., Biela, L. M., Chen, K., Getzy, M. D., Striegel, A., . . . Reist, N. E. (2011). Membrane penetration by synaptotagmin is required for coupling calcium binding to vesicle fusion in vivo. *J Neurosci*, 31(6), 2248-2257. doi:10.1523/JNEUROSCI.3153-09.2011
- Padovan-Neto, F. E., & West, A. R. (2017). Regulation of Striatal Neuron Activity by Cyclic Nucleotide Signaling and Phosphodiesterase Inhibition: Implications for the Treatment of Parkinson's Disease. *Adv Neurobiol*, 17, 257-283. doi:10.1007/978-3-319-58811-7_10
- Park, H. Y., Kang, Y. M., Kang, Y., Park, T. S., Ryu, Y. K., Hwang, J. H., . . . Kim, K. S. (2014). Inhibition of adenylyl cyclase type 5 prevents L-DOPA-induced dyskinesia in an animal model of Parkinson's disease. *J Neurosci*, 34(35), 11744-11753. doi:10.1523/JNEUROSCI.0864-14.2014

- Patel, T. B. (2004). Single transmembrane spanning heterotrimeric G protein-coupled receptors and their signaling cascades. *Pharmacol Rev*, *56*(3), 371-385. doi:10.1124/pr.56.3.4
- Pelosi, A., Menardy, F., Popa, D., Girault, J. A., & Herve, D. (2017). Heterozygous Gnal Mice Are a Novel Animal Model with Which to Study Dystonia Pathophysiology. *J Neurosci*, *37*(26), 6253-6267. doi:10.1523/JNEUROSCI.1529-16.2017
- Petrovski, S., Kury, S., Myers, C. T., Anyane-Yeboa, K., Cogne, B., Bialer, M., . . . Goldstein, D. B. (2016). Germline De Novo Mutations in GNB1 Cause Severe Neurodevelopmental Disability, Hypotonia, and Seizures. *Am J Hum Genet*, *98*(5), 1001-1010. doi:10.1016/j.ajhg.2016.03.011
- Pierre, S., Eschenhagen, T., Geisslinger, G., & Scholich, K. (2009). Capturing adenylyl cyclases as potential drug targets. *Nat Rev Drug Discov*, *8*(4), 321-335. doi:10.1038/nrd2827
- Putzel, G. G., Fuchs, T., Battistella, G., Rubien-Thomas, E., Frucht, S. J., Blitzer, A., . . . Simonyan, K. (2016). GNAL mutation in isolated laryngeal dystonia. *Mov Disord*, *31*(5), 750-755. doi:10.1002/mds.26502
- Quintana, A., Sanz, E., Wang, W., Storey, G. P., Guler, A. D., Wanat, M. J., . . . Palmiter, R. D. (2012). Lack of GPR88 enhances medium spiny neuron activity and alters motor- and cue-dependent behaviors. *Nat Neurosci*, *15*(11), 1547-1555. doi:10.1038/nn.3239
- Rickman, C., & Davletov, B. (2003). Mechanism of calcium-independent synaptotagmin binding to target SNAREs. *J Biol Chem*, *278*(8), 5501-5504. doi:10.1074/jbc.C200692200
- Rohena, L., Neidich, J., Truitt Cho, M., Gonzalez, K. D., Tang, S., Devinsky, O., & Chung, W. K. (2013). Mutation in SNAP25 as a novel genetic cause of epilepsy and intellectual disability. *Rare Dis*, *1*, e26314. doi:10.4161/rdis.26314
- Russwurm, C., Koesling, D., & Russwurm, M. (2015). Phosphodiesterase 10A Is Tethered to a Synaptic Signaling Complex in Striatum. *J Biol Chem*, *290*(19), 11936-11947. doi:10.1074/jbc.M114.595769
- Saitou, H., Fukai, R., Ben-Zeev, B., Sakai, Y., Mimaki, M., Okamoto, N., . . . Matsumoto, N. (2016). Phenotypic spectrum of GNAO1 variants: epileptic encephalopathy to

- involuntary movements with severe developmental delay. *Eur J Hum Genet*, 24(1), 129-134. doi:10.1038/ejhg.2015.92
- Sakamoto, S., Monden, Y., Fukai, R., Miyake, N., Saito, H., Miyauchi, A., . . . Yamagata, T. (2017). A case of severe movement disorder with GNAO1 mutation responsive to topiramate. *Brain Dev*, 39(5), 439-443. doi:10.1016/j.braindev.2016.11.009
- Salvi, J., Bertaso, F., Mausset-Bonnefont, A. L., Metz, A., Lemmers, C., Ango, F., . . . Mezghrani, A. (2014). RNAi silencing of P/Q-type calcium channels in Purkinje neurons of adult mouse leads to episodic ataxia type 2. *Neurobiol Dis*, 68, 47-56. doi:10.1016/j.nbd.2014.04.005
- Schirinzi, T., Garone, G., Travaglini, L., Vasco, G., Galosi, S., Rios, L., . . . Leuzzi, V. (2019). Phenomenology and clinical course of movement disorder in GNAO1 variants: Results from an analytical review. *Parkinsonism Relat Disord*, 61, 19-25. doi:10.1016/j.parkreldis.2018.11.019
- Schmidt, M., Dekker, F. J., & Maarsingh, H. (2013). Exchange protein directly activated by cAMP (epac): a multidomain cAMP mediator in the regulation of diverse biological functions. *Pharmacol Rev*, 65(2), 670-709. doi:10.1124/pr.110.003707
- Schorling, D. C., Dietel, T., Evers, C., Hinderhofer, K., Korinthenberg, R., Ezzo, D., . . . Kirschner, J. (2017). Expanding Phenotype of De Novo Mutations in GNAO1: Four New Cases and Review of Literature. *Neuropediatrics*, 48(5), 371-377. doi:10.1055/s-0037-1603977
- Shanley, L. J., O'Malley, D., Irving, A. J., Ashford, M. L., & Harvey, J. (2002). Leptin inhibits epileptiform-like activity in rat hippocampal neurones via PI 3-kinase-driven activation of BK channels. *J Physiol*, 545(3), 933-944. doi:10.1113/jphysiol.2002.029488
- Sharma, S., Hansen, J. T., & Notter, M. F. (1990). Effects of NGF and dibutyryl cAMP on neuronal differentiation of embryonal carcinoma cells. *Int J Dev Neurosci*, 8(1), 33-45.
- Shaw, C., Hisama, F., Friedman, J., & Bird, T. D. (1993). ADCY5-Related Dyskinesia. In M. P. Adam, H. H. Ardinger, R. A. Pagon, S. E. Wallace, L. J. H. Bean, K. Stephens, & A. Amemiya (Eds.), *GeneReviews((R))*. Seattle (WA).
- Signorini, S., Liao, Y. J., Duncan, S. A., Jan, L. Y., & Stoffel, M. (1997). Normal

cerebellar development but susceptibility to seizures in mice lacking G protein-coupled, inwardly rectifying K⁺ channel GIRK2. *Proc Natl Acad Sci U S A*, 94(3), 923-927. doi:10.1073/pnas.94.3.923

Simms, B. A., & Zamponi, G. W. (2014). Neuronal voltage-gated calcium channels: structure, function, and dysfunction. *Neuron*, 82(1), 24-45. doi:10.1016/j.neuron.2014.03.016

Sintas, C., Carreno, O., Fernandez-Castillo, N., Corominas, R., Vila-Pueyo, M., Toma, C., . . . Cormand, B. (2017). Mutation Spectrum in the CACNA1A Gene in 49 Patients with Episodic Ataxia. *Sci Rep*, 7(1), 2514. doi:10.1038/s41598-017-02554-x

Siuciak, J. A., McCarthy, S. A., Chapin, D. S., Martin, A. N., Harms, J. F., & Schmidt, C. J. (2008). Behavioral characterization of mice deficient in the phosphodiesterase-10A (PDE10A) enzyme on a C57/Bl6N congenic background. *Neuropharmacology*, 54(2), 417-427. doi:10.1016/j.neuropharm.2007.10.009

Steinrucke, S., Lohmann, K., Domingo, A., Rolfs, A., Baumer, T., Spiegler, J., . . . Munchau, A. (2016). Novel GNB1 missense mutation in a patient with generalized dystonia, hypotonia, and intellectual disability. *Neurol Genet*, 2(5), e106. doi:10.1212/NXG.000000000000106

Sudhof, T. C. (2012). Calcium control of neurotransmitter release. *Cold Spring Harb Perspect Biol*, 4(1), a011353. doi:10.1101/cshperspect.a011353

Sutton, K. G., McRory, J. E., Guthrie, H., Murphy, T. H., & Snutch, T. P. (1999). P/Q-type calcium channels mediate the activity-dependent feedback of syntaxin-1A. *Nature*, 401(6755), 800-804. doi:10.1038/44586

Szczepanik, E., Terczynska, I., Kruk, M., Lipiec, A., Dudko, E., Tryfon, J., . . . Hoffman-Zacharska, D. (2015). Glucose transporter type 1 deficiency due to SLC2A1 gene mutations--a rare but treatable cause of metabolic epilepsy and extrapyramidal movement disorder; own experience and literature review. *Dev Period Med*, 19(4), 454-463.

Tabarki, B., AlMajhad, N., AlHashem, A., Shaheen, R., & Alkuraya, F. S. (2016). Homozygous KCNMA1 mutation as a cause of cerebellar atrophy, developmental delay and seizures. *Hum Genet*, 135(11), 1295-1298. doi:10.1007/s00439-016-1726-y

- Takezawa, Y., Kikuchi, A., Haginoya, K., Niihori, T., Numata-Uematsu, Y., Inui, T., . . . Kure, S. (2018). Genomic analysis identifies masqueraders of full-term cerebral palsy. *Ann Clin Transl Neurol*, 5(5), 538-551. doi:10.1002/acn3.551
- Talvik, I., Moller, R. S., Vaher, M., Vaher, U., Larsen, L. H., Dahl, H. A., . . . Talvik, T. (2015). Clinical Phenotype of De Novo GNAO1 Mutation: Case Report and Review of Literature. *Child Neurol Open*, 2(2), 2329048X15583717. doi:10.1177/2329048X15583717
- Tong, J., Liu, X., Vickstrom, C., Li, Y., Yu, L., Lu, Y., . . . Liu, Q. S. (2017). The Epac-Phospholipase Cepsilon Pathway Regulates Endocannabinoid Signaling and Cocaine-Induced Disinhibition of Ventral Tegmental Area Dopamine Neurons. *J Neurosci*, 37(11), 3030-3044. doi:10.1523/JNEUROSCI.2810-16.2017
- Torrecilla, M., Marker, C. L., Cintora, S. C., Stoffel, M., Williams, J. T., & Wickman, K. (2002). G-protein-gated potassium channels containing Kir3.2 and Kir3.3 subunits mediate the acute inhibitory effects of opioids on locus ceruleus neurons. *J Neurosci*, 22(11), 4328-4334. doi:20026414
- Tucker, W. C., Weber, T., & Chapman, E. R. (2004). Reconstitution of Ca²⁺-regulated membrane fusion by synaptotagmin and SNAREs. *Science*, 304(5669), 435-438. doi:10.1126/science.1097196
- Ueda, K., Serajee, F., & Huq, A. (2016). Exome Sequencing Identifies Dual Mutations in Calcium Signaling Genes GNAO1 and ATP2B3 in a Patient with Early Infantile Epileptic Encephalopathy (EIEE) (P5.146). *Neurology*, 86.
- Waak, M., Mohammad, S. S., Coman, D., Sinclair, K., Copeland, L., Silburn, P., . . . Malone, S. (2017). GNAO1-related movement disorder with life-threatening exacerbations: movement phenomenology and response to DBS. *J Neurol Neurosurg Psychiatry*. doi:10.1136/jnnp-2017-315653
- Waak, M., Mohammad, S. S., Coman, D., Sinclair, K., Copeland, L., Silburn, P., . . . Malone, S. (2018). GNAO1-related movement disorder with life-threatening exacerbations: movement phenomenology and response to DBS. *J Neurol Neurosurg Psychiatry*, 89(2), 221-222. doi:10.1136/jnnp-2017-315653
- Wan, J., Mamsa, H., Johnston, J. L., Spriggs, E. L., Singer, H. S., Zee, D. S., . . . Investigators, C. (2011). Large Genomic Deletions in CACNA1A Cause Episodic Ataxia Type 2. *Front Neurol*, 2, 51. doi:10.3389/fneur.2011.00051

- Wang, J. L., Cao, L., Li, X. H., Hu, Z. M., Li, J. D., Zhang, J. G., . . . Tang, B. S. (2011). Identification of PRRT2 as the causative gene of paroxysmal kinesigenic dyskinesias. *Brain*, *134*(Pt 12), 3493-3501. doi:10.1093/brain/awr289
- Westenberger, A., Max, C., Bruggemann, N., Domingo, A., Grutz, K., Pawlack, H., . . . Klein, C. (2017). Alternating Hemiplegia of Childhood as a New Presentation of Adenylate Cyclase 5-Mutation-Associated Disease: A Report of Two Cases. *J Pediatr*, *181*, 306-308 e301. doi:10.1016/j.jpeds.2016.10.079
- Weston, M. C. (2017). The Role of PRRT2 in Synaptic Transmission May Not Be So Benign. *Epilepsy Curr*, *17*(3), 165-166. doi:10.5698/1535-7511.17.3.165
- Worley, P. F., Baraban, J. M., Van Dop, C., Neer, E. J., & Snyder, S. H. (1986). Go, a guanine nucleotide-binding protein: immunohistochemical localization in rat brain resembles distribution of second messenger systems. *Proc Natl Acad Sci U S A*, *83*(12), 4561-4565. doi:10.1073/pnas.83.12.4561
- Xie, Z., Adamowicz, W. O., Eldred, W. D., Jakowski, A. B., Kleiman, R. J., Morton, D. G., . . . Menniti, F. S. (2006). Cellular and subcellular localization of PDE10A, a striatum-enriched phosphodiesterase. *Neuroscience*, *139*(2), 597-607. doi:10.1016/j.neuroscience.2005.12.042
- Xiong, J., Peng, J., Duan, H. L., Chen, C., Wang, X. L., Chen, S. M., & Yin, F. (2018). [Recurrent convulsion and pulmonary infection complicated by psychomotor retardation in an infant]. *Zhongguo Dang Dai Er Ke Za Zhi*, *20*(2), 154-157.
- Yesil, G., Aralasmak, A., Akyuz, E., Icagasioglu, D., Uygur Sahin, T., & Bayram, Y. (2018). Expanding the Phenotype of Homozygous KCNMA1 Mutations; Dyskinesia, Epilepsy, Intellectual Disability, Cerebellar and Corticospinal Tract Atrophy. *Balkan Med J*, *35*(4), 336-339. doi:10.4274/balkanmedj.2017.0986
- Yilmaz, S., Turhan, T., Ceylaner, S., Gokben, S., Tekgul, H., & Serdaroglu, G. (2016). Excellent response to deep brain stimulation in a young girl with GNAO1-related progressive choreoathetosis. *Childs Nerv Syst*, *32*(9), 1567-1568. doi:10.1007/s00381-016-3139-6
- Yoda, A., Adelmant, G., Tamburini, J., Chapuy, B., Shindoh, N., Yoda, Y., . . . Lane, A. A. (2015). Mutations in G protein beta subunits promote transformation and kinase inhibitor resistance. *Nat Med*, *21*(1), 71-75. doi:10.1038/nm.3751

- Yu, J., Wang, S., Wu, C., & Yi, S. (2017). Deep Sequencing Reveals the Significant Involvement of cAMP-Related Signaling Pathways Following Sciatic Nerve Crush. *Neurochem Res*, 42(12), 3603-3611. doi:10.1007/s11064-017-2409-3
- Zamponi, G. W., & Currie, K. P. (2013). Regulation of Ca(V)₂ calcium channels by G protein coupled receptors. *Biochim Biophys Acta*, 1828(7), 1629-1643. doi:10.1016/j.bbamem.2012.10.004
- Zhang, Z. B., Tian, M. Q., Gao, K., Jiang, Y. W., & Wu, Y. (2015). De novo KCNMA1 mutations in children with early-onset paroxysmal dyskinesia and developmental delay. *Mov Disord*, 30(9), 1290-1292. doi:10.1002/mds.26216
- Zhu, X., Petrovski, S., Xie, P., Ruzzo, E. K., Lu, Y. F., McSweeney, K. M., . . . Goldstein, D. B. (2015). Whole-exome sequencing in undiagnosed genetic diseases: interpreting 119 trios. *Genet Med*, 17(10), 774-781. doi:10.1038/gim.2014.191
- Ztaou, S., Maurice, N., Camon, J., Guiraudie-Capraz, G., Kerkerian-Le Goff, L., Beurrier, C., . . . Amalric, M. (2016). Involvement of Striatal Cholinergic Interneurons and M1 and M4 Muscarinic Receptors in Motor Symptoms of Parkinson's Disease. *J Neurosci*, 36(35), 9161-9172. doi:10.1523/JNEUROSCI.0873-16.2016
- Zurawski, Z., Page, B., Chicka, M. C., Brindley, R. L., Wells, C. A., Preininger, A. M., . . . Hamm, H. E. (2017). Gbetagamma directly modulates vesicle fusion by competing with synaptotagmin for binding to neuronal SNARE proteins embedded in membranes. *J Biol Chem*, 292(29), 12165-12177. doi:10.1074/jbc.M116.773523
- Zurawski, Z., Rodriguez, S., Hyde, K., Alford, S., & Hamm, H. E. (2016). Gbetagamma Binds to the Extreme C Terminus of SNAP25 to Mediate the Action of Gi/o-Coupled G Protein-Coupled Receptors. *Mol Pharmacol*, 89(1), 75-83. doi:10.1124/mol.115.101600
- Zwart, R., Reed, H., Clarke, S., & Sher, E. (2016). A novel muscarinic receptor-independent mechanism of KCNQ2/3 potassium channel blockade by Oxotremorine-M. *Eur J Pharmacol*, 791, 221-228. doi:10.1016/j.ejphar.2016.08.037

CHAPTER 2: MOVEMENT DISORDER IN *GNAO1* ENCEPHALOPATHY ASSOCIATED WITH GAIN-OF-FUNCTION MUTATIONS

Modified from Feng, H., Sjögren, B., Karaj, B., Shaw, V., Gezer, A., & Neubig, R. R. (2017). Movement disorder in *GNAO1* encephalopathy associated with gain-of-function mutations. *Neurology*, 89(8), 762-770.

DOI: <https://doi.org/10.1212/WNL.0000000000004262>

With permission from the American Academy of Neurology. All rights reserved.

Gezer, A. performed plasmid mutagenesis for the first set of *GNAO1* mutations.

Wellhausen, N. did mutagenesis and cAMP assay in Figure S2.8.

Karaj, B. prepared six of the *GNAO1* mutant plasmids used in Figure 2.2.

Vincent Shaw made Figure S2.5.

2.1 Abstract

Objective: To define molecular mechanisms underlying the clinical spectrum of epilepsy and movement disorder in individuals with *de novo* mutations in the *GNAO1* gene.

Methods: We identified all *GNAO1* mutations reported in individuals with epilepsy (EIEE17) or movement disorders through April 2016; 15 *de novo* mutant alleles from 25 individuals were introduced into the $G\alpha_o$ subunit by site-directed mutagenesis in a mammalian expression plasmid. We assessed protein expression and function in vitro in HEK-293T cells by western blot and determined functional $G\alpha_o$ -dependent cyclic AMP inhibition with a co-expressed α_{2A} adrenergic receptor.

Results: Of the 15 clinical *GNAO1* mutations studied, 9 show reduced expression and loss of function (LOF, <90% maximal inhibition). Six other mutations show variable levels of expression but exhibit normal or even gain-of-function (GOF) behavior, as demonstrated by significantly lower EC_{50} values for α_{2A} adrenergic receptor-mediated inhibition of cAMP. The *GNAO1* LOF mutations are associated with epileptic encephalopathy while GOF mutants (such as G42R, G203R and E246K) or normally functioning mutants (R209) were found in patients with movement disorders with or without seizures.

Conclusions: Both LOF and GOF mutations in $G\alpha_o$ (encoded by *GNAO1*) are associated with neurological pathophysiology. There appears to be a strong predictive correlation between the in vitro biochemical phenotype and the clinical pattern of

epilepsy vs. movement disorder.

2.2 Introduction

Epilepsy is one of the most common neurological disorders in the United States. Severe early onset seizures can result in epileptic encephalopathy (Capovilla, Wolf, Beccaria, & Avanzini, 2013). There are at least 52 different gene mutations that cause early infantile epileptiform encephalopathy (EIEE) (McTague, Howell, Cross, Kurian, & Scheffer, 2016). Mutations in the same genes also cause other neurodevelopmental abnormalities (Berkovic et al., 2004; Sherr, 2003). A key challenge in genetic epilepsies has been understanding the genotype/phenotype relations of causal genes; this may require biochemical analysis (Noebels, 2015).

Mutations in the heterotrimeric G protein $G\alpha_o$ (*GNAO1* gene) cause an autosomal dominant epileptiform encephalopathy (EIEE17, OMIM: 615473) (Nakamura et al., 2013). In this original paper, all 4 mutations were characterized as having loss-of-function (LOF). More recently, an extended spectrum of “*GNAO1* encephalopathies” was identified in which individuals had movement disorders but minimal to no seizures (Ananth et al., 2016; Marce-Grau et al., 2016). Here, we use “*GNAO1* encephalopathy” to describe the entire clinical spectrum of individuals with pathological *GNAO1* mutations. A genotype-phenotype correlation was also recently noted (Menke et al., 2016); certain mutations (e.g. E246K and several R209 alleles) were found specifically in children with hypotonia, developmental delay, and chorea but no epilepsy. However, the mechanistic

basis for this genotype-phenotype correlation remains unknown.

GNAO1 encodes the α subunit of G_o , a heterotrimeric G protein (consisting of α and $\beta\gamma$ subunits) which is highly abundant in the central nervous system, comprising about 1% of brain membrane protein (Sternweis & Robishaw, 1984). $G\alpha_o$ mediates signals from a wide-range of inhibitory receptors including $GABA_B$, α_{2A} adrenergic, adenosine A_1 and dopamine D_2 receptors. A canonical function of $G\alpha_{i/o}$ family proteins is inhibition of cAMP (Ghahremani, Cheng, Lembo, & Albert, 1999). The identification of LOF mutations in *ADCY5* (which encodes adenylate cyclase 5, the enzyme that produces cAMP) in dyskinesia and chorea patients directly links reduced cAMP to involuntary movement disorders (Carapito et al., 2015; Chang et al., 2016; Mencacci et al., 2015; Morgan, Kurek, Davis, & Sethi, 2016; Raskind et al., 2017). This is inconsistent with LOF behavior of $G\alpha_o$.

Here we assessed expression and function of human mutations in *GNAO1* (Allen et al., 2013; Ananth et al., 2016; Consortium, Project, & Consortium, 2014; Dhamija, Mink, Shah, & Goodkin, 2016; Dietel, 2016; Epi KCEaekce, 2016; Kulkarni, Tang, Bhardwaj, Bernes, & Grebe, 2016; Law et al., 2015; Marce-Grau et al., 2016; Nakamura et al., 2013; Saito et al., 2016; Talvik, 2015; Zhu et al., 2015). Our biochemical analysis identified both loss- and gain-of-function behaviors; the latter are associated with movement disorders while the former are primarily found in individuals with epileptiform encephalopathies. This mechanistic insight has important implications for therapies of

GNAO1 encephalopathies.

Appendix B provides updated data on an additional list of 25 mutations analyzed after the publication of Feng et al. 2017.

2.3 Materials and Methods

2.3.1 Materials

UK14,304 was from Sigma Aldrich (St Louis, MO). Forskolin was from Calbiochem (San Diego, CA). Pertussis toxin (PTX) was from List Biological Laboratories (Campbell, CA). Protease inhibitor cocktail was from Roche (Roche, Indianapolis, IN). If not otherwise specified, all tissue culture reagents were from Thermo Fisher Scientific (Waltham, MA) and all chemicals were from Sigma Aldrich.

2.3.2 DNA constructs and mutagenesis

Cloning of the porcine α_{2A} AR in the pEGFP vector with an amino-terminal HA tag has been previously reported (Brink, Wade, & Neubig, 2000). PTX-insensitive murine $G\alpha_o$ (*Gnao1*; $G\alpha_o$ p.C351G PTXi) (Jeong & Ikeda, 2000) and RGS- and PTX-insensitive murine $G\alpha_o$ ($G\alpha_o$ p.G184S/C351G; RGS/PTXi) (Jeong & Ikeda, 2000) in the pCI vector were obtained from Dr. Stephen Ikeda (Guthrie Research Institute, Sayre, PA). Using the PTXi murine $G\alpha_o$ C351G as a template, 15 point mutations or deletions were introduced using the Stratagene Quickchange II Site-Directed Mutagenesis kit (Agilent Technologies, Santa Clara, CA). Primers for mutagenesis were designed using the algorithm described at <http://www.stratagene.com/sdmdesigner/default.aspx> (Table

S2.1). Mutations were verified by DNA sequencing at the RTSF Genomics Core at Michigan State University and sequences were analyzed using Clone Manager 9 (Sci-Ed Software, Denver, CO). The protein sequence of the human and murine $G\alpha_o$ are highly similar (98% identical) and do not differ in sequence at any of the mutated positions (Figure S2.1). As a positive control the RGS-insensitive GOF mutant $G\alpha_o$ p.G184S (Lan et al., 1998) was used.

2.3.3 Cell culture and transfections

Human embryonic kidney (HEK-293T) cells were maintained in a humidified incubator at 37°C with 5% CO₂ and grown to 95% confluence in Dulbecco's modified Eagle's medium (DMEM) supplemented with 10% fetal bovine serum (FBS), 100 U/ml penicillin and 100 µg/ml streptomycin. Cells were transfected using Lipofectamine 2000 according to the manufacturer's recommended protocol. All transfections were performed under serum-free conditions in Opti-MEM. Transfections were allowed to proceed for 4-5 h before the media was changed back to DMEM with 10 % FBS. Experiments were run 24 h after transfection.

For western blot, cells in 6-well plates were transfected using 2 µg of DNA and 8 µl of Lipofectamine 2000 per well. For cAMP assays, cells were plated in 60-mm dishes. DNA was kept constant at 4 µg (2 µg of $G\alpha_o$ or pcDNA and 2 µg of α_{2A} AR) and 10 µl of Lipofectamine2000 per plate was used. In the dominant-negative study, a total of 8 µg DNA was added to cells in 60-mm dishes with 10 µl Lipofectamine2000 per plate. In all

cases, empty vector (pcDNA3.1) was used to adjust the total amount of DNA.

2.3.4 SDS-PAGE and Western blot

Cells were harvested at 4°C in lysis buffer (20 mM Tris-HCl, pH7.4, 150 mM NaCl, 1 mM EDTA, 1 mM β -glycerophosphate, 1% Triton X-100, 0.1% SDS, with protease inhibitor) and then sonicated for 10 min at 4°C. Total protein concentrations in the cell lysates were determined by BCA protein assay (Pierce; Rockford, IL) and adjusted with an appropriate volume of Laemmli buffer (BioRad; Hercules, CA) with 5 % 2-mercaptoethanol (β -ME). Equal amounts of protein in each lane were resolved on a 12 % SDS-PAGE gel for 1 h at 160 V. Samples were transferred to an Immobilon-FL PVDF membrane (Millipore, Billerica, MA) for 1 h at 100 V, 400 mA on ice and subjected to Quantitative Infrared Western immunoblot analysis. The membrane was immersed in Odyssey blocking buffer (LI-COR Biosciences, Lincoln, NE) for 1 h with gentle shaking at room temperature. The membrane was simultaneously incubated with anti-G α_o (rabbit; 1:1,000; sc-387; Santa Cruz biotechnologies, Santa Cruz, CA) and anti-actin (goat; 1:1,000; sc-1615; Santa Cruz) antibodies diluted in Odyssey blocking buffer with 0.1% Tween-20 overnight at 4°C. Following four 5 min washes in phosphate-buffered saline, 0.1 % Tween-20 (PBS-T), the membrane was incubated for 1h at room temperature with secondary antibodies (both 1:10,000; IRDye® 800CW Donkey anti-rabbit; IRDye® 680RD Donkey anti-goat; LI-COR Biosciences) diluted in Odyssey blocking buffer with 0.1 % Tween-20. The membrane was subjected to four 5 min washes in PBS-T and a

final rinse in PBS for 5 min. The membrane was kept in the dark and the infrared signals at 680 and 800 nm were detected with an Odyssey Fc image system (LI-COR Biosciences). The $G\alpha_o$ polyclonal antibody recognizes an epitope located between positions 90-140 $G\alpha_o$ (Santa Cruz, personal communication), which shouldn't be affected by any of the mutations studied.

2.3.5 cAMP measurements

LANCE Ultra cAMP assays (Perkin Elmer; Waltham, MA) were performed in accordance with the manufacturer's instructions. Briefly, HEK-293T cells were transfected as indicated above. 100 ng/ml PTX was added the day before the assay to inhibit endogenous $G_{i/o}$ proteins. Cells were dissociated from dishes using Versene on the day of experiment. Then cells (2,000 cells/well in 5 μ l) were transferred to a white 384-well microplate (Perkin Elmer) and incubated with various concentrations of UK14,304 and Forskolin (final 1 μ M; 5 μ l/well) for 30 min at room temperature. A cAMP standard curve was generated in triplicate according to the manual. Finally, europium (Eu)-cAMP tracer (5 μ L) and ULIGHT™-anti-cAMP (5 μ L) were added to each well and incubated for 1h at room temperature. The plate was read on a TR-FRET microplate reader (Synergy NEO; Biotek, Winooski, VT).

2.3.6 Data analysis and statistics

Quantification of infrared (IR) Western blot signals was performed using Image Studio Lite (LI-COR Biosciences). Individual bands were normalized to the

corresponding actin signals, and WT $G\alpha_o$ was set as control. All data was analyzed using GraphPad Prism 6.0 (GraphPad; LaJolla, CA). Dose response curves were fit using non-linear least squares regression. Expression levels and Normalized % inhibition were analyzed with one-way ANOVA with Bonferroni's post hoc tests for multiple comparisons. Log EC_{50} values for the NF and GOF mutants were analyzed by paired t-test. Data are presented as mean \pm SEM. and a p -value less than 0.05 was considered significant.

2.4 Results

2.4.1 Most pathogenic *GNAO1* mutations cause reduced $G\alpha_o$ protein expression

To evaluate 15 mutations in *GNAO1* (Figure 2.1A and S2.1) that were previously identified in patients with epilepsy or other neurodevelopmental disorders (Allen et al., 2013; Ananth et al., 2016; Consortium et al., 2014; Dietel, 2016; Epi KCEaekce, 2016; Kulkarni et al., 2016; Law et al., 2015; Marce-Grau et al., 2016; Nakamura et al., 2013; Saitsu et al., 2016; Talvik, 2015; Zhu et al., 2015), we performed Western blots in HEK-293T cells transiently transfected with each mutant. The majority of mutants (12) showed significantly lower protein levels than wildtype (WT) $G\alpha_o$, whereas three separate Arg²⁰⁹ mutant alleles showed essentially normal expression as did the previously described GOF mutant G184S (Fu et al., 2004) (Figure 2.1B-E).

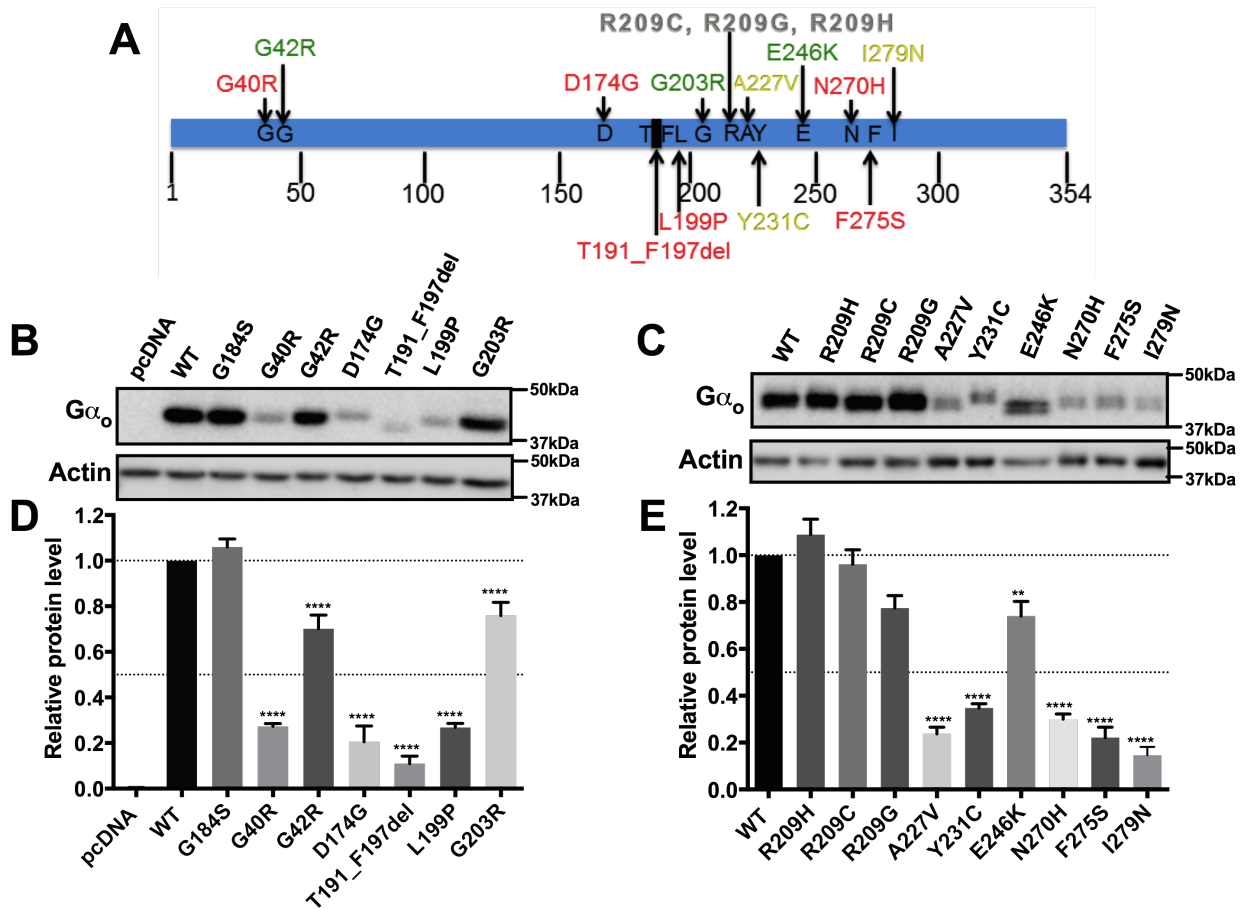


Figure 2.1 Location and protein expression levels of human *GNAO1* mutations related to epileptic encephalopathy.

(A) Location of 15 mutations (G40R, G42R, D174G, T191_F197del, L199P, G203R, R209C, R209G, R209H, A227V, Y231C, E246K, N270H, F275S, and I279N) mapped on the Gα_o amino acid sequence. (B, C) Representative Western blots of Gα_o protein expression from HEK293T cells transiently transfected with each Gα_o mutant. (D, E) Quantification of relative protein levels of each Gα_o mutant compared to WT Gα_o. Graphs are the result of 3 independent experiments and data are presented as mean ± SEM. p<0.01**, p<0.0001**** using One-way ANOVA with Bonferroni's post-hoc test for pairwise comparison.

2.4.2 Validation of an in vitro assay to assess function of *GNAO1* mutations

We used inhibition of forskolin-stimulated cAMP levels as a functional readout to allow efficient quantification of $G\alpha_o$ effects with full concentration curves for agonist-mediated signaling. We co-transfected $G\alpha_o$ plasmids with α_{2A} adrenergic receptor (α_{2A} AR) cDNA (Goldenstein et al., 2009). Robust inhibition of cAMP by the α_2 adrenergic agonist UK14,304 depends on both the transfected receptor and the $G\alpha_o$ protein (Figure S2.2A, S2.2B). A pertussis toxin (PTX)-insensitive $G\alpha_o$ (C351G) (Ikeda & Jeong, 2004) was used to create all mutant constructs and WT, enabling inactivation of endogenous $G_{i/o}$ proteins using PTX.

When PTX eliminates the inhibitory signaling through $G_{i/o}$, α_{2A} AR couples weakly to G_s and stimulates adenylate cyclase (AC) (Wade et al., 1999), resulting in increased cAMP levels after PTX treatment in the absence of a transfected $G\alpha_o$ (Figure S2.2B). Consequently, the fractional inhibition of AC by $G\alpha_o$ mutants was assessed as the decrease from the high control level of cAMP (PTX but no $G\alpha_o$ - 0%) to the low level with WT $G\alpha_o$ (PTX and PTXi $G\alpha_o$ - 100%). This is termed Normalized % inhibition. PTX treatment did not alter the ability of the PTX-insensitive $G\alpha_o$ to mediate α_{2A} AR-stimulated cAMP inhibition (Figure S2.2C). Hence, this is a good system to study functional consequences of $G\alpha_o$ mutations.

2.4.3 Nine *GNAO1* mutations result in loss- (LOF) or partial loss-of-function (PLOF)

Six mutants showed essentially complete loss-of-function (LOF) with normalized inhibition below 40% (Figure 2.2A and Table 2.1). All of these mutants also showed low expression levels (11-35% of control; Figure 2.1). Three mutants (A227V, Y231C, and I279N; Figure 2.2A, 2.2E and Table 2.1) had intermediate effects and were classified as partial loss-of-function (PLOF) mutants. The I279N mutation showed a modestly reduced maximal inhibition of cAMP levels (Figure 2.2E and Table 2.1). This mutant also produced a very low EC₅₀ value (0.7 nM vs 25 nM for WT Gα_o), which might explain the discrepancy between the quite low expression levels (15% of WT) while maintaining good maximal inhibition in the cAMP inhibition assay. Based on the maximum inhibition below 90% of control, however, we classified this mutation as PLOF (Tables 2.1 and 2.3).

The dominant nature of the clinical picture in the *GNAO1* encephalopathies raised the question of whether the LOF mutations are actually dominant negative mutations that interfere with the function of the remaining normal Gα_o protein expressed in heterozygous individuals. However, in co-expression studies of WT and mutant Gα_o at plasmid ratios of 1:1 or 1:2, there was no evidence of a dominant negative action (Figure S2.3). This suggests that the effect of LOF mutations is through a haploinsufficiency mechanism rather than a dominant negative one.

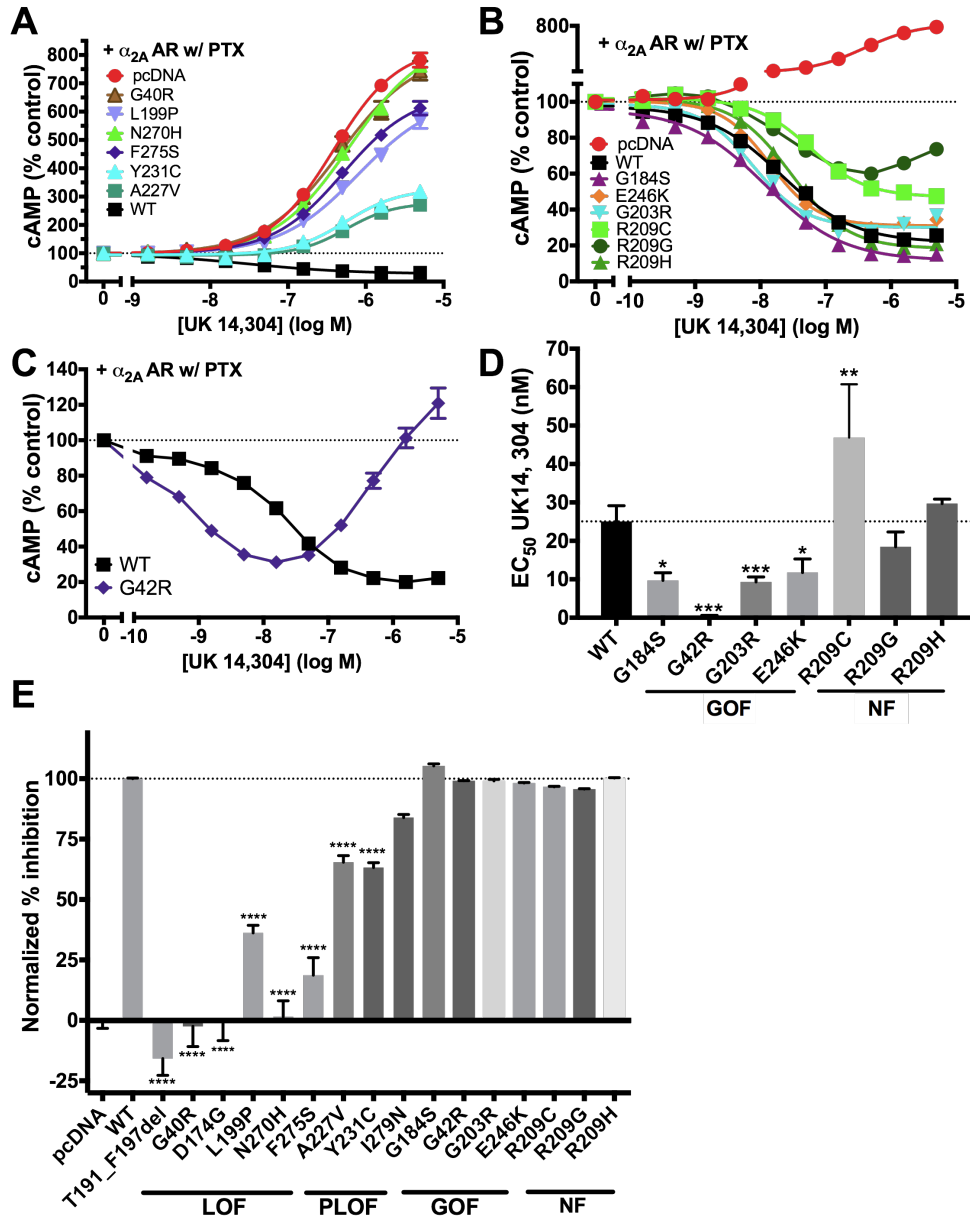


Figure 2.2 Effect on α_{2A} AR-mediated cAMP inhibition by *GNAO1* mutants.

(A-C) Dose-response curves of representative *GNAO1* mutants. **(A)** Dose-response curves of LOF and PLOF mutants (G40R, L199P, N270H, F275S, A227V, Y231C) showing changes in cAMP production in response to the AC activator forskolin and α_2 AR agonist UK14,304, compared to the positive control (WT) and negative control (pcDNA). **(B)** Dose-response curves of functioning $G\alpha_o$ mutants showing changes in cAMP production in response to the α_2 AR agonist UK14,304. All dose-response curves are shown in comparison with WT and G184S. **(C)** G42R displays a biphasic dose-response

Figure 2.2 (cont'd) curve with cAMP inhibition at low concentrations (GOF), followed by enhancement of cAMP levels at higher concentrations of UK14,304. (D) Quantification of EC₅₀ of functioning Gα_o mutants. G42R, G203R and E246K exhibit significantly increased potency for α_{2A} AR-mediated cAMP inhibition similar to the known GOF mutation G184S. p<0.05*, p<0.01**, p<0.001*** using paired t test between WT and each mutant separately (Figure S2.4). **E.** Percentage of maximum inhibition (n=5) was normalized to pcDNA (0%; resulting in activation of cAMP) and WT (100%). p<0.0001**** using One-way ANOVA with Bonferroni's post-hoc test for pairwise comparison. Note that the maximum inhibition of G42R was calculated at UK14,304 of 15.8 nM.

Table 2.1 Functional data for loss-of-function (LOF) and partial loss-of-function (PLOF) mutants.

Mutations			Expression (% of WT) [†]	cAMP at 5μM UK14,304 (% of un-stimulated) [†]	Normalized % inhibition [†]	LogEC ₅₀ [†]	EC ₅₀ (nM)
pcDNA (no Gα _o)			0	880 ± 30	0	-6.48 ± 0.05	526
WT			100	23 ± 1	100	-7.71 ± 0.07	25
118G>A	Gly40Arg	G40R	27 ± 1 ****	900 ± 70	-2 ± 8 ****	-6.52 ± 0.13	355
521A>G	Asp174Gly	D174G	21 ± 7 ****	250 ± 20	-1 ± 7 ****	-6.41 ± 0.19	502
517_592del	Thr191_Phe197del	T191_F197del	11 ± 3 ****	290 ± 20	-16 ± 7 ****	-6.36 ± 0.20	525
596T>C	Leu199Pro	L199P	27 ± 2 ****	570 ± 30	36 ± 3 ****	-6.12 ± 0.07	784
680C>T	Ala227Val	A227V	24 ± 3 ****	320 ± 20	65 ± 3 ****	-6.32 ± 0.13	586
808A>C	Asp270His	N270H	30 ± 2 ****	860 ± 60	2 ± 7 ****	-6.42 ± 0.16	499
692A>G	Tyr231Cys	Y231C	35 ± 2 ****	340 ± 20	63 ± 2 ****	-6.34 ± 0.06	472
824T>C	Phe275Ser	F275S	22 ± 4 ****	720 ± 60	19 ± 7 ****	-6.46 ± 0.12	395
836T>A	Ile279Asp	I279N	15 ± 4 ****	100 ± 10	84 ± 1	-9.18 ± 0.15	<u>0.7</u>

[†] Mean ± SEM; **, p < 0.01; ***, p < 0.001; ****, p < 0.0001, one-way ANOVA

2.4.4 Six *GNAO1* mutations result in gain-of-function (GOF) or normal function (NF)

Unexpectedly, a significant number of pathological *GNAO1* mutants showed essentially normal or even GOF behavior (Figure 2.2B-E and Table 2.2). As a benchmark for GOF behavior, we used our previously described RGS-insensitive G184S mutant (Fu et al., 2004; Goldenstein et al., 2009; Kehrl et al., 2014; Lan et al., 1998), which shows a mild seizure phenotype in mouse models (Kehrl et al., 2014). It produced a small increase in the maximum inhibition of forskolin-stimulated cAMP levels in response to UK14,304 (Table 2.2). More importantly, it had a significantly more potent response to the α_{2A} R agonist UK14,304 (Figure 2.2D & S2.4A). This represents a 2-3-fold increase in signal strength at low agonist concentrations. Three of the human pathological *GNAO1* mutants also showed GOF behavior by this criterion. The G203R, E246K and G42R mutants produced robust inhibition of cAMP with significantly lower EC_{50} values for the α_{2A} R agonist UK14,304 (Figure 2.2D, S2.4 and Table 2.2). G203R and E246K showed normal inhibition with modest decreases in EC_{50} (Table 2.2, Figure 2.2D, 2.2E and S.4). This is similar to the effect on EC_{50} seen for the *bona fide* GOF mutant G184S. The G42R mutant showed the lowest EC_{50} of any of the mutants (Figure S2.4), at least 50-fold lower than the WT protein (Figure 2.2C, 2.2D). However, the inhibition mediated by G42R is followed by activation of cAMP with increasing concentrations of UK14,304 (Figure 2.2C). The calculated Normalized % inhibition for

the G42R mutant is essentially identical to that of WT $G\alpha_o$ which combined with its very high potency for agonist-mediated inhibition suggests GOF behavior.

Three other patient-derived mutations (R209G, R209H, and R209C) showed almost completely normal function and nearly normal expression levels and are designated as normal function (NF) mutants (Figure 2.2B, 2.2D-E, S2.4, and Tables 2.2 & 2.3). The EC_{50} values for R209G and R209H mutant were not significantly different from WT, while the value for R209C was modestly but significantly higher (Table 2.2, Figure 2.2D & S2.4).

Table 2.2 Functional data for normal and gain-of-function (GOF) mutants.

Group			Expression (% of WT) ⁺	cAMP at 5 μ M UK14,304 (% of unstimulated) ⁺	Normalized % inhibition ⁺	LogEC ₅₀ ⁺	EC ₅₀ (nM)
pcDNA (no G α_o)			0	880 \pm 30	0	-6.48 \pm 0.05	525
WT			100	23 \pm 1	100	-7.71 \pm 0.07	25
550G>A ⁺⁺	Gly184Ser	G184S	105 \pm 5	15 \pm 1	108 \pm 0.1	-8.06 \pm 0.09 [†]	<u>9.7</u>
124G>C	Gly42Arg	G42R	70 \pm 6 ****	170 \pm 10	99 \pm 0.1	-9.34 \pm 0.09 ^{†††}	<u>0.5</u>
607G>A	Gly203Arg	G203R	72 \pm 9 ****	31 \pm 3	100 \pm 1.3	-8.06 \pm 0.06 ^{†††}	<u>9.3</u>
736G>A	Glu246Lys	E246K	74 \pm 6 **	39 \pm 2	98 \pm 0.2	-8.00 \pm 0.12 [†]	<u>12</u>
625C>G	Arg209Gly	R209G	77 \pm 5	74 \pm 4	96 \pm 0.2	-7.75 \pm 0.09	18
626G>A	Arg209His	R209H	109 \pm 7	21 \pm 1	100 \pm 0.1	-7.52 \pm 0.02	30
625C>T	Arg209Cys	R209C	96 \pm 6	52 \pm 2	97 \pm 0.2	-7.39 \pm 0.08 ^{††}	<u>47</u>

⁺ Mean \pm SEM; ⁺⁺ Not a human mutation; Underlined EC₅₀ Values are significantly different from that of WT; **, p < 0.01; ***, p < 0.001; ****, p < 0.0001, one-way ANOVA; [†], p < 0.05; ^{††}, p < 0.01; ^{†††}, p < 0.001 by paired t-test

Table 2.3 Correlation between cAMP inhibition and clinical diagnosis.

#	Human <i>GNAO1</i> Mutations			cAMP Inh.	Epilepsy	Movement Disorder	Age	Sex	Ref.
1	124G>C	Gly42Arg	G42R	GOF		++	Unknown	F	(Zhu et al., 2015)
2	736G>A	Glu246Lys	E246K	GOF		++	13 yrs	F	(Saitsu et al., 2016)
3	736G>A	Glu246Lys	E246K	GOF		++	5.5 yrs (twins)	M	(Ananth et al., 2016)
4	736G>A	Glu246Lys	E246K	GOF		++	5.5 yrs (twins)	F	(Ananth et al., 2016)
5	736G>A	Glu246Lys	E246K	GOF		++	Deceased at 10 yrs 3 months	F	(Ananth et al., 2016)
6	736G>A	Glu246Lys	E246K	GOF		++	15 yrs	M	(Ananth et al., 2016)
7	625C>G	Arg209Gly	R209G	NF		++	Deceased at 4 yrs 7 months	F	(Ananth et al., 2016)
8	626G>A	Arg209His	R209H	NF		++	16 yrs	M	(Ananth et al., 2016)

Table 2.3 (cont'd)

9	626G>A	Arg209His	R209H	NF		++	8 yrs	M	(Kulkarni et al., 2016)
10	626G>A	Arg209His	R209H	NF		++	6yrs	M	(Kulkarni et al., 2016)
11	626G>A	Arg209His	R209H	NF		++	5 yrs	M	(Radhika Dhamija, 2016)
12	625C>T	Arg209Cys	R209C	NF	+	++	18 yrs	F	(Saitsumi et al., 2016)
13	607G>A	Gly203Arg	G203R	GOF	++	++	8 yrs	F	(Nakamura et al., 2013)
14	607G>A	Gly203Arg	G203R	GOF	+	++	14 months	F	(Saitsumi et al., 2016)
15	607G>A	Gly203Arg	G203R	GOF	++	++	3 yrs	F	(Dietel, 2016)
16	692A>G	Tyr231Cys	Y231C	PLOF	++		4 yrs 9 months	F	(Talvik, 2015)
17	680C>T	Ala227Val	A227V	PLOF	++		20 months	F	(Saitsumi et al., 2016)

Table 2.3 (cont'd)

18	836T>A	Ile279Asp	I279N	PLOF	++		13 yrs	F	(Nakamura et al., 2013)
19	836T>A	Ile279Asp	I279N	PLOF	++		2 yrs	M	(EpiKCEaekce, 2016)
20	118G>A	Gly40Arg	G40R	LOF	++		10 months	F	(Law et al., 2015)
21	521A>G	Asp174Gly	D174G	LOF	++		4 yrs 1 month	F	(Nakamura et al., 2013)
22	517_59 2del	Thr191_ Phe197del	T191_ F197del	LOF	++	+	Deceased at 11 months	F	(Nakamura et al., 2013)
23	596T>C	Leu199Pro	L199P	LOF	++	+	20 months	F	(Marce-Grau et al., 2016)
24	824T>C	Phe275Ser	F275S	LOF	++		9 yrs	F	(Allen et al., 2013)
25	808A>C	Asp270His	N270H	LOF	++		3 yrs	F	(Consortium et al., 2014)

GOF: gain of function; **NF**: normal function; **PLOF**: partial loss of function; **LOF**: loss of function. ++: major symptoms, +: minor symptoms

2.4.5 Clinical correlation with biochemical behavior of mutant *GNAO1* alleles

To address genotype/phenotype correlations for *GNAO1* encephalopathy, we reviewed the case reports of all 25 individuals who had *GNAO1* mutations that had been reported by April, 2016. They have a range of clinical patterns, which extend from early severe epileptic encephalopathy with prominent tonic seizure activity to individuals with a dominant choreo-athetotic movement disorder with virtually no evidence of seizures. There are also individuals (Dietel, 2016; Saitsu et al., 2016), including one of the original 4 cases (Nakamura et al., 2013) (patient #13 – G203R; Table 2.3), who had multiple seizures but also showed prominent choreo-athetosis.

In 2016, a clinical report (Ananth et al., 2016) described a unique series of 6 patients with *GNAO1* mutations and a pronounced movement disorder, virtually without seizures. They had global developmental delay and hypotonia from infancy and all developed chorea by ages 4-11. In the majority of cases it was intractable, leading to death in two cases. Four patients carried the E246K allele, which we have found to be a GOF mutation. The other two mutations found in this group (R209G and R209C) exhibited essentially normal function in our cAMP inhibition measurements. There are several other reports (Allen et al., 2013; Ananth et al., 2016; Consortium et al., 2014; Epi KCEaekce, 2016; Kulkarni et al., 2016; Law et al., 2015; Marce-Grau et al., 2016; Saitsu et al., 2016; Talvik, 2015; Zhu et al., 2015) of *GNAO1* mutations in individuals with a predominant movement disorder with or without seizures. This distinction of clinical

patterns based on certain mutant alleles in *GNAO1* encephalopathy patients was noted very recently (Menke et al., 2016) but without information about biochemical mechanisms. Table 2.3 summarizes the $G\alpha_o$ biochemical function from the present report and its relation to seizure disorder or movement disorder in literature reports for these mutations. GOF and NF mutations are nearly always found when movement disorder is the predominant feature of the clinical pattern. Mutations that have pure LOF or PLOF biochemical phenotypes are seen in individuals with epileptic encephalopathy without pronounced choreoathetosis. A number of patients exhibit both seizures and movement disorder. We have indicated in Table 2.3 with + or ++ which of these features is predominant or less so. Further studies will be needed based on new cases and/or additional mutations, but there does appear to be a clear pattern emerging about a genotype-phenotype correlation that is driven by a GOF/LOF difference in mutant *GNAO1* alleles.

2.4.6 Location of mutations linked to *GNAO1* encephalopathies in the $G\alpha_o$ protein

To investigate the structural basis for the effects of mutations in $G\alpha_o$, the mutations were modelled onto the published crystal structure of $G\alpha_o$ in complex with RGS16 (PDB: 3C7K; Figure S2.5). The locations of mutations within the $G\alpha_o$ structure segregated according to their function. The GOF mutations are all near G184S and close to the ribose and phosphate moieties of the bound GDP. The LOF mutants are more broadly scattered throughout the GTPase domain and may destabilize protein folding or stability

consistent with their markedly reduced expression levels. The PLOF mutations are clustered in the GTPase domain but away from the bound GDP. This striking structure-function correlation may facilitate prediction of the function of new mutations but ultimately a rigorous biochemical analysis will provide definitive understanding of function.

2.5 Discussion

The concept of a “*GNAO1* encephalopathy” has developed based on the identification of at least 15 different mutations in the *GNAO1* gene (Allen et al., 2013; Ananth et al., 2016; Consortium et al., 2014; Epi KCEaekce, 2016; Kulkarni et al., 2016; Law et al., 2015; Marce-Grau et al., 2016; Nakamura et al., 2013; Saitsu et al., 2016; Talvik, 2015; Zhu et al., 2015) associated with various combinations of epilepsy, developmental delay, hypotonia, and choreo-athetotic movement disorders. Our study demonstrates GOF as well as LOF mutations in *GNAO1* and describes a clear correlation between biochemical and clinical characteristics. The existence of these unexpected GOF mutations has important therapeutic implications. Specifically, one might expect that different approaches to therapy would be needed for different mutations (i.e. agonists for LOF and antagonists for GOF mutants).

We chose inhibition of cAMP production as the functional readout to assess the $G\alpha_o$ mutants because of the robust measurements permitting complete agonist concentration-response studies. This was critical to our findings since the GOF mutants

were detected primarily through their ability to increase signals at low agonist concentrations (Figure 2.2 and Table 2.2). Our previously studied GOF mutant (G184S) which is insensitive to the inhibitory influence of RGS proteins shows such a “left-shift” of agonist concentration response curves *in vitro* (Clark, Harrison, Zhong, Neubig, & Traynor, 2003; Fu et al., 2004) and *in vivo* (Goldenstein et al., 2009; Lamberts et al., 2013), and also has a mild seizure phenotype in a mouse model (Kehrl et al., 2014). One might argue that cAMP is not the best choice of functional measures for epilepsy since N-type Ca^{++} channels or the synaptic release mechanism proteins are critical for regulation of neurotransmitter release. However, the apparent correlation of clinical patterns with the biochemical behavior in our cAMP assay does suggest that function assessed in this way is relevant to functionality in humans. The clear pathological effect of the R209 mutations (with at least 3 individuals carrying distinct alleles), however, does raise the question of why a protein with normal expression and function would cause pathology. It is possible that the R209 mutations have a selective loss of one of the other functional outputs while retaining a normal ability to inhibit AC. Alternatively; there may be selective alterations in expression or localization in neurons that are not accurately reflected in our HEK-293T cell studies of cAMP regulation. A full understanding of the causal mechanisms in *GNAO1* encephalopathies requires additional studies of these mutant $\text{G}\alpha_0$ proteins in neurons and with different functional readouts.

The locations of mutations in the protein structure may partially explain their

functional influences. All functioning mutants (NF and GOF) are located around the RGS binding domain, while most of the LOF or PLOF mutants are near the GDP binding region. Two exceptions are D174G and T191_F197del. D174 forms a salt bridge with R162 and mutations in this position may disrupt this interaction. T191_F197del truncates two beta sheets as well as their linking region, which would be expected to decrease protein stability of $G\alpha_o$.

A dominant genetic effect from GOF mutants is not unusual but the fact that the LOF mutations result in a severe autosomal dominant disorder is a bit surprising. We have ruled out a biochemical dominant negative mechanism of these mutations, at least for cAMP regulation, suggesting a haploinsufficiency mechanism. In mice, homozygous $G\alpha_o$ knockouts exhibit seizures as well as hyperactive turning behavior (Jiang et al., 1998). We did not, however, observe spontaneous seizures or an increased sensitivity to pentylenetetrazol (PTZ) kindling in heterozygous *Gnao1*^{+/-} knockouts (Kehrl et al., 2014). This suggests that humans are more susceptible to haploinsufficiency of $G\alpha_o$ than are mice. In contrast, we observed enhanced kindling sensitivity and reduced survival in our *Gnao1*^{+/^{G184S}} knock-in mouse model possibly due to seizures (Kehrl et al., 2014). Furthermore, these mice display early neonatal lethality (Kehrl et al., 2014) of unclear mechanism which may be similar to the hypotonia seen in human patients carrying GOF mutations. We do not know whether the abnormalities in these mice are due to brain developmental abnormalities or acute signaling effects. Further studies are needed to

better understand this and to determine whether our *Gnao1*^{+/*G184S*} mutant mouse might represent a useful pre-clinical model for individuals with *GNAO1* GOF mutations.

To date, all characterized *GNAO1* mutants have been reported as LOF mutations. The G203R mutant in the original paper (Nakamura et al., 2013) was reported as a LOF mutant for regulation of N-type Ca⁺⁺ channels. Similarly, a G42R mutation in Gα_{i1} was reported as a LOF mutant based on biochemical studies (Bosch et al., 2012). The unique approach that we have taken with detailed cAMP dose-response studies in a mammalian cell model permitted our recognition of the GOF mechanisms (e.g. the Gα_o G42R mutation). The patient with the G203R mutation, which we found to have GOF for cAMP inhibition, had a very different clinical pattern than the other 3 patients in the original study. She had a much later onset of disease (7 months) as well as developmental delay and severe chorea with only localized seizures (Nakamura et al., 2013). A similar clinical pattern was observed in two more, recently described, patients with this same mutation (Dietel, 2016; Saitsu et al., 2016). All patients carrying the GOF mutations identified here appear distinct from the strict EIEE pattern (see Table 3). In comparison, patients with LOF or PLOF mutations were diagnosed with either Ohtahara syndrome (Y231C, I279N, D174G, T191_F197del) or early-infantile epileptic encephalopathy (A227V, L199P, N270H, F275S). Thus GOF and LOF mutations in Gα_o appear to result in different disease mechanisms likely requiring different therapeutic approaches.

It has remained challenging to convert knowledge about genetic epilepsy mutations

into therapies. The *GNAO1* encephalopathies may be different because of the eminently targettable nature of the receptors that drive $G\alpha_o$ signaling pathways. A critical question then becomes which receptors might be involved. Interestingly, activation of many $G_{i/o}$ -coupled receptors is associated with suppression of seizures. Adenosine A1 receptors may play a role in the efficacy of the ketogenic diet (Masino et al., 2011) and agonists at group II metabotropic glutamate receptors are anticonvulsant in various models (Dalby & Thomsen, 1996). The opposite situation is also seen; $GABA_B$ R agonists exacerbate absence seizures while $GABA_B$ R antagonists suppress them (Han HA, 2012). Identifying which receptors or downstream signaling effectors of $G\alpha_o$ contribute to mechanisms of encephalopathy from LOF or GOF *GNAO1* mutations could therefore reveal potential targets for novel anti-convulsant drug development.

We have identified distinct biochemical mechanisms of pathogenic human *GNAO1* mutations that may improve the understanding of the heterogeneous clinical spectrum of *GNAO1*-associated epilepsy and movement disorders. Furthermore, these results also carry significant implications for personalized therapeutics in *GNAO1* encephalopathies.

APPENDICES

APPENDIX A

SUPPLEMENTAL DATA

Table S2.1 Primer sequences for mutagenesis to create *GNAO1* mutants.

Mutation		Primer Sequences
Protein	DNA	
R209H (Arg209His)	626 G>A	F: 5'-GTGGATCCACTTCTTGTGTTTCAGATCGCTGGCC-3' R: 5'-GGCCAGCGATCTGAACACAAGAAGTGGATCCAC-3'
G203R (Gly203Arg)	607 G>A	F: 5'-AGATCGCTGGCCTCTGACGTCAAACAGCC-3', R: 5'-GGCTCTTTGACGTCAGAGGCCAGCGATCT-3'
E246K (Glu246Lys)	736 G>A	F: 5'-AAGAGCATGAGAGACTTGTGCATGCGGTTTCGTG-3' R: 5'-CACGAACCGCATGCACAAGTCTCTCATGCTCTT-3'
G42R (Gly42Arg)	124 G>C	F: 5'-TTTTTCCTGATTCTCGAGCCCCCAGCAGGAG-3' R: 5'-CTCCTGCTGGGGGCTCGAGAATCAGGAAAAA-3'
R209C (Arg209Cys)	625 C>T	F: 5'-GATCCACTTCTTGCATTCAGATCGCTGGCCCC-3' R: 5'-GGGGCCAGCGATCTGAATGCAAGAAGTGGATC-3'
I279N (Ile279Asp)	836T >A	F: 5'-GTCAAAGGTGACTTCTTGTTCCTTCTCGCCAAAGAGA-3' R: 5'-ATCTCTTTGGCGAGAAGAACAAGAAGTCACCTTTGAC-3'
T191_F197del (Thr191_Phe197del)	572_ 592d el	F: 5'-GCATCGTAGAAACCCACTTCAGGCTGTTTGACGTC-3', R: 5'-GACGTCAAACAGCCTGAAGTGGGTTTCTACGATGC-3'
R209G (Arg209Gly)	625 C>G	Forward 5'-ATCCACTTCTTGCCTTCAGATCGCTGGCCCC-3' Reverse 5'-GGGCCAGCGATCTGAAGGCAAGAAGTGGAT-3'
A227V (Ala227Val)	680 C>T	F: 5'-GGTCATAGCCGCTGAGTACGACACAGAAGATGATG-3', R: 5'-CATCATCTTCTGTGTCGTACTIONCAGCGGCTATGACC-3'
F275S (Phe275Ser)	824T >C	F: 5'-ATCTTCTCGCCAGAGAGGTCTTTCTTGTGAGGAAG-3', R: 5'-CATTCTCAACAAGAAAGACCTCTCTGGCGAGAAGAT-3'
N270H (Asp270His)	808A >C	F: 5'-CAAAGAGGTCTTTCTTGTGGAGGAAGAGGATGATGGA-3 R: 5'-TCCATCATCCTCTTCTCCACAAGAAAGACCTCTTTG-3'
G40R (Gly40Arg)	118 G>A	F: 5'-CCTGATTCTCCAGCCCTCAGCAGGAGTAATTTTC-3' R: 5'-GAAATTACTCCTGCTGAGGGCTGGAGAATCAGG-3'

Table S2.1 (cont'd)

D174G (Asp174Gly)	521A>G	F: 5'-GGTTCGGAGGATGCCCTGCTCGGTGGG-3', R: 5'-CCCACCGCGCAGGGCATCCTCCGAACC-3'
L199P (Leu199Pro)	596T>C	F: 5'-CCCCGACGTCAAACGGCCTGAAGTGGAGG-3' R: 5'-CCTCCACTTCAGGCCGTTTGACGTCGGGG-3'
Y231C (Tyr231Cys)	692A>G	F: 5'-AGCACCTGGTCACAGCCGCTGAGTGCG-3' R: 5'-CGCACTCAGCGGCTGTGACCAGGTGCT-3'

```

                                G40R G42R
Gαo HUMAN NP_066268 MGCTLSAEERAALERSKAIEKNLKEDGISAAKDVKLLLLGAGESGKSTIVKQMKIIHEDG 60
Gαo MOUSE NP_034438 MGCTLSAEERAALERSKAIEKNLKEDGISAAKDVKLLLLGAGESGKSTIVKQMKIIHEDG 60
*****

Gαo HUMAN NP_066268 FSGEDVKQYKPVVYSNTIQSLAAIVRAMDTLGIEYGDKERKADAKMVCDDVSRMEDTEPF 120
Gαo MOUSE NP_034438 FSGEDVKQYKPVVYSNTIQSLAAIVRAMDTLGVEYGDKERKTD SKMVCDDVSRMEDTEPF 120
*****

                                D174G
Gαo HUMAN NP_066268 SAELLSAMMRLWGD SGIQECFNRSREYQLNDSAKY YLDSLDRIGAADYQPT EQDILRTRV 180
Gαo MOUSE NP_034438 SAELLSAMMRLWGD SGIQECFNRSREYQLNDSAKY YLDSLDRIGAGDYQPT EQDILRTRV 180
*****

G184S ΔT191-F197 L199P G203R/T R209G/H/C A227V Y231C
Gαo HUMAN NP_066268 KTTGIVETHFTFKNLHFR LFDVGGQRSE RKKWIHCFEDVTA IIFCVALS GYDQVLHEDET 240
Gαo MOUSE NP_034438 KTTGIVETHFTFKNLHFR LFDVGGQRSE RKKWIHCFEDVTA IIFCVALS GYDQVLHEDET 240
*****

E246K N270H F275S I279N
Gαo HUMAN NP_066268 TNRMHESLMLFDS ICNKNKFFIDT SII LFLNKKDL FGEKIKKSPL TICFPEY TGPNTYEDA 300
Gαo MOUSE NP_034438 TNRMHESLMLFDS ICNKNKFFIDT SII LFLNKKDL FGEKIKKSPL TICFPEY PGSNTYEDA 300
*****

Gαo HUMAN NP_066268 AAYIQAQFESKNRSPNKEIYCHMTCATDTNNIQVV FDAVTDII IANNL RGCGLY 354
Gαo MOUSE NP_034438 AAYIQTFESKNRSPNKEIYCHMTCATDTNNIQVV FDAVTDII IANNL RGCGLY 354
*****

```

Figure S2.1 Alignment of the human and mouse Gα_o protein sequences.

Human Gα_o (NCBI accession number NP_066268.1) and mouse Gα_o (NCBI accession number NP_034438.1) were aligned using Clustal Omega(Sievers et al., 2011). The Sequences are 98% identical at the protein level. All the mutations in the current study are highlighted in blue and the inter-species homology is 100% in all those positions. The known gain-of-function mutation G184S is highlighted in green.

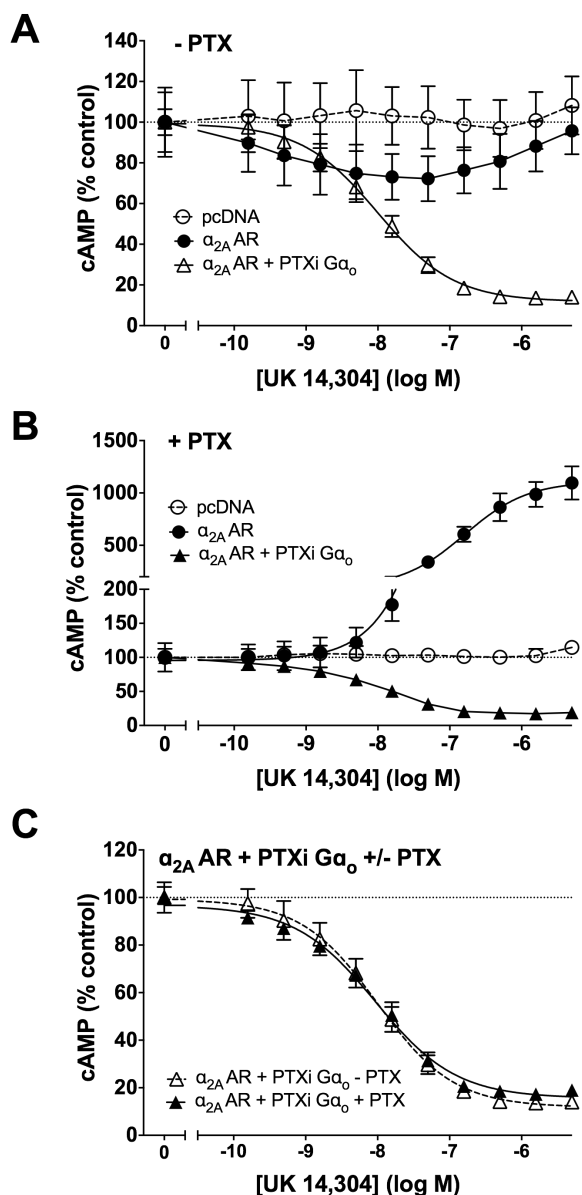


Figure S2.2 Validation of the Lance Ultra cAMP assay with transient transfection of α_{2A} adrenergic receptor (α_{2A} AR) and Pertussis toxin (PTX)-insensitive $G\alpha_o$. (A) Co-expression of both α_{2A} AR and $G\alpha_o$ C351G (PTX insensitive) results in strong inhibition of forskolin-stimulated cAMP levels. In the absence of $G\alpha_o$ the α_{2A} AR produces a very modest inhibitory effect. (n=3). (B) α_{2A} AR activation results in cAMP activation in the presence of PTX (n=3). (C) Dose-response curves of co-expression of α_{2A} AR and $G\alpha_o$ C351G exhibit similar EC_{50} in the absence and presence of PTX (with PTX EC_{50} =9.4nM; without PTX EC_{50} =9.9nM, n=3).

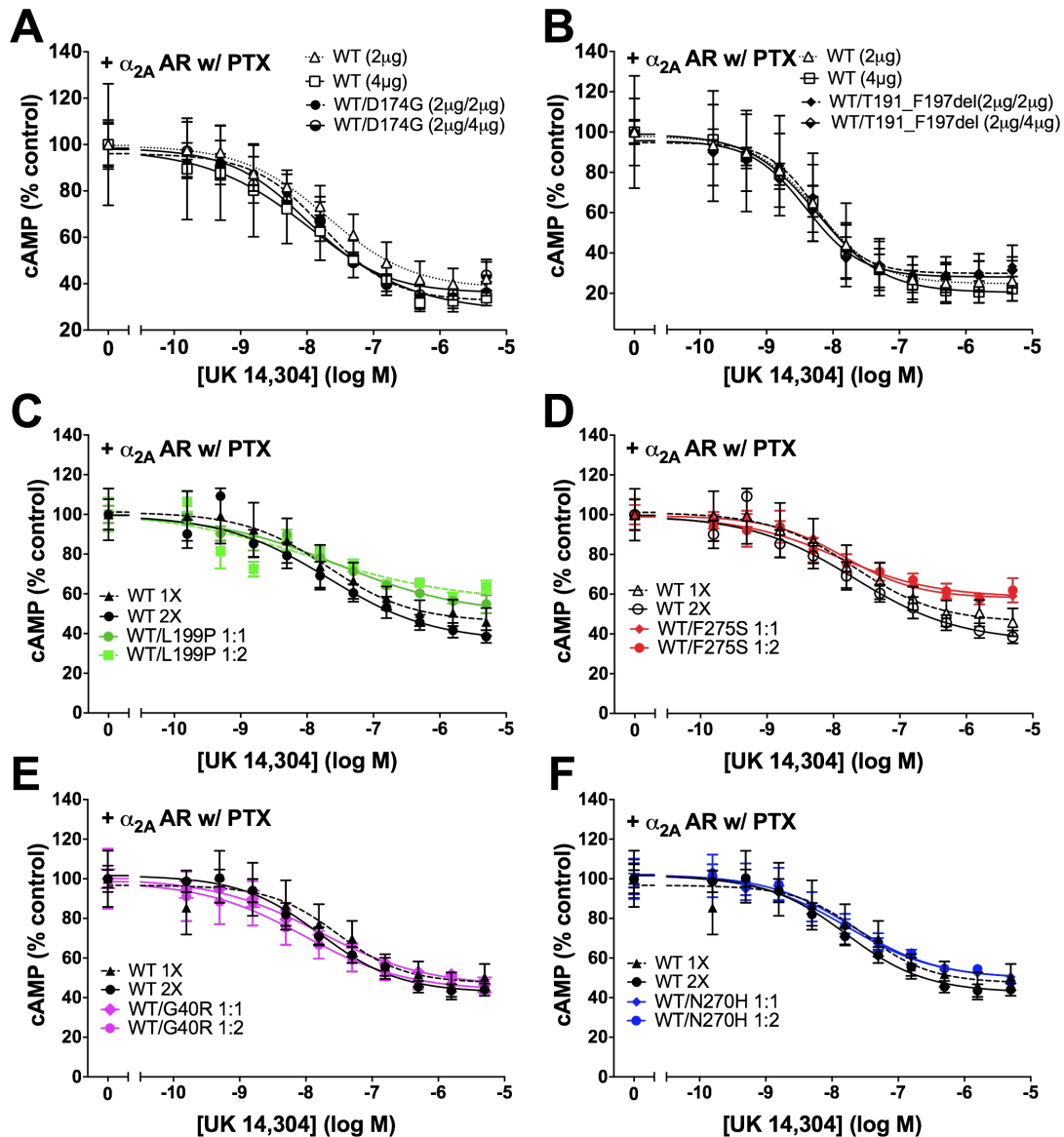


Figure S2.3 Assessment of dominant-negative effect of complete LOF mutants G40R, N270H, D174G, T191_F197del, L199P, and F275S.

(A) Dose response curves of changes in cAMP production of HEK293T cells co-transfected with different combinations of WT/D174G and α_{2A} AR. D174G did not show an increase of inhibition when co-transfected with WT in different concentrations (n=3). (B) Dose response curves of changes in cAMP production of HEK293T cells co-transfected with different combination of WT/T191_F197del and α_{2A} AR. Although a slight upward shift was observed with WT/T191_F197del 2 μ g/4 μ g, the trend did not continue with WT/T191_F197del 2 μ g/4 μ g (n=3). (C) Dose response curves of changes

Figure S2.3 (cont'd) in cAMP production of HEK293T cells co-transfected with different combination of WT/L199P and α_{2A} AR (n=2). (D) Dose response curves of changes in cAMP production of HEK293T cells co-transfected with different combination of WT/F275S and α_{2A} AR (n=2). (E) Dose response curves of changes in cAMP production of HEK293T cells co-transfected with different combination of WT/G40R and α_{2A} AR (n=2). (F) Dose response curves of changes in cAMP production of HEK293T cells co-transfected with different combinations of WT/N270H and α_{2A} AR (n=2).

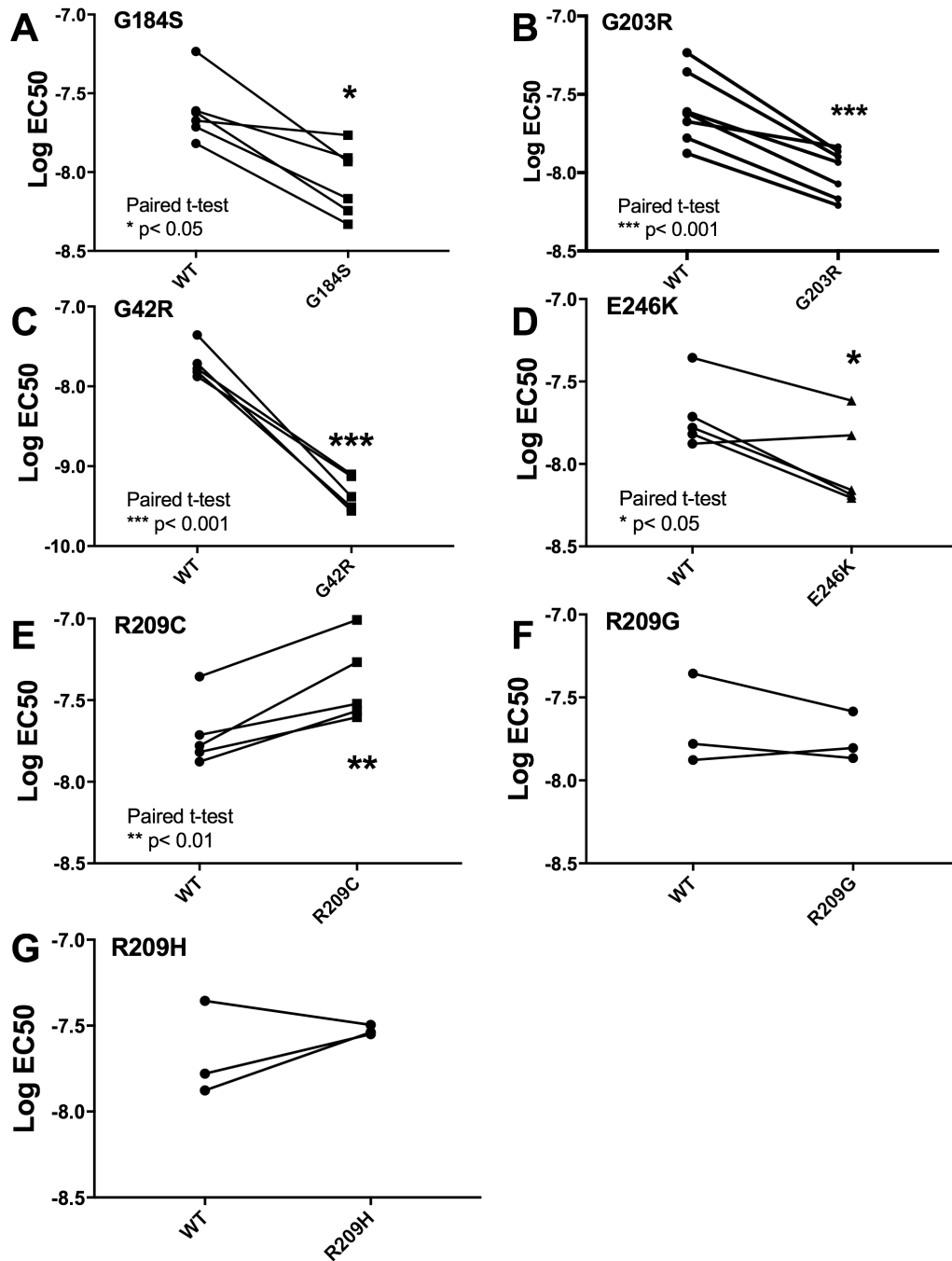


Figure S2.4 Paired t-test analysis of LogEC₅₀ values for normal and GOF mutants.

(A-D) Apart from the known gain of function mutant G184S, G42R, G203R and E246K show a significant decrease of EC₅₀ (n=5). (E) R209C shows an increase of EC₅₀ (n=5). (F, G) R209G and R209H do not display any significant change in EC₅₀ (n=3).

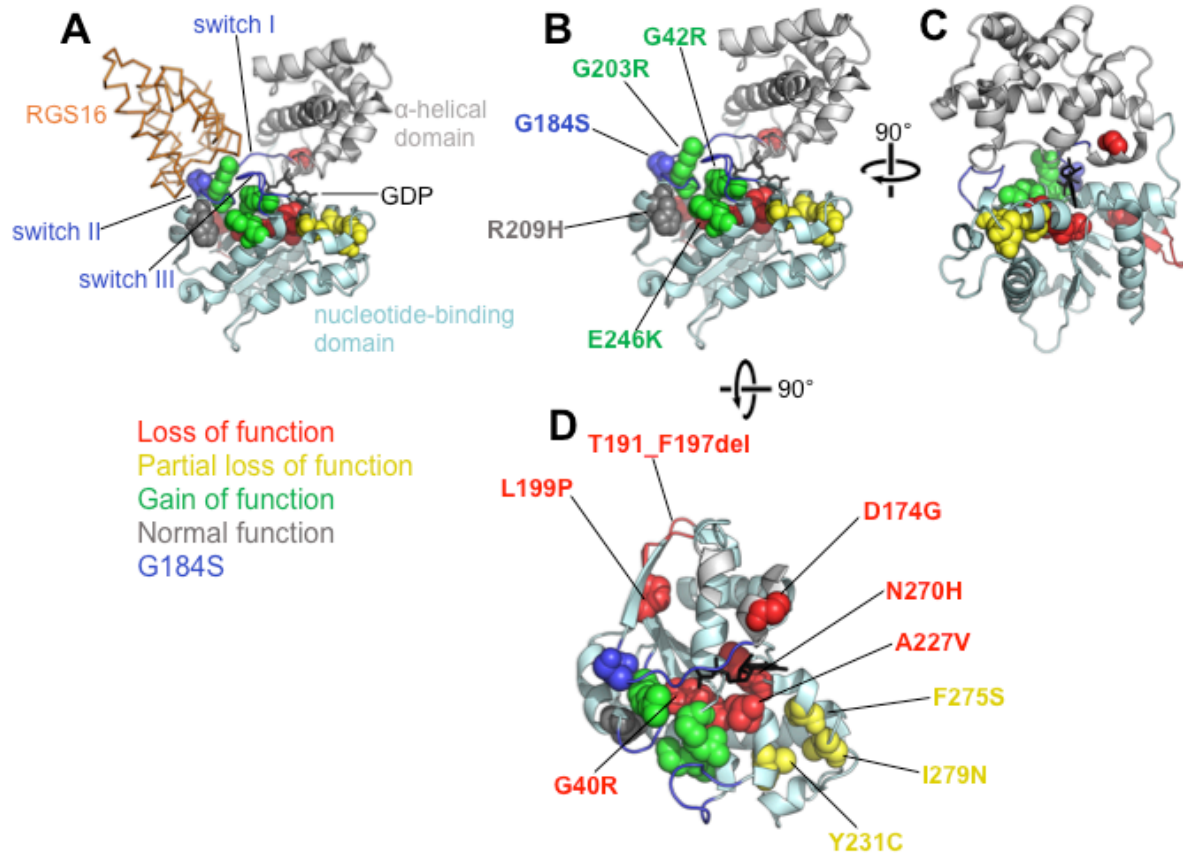


Figure S2.5 Mapping of mutations on the structure of $G\alpha_o$ -GDP bound to RGS16.

(A) $G\alpha_o$ -GDP · RGS16 complex with the nucleotide-binding domain in cyan, α -helical domain in grey, switch regions in blue and RGS16 in orange (PDB: 3C7K). (B-D) Localization of mutations on the $G\alpha_o$ -GDP complex. LOF mutants are in red, PLOF mutants are in yellow, GOF mutants are in green and NF mutants are in grey. Each mutant presented in the structure has been changed to its mutated amino acid. (B) R209H serves as a representative to all three mutants at R²⁰⁹. (D) T191_F197del has only been labeled out in red. Protein structure adapted from Slep *et al.* (Slep *et al.*, 2008) using Pymol (The PyMOL Molecular Graphics System, Version 1.8 Schrödinger, LLC)

APPENDIX B

VALIDATION OF THE GENOTYPE-PHENOTYPE CORRELATION OF *GNAO1*-ASSOCIATED NEUROLOGICAL DISORDERS

Since the first fifteen *GNAO1* mutations covered by our previous study (Feng et al., 2017), many more *GNAO1* mutations have been reported. To validate our genotype-phenotype correlation model, we have tested twenty-five newly reported mutations' functional changes using our cAMP assay. Previously, we used HEK293T cells transiently transfected with $\alpha_{2A}R$ and $G\alpha_o$ proteins for all of our assays. However, in HEK293T cells, $\alpha_{2A}R$ couples to $G\alpha_s$ when the system lacks $G\alpha_i$ or $G\alpha_o$ protein (Figure S2.6C) (Wade et al., 1999). This complicates the interpretation of the results. When HEK293T cells are transfected with LOF mutations or only pcDNA, stimulation of the $\alpha_{2A}R$ results in an increase in cAMP concentration (Figure S2.6C). Here we used another HEK cell line without the $G\alpha_s$ protein (kindly provided by Dr. Kirill Martemyanov from the Scripps Institute; *GNAS* KO cell line; Figure S2.6) (Masuho et al., 2018), and tested the functions of newly reported *GNAO1* mutations. The maximum inhibition of cAMP is less prominent in the *GNAS* KO cell line (Figure S2.6A & S2.6B). However, in this new system, non-functioning mutations transfected cells, including cells only transfected with pcDNA and $\alpha_{2A}R$, show no effects on cAMP production (Figure S2.6C, S2.6D & S2.7F, S2.8D). The functioning mutations inhibited the cAMP production when $\alpha_{2A}R$ was activated by UK14,304 (Figure S2.6B, D, F & S2.7E & S2.8C). One interesting aspect using the *GNAS* KO cell line is that there is a clear rightward shift in the concentration-response curve when the system contains more $G\alpha_o$ protein (Figure S2.6B: without PTX, EC_{50} for $\alpha_{2A}R$ vs EC_{50} for $\alpha_{2A}R + G\alpha_o$: 1.2 nM vs 10.6 nM); S2.6F: EC_{50} for

$\alpha_{2A}R + G\alpha_o - PTX$ vs EC_{50} for $\alpha_{2A}R + G\alpha_o + PTX$: 10.6 nM vs 42.6 nM). This rightward shift can be explained by the $G\beta\gamma$ -mediated cAMP inhibition.

All adenylyl cyclase (AC) isoforms can be stimulated by forskolin, however, stimulated AC activities can be further regulated in a subtype specific manner (Ammer & Christ, 2002). For example, type I AC not only can be inhibited by $G\alpha_o$, but also by $G\beta\gamma$ directly (Bayewitch et al., 1998a; Taussig, Quarmby, & Gilman, 1993), while type V AC is not affected by $G\alpha_o$ but can be inhibited by $G\alpha_i$ subunits and $G\beta\gamma$ (Bayewitch et al., 1998b; Taussig & Gilman, 1995). $G\beta\gamma$ subunits exhibit a surprising stimulatory effect on type II and type IV ACs, although this effect is highly conditional and only detectable with the presence of $G\alpha_s$ (Bayewitch et al., 1998a; Gao & Gilman, 1991; Tang & Gilman, 1991; Taussig & Gilman, 1995). In particular, stimulation of type II AC by $G\beta\gamma$ requires a significantly higher concentration of $G\beta\gamma$ than $G\alpha_s$ (Taussig & Gilman, 1995). Human kidney, from which HEK293 cells are developed, mainly expresses Type VI AC (Defer, Best-Belpomme, & Hanoune, 2000), which can be inhibited by $G\beta\gamma$ dimers (Bayewitch et al., 1998b). It is possible that in this system $G\alpha_o$ functions as a restraint for $G\beta\gamma$'s inhibition of AC; therefore with more $G\alpha_o$ present, the EC_{50} increases significantly.

Similar to our previously described trend, functioning $G\alpha_o$ mutants showed a relatively normal protein expression pattern comparing to WT $G\alpha_o$ (Figure S2.7A, C & S2.8A, B) with the exception of Q223P (Figure S2.7; 0.066 ± 0.019). Non-functioning *GNAO1* mutations all exhibited significantly reduced protein expression pattern (Figure

S2.7B, D & S2.8A, B). Some of the mutant alleles identified were obtained from genomic database or personal communication from families so clinical information is limited in these cases.

However, it is still clear that functioning *GNAO1* mutations are associated with movement disorder patients, while non-functioning *GNAO1* mutations are mainly related to the onset of epilepsy (Table S2.4). The genotype-phenotype between the mutation functions and the onset of epilepsy or movement disorders still stand with the new HEK cell line (Table S2.4).

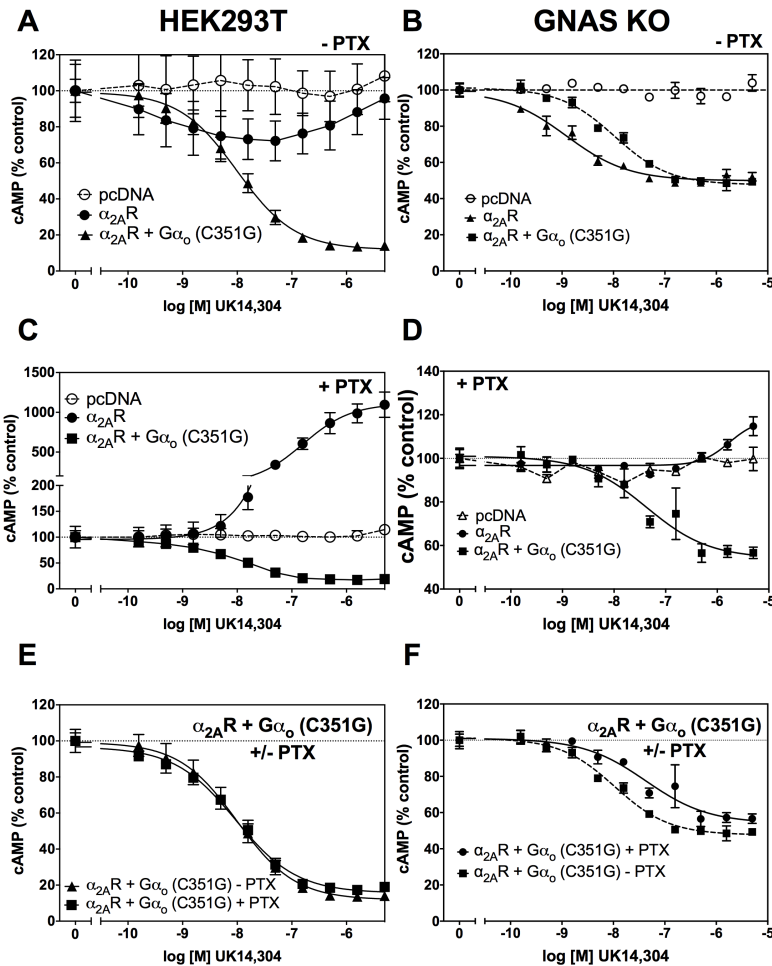


Figure S2.6 Comparison of validation of the Lance Ultra cAMP assay between HEK293T and GNAS KO HEK293 cells with transient transfection of α_{2A} adrenergic receptor ($\alpha_{2A}R$) and Pertussis toxin (PTX)-insensitive $G\alpha_o$. Figure S2.6A, S2.6C, & S2.6E are taken from Figure S2.2. (A, B) Co-expression of both $\alpha_{2A}R$ and $G\alpha_o$ C351G (PTX insensitive) results in strong inhibition of forskolin-stimulated cAMP levels in both cell lines. In the absence of $G\alpha_o$ the $\alpha_{2A}R$ produces a very modest inhibitory effect in HEK 293T cells but a strong inhibition effect in GNAS KO cells ($n=3$). (C, D) $\alpha_{2A}R$ activation results in cAMP activation in the presence of PTX in HEK293T but no effect in GNAS KO cells due to the lack of $G\alpha_s$ ($n=3$). (E, F) Dose-response curves of co-expression of $\alpha_{2A}R$ and $G\alpha_o$ C351G exhibit similar EC_{50} in the absence and presence of PTX in both cell line (HEK 293T: with PTX $EC_{50}=9.4$ nM; without PTX $EC_{50}=9.9$ nM, $n=3$. GNAS KO: with PTX $EC_{50}=42.6$ nM; without PTX $EC_{50}=10.6$ nM, $n=3$).

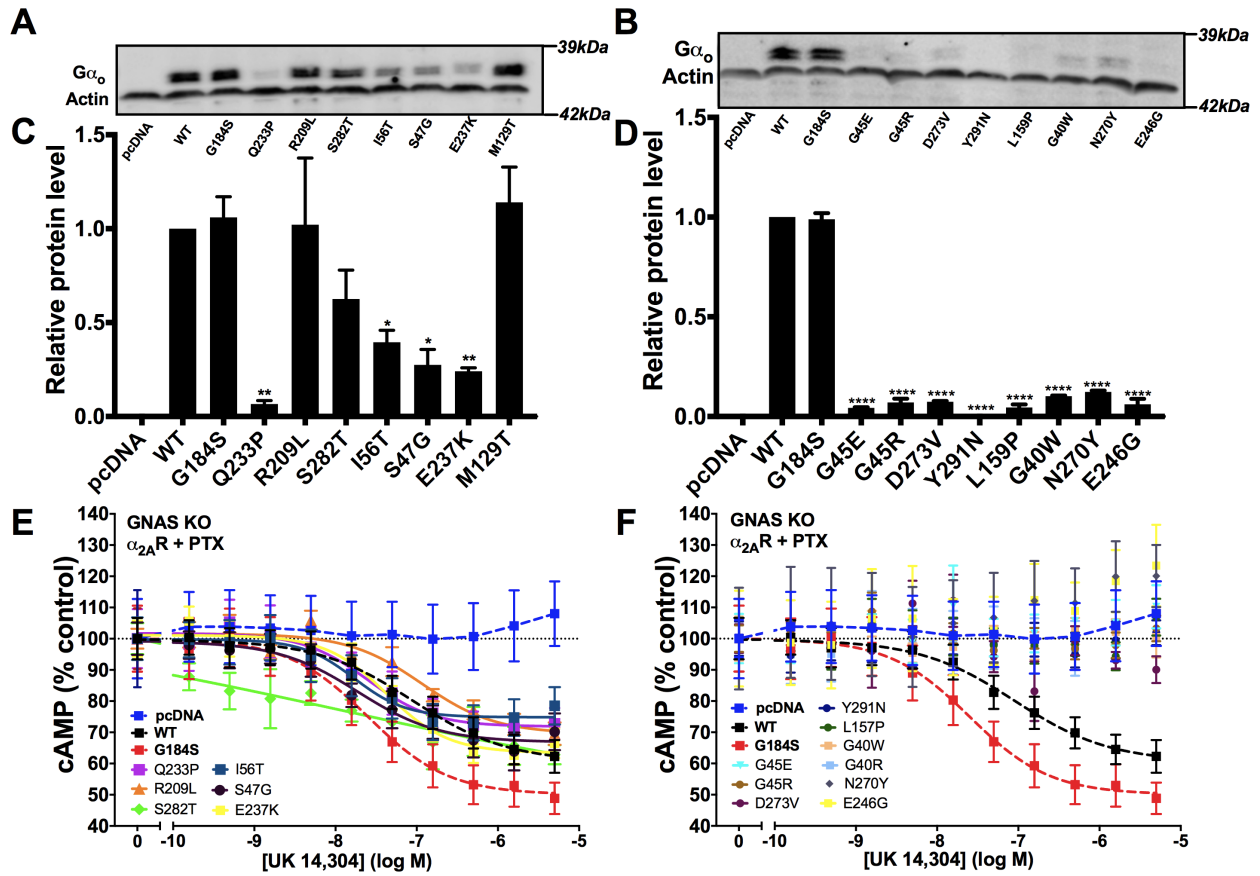


Figure S2.7 *GNAO1* mutations' functionalities correlate to their protein expression patterns. (A-D) Representative and quantification of relative protein levels of each Gα_o mutant compared to wild-type Gα_o grouped by functioning mutants (A, C) and non-functioning mutants (B, D). (E, F) Dose-response curves for α₂ agonist-mediated inhibition of AC with different *GNAO1* mutants. In the GNAS KO HEK cell line, functioning *GNAO1* mutants inhibit cAMP production (E) while non-functioning *GNAO1* mutants do not show any inhibition of cAMP production (F). Graphs are the results of 3 independent experiments and data are presented as mean ± SEM. *p<0.05, **p<0.01, ****p<0.001 using one-way ANOVA analysis of variance with Bonferroni post-hoc test for pairwise comparison. PTX = pertussis toxin.

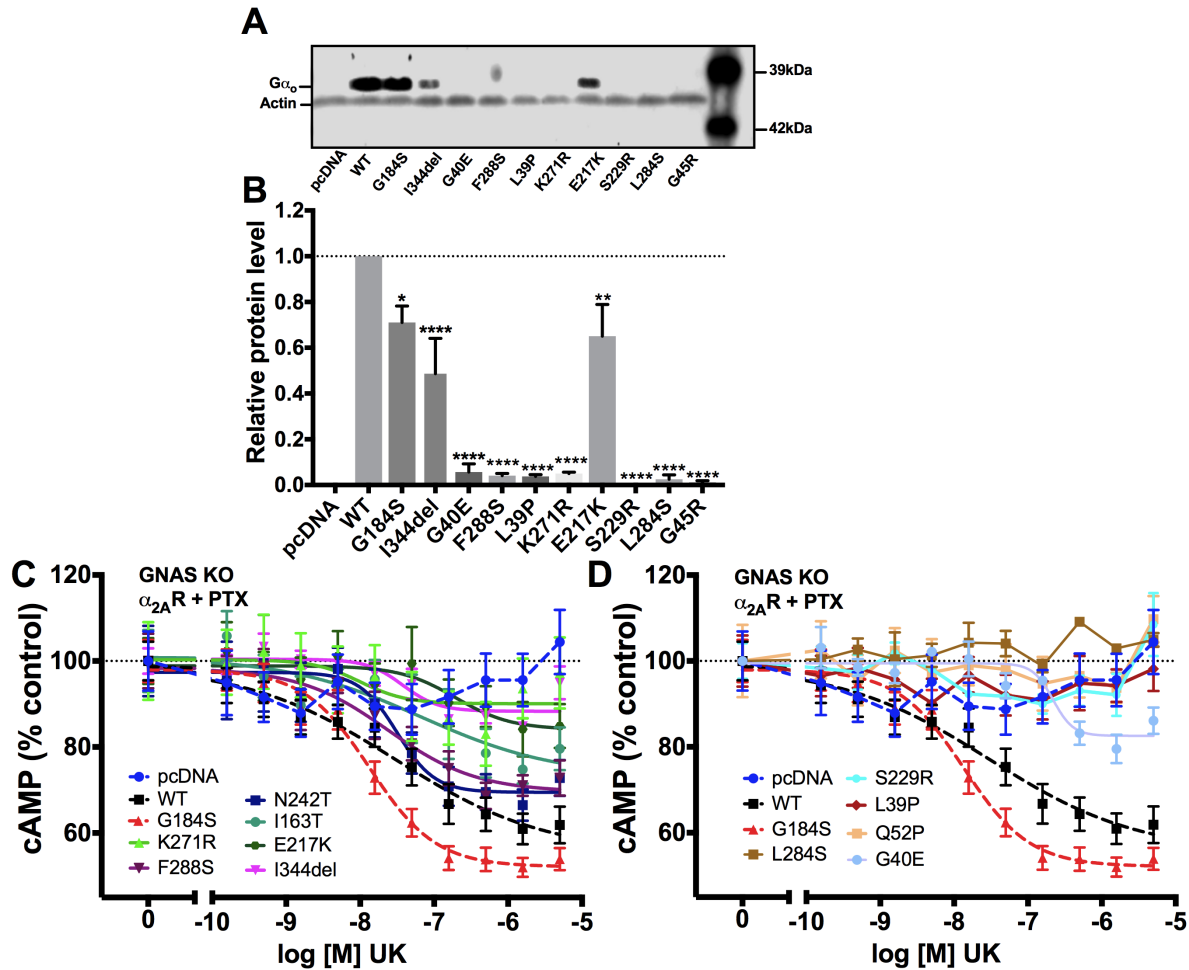


Figure S2.8 *GNAO1* mutations' functionalities correlate to their protein expression patterns (assays done by Nils Wellhausen with a different group of mutations from those in Figure S2.7). (A) Representative mutations of and (B) quantification of relative protein levels of each G α_o mutant compared to wild-type G α_o . (C, D) Dose-response curves for $\alpha_{2A}R$ regulation of AC with *GNAO1* mutants. In GNAS KO HEK cell line, functioning *GNAO1* mutants inhibit cAMP production (C) while non-functioning *GNAO1* mutants do not show any inhibition of cAMP production (D). Graphs are the results of 3 independent experiments and data are presented as mean \pm SEM. *p < 0.05, **p < 0.01, ****p < 0.001 using one-way ANOVA analysis of variance with Bonferroni post-hoc test for pairwise comparison. PTX = pertussis toxin.

Table S2.2 All non-functioning *GNAO1* mutations tested with *GNAS* KO cells

Group			Expression (% of WT)	cAMP at 5 μ M UK14, 304 (% of unstimulated)	Normalized % Inhibition	LogEC50	EC50 (nM)
pcDNA			0	116 \pm 12	0	-5.70 \pm 1.30	2014
WT			100	64 \pm 4	100	-7.14 \pm 0.67	73
550G>A	G184S	Gly184Ser	99 \pm 3	60 \pm 7	129 \pm 14	-7.43 \pm 0.07	38
134G>A	G45E	Gly45Gln	4	110 \pm 7	13 \pm 14	-	-
133G>C	G45R	Gly45Arg	7 \pm 2	103 \pm 4	29 \pm 9	-	-
818A>T	D273V	Asp273Val	7	90 \pm 4	60 \pm 9	-	-
871T>A	Y291N	Tyr291Asn	0	102 \pm 4	32 \pm 8	-	-
470T>C	L157P	Leu157Pro	5 \pm 2	107 \pm 6	21 \pm 12	-	-
118G>T	G40W	Gly40Trp	10	101 \pm 7	35 \pm 14	-	-
808A>T	N270Y	Asn270Tyr	12 \pm 1	120 \pm 10	-10 \pm 21	-	-
737A>G	E246G	Glu246Gly	6 \pm 3	123 \pm 13	-18 \pm 27	-	-
851T>C	L284S	Leu284Ser	3 \pm 2	105 \pm 2	-1 \pm 4	-	-
687C>A	S229R	Ser229Arg	-2 \pm 5	108 \pm 7	-10 \pm 17	-	-
116T>C	L39P	Leu39Pro	4 \pm 1	98 \pm 5	15 \pm 12	-	-
155A>C	Q52P	Gln52Pro	-	110 \pm 5	-31 \pm 16	-	-
119G>A	G40E	Gly40Glu	6 \pm 4	86 \pm 3	43 \pm 7	-6.66 \pm 0.17	218

Table S2.3 All functioning *GNAO1* mutations tested with *GNAS* KO cells

Group			Expression (% of WT)	cAMP at 5 μ M UK14, 304 (% of unstimulated)	Normalized % Inhibition	LogEC50	EC50 (nM)
pcDNA			0	116 \pm 12	0	-5.70 \pm 1.30	2014
WT			100	64 \pm 4	100	-7.14 \pm 0.67	73
550G>A	G184S	Gly184Ser	106 \pm 11	60 \pm 7	129 \pm 14	-7.43 \pm 0.07	38
698A > C	Q233P	Gln233Pro	7 \pm 2	73 \pm 5	100 \pm 10	-7.60 \pm 0.32	25
626G>T	R209L	Arg209Leu	102 \pm 36	70 \pm 4	107 \pm 7	-6.93 \pm 0.19	116
844T>A	S282T	Ser282Thr	63 \pm 15	63 \pm 3	123 \pm 6	-7.85 \pm 5.08	14
167T>C	I56T	Ile56Thr	39 \pm 6	79 \pm 6	87 \pm 12	-7.77 \pm 0.31	17
139A>G	S47G	Ser47Gly	27 \pm 8	70 \pm 6	106 \pm 12	-7.72 \pm 0.29	19
709G>A	E237K	Glu237Lys	24 \pm 2	66 \pm 5	115 \pm 10	-7.37 \pm 0.17	43
812A>G	K271R	Lys271Arg	5 \pm 1	97 \pm 8	17 \pm 19	-8.00 \pm 0.88	10
863T>C	F288S	Phe288Ser	4 \pm 1	73 \pm 4	74 \pm 10	-7.62 \pm 0.31	24
725A>C	N242T	Asn242Thr	-	73 \pm 4	93 \pm 10	-7.50 \pm 0.24	31
448T>C	I163T	Ile163Thr	-	80 \pm 4	37 \pm 11	-7.17 \pm 1.12	67
649G>A	E217K	Glu217Lys	65 \pm 14	85 \pm 5	46 \pm 12	-6.71 \pm 0.64	195
1030_1032 delATT	I344del	Ile344del	49 \pm 15	95 \pm 4	22 \pm 9	-7.42 \pm 0.22	38

Table S2.4 Genotype-phenotype correlation of the newly reported *GNAO1* mutations

GNAO1 Mutations	cAMP Inhibition	Epilepsy	Movement Disorder	Age of onset	Gender
R209L	Functioning		++	birth	M
I56T	Functioning	+	++	4 y	F
Q233P	Functioning	+	++	13 mo	F
E237K	Functioning		+	4 mo	M
E237K	Functioning		+	3 mo	M
S282T*	Functioning		+	NA	F
S47G	Functioning	+	++	5 mo	M
I344del	Functioning		+	12 mo	F
G45E	Non-Functioning	++		infancy	F
G45R	Non-Functioning	++	+	NA	M
E246G	Non-Functioning	++	+	6 mo	F
N270Y*	Non-Functioning	+		NA	F
G40W*	Non-Functioning	++	+	birth	F
Y291N*	Non-Functioning	+		2.5 mo	F
L157P*	Non-Functioning	++	+	NA	M
D273V*	Non-Functioning	+		NA	F
G40E	Non-Functioning	+		15 hr	M
G40E	Non-Functioning	++	+	2 hr	F
L284S	Non-Functioning	+		11 d	F

* Personal communication from *GNAO1* patient support

NA: not available

++ Severe symptoms; + Mild symptoms

REFERENCES

REFERENCES

- Allen, A. S., Berkovic, S. F., Cossette, P., Delanty, N., Dlugos, D., Eichler, E. E., . . . Project, E. P. G. (2013). De novo mutations in epileptic encephalopathies. *Nature*, *501*(7466), 217-221. doi:10.1038/nature12439
- Ammer, H., & Christ, T. E. (2002). Identity of adenylyl cyclase isoform determines the G protein mediating chronic opioid-induced adenylyl cyclase supersensitivity. *J Neurochem*, *83*(4), 818-827.
- Ananth, A. L., Robichaux-Viehoever, A., Kim, Y. M., Hanson-Kahn, A., Cox, R., Enns, G. M., . . . Bernstein, J. A. (2016). Clinical Course of Six Children With GNAO1 Mutations Causing a Severe and Distinctive Movement Disorder. *Pediatr Neurol*. doi:10.1016/j.pediatrneurol.2016.02.018
- Bayewitch, M. L., Avidor-Reiss, T., Levy, R., Pfeuffer, T., Nevo, I., Simonds, W. F., & Vogel, Z. (1998a). Differential modulation of adenylyl cyclases I and II by various G beta subunits. *J Biol Chem*, *273*(4), 2273-2276. doi:10.1074/jbc.273.4.2273
- Bayewitch, M. L., Avidor-Reiss, T., Levy, R., Pfeuffer, T., Nevo, I., Simonds, W. F., & Vogel, Z. (1998b). Inhibition of adenylyl cyclase isoforms V and VI by various Gbetagamma subunits. *FASEB J*, *12*(11), 1019-1025. doi:10.1096/fasebj.12.11.1019
- Berkovic, S. F., Heron, S. E., Giordano, L., Marini, C., Guerrini, R., Kaplan, R. E., . . . Scheffer, I. E. (2004). Benign familial neonatal-infantile seizures: characterization of a new sodium channelopathy. *Ann Neurol*, *55*(4), 550-557. doi:10.1002/ana.20029
- Bosch, D. E., Willard, F. S., Ramanujam, R., Kimple, A. J., Willard, M. D., Naqvi, N. I., & Siderovski, D. P. (2012). A P-loop mutation in Gα subunits prevents transition to the active state: implications for G-protein signaling in fungal pathogenesis. *PLoS Pathog*, *8*(2), e1002553. doi:10.1371/journal.ppat.1002553
- Brink, C. B., Wade, S. M., & Neubig, R. R. (2000). Agonist-directed trafficking of porcine alpha(2A)-adrenergic receptor signaling in Chinese hamster ovary cells: l-isoproterenol selectively activates G(s). *J Pharmacol Exp Ther*, *294*(2), 539-547.

- Capovilla, G., Wolf, P., Beccaria, F., & Avanzini, G. (2013). The history of the concept of epileptic encephalopathy. *Epilepsia*, *54 Suppl 8*, 2-5. doi:10.1111/epi.12416
- Carapito, R., Paul, N., Untrau, M., Le Gentil, M., Ott, L., Alsaleh, G., . . . Bahram, S. (2015). A de novo ADCY5 mutation causes early-onset autosomal dominant chorea and dystonia. *Mov Disord*, *30*(3), 423-427. doi:10.1002/mds.26115
- Chang, F. C., Westenberger, A., Dale, R. C., Smith, M., Pall, H. S., Perez-Duenas, B., . . . Fung, V. S. (2016). Phenotypic insights into ADCY5-associated disease. *Mov Disord*, *31*(7), 1033-1040. doi:10.1002/mds.26598
- Clark, M. J., Harrison, C., Zhong, H., Neubig, R. R., & Traynor, J. R. (2003). Endogenous RGS protein action modulates mu-opioid signaling through Galphao. Effects on adenylyl cyclase, extracellular signal-regulated kinases, and intracellular calcium pathways. *J Biol Chem*, *278*(11), 9418-9425. doi:10.1074/jbc.M208885200
- Consortium, E.-R., Project, E. P. G., & Consortium, E. K. (2014). De novo mutations in synaptic transmission genes including DNMT1 cause epileptic encephalopathies. *Am J Hum Genet*, *95*(4), 360-370. doi:10.1016/j.ajhg.2014.08.013
- Dalby, N. O., & Thomsen, C. (1996). Modulation of seizure activity in mice by metabotropic glutamate receptor ligands. *J Pharmacol Exp Ther*, *276*(2), 516-522.
- Defer, N., Best-Belpomme, M., & Hanoune, J. (2000). Tissue specificity and physiological relevance of various isoforms of adenylyl cyclase. *Am J Physiol Renal Physiol*, *279*(3), F400-416. doi:10.1152/ajprenal.2000.279.3.F400
- Dhamija, R., Mink, J. W., Shah, B. B., & Goodkin, H. P. (2016). GNAO1-Associated Movement Disorder. *Mov Disord Clin Pract*, *3*(6), 615-617. doi:10.1002/mdc3.12344
- Dietel, T. (2016). Genotype and phenotype in GNAO1-Mutation – Case report of an unusual course of a childhood epilepsy. In G. S. T. B. Haack , I. Cordes , R. Trollmann , T. Bast (Ed.), (Vol. 47, pp. P01-17). Neuropediatrics: Thieme.
- Epi KCEaekce, E. K. (2016). De Novo Mutations in SLC1A2 and CACNA1A Are Important Causes of Epileptic Encephalopathies. *Am J Hum Genet*. doi:10.1016/j.ajhg.2016.06.003

- Feng, H., Sjogren, B., Karaj, B., Shaw, V., Gezer, A., & Neubig, R. R. (2017). Movement disorder in GNAO1 encephalopathy associated with gain-of-function mutations. *Neurology*, *89*(8), 762-770. doi:10.1212/WNL.0000000000004262
- Fu, Y., Zhong, H., Nanamori, M., Mortensen, R. M., Huang, X., Lan, K., & Neubig, R. R. (2004). RGS-insensitive G-protein mutations to study the role of endogenous RGS proteins. *Methods Enzymol*, *389*, 229-243. doi:10.1016/S0076-6879(04)89014-1
- Gao, B. N., & Gilman, A. G. (1991). Cloning and expression of a widely distributed (type IV) adenylyl cyclase. *Proc Natl Acad Sci U S A*, *88*(22), 10178-10182. doi:10.1073/pnas.88.22.10178
- Ghahremani, M. H., Cheng, P., Lembo, P. M., & Albert, P. R. (1999). Distinct roles for Galphai2, Galphai3, and Gbeta gamma in modulation of forskolin- or Gs-mediated cAMP accumulation and calcium mobilization by dopamine D2S receptors. *J Biol Chem*, *274*(14), 9238-9245.
- Goldenstein, B. L., Nelson, B. W., Xu, K., Luger, E. J., Pribula, J. A., Wald, J. M., . . . Doze, V. A. (2009). Regulator of G protein signaling protein suppression of Galphao protein-mediated alpha2A adrenergic receptor inhibition of mouse hippocampal CA3 epileptiform activity. *Mol Pharmacol*, *75*(5), 1222-1230. doi:mol.108.054296 [pii]10.1124/mol.108.054296
- Han HA, C. M., Snead OC III. (2012). *GABAB Receptor and Absence Epilepsy*. (4th edition. ed.). Jasper's Basic Mechanisms of the Epilepsies [Internet]. Bethesda (MD): National Center for Biotechnology Information (US).
- Ikeda, S. R., & Jeong, S. W. (2004). Use of RGS-insensitive Galpha subunits to study endogenous RGS protein action on G-protein modulation of N-type calcium channels in sympathetic neurons. *Methods Enzymol*, *389*, 170-189. doi:10.1016/S0076-6879(04)89011-6
- Jeong, S. W., & Ikeda, S. R. (2000). Effect of G protein heterotrimer composition on coupling of neurotransmitter receptors to N-type Ca(2+) channel modulation in sympathetic neurons. *Proc Natl Acad Sci U S A*, *97*(2), 907-912.
- Jiang, M., Gold, M. S., Boulay, G., Spicher, K., Peyton, M., Brabet, P., . . . Birnbaumer, L. (1998). Multiple neurological abnormalities in mice deficient in the G protein Go. *Proc Natl Acad Sci U S A*, *95*(6), 3269-3274. doi:10.1073/pnas.95.6.3269

- Kehrl, J. M., Sahaya, K., Dalton, H. M., Charbeneau, R. A., Kohut, K. T., Gilbert, K., . . . Neubig, R. R. (2014). Gain-of-function mutation in *Gnao1*: a murine model of epileptiform encephalopathy (EIEE17)? *Mamm Genome*, *25*(5-6), 202-210. doi:10.1007/s00335-014-9509-z
- Kulkarni, N., Tang, S., Bhardwaj, R., Bernes, S., & Grebe, T. A. (2016). Progressive Movement Disorder in Brothers Carrying a *GNAO1* Mutation Responsive to Deep Brain Stimulation. *J Child Neurol*, *31*(2), 211-214. doi:10.1177/0883073815587945
- Lamberts, J. T., Smith, C. E., Li, M. H., Ingram, S. L., Neubig, R. R., & Traynor, J. R. (2013). Differential control of opioid antinociception to thermal stimuli in a knock-in mouse expressing regulator of G-protein signaling-insensitive *Galphao* protein. *J Neurosci*, *33*(10), 4369-4377. doi:10.1523/JNEUROSCI.5470-12.2013
- Lan, K. L., Sarvazyan, N. A., Taussig, R., Mackenzie, R. G., DiBello, P. R., Dohlman, H. G., & Neubig, R. R. (1998). A point mutation in *Galphao* and *Galphai1* blocks interaction with regulator of G protein signaling proteins. *J Biol Chem*, *273*(21), 12794-12797.
- Law, C. Y., Chang, S. T., Cho, S. Y., Yau, E. K., Ng, G. S., Fong, N. C., & Lam, C. W. (2015). Clinical whole-exome sequencing reveals a novel missense pathogenic variant of *GNAO1* in a patient with infantile-onset epilepsy. *Clin Chim Acta*, *451*(Pt B), 292-296. doi:10.1016/j.cca.2015.10.011
- Marce-Grau, A., Dalton, J., Lopez-Pison, J., Garcia-Jimenez, M. C., Monge-Galindo, L., Cuenca-Leon, E., . . . Macaya, A. (2016). *GNAO1* encephalopathy: further delineation of a severe neurodevelopmental syndrome affecting females. *Orphanet J Rare Dis*, *11*, 38. doi:10.1186/s13023-016-0416-0
- Masino, S. A., Li, T., Theofilas, P., Sandau, U. S., Ruskin, D. N., Fredholm, B. B., . . . Boison, D. (2011). A ketogenic diet suppresses seizures in mice through adenosine A_1 receptors. *J Clin Invest*, *121*(7), 2679-2683. doi:10.1172/JCI57813
- Masuh, I., Chavali, S., Muntean, B. S., Skamangas, N. K., Simonyan, K., Patil, D. N., . . . Martemyanov, K. A. (2018). Molecular Deconvolution Platform to Establish Disease Mechanisms by Surveying GPCR Signaling. *Cell Rep*, *24*(3), 557-568 e555. doi:10.1016/j.celrep.2018.06.080
- McTague, A., Howell, K. B., Cross, J. H., Kurian, M. A., & Scheffer, I. E. (2016). The

- genetic landscape of the epileptic encephalopathies of infancy and childhood. *Lancet Neurol*, 15(3), 304-316. doi:10.1016/S1474-4422(15)00250-1
- Mencacci, N. E., Erro, R., Wiethoff, S., Hersheson, J., Ryten, M., Balint, B., . . . Bhatia, K. P. (2015). ADCY5 mutations are another cause of benign hereditary chorea. *Neurology*, 85(1), 80-88. doi:10.1212/WNL.0000000000001720
- Menke, L. A., Engelen, M., Alders, M., Odekerken, V. J., Baas, F., & Cobben, J. M. (2016). Recurrent GNAO1 Mutations Associated With Developmental Delay and a Movement Disorder. *J Child Neurol*. doi:10.1177/0883073816666474
- Morgan, J. C., Kurek, J. A., Davis, J., & Sethi, K. D. (2016). ADCY5 mutations are another cause of benign hereditary chorea. *Neurology*, 86(10), 978-979. doi:10.1212/WNL.0000000000002479
- Nakamura, K., Kodera, H., Akita, T., Shiina, M., Kato, M., Hoshino, H., . . . Saitsu, H. (2013). De Novo mutations in GNAO1, encoding a Gαo subunit of heterotrimeric G proteins, cause epileptic encephalopathy. *Am J Hum Genet*, 93(3), 496-505. doi:10.1016/j.ajhg.2013.07.014
- Noebels, J. (2015). Pathway-driven discovery of epilepsy genes. *Nat Neurosci*, 18(3), 344-350. doi:10.1038/nn.3933
- Raskind, W. H., Friedman, J. R., Roze, E., Meneret, A., Chen, D. H., & Bird, T. D. (2017). ADCY5-related dyskinesia: Comments on characteristic manifestations and variant-associated severity. *Mov Disord*, 32(2), 305-306. doi:10.1002/mds.26888
- Saitsu, H., Fukai, R., Ben-Zeev, B., Sakai, Y., Mimaki, M., Okamoto, N., . . . Matsumoto, N. (2016). Phenotypic spectrum of GNAO1 variants: epileptic encephalopathy to involuntary movements with severe developmental delay. *Eur J Hum Genet*, 24(1), 129-134. doi:10.1038/ejhg.2015.92
- Sherr, E. H. (2003). The ARX story (epilepsy, mental retardation, autism, and cerebral malformations): one gene leads to many phenotypes. *Curr Opin Pediatr*, 15(6), 567-571.
- Sievers, F., Wilm, A., Dineen, D., Gibson, T. J., Karplus, K., Li, W., . . . Higgins, D. G. (2011). Fast, scalable generation of high-quality protein multiple sequence alignments using Clustal Omega. *Mol Syst Biol*, 7, 539. doi:10.1038/msb.2011.75

- Slep, K. C., Kercher, M. A., Wieland, T., Chen, C. K., Simon, M. I., & Sigler, P. B. (2008). Molecular architecture of Galphao and the structural basis for RGS16-mediated deactivation. *Proc Natl Acad Sci U S A*, *105*(17), 6243-6248. doi:10.1073/pnas.0801569105
- Sternweis, P. C., & Robishaw, J. D. (1984). Isolation of two proteins with high affinity for guanine nucleotides from membranes of bovine brain. *J Biol Chem*, *259*(22), 13806-13813.
- Talvik, I. (2015). Clinical Phenotype of De Novo GNAO1 Mutation: Case Report and Review of Literature. In M. V. Rikke S. Møller, Ulvi Vaheer, Line HG Larsen, Hans A. Dahl, Pilvi Ilves, and Tiina Talvik (Ed.), (Vol. 2). Child Neurology Open.
- Tang, W. J., & Gilman, A. G. (1991). Type-specific regulation of adenylyl cyclase by G protein beta gamma subunits. *Science*, *254*(5037), 1500-1503. doi:10.1126/science.1962211
- Taussig, R., & Gilman, A. G. (1995). Mammalian membrane-bound adenylyl cyclases. *J Biol Chem*, *270*(1), 1-4. doi:10.1074/jbc.270.1.1
- Taussig, R., Quarmby, L. M., & Gilman, A. G. (1993). Regulation of purified type I and type II adenylyl cyclases by G protein beta gamma subunits. *J Biol Chem*, *268*(1), 9-12.
- Wade, S. M., Lim, W. K., Lan, K. L., Chung, D. A., Nanamori, M., & Neubig, R. R. (1999). G(i) activator region of alpha(2A)-adrenergic receptors: distinct basic residues mediate G(i) versus G(s) activation. *Mol Pharmacol*, *56*(5), 1005-1013.
- Zhu, X., Petrovski, S., Xie, P., Ruzzo, E. K., Lu, Y. F., McSweeney, K. M., . . . Goldstein, D. B. (2015). Whole-exome sequencing in undiagnosed genetic diseases: interpreting 119 trios. *Genet Med*, *17*(10), 774-781. doi:10.1038/gim.2014.191

CHAPTER 3: BEHAVIORAL ASSESSMENT OF MOUSE MODELS WITH GNAO1-ASSOCIATED MOVEMENT DISORDER AND EPILEPSY

Modified from Feng, H., Larrivee, C. L., Demireva, E. Y., Xie, H., Leipprandt, J. R., & Neubig, R. R. (2019). Mouse models of *GNAO1*-associated movement disorder: Allele- and sex-specific differences in phenotypes. *PloS one*, 14(1), e0211066.

DOI:10.1371/journal.pone.0211066

With permission from PLOS ONE. All rights reserved.

&

From Larrivee, C. L., Feng, H., Leipprandt, J. R., Demireva, E. Y., Xie, H., & Neubig, R. R. (2019). Mice with *GNAO1* R209H Movement Disorder Variant Display Hyperlocomotion Alleviated by Risperidone. *bioRxiv*, 662031.

DOI: <https://doi.org/10.1101/662031>

Demireva, E. Y. and Xie, H. did the design and production of the G203R and R209H mutant mice.

Larrivee C. L. performed Rotarod and Open Field studies for the G203R and R209H mutant mice.

Leipprandt, J. R. did the breeding and genotyping for the mutant mice.

3.1 Abstract

Infants and children with dominant *de novo* mutations in *GNAO1* exhibit movement disorders, epilepsy, or both. Children with loss-of-function (LOF) mutations and partial-loss-of-function (PLOF) mutations exhibit Epileptiform Encephalopathy 17 (EIEE17). Gain-of-function (GOF) or those with normal functioning (NF) mutations in an *in vitro* assay are found in patients with Neurodevelopmental Disorder with Involuntary Movements (NEDIM). There is no animal model with a human mutant *GNAO1* allele.

Here we assess the behavioral patterns in several mouse models. Mouse models with *Gnao1* knock-in mutation G203R (GOF), R209H (NF) or Δ T191F197 (LOF) were created by CRISPR/Cas9 methods to determine whether the clinical features of patients with a particular *GNAO1* mutation which could include epilepsy and/or movement disorder would be evident in the mouse model. These three newly developed models are compared with previously developed *Gnao1* mouse model, *Gnao1*^{+/_{G184S}} and *Gnao1*^{+/-}.

Gnao1^{+/_{G203R}} mutant mice were viable and gained weight comparably to controls. Homozygotes were not non-viable. Grip strength was decreased in both males and females. Male *Gnao1*^{+/_{G203R}} mice were strongly affected in movement assays (RotaRod and DigiGait) while females were not. Male *Gnao1*^{+/_{G203R}} mice also showed enhanced seizure propensity in the pentylenetetrazole kindling test. Mice with a G184S GOF knock-in also showed movement-related behavioral phenotypes but females were more strongly affected than males. In contrast, the *Gnao1*^{+/_{R209H}} mouse model exhibited

hyperkinetic movements, which have not been seen in any other *Gnao1* mutant mouse line. *Gnao1*^{+/*R209H*} mice also did not show a strong sex difference in our behavioral battery test. Mice carrying the strong epilepsy allele, *Gnao1*^{+/*ΔT191F197*} did not gain weight like their WT siblings and the mutant mice developed seizures around P7 and all mutant mice died before P16. In contrast, *Gnao1*^{+/-} mice survived and never developed spontaneous seizures.

Gnao1^{+/*G203R*}, *Gnao1*^{+/*R209H*} and *Gnao1*^{+/*ΔT191F197*} mice all shared similar phenotypes regarding to the onset of epilepsy and/or movement disorders as children with the same heterozygous *GNAO1* mutations. Although *Gnao1*^{+/*ΔT191F197*} mice did not survive to breeding age and the line was lost, both *Gnao1*^{+/*G203R*} and *Gnao1*^{+/*R209H*} mouse models should be useful tools in mechanistic and preclinical studies of *GNAO1*-related movement disorders and epilepsy.

3.2 Introduction

Neurodevelopmental Disorder with Involuntary Movements (NEDIM) is a newly defined neurological disorder associated with mutations in *GNAO1*. It is characterized by “hypotonia, delayed psychomotor development, and infantile or childhood onset of hyperkinetic involuntary movements” (OMIM 617493). NEDIM is monogenetic and associated with GOF mutations and NF mutations in *GNAO1* (Feng et al., 2017). The *GNAO1* gene has also been associated with early infantile epileptic encephalopathy 17 (EIEE17; OMIM 615473). However, 36% of patients showed both epilepsy and

movement disorder phenotypes. This includes many different *GNAO1* alleles such as: G40R, G45R, S47G, I56T, T191_F197del, L199P, G203R, R209C, A227V, Y231C and E246G (Feng, Khalil, Neubig, & Sidiropoulos, 2018).

GNAO1 encodes $G\alpha_o$, the most abundant membrane protein in the mammalian central nervous system (Jiang & Bajpayee, 2009). $G\alpha_o$ is the α -subunit of the G_o protein, a member of the $G_{i/o}$ family of heterotrimeric G proteins. $G_{i/o}$ proteins couple to many important G protein-coupled-receptors (GPCRs) involved in movement control like $GABA_B$, dopamine D_2 , adenosine A_1 and adrenergic α_{2A} receptors (Franek et al., 1999; Gazi, Nickolls, & Strange, 2003; Lorenzen, Lang, & Schwabe, 1998; Tian, Duzic, Lanier, & Deth, 1994). Upon activation, $G\alpha_o$ and $G\beta\gamma$ separate from each other and modulate separate downstream signaling pathways. $G\alpha_o$ mediates inhibition of cyclic AMP (cAMP), and $G\beta\gamma$ mediates inhibition of AC and N-type calcium channels while activating G-protein activated inward rectifying potassium channels (GIRK channels) (Zhang, Pacheco, & Doupnik, 2002). G_o is expressed mainly in the central nervous system and it regulates neurotransmitter release by modulating intracellular calcium concentrations in pre-synaptic cells (Li et al., 2004). It has also been suggested that G_o plays a role in neurodevelopmental processes like neurite outgrowth and axon guidance (Bromberg, Iyengar, & He, 2008; Strittmatter, Fishman, & Zhu, 1994). Consequently, G_o is an important modulator of neurological functions.

Previously, we defined a functional genotype-phenotype correlation for *GNAO1*

disorders (Feng et al., 2017); GOF and NF mutations are found in patients with movement disorders, while loss-of-function (LOF) and partial-loss-of-function (PLOF) mutations are associated with epilepsy (Feng et al., 2017). I recently published a mechanistic review of this genotype-phenotype correlation (Feng et al., 2018). The experimental study of human *GNAO1* mutant alleles, however, was done in HEK293T cells, which lack complex physiological context of the brain. Therefore, it was important to see whether mouse models with *GNAO1* mutations would share clinical characteristics of the human patients. Such a result would verify the previously - reported genotype-phenotype correlation and would provide a system for more detailed mechanistic studies and preclinical testing models for possible new therapeutics. Previously, we reported that *Gnao1*^{+/*G184S*} mutant mice carrying a human-engineered GOF mutation (G184S) showed heightened sensitization to pentylentetrazol (PTZ) kindling and had an elevated frequency of interictal epileptiform discharges on EEG (Kehrl et al., 2014). Here, we tested whether the *Gnao1*^{+/*G184S*} mice also exhibit movement disorders although G184S has not been found in human (Feng et al., 2019). A *Gnao1*^{+/-} mouse model was also described previously. They are hyperalgesic and display severe motor control impairment (Jiang et al., 1998). *Gnao1*^{-/-} mice are hyperactive and also exhibit an abnormal turning behavior (Jiang et al., 1998). In our hands, they are poorly viable.

The G203R is a GOF *GNAO1* mutation in the cAMP assay (Feng et al., 2017). It is

one of the most common *GNAO1* mutations found clinically (Table 3.1) (Arya, Spaeth, Gilbert, Leach, & Holland, 2017; Feng et al., 2018; Nakamura et al., 2013; Saitsu et al., 2016; Schorling et al., 2017; Xiong et al., 2018). Most patients with this mutation exhibit both seizures and movement disorders (Arya et al., 2017; Feng et al., 2018; Nakamura et al., 2013; Saitsu et al., 2016; Schorling et al., 2017; Xiong et al., 2018).

The R209 is a mutation hotspot in the $G\alpha_o$ protein, which has been reported in over ten patients. Previously, the R209H mutation was in more than seven patients (Ananth et al., 2016; R. Dhamija, Mink, Shah, & Goodkin, 2016; Kelly et al., 2019; Kulkarni, Tang, Bhardwaj, Bernes, & Grebe, 2016; Marecos, Duarte, Alonso, Calado, & Moreira, 2018), all of who develop severe chorea/athetosis, dystonia, hypotonia and developmental delay (Table 3.1). All three previously reported R209 mutations (R209H, R209C, and R209G) were NF *GNAO1* mutations in our cAMP assay (Feng et al., 2017). However, it remained a question why *GNAO1* mutations that showed normal function in the cellular assay were pathogenic.

The $\Delta T191F197$ in-frame deletion mutation was the most severe LOF pathogenic *GNAO1* mutation reported in patients (Feng et al., 2017; Nakamura et al., 2013) (Table 3.1). It is the most representative LOF mutation with the lowest protein expression level and lowest % inhibition (Feng et al., 2017); therefore it was a good candidate for generating a LOF mouse model that would possibly develop spontaneous neurological disorders. However, since all mutant $\Delta T191F197$ mice died before P16, we were not

able to generate a line carrying this mutation. In this chapter, I only provide limited data on survival and growth of this mouse model.

Table 3.1 The status of *Gnao1* mutant mice

Allele	cAMP Inhibition	Clinical	Mouse Status
G184S	GOF	N/A	Rare adult lethality; breeds well (Kehrl et al., 2014)
KO	LOF	N/A	Homozygous early lethality (Jiang et al., 1998)
G203R	GOF	EIEE17 & MD	Rare adult lethality; breeds well (Feng et al., 2019)
R209H	NF	MD	Hyperactivity; gait phenotypes (Larrivee et al., 2019)
Δ T191F197	LOF	EIEE17	Heterozygous early lethality (P7-P14); loss of strains (Figure 3.4)

We intended to develop mouse models with the representative human GOF (G203R), NF (R209H), and LOF (Δ T191F197) mutations to see if they replicated the clinical phenotype of *GNAO1* mutation-associated neurological disorders. If so, they would be valuable tools to understand neural mechanisms underlying the complex phenotypic spectrum of patients with *GNAO1* mutations. In this chapter, I show the behavioral assessment of two mouse lines carrying α_o GOF mutation *Gnao1*^{+/G203R} and NF mutation *Gnao1*^{+/R209H}. They are compared with two previously described mouse models: one with a known GOF function mutation G184S (*Gnao1*^{+/G184S}) and the other the *Gnao1* KO model (*Gnao1*^{+/-}). These two mouse models (*Gnao1*^{+/G203R} and *Gnao1*^{+/R209H}) present

the possibility of studying *GNAO1*-associated neurological defects in animal models.

3.3 Materials and Methods

3.3.1 Animals

Animal studies were performed in accordance with the Guide for the Care and Use of Laboratory Animals established by the National Institutes of Health. All experimental protocols and personnel were approved by the Michigan State University Institutional Animal Care and Use Committee (IACUC). Mice were housed on a 12-h light/dark cycle and had free access to food and water. They were studied between 8-12 weeks old.

3.3.2 Generation of *Gnao1* mutant mice

3.3.2.1 Generation of *Gnao1*^{+/*G203R*} mouse model

Gnao1^{+/*G184S*} (Feng et al., 2017; Fu et al., 2004; Goldenstein et al., 2009; Kehrl et al., 2014) and *Gnao1*^{+/-} mice (Kehrl et al., 2014) were generated as previously described and used as N10 or greater backcross on the C57BL/6J background.

Gnao1^{*G203R*} mutant mice were generated using CRISPR/Cas9 genome editing on the C57BL/6NCrl strain. gRNA targets within exon 6 of the *Gnao1* locus (ENSMUSG00000031748) were used to generate the *G203R* mutation (Figure 3.1A). Synthetic single-stranded DNA oligonucleotides (ssODN) were used as repair templates carrying the desired mutation and short homology arms (Table 3.2). CRISPR reagents were delivered as ribonucleoprotein (RNP) complexes. RNPs were assembled in vitro using wild-type *S.p.* Cas9 Nuclease 3NLS protein, and synthetic tracrRNA and crRNA

(Integrated DNA Technologies, Inc.). TracrRNA and crRNA were denatured at 95°C for 5 min and cooled to room temperature in order to form RNA hybrids, which were incubated with Cas9 protein for 5 min at 37°C. RNPs and ssODN templates were electroporated into C57BL/6NCrI zygotes as described previously (Qin et al., 2015), using a Genome Editor electroporator (GEB15, BEX CO, LTD). C57BL/6NCrI embryos were implanted into pseudo-pregnant foster dams. Founders were genotyped by PCR (Table 3.2) followed by T7 Endonuclease I assay (M0302, New England BioLabs) and validated by Sanger sequencing.

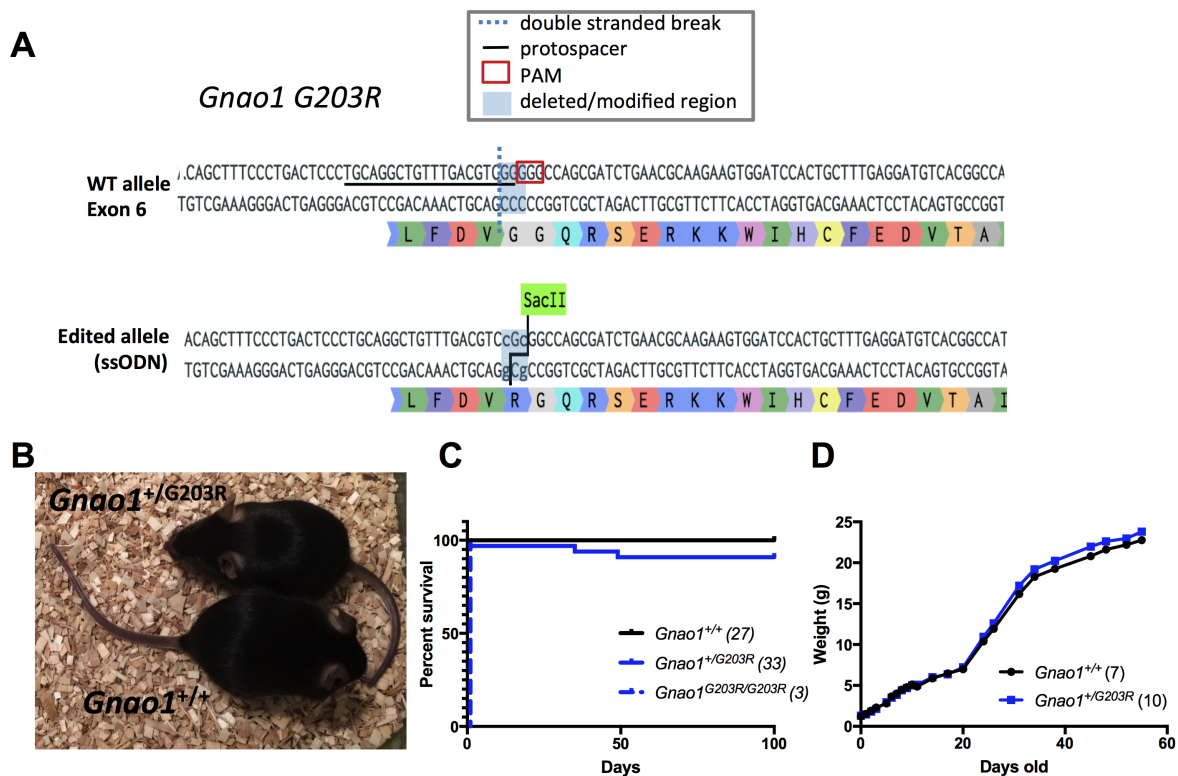


Figure 3.1 Development of *Gnao1*^{+/*G203R*} mouse model. (A) Targeting of the *Gnao1* locus. The location of the gRNA target protospacer and the PAM, and double stranded breaks following Cas9 cleavage are indicated on the WT allele. Deleted or modified sequences are highlighted in blue. The resulting edited allele sequence and translation

Figure 3.1 (cont'd) are presented along with the sequences used as references for ssODN synthesis. (B) Heterozygous *Gnao1*^{+/*G203R*} mutant mice are largely normal in size and behavior. Photo comparing mutant mouse with its littermate control is shown. (C) *Gnao1*^{+/*G203R*} mice have a relatively normal survival; while homozygous *Gnao1*^{*G203R*/*G203R*} mice die perinatally (P0-P1). (D) *Gnao1*^{+/*G203R*} mice develop normally and gain weight similarly to their WT littermate controls.

Table 3.2 Location, sequence and genotyping of gRNA targets in the *Gnao1* locus.

	<i>Gnao1</i> G203R
DSB location	chr 8: 93,950,314
gRNA target	5' TGCAGGCTGTTTGACGTCGG GGG 3' (+)
ssODN	5' ATGGCCGTGACATCCTCAAAGCAGTGGATCCAC TTCTTGCGTTCAGATCGCTGGCC GCG GACGTCAA CAGTTTGCAGGGAGTCAGGGAAAGCTGT 3'
PCR primers	Fwd: 5' GACAGGTGTCACAGGGGATG 3' Rev: 5' TCCTAGCCAAGACCCCAACT 3' PCR product = 462bp
Genotyping	SacII site created by G203R mutation

gRNA target – 20bp protospacer and PAM sequences are listed, strand orientation indicated by (+) or (-). The sequence of the ssODN used as a repair template is listed. For G203R, the mutated codon is highlighted in bold. DSB – double stranded break. PAM – protospacer adjacent motif.

The likelihood of an off-target site being edited is very low. Based on the number and position of mismatches several predictive algorithms were used to assign guide

specificity scores from 0 to 100 (100 is the best) to rank gRNAs by specificity with respect to off-targets occurring (Doench et al., 2016; Haeussler M, 2016; Hsu et al., 2013). The gRNA target used for this experiment has a specificity score of 94, which is the highest seen by the MSU Transgenic and Gene Editing Facility in over 40 similar targeting experiments (E. Demivera personal communication). This greatly reduces the probability of an off-target edits occurring. After examining the off-target lists (Table S3.9), we did not identify any off-target loci with less than 3 mismatches or with an off-target binding score > 0.5 which we deem as thresholds for further validation. We also did not identify any off-target loci with significant scores that were on the same chromosome and would be less likely to be removed from the genome after breeding of several generations. Furthermore, the RNP (ribonucleoprotein) approach of delivering CRISPR reagents to mouse embryos we employed further lowers the risk of off-target events (Iyer et al., 2018).

Nevertheless, we directly validated several predicted off-target loci within coding regions for the G203 gRNA target TGCAGGCTGTTTGACGTCGG GGG. One off-target site with 4 mismatches and a score of 0.52 was validated for locus ENSMUSG00000041390. We also analyzed two other off-target sites with 4 mismatches and scores of 0.15 and 0.069 respectively, predicted to occur on the same chromosome (chr 8) ENSMUSG00000086805 and ENSMUSG00000097637. To test these 3 off-target sites, DNA from WT and founder animals from which the line was expanded were

analyzed by PCR and sequencing and we found that no off-target effects had occurred for all 3 off-target loci analyzed (see Supplemental Materials).

3.3.2.2 Generation of *Gnao1*^{+/*R209H*} mouse model

Mutant *Gnao1*^{+/*R209H*} mice were generated via CRISPR/Cas9 genome editing on a C57BL/6J genomic background. CRISPR gRNA selection and locus analysis were performed using the Benchling platform (Benchling, Inc. San Francisco, CA.). A gRNA targeting exon 6 of the *Gnao1* locus (ENSMUSG00000031748) was chosen to cause a double strand break (DSB) 3bp downstream of codon R209. A single-stranded oligodeoxynucleotide (ssODN) carrying the R209H mutation CGC > CAC with short homology arms was used as a repair template (Figure 3.2 and Table 3.3). Ribonucleoprotein (RNP) complexes consisting of a synthetic crRNA/tracrRNA hybrid and Alt-R® S.p. Cas9 Nuclease V3 protein (Integrated DNA Technologies, Inc. Coralville, IA), were used to deliver CRISPR components along with the ssODN to mouse zygotes via electroporation as previously described (Feng et al., 2019). Edited embryos were implanted into pseudo-pregnant dams using standard techniques. Resulting litters were screened by PCR (Phire Green HSII PCR Mastermix, F126L, Thermo Fisher, Waltham, MA.), T7 Endonuclease I assay (M0302, New England Biolabs Inc.) and Sanger sequencing (GENEWIZ, Inc. Plainfield, NJ) for edits of the target site.

Table 3.3 Location and sequence of gRNA and ssODN template for CRISPR-Cas targeting *Gnao1* locus; primers and genotyping method for *Gnao1*^{+/*R209H*} mice

	<i>Gnao1</i> R209H
Location	Chr 8: 93,950,334
gRNA target 5' N20-PAM -3'	5' AGCGATCTGAACGCAAGAAG TGG 3'
ssODN template (reverse complement)	GTTTCGTCCTCGTGGAGCACCTGGTTCATAGCCGCT GAGTGCACACAGAAGATGATGGCCGTGACATCCTCAA GCAGTGGATCCACTTCTTGtGTTTCAGATCGCTGGCCCCG ACGTCAAACAGCCTGCAGGGAGTCAGGGAAAGCTGTGA GGGCGGGGACGCCTA
PCR primers	O586 FWD: 5' GGACAGGTGTCACAGGGGAT 3' O587 REV: 5' ACTGGCCTCCCTTGGCAATA 3'
Genotyping	By Sanger Sequencing

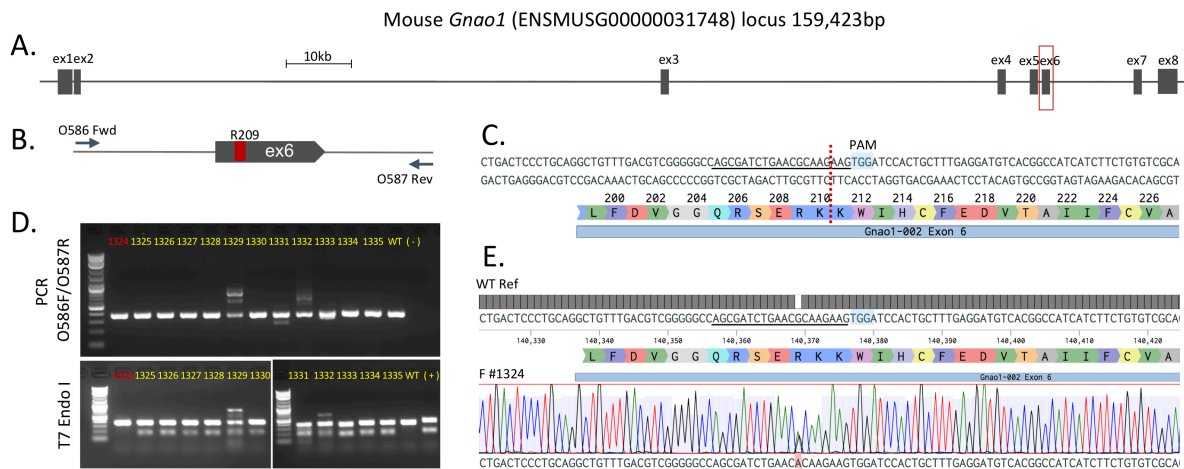


Figure 3.2 Targeting of the mouse *Gnao1* locus. (A) Mouse *Gnao1* genomic locus (exon size not to scale), red outline is magnified in (B) showing exon 6 and relative location of codon 209, and PCR primers O586 and O587. (C) Location and exact sequence of gRNA target within exon 6, dotted red line denotes DSB, PAM is highlighted

Figure 3.2 (cont'd) and sequence corresponding to gRNA protospacer is underlined (also in E). (D) Raw gel electrophoresis images showing PCR of the target region and T7 Endonuclease I (T7 Endo I) digestion analysis of founders 1324 – 1335 (n=12), with WT, H₂O (-) and T7Endo I (+) controls. Founder 1324 (red number) was positive for the mutation on one allele and WT on the other, note that the single bp mismatch was not reliably detected by T7 Endo I assay. (E) Exact sequence of edited founder 1324 as aligned to WT reference genome, two peaks (G and A) are detected on the sequence chromatogram, indicating the presence of both WT and edited R209H allele.

3.3.3 Genotyping and Breeding

3.3.3.1 Genotyping *Gnao1*^{+/*G203R*} mice

Heterozygous *Gnao1*^{+/*G203R*} mutant founder mice were crossed against C57BL/6J mice to generate *Gnao1*^{+/*G203R*} heterozygotes (N1 backcross). Further breeding was done to produce N2 backcross heterozygotes while male and female N1 heterozygotes were crossed to produce homozygous *Gnao1*^{*G203R*/*G203R*} mutants. Studies were done on N1 or N2 *G203R* heterozygotes with comparisons to littermate controls.

All mice had ears clipped before weaning. DNA was extracted from earclips by an alkaline lysis method (Truett et al., 2000). The *G203R* allele of *Gα_o* was identified by *Sac* II digests (WT 462 Bp and *G203R* 320 & 140Bp) of genomic PCR products generated with primers (Fwd 5' GACAGGTGTCACAGGGGATG 3'; Rev 5' TCCTAGCCAAGACCCCAACT 3'). Reaction conditions were: 0.8 μl template, 4 μl 5x Promega PCR buffer, 0.4 μl 10 mM dNTPs, 1 μl 10 μM Forward Primer, 1 μl 10 μM Reverse Primer, 0.2 μl Promega GoTaq and 12.6 μl DNase free water (Promega catalog

M3005, Madison WI). Samples were denatured for 4 minutes at 95 °C then underwent 32 cycles of PCR (95 °C for 30 seconds, 60 °C for 30 seconds, and 72 °C for 30 seconds) followed by a final extension (7 minutes at 72 °C). After PCR, samples were incubated with Sac II restriction enzyme for 2 hrs.

3.3.3.2 Genotyping *Gnao1*^{+/*R209H*} mice

Studies were done on N1 R209H heterozygotes with comparisons to littermate controls. To generate *Gnao1*^{+/*R209H*} heterozygotes (N1 backcross), 2 founder *Gnao1*^{+/*R209H*} mice, 1 male and 1 female, were crossed with C57BL/6J mice.

DNA was extracted by an alkaline method (Hirata, Takahashi, Shimoda, & Koide, 2016) from ear clips done before weaning. PCR products were generated with primers flanking the mutation site (Fwd 5' GGACAGGTGTCACAGGGGAT 3'; 5' ACTGGCCTCCCTTGGCAATA 3'). Reaction conditions were: 0.8 µl template, 4 µl 5x Promega PCR buffer, 0.4 µl 10mM dNTPs, 1 µl 10 µM Forward Primer, 1 µl 10 µM Reverse Primer, 0.2 µl Promega GoTaq and 12.6 µl DNase free water (Promega catalog # M3005, Madison WI). Samples were denatured for 4 minutes at 95 °C then underwent 32 cycles of PCR (95 °C for 30 seconds, 63 °C for 30 seconds, and 72 °C for 30 seconds) followed by a 7-minute final extension at 72 °C. Ethanol precipitation was done on the PCR products and then samples were sent for Sanger sequencing (GENEWIZ, Inc. Plainfield, NJ).

3.3.4 Behavioral Studies

Researchers conducting behavioral experiments were blinded until the data analysis was completed. Before each experiment, mice were acclimated in the testing room for at least 10 min. The timeline of behavioral protocols is described in Figure 3.3. Female experimenters conducted all behavioral studies.

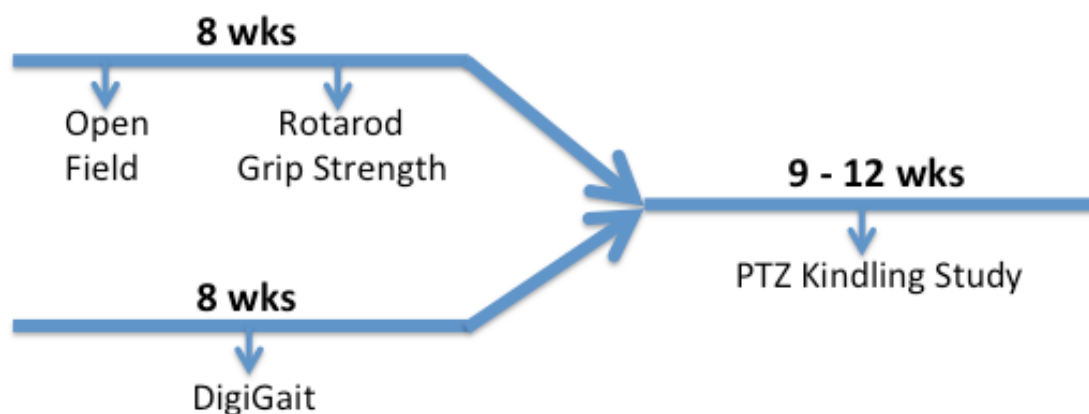


Figure 3.3 The timeline for utilizing animals in this study. Open field, Rotarod and Grip strength tests were performed on the same group of 8-week-old animals in this as showed above. DigiGait tests were done on naïve 8-week-old animals. Animals finishing the motor behavior studies were used for the PTZ kindling study for 3 weeks.

3.3.4.1 Open Field

The Open Field test was conducted in Fusion VersaMax 42 cm x 42 cm x 30 cm arenas (Omnitech Electronics, Inc., Columbus, OH). Mice and their littermate controls were placed in the arena for 30 minutes to observe spontaneous activities. Using the Fusion Software, distance traveled (cm) was evaluated for novel (first 10 minutes),

sustained (10-30 minutes), and total (0-30 minutes) activity. Center Time was also measured. Center Time was defined as the time spent in the center portion (20.32cm x 20.32cm) of the Open Field cage.

3.3.4.2 RotaRod

Motor skills were assessed using an Economex accelerating RotaRod (Columbus Instruments, Columbus, OH). The entire training and testing protocol took two days. On day 1, mice were trained for three 2-minute sessions, with a 10-minute rest between each training period. During the first two sessions, the RotaRod was maintained at a constant speed of 5 rpm. In the third training session, the rod was started at 5 rpm and accelerated at 0.1 rpm/sec for 2 minutes. On day 2, mice were trained with two more accelerating sessions for 2 minutes each with a 10-minute break in between. The final test session was 5 minutes long, starting at 5 rpm then accelerating to 35 rpm (0.1 rpm/sec). For all training and test trials, the time to fall off the rod was recorded. RotaRod learning curves were done on a separate group of mice with 10 tests in one day with a 5-min rest between each test. The learning rate of each group of animals was calculated as described (Hirata et al., 2016).

3.3.4.3 Grip Strength

Mouse grip strength data was collected following a protocol adapted from Deacon et al (Deacon, 2013) using seven home-made weights (10, 18, 26, 34, 42, 49, 57 grams). Briefly, the mouse was held by the middle/base of the tail and lowered to grasp a weight.

A total of three seconds was allowed for the mouse to hold the weight with its forepaws and to lift the weight until it was clear of the bench. Three trials were done starting with the 10g weight to permit the mice to lift the weights with a 10-second rest between each trial. If the mouse successfully held a weight for 3 seconds, the next heavier weight was given; otherwise the maximum time/weight achieved was recorded. A final total score was calculated based on the heaviest weight the mouse was able to lift up and the time that it held it (Deacon, 2013). The final score was normalized to the body weight of each mouse, which was measured before the trial.

3.3.4.4 DigiGait

Mouse gait data were collected using a DigiGait Imaging System (Mouse Specifics, Inc., Framingham, MA) (Hansen & Pulst, 2013). The test is used for assessment of locomotion as well as the integrity of the cerebellum and muscle tone/equilibrium (Franco-Pons, Torrente, Colomina, & Vilella, 2007). Briefly, after acclimation, mice were allowed to walk on a motorized transparent treadmill belt. A high-speed video camera was mounted below to capture the paw prints on the belt. Each paw image was treated as a paw area and its position recorded relative to the belt. Seven speeds (18, 20, 22, 25, 28, 32 and 36 cm/s) were tested per animal with a 5-minute rest between each speed. An average of 4-6 s of video was saved for each mouse, which is sufficient for the analysis of gait behaviors in mice (Franco-Pons et al., 2007). For each speed, left & right paws were averaged for each animal while fore and

hind paws were evaluated separately. Stride length was normalized to animal body length.

3.3.5 PTZ Kindling Susceptibility

A PTZ kindling protocol was performed as described before (Kehrl et al., 2014) to assess epileptogenesis. Briefly, PTZ (40 mg/kg, i.p. in 5 mg/ml) was administered every other day starting at 8 weeks of age. Mice were monitored and scored for 30 minutes for behavioral signs of seizures as described (Grecksch et al., 2004; Kehrl et al., 2014; Wilczynski et al., 2008). Kindling is defined as death or the onset of a tonic-clonic seizure on two consecutive treatment days. The number of injections for each mouse to reach a sensitization was reported in survival curves. This experiment lasted up to 4 weeks with a maximum of 12 doses. Each animal in the study was checked every day for health and seizure development.

Animals were humanely euthanized with CO₂ immediately after kindling or after 12 PTZ injections and observation. In total, 40 animals were used for this study, among which 27 died of tonic-clonic seizures and 13 were euthanized after 12 doses of PTZ injections.

3.3.6 Data Analysis

All data was analyzed using GraphPad Prism 7.0 (GraphPad; La Jolla, CA). Data are presented as mean \pm SEM and a p value less than 0.05 was considered significant. All statistical tests are detailed in Figure Legends. Multiple comparison correction of the

dataset from DigiGait was performed via a false discovery rate (FDR) correction at a threshold value of 0.01 in an R environment using the psych package.

3.4 Results

3.4.1 The growth patterns of the three newly developed *Gnao1* mutant mouse models (G203R, R209H and Δ T191F197)

3.4.1.1 *Gnao1*^{+G203R} mice showed normal viability and growth.

Genotypes of offspring of *Gnao1*^{+G203R} x WT crosses (N1 - C57BL/6NCrl x C57BL/6J) were observed at the expected frequency (29 WT and 27 heterozygous). All three homozygous mice from *Gnao1*^{+G203R} x *Gnao1*^{+G203R} crosses died by P1. The small numbers of offspring observed from these crosses so far, however, were not significantly different from expected frequencies (4 wt, 14 het, and 3 homozygous). Heterozygous *Gnao1*^{+G203R} mice did not show any growth abnormalities compared to *Gnao1*^{+/+} mice (Figure 3.1B & 3.1D) and they had relatively normal survival. There were two spontaneous deaths (~5-7 weeks) seen for *Gnao1*^{+G203R} mice out of 33 (Figure 3.1C). This is reminiscent of the spontaneous deaths seen previously with the *Gnao1*^{+G184S} GOF mutant mice (Kehrl et al., 2014). *Gnao1*^{+G203R} mice did not exhibit any obvious spontaneous seizures or abnormal movements.

3.4.1.2 *Gnao1*^{+R209H} mice have expected frequency and normal viability

Two founder *Gnao1*^{+R209H} mice, 1 male and 1 female, were crossed with C57BL/6J mice. Out of 98 offspring of a cross of *Gnao1*^{+R209H} with WT mice, 51 heterozygotes and

47 WT were observed. *Gnao1*^{+/*R209H*} mice exhibit no overt postural or movement abnormalities or seizures at basal conditions. Adult mice showed no statistically significant differences in weight between WT and *Gnao1*^{+/*R209H*} genotypes of either sex (data not shown).

3.4.1.3 *Gnao1*^{+/ Δ T191F197} mice developed spontaneous seizures at P7 and died before P16.

Gnao1 ^{Δ T191F197} mutant mice were generated using CRISPR/Cas9 genome editing on the C57BL/6NCrl strain. gRNA targets within exon 6 of the *Gnao1* locus (ENSMUSG00000031748) were used to generate the Δ T191F197 mutation (Figure 3.4A). Only one viable founder (male) was obtained. Genotypes of offsprings of this male founder *Gnao1*^{+/ Δ T191F197} x WT crosses (C57BL/6NCrl x C57BL/6J) were observed. Heterozygous *Gnao1*^{+/ Δ T191F197} mice were very rare and all died perinatally within P16 (Figure 3.4C & 3.2D). *Gnao1*^{+/ Δ T191F197} mice also developed spontaneous seizure at P7 (Figure 3.4B). Previously, we described that *Gnao1* G184S heterozygous mutant mice on a 129 background (N6 129S1/SvImJ) lived a relatively normal life (Kehrl et al., 2014). To investigate whether a 129 background is also protective towards the Δ T191F197 mutant mice, we crossed our *Gnao1*^{+/ Δ T191F197} with WT mice on the 129 background and assessed their offsprings. Unfortunately, 129 alleles did not appear to provide a dominant protective effect against the spontaneous death observed in the heterozygous Δ T191F197 mutant mice (Figure 3.4C).

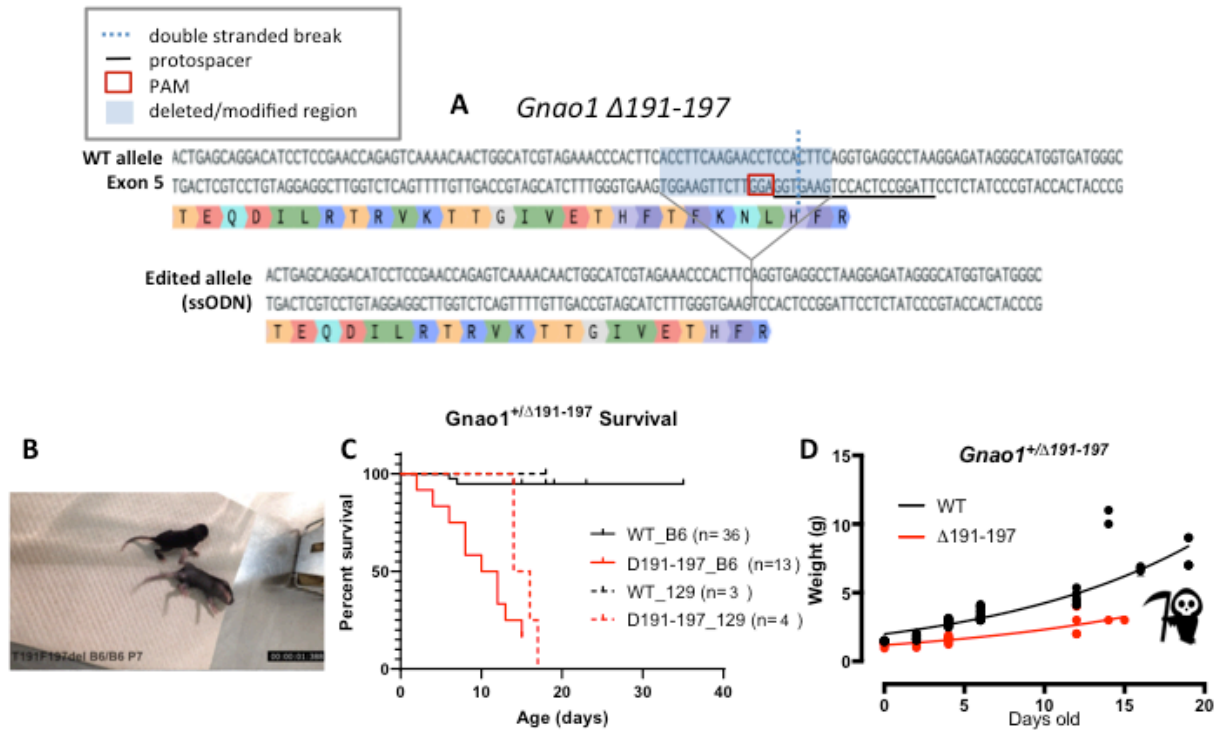


Figure 3.4 *Gnao1*^{+/ $\Delta T191F197$} mice developed spontaneous seizures at P7 and died before P16. (A) Targeting of the *Gnao1* locus. The location of the gRNA target protospacer and the PAM, and double stranded breaks following Cas9 cleavage are indicated on the WT allele. Deleted or modified sequences are highlighted in blue. The resulting edited allele sequence and translation are presented along with the sequences used as references for ssODN synthesis. (B) Video snapshot of one heterozygous *Gnao1*^{+/ $\Delta T191F197$} mutant mouse developed spontaneous seizure at P7. Photo comparing mutant mouse with its littermate control is shown. (C) *Gnao1*^{+/ $\Delta T191F197$} on both C57BL/6J and B6/129 backgrounds died prematurely. (D) *Gnao1*^{+/ $\Delta T191F197$} mice did not develop or gain weight normally comparing to WT littermate controls.

3.4.2 Behavioral assessment of mutant *Gnao1* mouse models (G184S, G203R, R209H and KO) for movement patterns

3.4.2.1 Female *Gnao1*^{+G184S} and male *Gnao1*^{+G203R} mice show similar movement abnormalities and gait disturbances

Since GOF alleles of *GNAO1* in children result primarily in movement disorder, we tested motor coordination in two mouse lines with GOF mutations. One carried an engineered GOF mutant G184S, designed to block RGS protein binding (DiBello et al., 1998; Fu et al., 2004; Lan et al., 1998). The other is the G203R GOF mutant, which has been seen in at least 9 children (Chapter 1) (Feng et al., 2018; Feng et al., 2017). First, we used a two-day training and testing procedure on the RotaRod (Figure 3.5A & 3.5B). *Gnao1*^{+G184S} and *Gnao1*^{+G203R} mice were compared to their same-sex littermate controls. Female *Gnao1*^{+G184S} mice exhibited a reduced retention time on the accelerating RotaRod (unpaired t-test, $p < 0.001$, Figure 3.5A) while male mice remained unaffected. In contrast, male *Gnao1*^{+G203R} mice exhibited reduced time to stay on the rotating rod (unpaired t-test, $p < 0.05$, Figure 3.5B) while female *Gnao1*^{+G203R} mice did not show any abnormalities. Results from all the RotaRod training and testing sessions are shown in Figure S1. Neither *Gnao1*^{+G184S} nor *Gnao1*^{+G203R} mice showed a significant difference in learning rate on RotaRod (Figure S3.3), suggesting that the differences we observed in the RotaRod study was due to movement deficits rather than learning difficulties.

Grip strength was assessed as described (Deacon, 2013). This test is widely done in

combination with the RotaRod motor coordination test. This may be relevant to the hypotonia, seen in many *GNAO1* patients (Ananth et al., 2016; Bruun et al., 2018; Danti et al., 2017; Euro, Epilepsy Phenome/Genome, & Epi, 2014; Gawlinski et al., 2016; Honey et al., 2018; Kulkarni et al., 2016; Law et al., 2015; Marce-Grau et al., 2016; Saitsu et al., 2016; Schorling et al., 2017; Waak et al., 2018; Yilmaz et al., 2016; Zhu et al., 2015). Similar to the RotaRod results, female *Gnao1*^{+/*G184S*} mice also showed reduced forepaw grip strength compared to their littermate controls (unpaired student t-test, $p < 0.05$, Figure 3.5C) while males did not exhibit a significant difference (Figure 3.5C). In contrast, both male and female *Gnao1*^{+/*G203R*} mice displayed reduced forepaw grip strength (unpaired t-test, $p < 0.05$, Figure 3.5D).

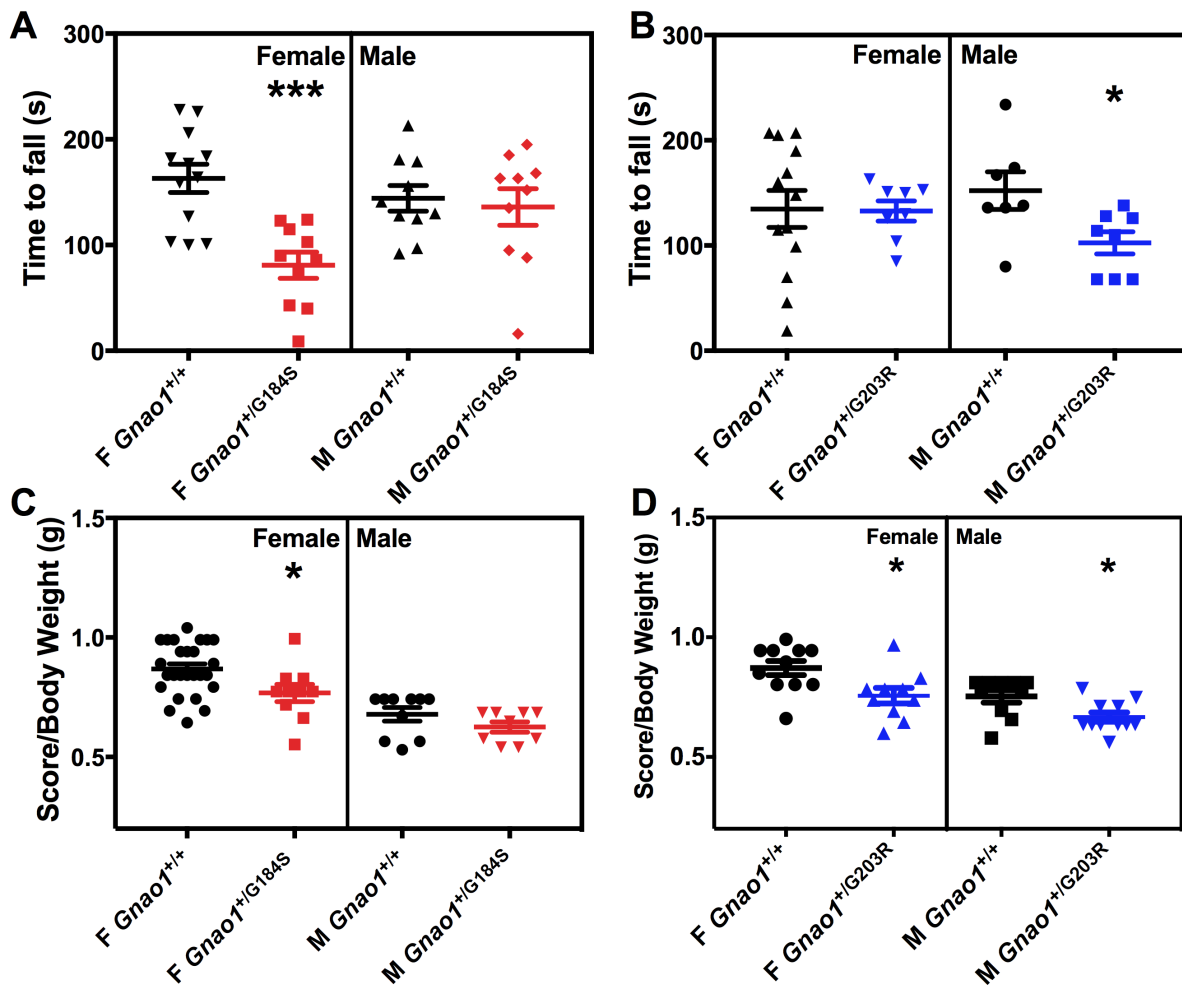


Figure 3.5 Female *Gnao1*^{+G184S} mice and male *Gnao1*^{+G203R} mice show reduced time on RotaRod and reduced grip strength. (A&B) Quantification of RotaRod studies. (A) Female *Gnao1*^{+G184S} mice lose the ability to stay on a RotaRod (unpaired t-test; *** $p < 0.001$), while male *Gnao1*^{+G184S} mice appeared unaffected. (B) Male *Gnao1*^{+G203R} also showed reduced motor coordination on RotaRod (unpaired t-test, * $p < 0.01$). (C&D) Quantification of grip strength results. Scores for each mouse were normalized to the body weight of the animal measured. (C) Female *Gnao1*^{+G184S} mice are less capable of lifting weights compared to their *Gnao1*^{+/+} siblings (unpaired t-test, * $p < 0.05$). (D) Both male and female *Gnao1*^{+G203R} mice showed reduced ability to hold weights (unpaired t-test, * $p < 0.05$). Data are shown as mean \pm SEM.

The open field test provides simultaneous measurements of locomotion, exploration and surrogates of anxiety. It is a useful tool to assess locomotive impairment in rodents (Tatem et al., 2014), however, environmental salience may reduce the impact of the motor impairment on behaviors (Parr & Friston, 2017). Therefore, we divided the 30-min open field measurements into two periods, with the first 10 min assessing activity in a novel environment and the 10-30 minute period designated as sustained activity (Figure 3.6C & 3.6D). The novelty measurement showed a significant difference between *Gnao1*^{+G184S} mice and their littermate controls for both male and female mice (2-way ANOVA, $p < 0.01$ for female, $p < 0.05$ for male, Figure 3.6C). Female, but not male, *Gnao1*^{+G184S} mice showed reduced activity in the sustained phase of open field testing (2-way ANOVA, * $p < 0.05$, ** $p < 0.01$, **** $p < 0.0001$). Both male and female *Gnao1*^{+G184S} mice also showed reduced total activity (2-way ANOVA, $p < 0.001$, Figure 3.6A & 3.6C). Neither male nor female *Gnao1*^{+G203R} mice performed differently in the open field arena compared to their littermate controls (Figure 3.6B & 3.6D). No significant difference was observed in the time mice spent in the center of the arena (Figure S3.2).

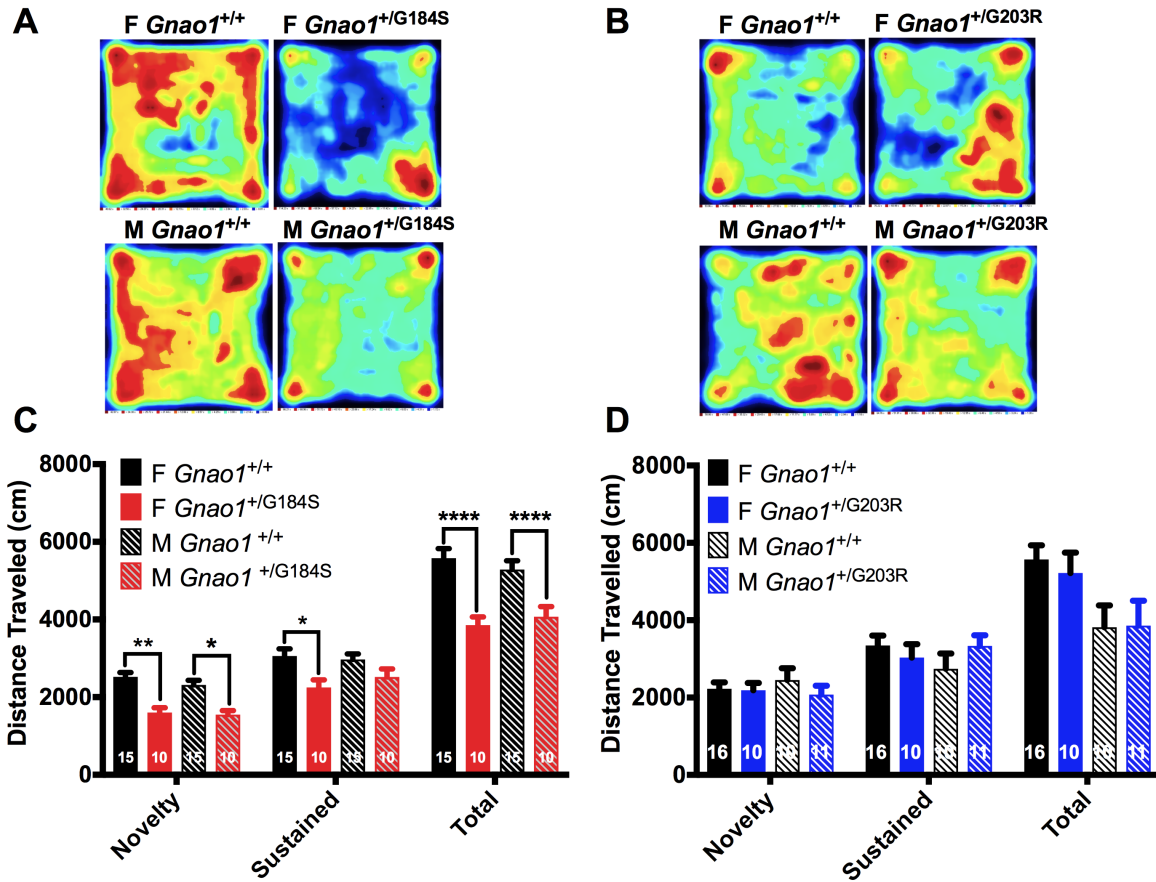


Figure 3.6 *G184S* mutant mice showed reduced activities in Open Field Test but *G203R* mutants do not. (A&C) Female and male *Gnao1*^{+/G184S} mice showed decreased activity in the open field test. A total of 30 min activity was recorded which was divided into Novelty (0-10 min) and Sustained (10-30 min) period. (A) Representative heat map of overall activity comparison between *Gnao1*^{+/+} and *Gnao1*^{+/G184S} mice in both sexes. (C) Quantitatively, both male and female *Gnao1*^{+/G184S} travelled less in the open field arena (2-way ANOVA; ****p< 0.0001, **p<0.01, *p<0.05). (B & D) Neither male nor female *Gnao1*^{+/G203R} mice showed abnormalities in the open field arena. (B) Sample heat map tracing both female and male mouse movement in open field. (D) Quantification showed no difference between *Gnao1*^{+/+} and *Gnao1*^{+/G203R} mice in distance traveled (cm) in the open field arena (2-way ANOVA; n.s.). Data are shown as mean ± SEM. Numbers of animals are indicated on bars.

In addition to the above behavioral tests, we also performed gait assessment on *Gnao1*^{+/^{G184S} and *Gnao1*^{+/^{G203R mice of both sexes. Gait is frequently perturbed in rodent models of human movement disorders even when the actual movement behavior seen in the animals does not precisely phenocopy the clinical movement pattern (Song, Fan, Exeter, Hess, & Jinnah, 2012; Stroobants, Gantois, Pooters, & D'Hooge, 2013). The multiple parameters assessed in DigiGait allow it to pick up subtle neuromotor defects and makes it more informative than the RotaRod test.}}}

The gait analysis largely confirmed the sex differences between the two strains in RotaRod tests. Thirty-seven parameters were measured for both front and hind limbs. Given the large number of measurements, we used false discovery rate (FDR) analysis with a Q of 1% as described in Methods to reduce the probability of Type I errors (Figure S3.4 & S3.5, Table S3.1-S3.4). *Gnao1*^{+/^{G184S female mice showed 22 significant differences (Q<0.01) and males showed 8 (Figure S3.4, Table S3.3 & S3.4). For *Gnao1*^{+/^{G203R mice, the opposite sex pattern was seen with 27 parameters in females and 8 parameters in males showing significant differences from WT (Figure S3.5, Table S3.1 & S3.2). Two of the most highly significant parameters and ones that had face validity in terms of clinical observations (stride length and paw angle variability) were chosen for further analysis.}}}}

Across the range of treadmill speeds, female *Gnao1*^{+/^{G184S mice showed significantly reduced stride length (2-way ANOVA, p<0.01, Figure 3.7A) and increased paw angle}}

variability (2-way ANOVA, $p < 0.0001$, Figure 3.7E) compared to WT littermates. Male *Gnao1*^{+G184S} mice only had a difference in paw angle variability (2-way ANOVA, $p < 0.0001$), not in stride length (Figure 3.7C & 3.7G). These results are consistent with the results of RotaRod and grip strength measurements in that female *Gnao1*^{+G184S} mice showed a stronger phenotype than males. In contrast to the *Gnao1*^{+G184S} mice, male *Gnao1*^{+G203R} mice appeared to be more severely affected in gait compared to female *Gnao1*^{+G203R} mice. Male *Gnao1*^{+G203R} mice had highly significantly reduced stride length (2-way ANOVA, $p < 0.0001$, Figure 3.7D) and increased paw angle variability (2-way ANOVA, $p < 0.05$, Figure 3.7H). In contrast, female *Gnao1*^{+G203R} mice did not show any significant differences in stride length or paw angle variability (Figure 3.7B & 3.7F). In addition to these quantitative gait abnormalities a qualitative defect was seen. A significant number of *Gnao1*^{+G203R} mice of both sexes failed to run when the belt speed exceeded 22 cm/s (Mann-Whitney test, female and male $p < 0.05$, Figure 3.7J). For reasons that are not clear such a difference was not seen for *Gnao1*^{+G184S} mice (Figure 3.7I).

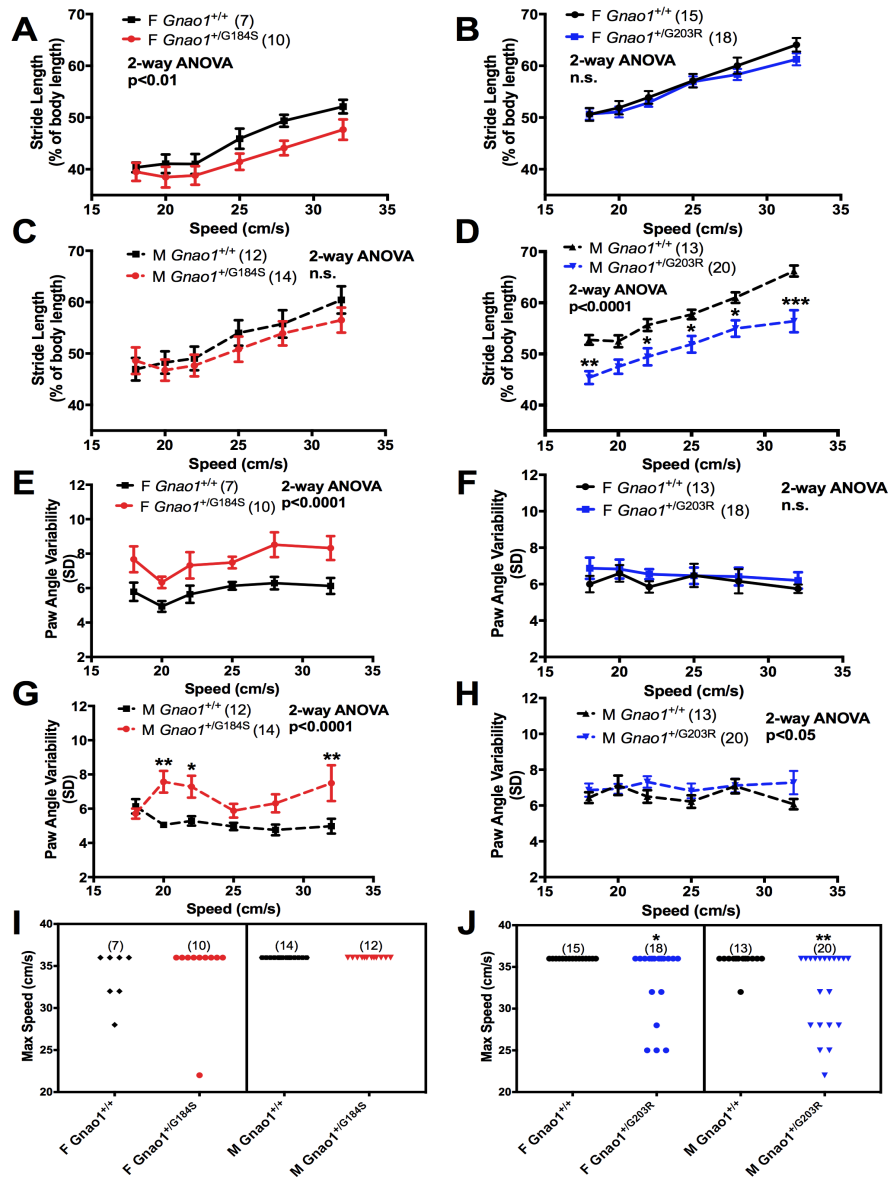


Figure 3.7 DigiGait Imaging System reveals sex-specific gait abnormalities in *Gnao1*^{+/G184S} mice and *Gnao1*^{+/G203R} mice. (A-D) Female *Gnao1*^{+/G184S} mice showed significant gait abnormalities, while female *Gnao1*^{+/G203R} mice remain normal. (A & B) Female *Gnao1*^{+/G184S} mice showed reduced stride length (2-way ANOVA with Bonferroni multiple comparison post-test) while female *Gnao1*^{+/G203R} mice were unchanged from control (2-way ANOVA; n.s.). (C) Female *Gnao1*^{+/G184S} mice also showed increased paw angle variability (2-way ANOVA, $p < 0.0001$) while female *Gnao1*^{+/G203R} mice showed normal paw angle variability. (E-H) Male *Gnao1*^{+/G203R} and *Gnao1*^{+/G184S} mutant mice showed distinct gait abnormalities. (E & G) Male *Gnao1*^{+/G184S} mice showed significantly

Figure 3.7 (cont'd) increased paw angle variability (2-way ANOVA $p < 0.0001$ overall with significant Bonferroni multiple comparison tests; $**p < 0.01$ and $*p < 0.05$). There was no effect on stride length. (F & H) In contrast, male *Gnao1*^{+/^{G203R} mice showed markedly reduced stride length (2-way ANOVA $p < 0.0001$ with Bonferroni multiple comparison post-test; $***p < 0.001$, $**p < 0.01$, and $*p < 0.05$) and modestly elevated paw angle variability (overall $p < 0.05$). (I) *Gnao1*^{+/^{G184S} mice did not show significant differences in the highest treadmill speed successfully achieved. (J) Both male and female *Gnao1*^{+/^{G203R} mice showed reduced capabilities to run on a treadmill at speeds greater than 25 cm/s (Mann-Whitney test; $*p < 0.05$).}}}

3.4.2.2 *Gnao1*^{+/^{R209H} mouse model exhibits unique hyperactive behavior in the open field arena but no abnormal motor coordination in other behavior tests and minor disturbance in gait analysis}

All patients with R209H mutation were diagnosed with hyperkinetic movements including chorea/athetosis and dystonia (Ananth et al., 2016; R. Dhamija et al., 2016; Kelly et al., 2019; Kulkarni et al., 2016; Marecos et al., 2018). To assess whether *Gnao1*^{+/^{R209H} mice phenocopy the patients' symptoms, we repeated the above behavior tests with the newly developed heterozygous R209H mice.}

Unlike *Gnao1*^{+/^{G184S} and *Gnao1*^{+/^{G203R} mice, both sexes of *Gnao1*^{+/^{R209H} mice were hyperactive in the open field arena (Figure 3.8A& 3.8B) but completely normal in Rotarod (Figure 3.8C) and grip strength assessment (Figure 3.8D). Male and female *Gnao1*^{+/^{R209H} mice also showed reduced time spent in the center of the arena (Figure 3.8A & 3.8B), which is an indication for possible anxiety-linked behavior (Wilmshurst,}}}}

Byrne, & Webb-Peploe, 1989).

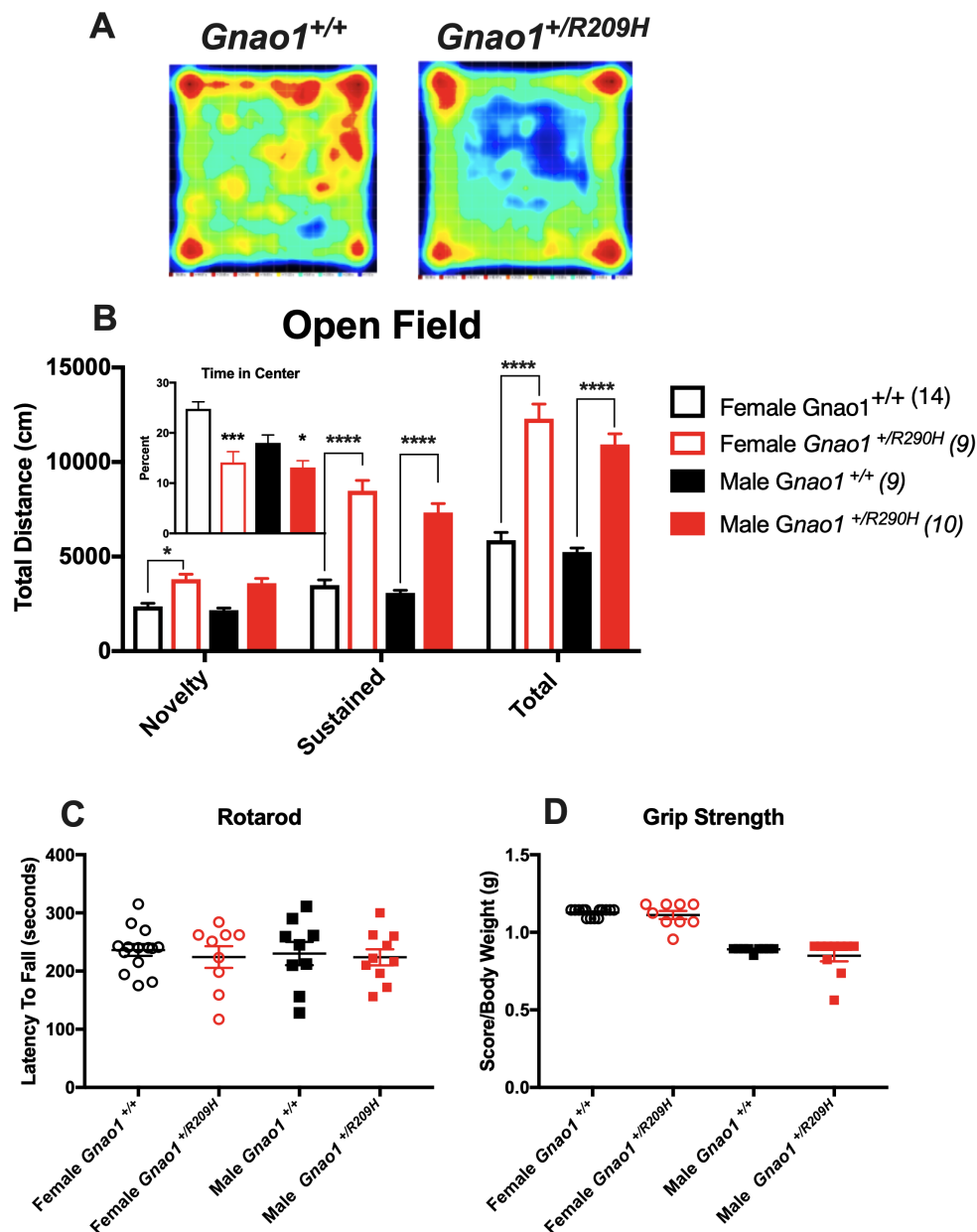


Figure 3.8 *Gnao1*^{+/R209H} mice show significant hyperactivity and reduced time in center in the open field arena. (A) Representative heat maps of *Gnao1*^{+/R209H} mice and *Gnao1*^{+/+} mice in the open field arena (B) Time spent in the open field arena was separated into 0-10 minutes (novelty) and 10-30 minutes (sustained). *Gnao1*^{+/R209H} male and female mice exhibit increased locomotion in the novelty period. Hyperactivity was maintained throughout the sustained period as mice continued to show significant

Figure 3.8 (cont'd) increase in distance traveled (2-way ANOVA; **** $p < 0.0001$, *** $p < 0.001$, * $p < 0.05$). *Gnao1*^{+/^{R209H} mice of both sexes spend less time in center areas of the open field arena compared to WT littermates. (C) Neither male nor female *Gnao1*^{+/^{R209H} mice show significant differences on the Rotarod. (D) There is no significant difference between grip strength between WT and *Gnao1*^{+/^{R209H} mice. Data are shown as mean \pm SEM.}}}

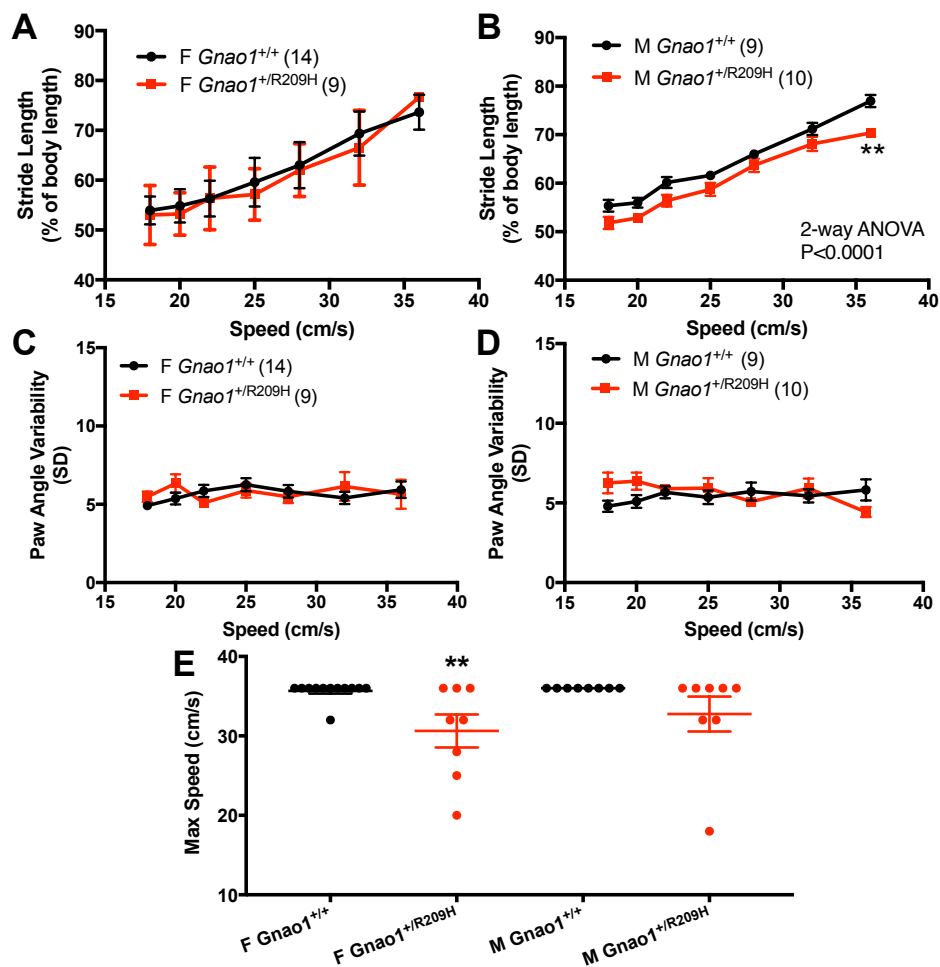


Figure 3.9 Male and female *Gnao1*^{+/^{R209H} mice shows gait abnormalities in different tests on the DigiGait imaging system. (A & B) Male *Gnao1*^{+/^{R209H} mice showed reduced stride length compared to wildtype littermates (2-way ANOVA with Bonferroni multiple comparison post-test), while female *Gnao1*^{+/^{R209H} mice show a normal stride}}}

Figure 3.9 (cont'd) length. (C & D) Neither male nor female *Gnao1*^{+/^{R209H} exhibited significant differences in paw angle variability compared to WT littermates. (E) At speeds greater than 25 cm/s female *Gnao1*^{+/^{R209H} shows reduced ability to run on a treadmill.}}

Gait analysis was done with a Digigait video system. Similar to *Gnao1*^{+/^{G203R} mouse model, male *Gnao1*^{+/^{R209H} mice showed a highly significant genotype effect with reduced stride length compared to wildtype littermates (**p<0.01, 2-way ANOVA). Females showed no difference from WT. No difference was seen in paw angle variability of *Gnao1*^{+/^{R209H} of either sex. However, both male and female *Gnao1*^{+/^{R209H} mice failed to consistently run at higher speeds (>20 cm/s; Figure 3.9E, **p<0.01, Student's t-test). The difference observed was not due to a reduced body length (WT: 9.54 cm vs R209H: 10.17 cm) or weight. Comparisons of other parameters assessed by the Digigait system were shown in the appendix (Figure S3.6 & Table S3.5-S3.6). Compared to the number of parameters with significant difference detected for *Gnao1*^{+/^{G203R} and *Gnao1*^{+/^{G184S} mice respectively, *Gnao1*^{+/^{R209H} mice only did not display as many significantly different gait abnormalities (Figure S3.6).}}}}}}}

3.4.2.3 Previously described *Gnao1*^{+/-} mouse model did not show any abnormalities in the behavioral test battery

A *Gnao1*^{+/-} KO mouse model was previously described for the study of the mechanisms of G_o protein (Jiang et al., 1998; Valenzuela et al., 1997). In these reports, homozygous *Gnao1*^{-/-} mice lived but exhibited a reduced lifespan and developed severe

motor control impairment (Jiang et al., 1998). *Gnao1*^{-/-} mice were also reported to be hyperactive and had an abnormal turning behavior (Jiang et al., 1998). Heterozygous *Gnao1*^{+/-} mice did not have any spontaneous abnormal behavior (Jiang et al., 1998). We have been unable to generate homozygous (*Gnao1*^{-/-}) KO mice. In our behavior battery, heterozygous *Gnao1*^{+/-} mice did not show any abnormalities in open field (Figure 3.10A-D), Rotarod (Figure 3.10E), or grip strength (Figure 3.10F). However, male *Gnao1*^{+/-} mice did exhibit significantly reduced stride length (Figure 3.11B, p<0.001, 2-way ANOVA). Furthermore, male *Gnao1*^{+/-} mice also showed several DigiGait parameters that are significantly different compared to the WT mice (Figure S3.7 & Table S3.7-S3.8). To our surprise, *Gnao1*^{+/-} mice also did not develop any spontaneous seizure activity in contrast to the LOF mutant mice *Gnao1*^{+/ Δ T191F197}, which were severely impaired by spontaneous seizures perinatally and died prematurely (Figure 3.4).

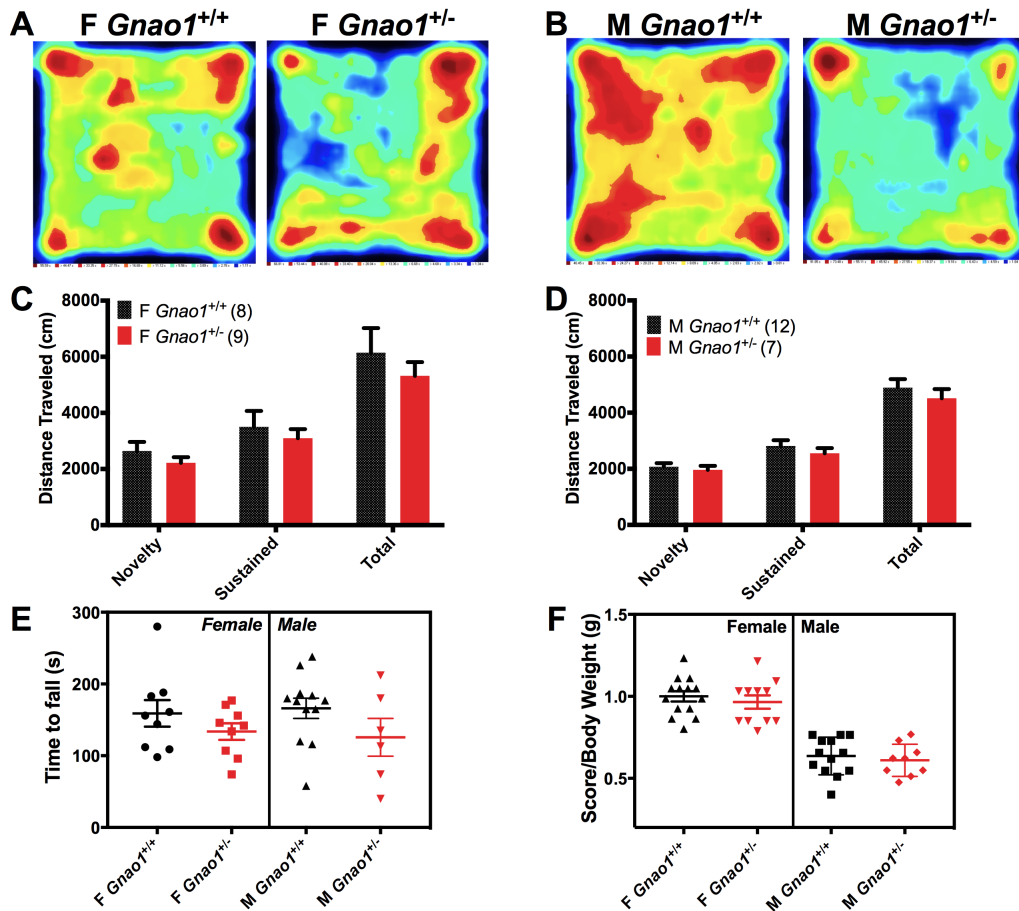


Figure 3.10 Male and female *Gnao1*^{+/-} mice do not show any abnormalities in the behavioral tests including open field, Rotarod, and grip strength. (A-D) Neither sex of *Gnao1*^{+/-} mice has normal activity in the open field arena in any time period. The activity pattern of *Gnao1*^{+/-} mice (A) is also similar to *Gnao1*^{+/+} (B). The overall activity is also comparable between male (D) and female (C) WT and *Gnao1*^{+/-} mice. (E) *Gnao1*^{+/-} mice do not show any reduced motor coordination capability in Rotarod. (F) Grip strength test shows that neither sex of *Gnao1*^{+/-} mice decreases their capability of lifting heavy weight.

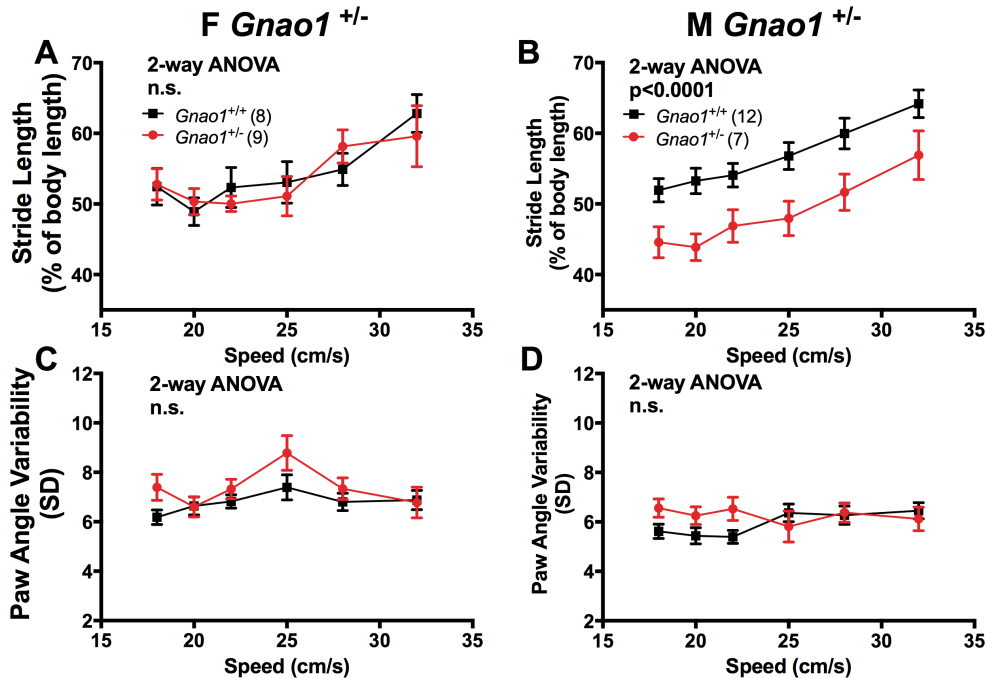


Figure 3.11 DigiGait Imaging System reveals the decreased stride length in male *Gnao1*^{+/-} mice. Female *Gnao1*^{+/-} mice do not show any difference comparing to female *Gnao1*^{+/-} mice in either stride length (A) or paw angle variability (C). (B) However, male *Gnao1*^{+/-} mice exhibit a significantly decreased stride length ($p < 0.0001$, 2-way ANOVA) but not (D) paw angle variability.

3.4.3 PTZ kindling study of G203R and R209H mice.

Kindling studies for *Gnao1*^{+/*G184S*} and *Gnao1*^{+/-} mice have been reported previously by Kehrl et al (Kehrl et al., 2014).

3.4.3.1 Male *Gnao1*^{+/*G203R*} mice are sensitized to PTZ kindling.

Epilepsy has been observed in 100% of patients with *GNAO1* G203R mutations (Arya et al., 2017; Feng et al., 2018; Nakamura et al., 2013; Saito et al., 2016; Xiong et al., 2018). Also in the *Gnao1*^{+/*G184S*} GOF mutant mice, we previously reported spontaneous lethality as well as increased susceptibility to kindling by the chemical

anticonvulsant PTZ for both males and females (Kehrl et al., 2014). Kindling is a phenomenon where a sub-convulsive stimulus, when applied repetitively and intermittently, leads to the generation of full-blown convulsions. To determine if the G203R GOF mutant mice mimicked the G184S mutants and phenocopied the human epilepsy pattern of children with the G203R mutation, we assessed PTZ-induced kindling in *Gnao1*^{+G203R} mutant mice. As expected for C57BL/6 mice, females were more prone to kindling than male mice, half kindled at 4 and 8-10 injections, respectively (Figure 3.12A & 3.12B). Despite the increased sensitivity of females in general, female *Gnao1*^{+G203R} mice did not show significantly higher sensitivity to PTZ compared to their littermate controls (Figure 3.12A). On the contrary, male *Gnao1*^{+G203R} mice were more sensitive to PTZ kindling than controls (Figure 3.12B, Mantel-Cox Test, $p < 0.05$). Also, three spontaneous deaths were seen (two male and one female) among the 33 G203R mice observed for at least 100 days, similar to the early lethality seen in G184S mutant mice. We cannot, however, attribute those deaths to seizures at this point.

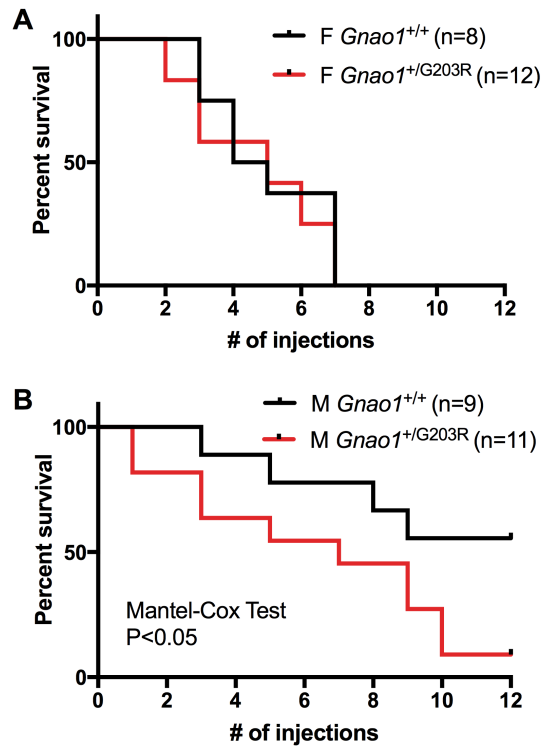


Figure 3.12 *Gnao1*^{+/G203R} male mice have an enhanced Pentylentetrazol (PTZ)-Kindling response. (A) Female *Gnao1*^{+/G203R} did not show heightened sensitivity to PTZ injection. (B) Male *Gnao1*^{+/G203R} mice developed seizures earlier after repeated PTZ injections (Mantel-Cox Test; $p < 0.05$).

3.4.3.2 R209H mutant mice are not hypersensitive to PTZ kindling

Repeated application of a sub-threshold convulsive stimulus, leads to the generation of full-blown convulsions (Dhir, 2012). *GNAO1* variants differ in their ability to cause epileptic seizures in patients. Children carrying the R209H mutant allele do not exhibit a seizure disorder. In accordance with the patients' pattern, *Gnao1*^{+/R209H} mice did not show increased susceptibility to kindling-induced seizures (Figure 3.13A & 3.13B). This contrasts with the increased kindling sensitivity in male G203R mutant mice (Figure 3.13) (Feng et al., 2019; Larrivee et al., 2019).

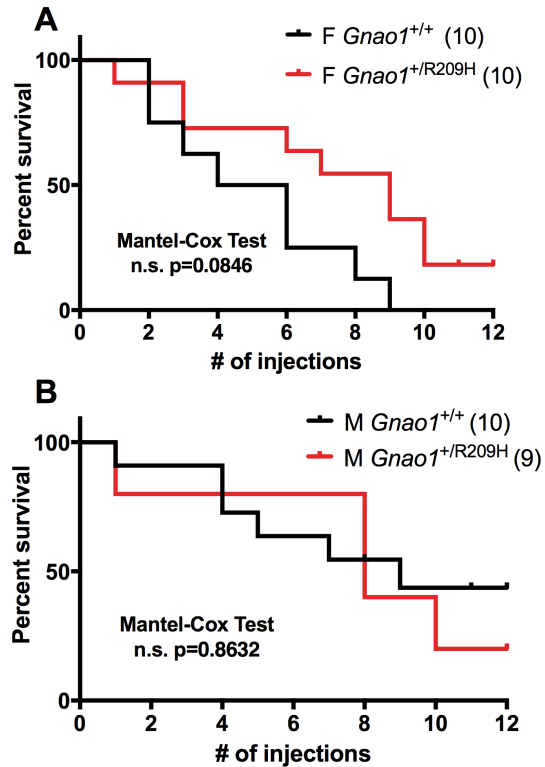


Figure 3.13 *Gnao1*^{+/R209H} mice do not have an enhanced pentylenetetrazol (PTZ) kindling response. (A&B) Neither male nor female *Gnao1*^{+/R209H} mice showed significant differences in sensitivity to PTZ injection compared to WT littermates (n.s.; Mantel-Cox test).

3.5 Discussion

In this chapter, I describe three newly developed *Gnao1* mutant mouse models (Δ T191F197, G203R, and R209H) and compare them with two previously published mouse models (G184S and KO). These data verify the genotype-phenotype correlation that I describe in chapter 2. Also, among the three different newly developed mouse models, only two mouse models (G203R and R209H) produced viable strains (Table

3.3). Through the established behavioral pattern of the mouse models, we intend to explore mechanisms of *Gnao1*-associated movement disorders in the next chapter.

Heterozygous male mice carrying the G203R mutation (GOF) in *Gnao1* exhibit both a mild increase in seizure propensity and evidence of abnormal movements. This fits precisely with the variable seizure pattern of the children who carry this mutation as well as their severe choreo-athetotic movements (Arya et al., 2017; Dietel, 2016; Feng et al., 2018; Nakamura et al., 2013; Saitsu et al., 2016; Schirinzi et al., 2019; Schorling et al., 2017; Xiong et al., 2018). Heterozygous mice carrying the R209H mutation (NF) only develop hyperkinetic movements without loss of motor coordination on RotaRod or loss of capability of lifting heavy weights (Figure 3.8). This mimics patients with R209H mutations (Ananth et al., 2016; Blumkin et al., 2018; R. M. Dhamija, J. W.; Shah, B. B.; Goodkin, H. P., 2016; Kelly et al., 2019; Kulkarni et al., 2016; Marecos et al., 2018; Menke et al., 2016). In comparison, mice model with the LOF mutation $\Delta T191F197$ developed spontaneous seizures at an early age and died prematurely before P16. This fits the clinical description of the patient carrying the same mutation (Nakamura et al., 2013) who died at 11 months (Figure 3.4). A summary of phenotypes of viable mutant mice is shown in Table 3.4. For comparison purposes, we have also tested the previously reported GOF mutant mouse model (G184S) and KO mouse model. The G184S mouse model exhibits a sex-dependent movement disorder while KO mice did not show any severe motor disability.

Table 3.4 Phenotypes of *Gnao1* mutant mice

	G203R	R209H	G184S	KO
Open Field	Normal	Hyperactivity	Hypoactivity	Normal
Balance (RotaRod)	Reduced	Normal	Reduced	Normal
Grip Strength	Reduced	Normal	Reduced	Normal
Gait Analysis	↓↓ stride length ↑ variability	↓ stride length	↓ stride length ↑↑ variability	↓ stride length
Seizure Susceptibility	Increased	Normal	Increased (Kehrl et al., 2014)	Normal (Kehrl et al., 2014)

In mouse models of movement disorders, the mouse phenotype is usually not as striking or as easily observed as the clinical abnormalities in the patients (Oleas, Yokoi, DeAndrade, Pisani, & Li, 2013; Wilson & Hess, 2013), however they are often informative about mechanism and therapeutics. The male *Gnao1*^{+/*G203R*} mutant mouse carrying patient-derived mutation very closely replicates the mild seizure phenotype of female *Gnao1*^{+/*G184S*} mice (Kehrl et al., 2014). I now show that the female *Gnao1*^{+/*G184S*} mice also exhibit gait and motor abnormalities. Both the *GNAO1* G203R and the G184S mutations show a definite but modest GOF phenotype in biochemical measurements of cAMP regulation (Feng et al., 2017). In each case, the maximum percent inhibition of cAMP is not greatly increased but the potency of the α_{2A} adrenergic agonist, used in those studies to reduce cAMP levels, was increased about 2-fold (Feng et al., 2017). This effectively doubles signaling through these two mutant G proteins at low

neurotransmitter concentrations (i.e. those generally produced during physiological signaling). This, however, does not prove that cAMP is the primary signal mechanism involved in pathogenesis of the disease. The heterotrimeric G protein, G_o , is the defining subunit to many different effectors (Feng et al., 2018; Strittmatter et al., 1994; Wettschureck & Offermanns, 2005). We recently reviewed the mutations associated with genetic movement disorders and identified both cAMP regulation and control of neurotransmitter release as two mechanisms that seem highly likely to account for the pathophysiology of *GNAO1* mutants (Chapter 1) (Feng et al., 2018). Since many G_o signaling effectors (including cAMP and neurotransmitter release) can be mediated by the $G_{\beta\gamma}$ subunit released from the G_o heterotrimer, other effectors could also be involved in the disease mechanisms. A recent hypothesis has also been raised that intracellular signaling by G_{α_o} may be involved (Solis & Katanaev, 2018). The observation that one of the most common movement disorder-associated alleles (R209H and other mutations in Arg²⁰⁹) does not markedly alter cAMP signaling in *in vitro* models, does suggest that the mechanism is more complex than a simple GOF vs LOF distinction at cAMP regulation.

The R209H mutation was only tested for regulation of cAMP levels. It remains an unanswered question why a NF mutation still would lead to movement disorder in human patients and hyperactivity in our mouse models. This is a potential drawback of our *in vitro* assessment of cAMP only in an engineered HEK293T cell system. Since G_{α_o} regulates at least six different pathways (Jiang & Bajpayee, 2009), cAMP may not be the

affected downstream target of the R209H mutation. Therefore, the R209H animal model should be more valuable for mechanistic studies since it will provide a more relevant physiological environment for studying the regulation of Ga_o in isolated neurons.

Another interesting observation lies in the comparison between the KO mouse model and the LOF mouse model $\Delta T191F197$. Although $\Delta T191F197$ proved to be an epileptogenic and lethal mutation in both mouse and human, the actual KO mouse model did not develop any obvious seizure phenotype. Previously, homozygous *Gnao1* KO mice were reported with a mild seizure phenotype (Jiang et al., 1998), however, heterozygous KO mice were relatively normal. One explanation could be the compensation effect of Ga_i protein, which takes over the mechanistic pathways that were once regulated by Ga_o protein. More likely, $\Delta T191F197$ has some unknown mechanism, which would lead to the abnormal fetal development and infantile lethality.

We also observed a striking sex difference in the phenotypes of our mouse models. Female *Gnao1*^{+/*G184S*} mice and male *Gnao1*^{+/*G203R*} mice showed much more prominent movement abnormalities than male G184S and female G203R mutants. However, the patterns of changes in the behavioral tests did not exactly overlap. G184S mutants showed significant changes in open field tests while G203R mutants did not. Conversely, G203R mutants showed a striking reduction in ability to walk/run at higher treadmill speeds while G184S mutants did not. For both mutant alleles, the seizure phenotype was also worse in the sex with more prominent movement disorder. For the NF mutant

line, *Gnao1*^{+/*R209H*} mice did not show any sex difference in their hyperkinetic movements in the open field arena (Figure 3.8), but they did have male dominated gait abnormalities, shown as decreased stride length (Figure 3.9).

GNAO1 encephalopathies are slightly more prevalent (60:40) in female than male patients (Feng et al., 2018). It is not uncommon to have sex differences in epilepsy or movement disorder disease progression. One possible explanation is that estrogen prevents dopaminergic neuron depletion (Smith & Dahodwala, 2014). The $G_{i/o}$ coupled estrogen receptor, GPR30, contributes to estrogen physiology and pathophysiology (Revankar, Cimino, Sklar, Arterburn, & Prossnitz, 2005). Also, PD is more common in male than female human patients (Wooten, Currie, Bovbjerg, Lee, & Patrie, 2004), therefore, the pro-dopaminergic properties of estrogen may exacerbate conditions mediated by hyper-dopaminergic symptoms like chorea in Huntington's disease (HD) (Smith & Dahodwala, 2014). Chorea/athetosis is the most prevalent movement pattern seen in *GNAO1*-associated movement disorders (Feng et al., 2018) so the female predominance correlates with that in HD. Clearly mechanisms of sex differences are complex including differences in synaptic patterns, neuronal densities and hormone secretion (Gillies, Murray, Dexter, & McArthur, 2004; Kompoliti, 1999; Smith & Dahodwala, 2014), but it is beyond the scope of this chapter to explain how the molecular differences contribute to the distinct behavioral patterns. A more detailed analysis on sex difference is provided in Chapter 5.

Since *GNAO1* encephalopathy is often associated with developmental delay and cognitive impairment (Feng et al., 2018), it would be interesting to see whether the movement phenotype we have seen in female *Gnao1*^{+/^{G184S}, male *Gnao1*^{+/^{G203R} or *Gnao1*^{+/^{R209H} mice is due to a neurodevelopmental malfunction or to ongoing active signaling alterations. G_o-coupled GPCRs play an important role in hippocampal memory formation (Madalan, Yang, Ferris, Zhang, & Roman, 2012; Schutsky, Ouyang, & Thomas, 2011). Additional behavioral tests will be valuable to assess the learning and memory ability of the *Gnao1* mutant mice.}}}

With the increasing recognition of *GNAO1*-associated neurological disorders, it is important to learn about the role of G_o in the regulation of central nervous system. The novel *Gnao1* G203R and R209H mutant mouse models reported here, and further models under development, should facilitate our understanding of *GNAO1* mechanisms in the *in vivo* physiological background rather simply in *in vitro* cell studies. The animal models can also be used for preclinical drug testing and may permit a true allele-specific personalized medicine approach in drug repurposing for the associated movement disorders or epilepsy.

APPENDIX

APPENDIX

SUPPLEMENTAL DATA

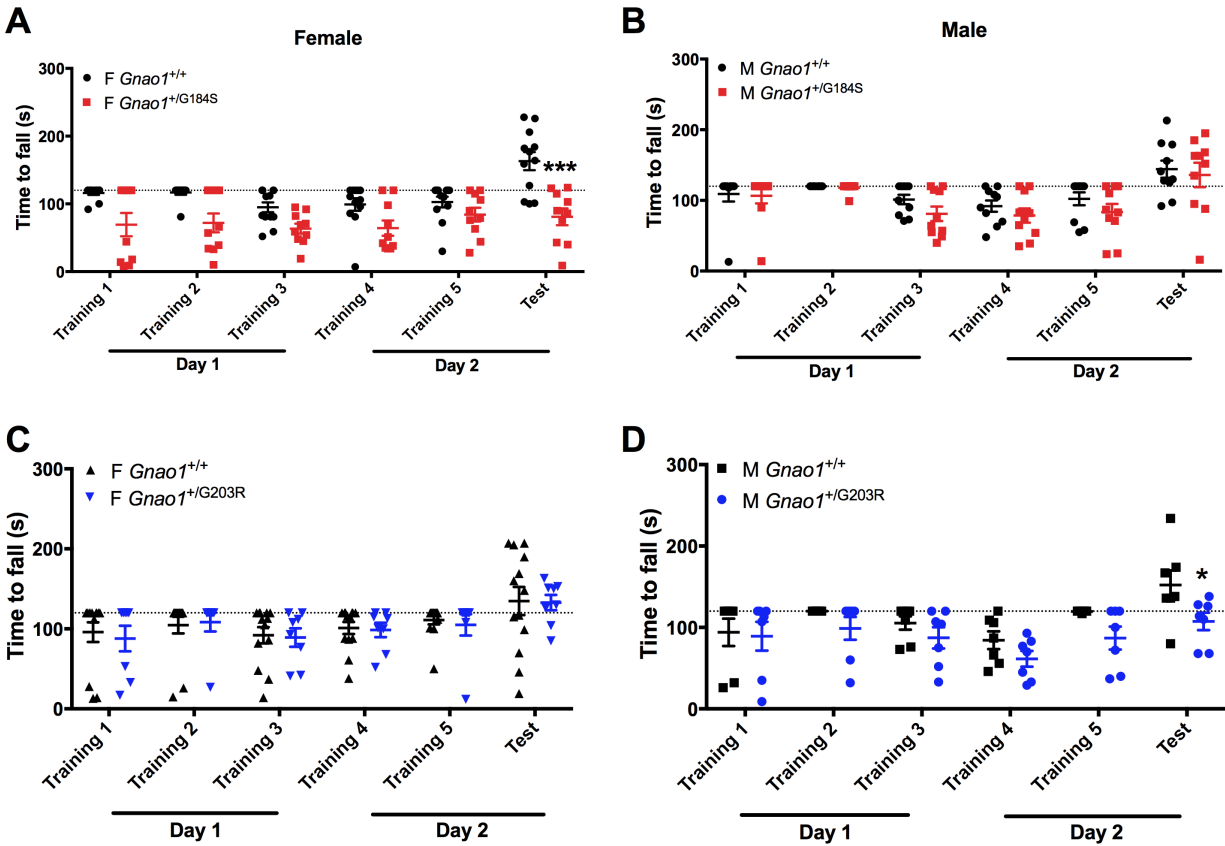


Figure S3.1 RotaRod test was conducted with 5 training sessions and 1 test session over two consecutive days. (A) Female *Gnao1*^{+/^{G184S} mice showed significantly motor abnormalities in test trial at day 2 (unpaired t-test; ****p*<0.001). (B) Male *Gnao1*^{+/^{G184S} mice did not show any significance in any training or test session. (C) Female *Gnao1*^{+/^{G203R} mice did not exhibit any motor abnormalities in any RotaRod trial or test session. (D) Male *Gnao1*^{+/^{G203R} mice showed significantly decreased capability in motor balance (unpaired t-test; **p*<0.05).}}}}

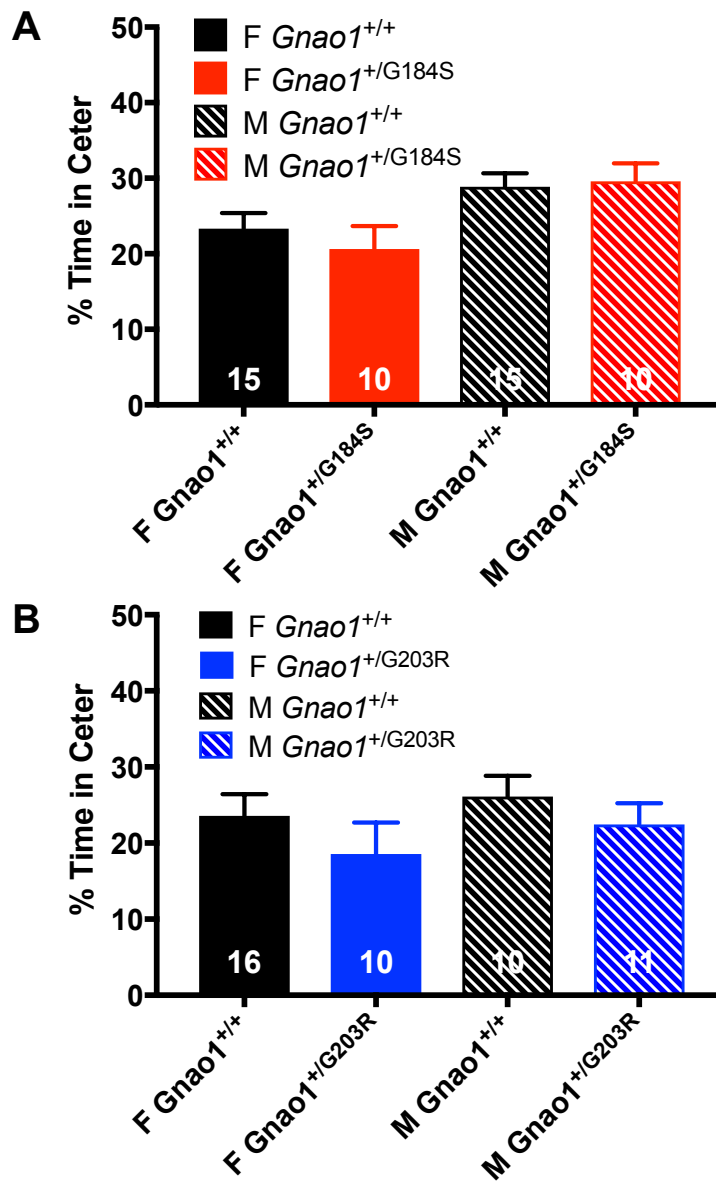


Figure S3.2 Time spent at the center in the Open Field Test. (A) No significant differences were observed between *Gnao1*^{+/G184S} mice and their littermate controls. (B) No significant differences were observed between *Gnao1*^{+/G203R} mice and their littermate controls.

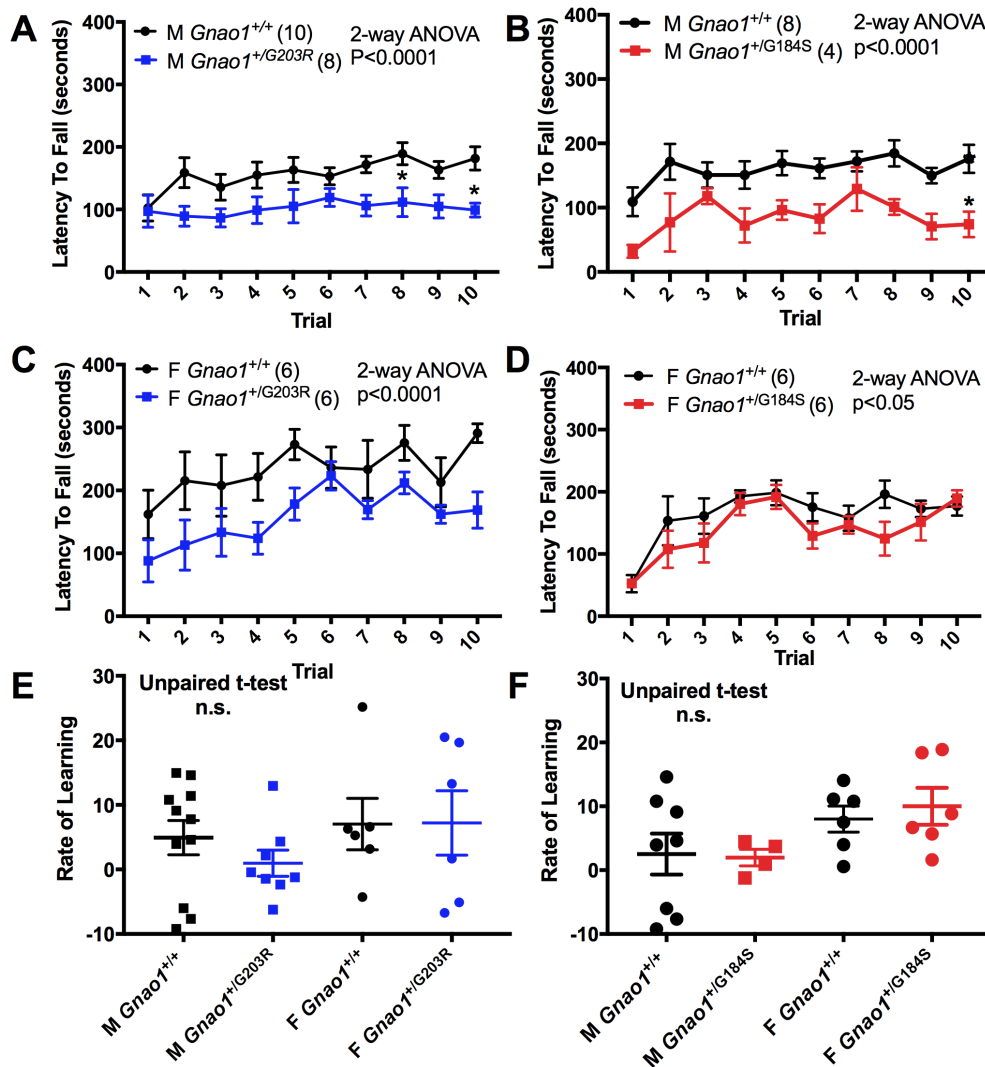


Figure S3.3 RotaRod learning curve was collected in 10 consecutive tests with a 5-min break between each test. (A, C & E) Short-term learning curve comparison between $Gnao1^{+/+}$ and $Gnao1^{+/G203R}$ in both sexes. (A & C) Both male and female $Gnao1^{+/G203R}$ mice showed reduced capability of keeping balance on RotaRod. (E) No significant difference in either sex between $Gnao1^{+/+}$ and $Gnao1^{+/G203R}$ mice was observed comparing the rate of learning. (B, D & F) Short-term learning curve comparison between $Gnao1^{+/+}$ and $Gnao1^{+/G184S}$ in both sexes. (B & D) Both male and female $Gnao1^{+/G184S}$ mice showed reduced capability of keeping balance on RotaRod. (F) No significant difference in either sexes between $Gnao1^{+/+}$ and $Gnao1^{+/G184S}$ mice was observed comparing the rate of learning.

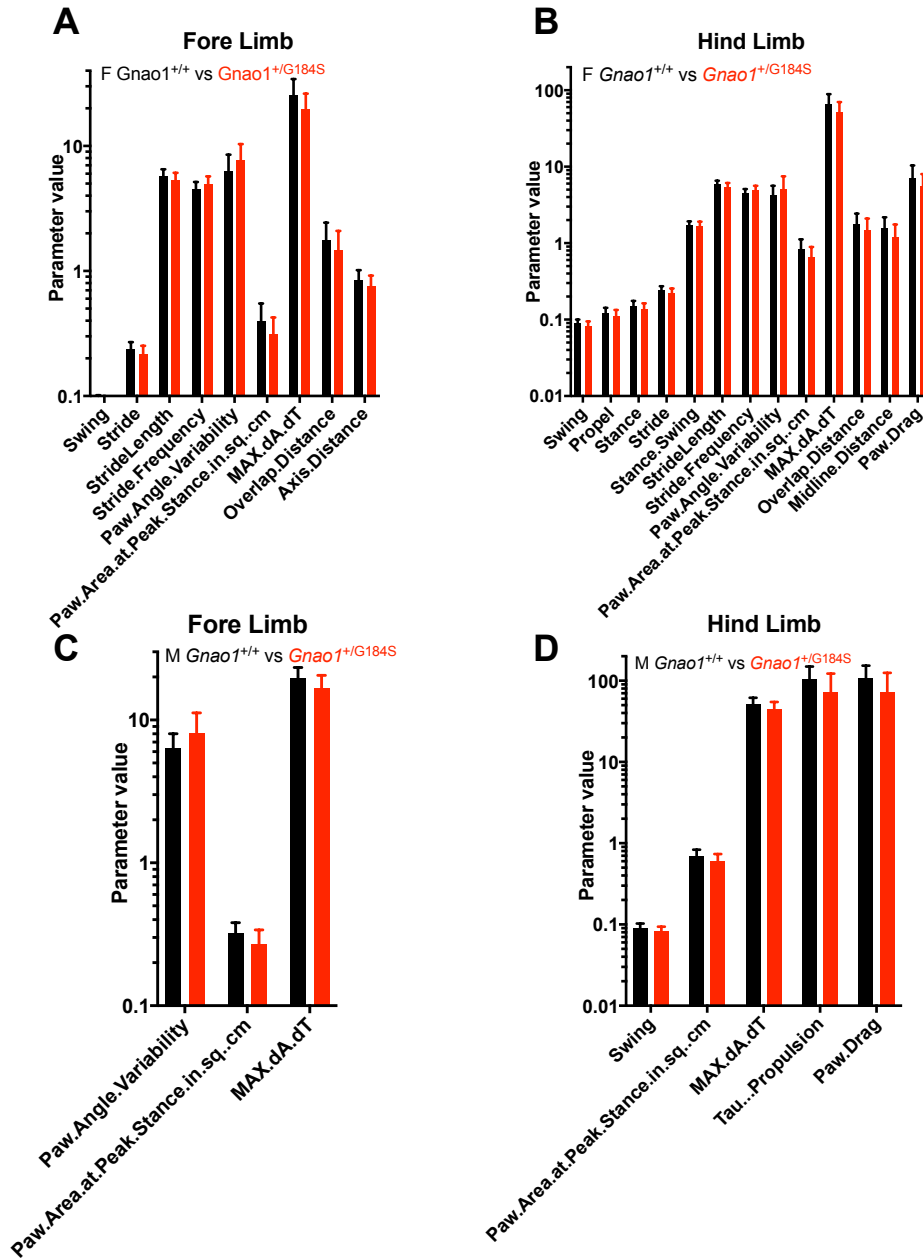


Figure S3.4 False discovery rate (FDR) calculation probed of significantly different parameters from the DigiGait data in *Gnao1*^{+/G184S} mice. All parameters that showed significance at belt speed 25 cm/s are plotted. (A&B) Female *Gnao1*^{+/G184S} and their littermate controls showed parameters with significance detected by the FDR analysis. (C&D) Male *Gnao1*^{+/G184S} and their littermates controls showed parameters with significance detected by the FDR analysis. FDR is calculated by a two-stage step-up method of Benjamini, Krieger and Yekutieli. Significant values are defined as $q < 0.01$.

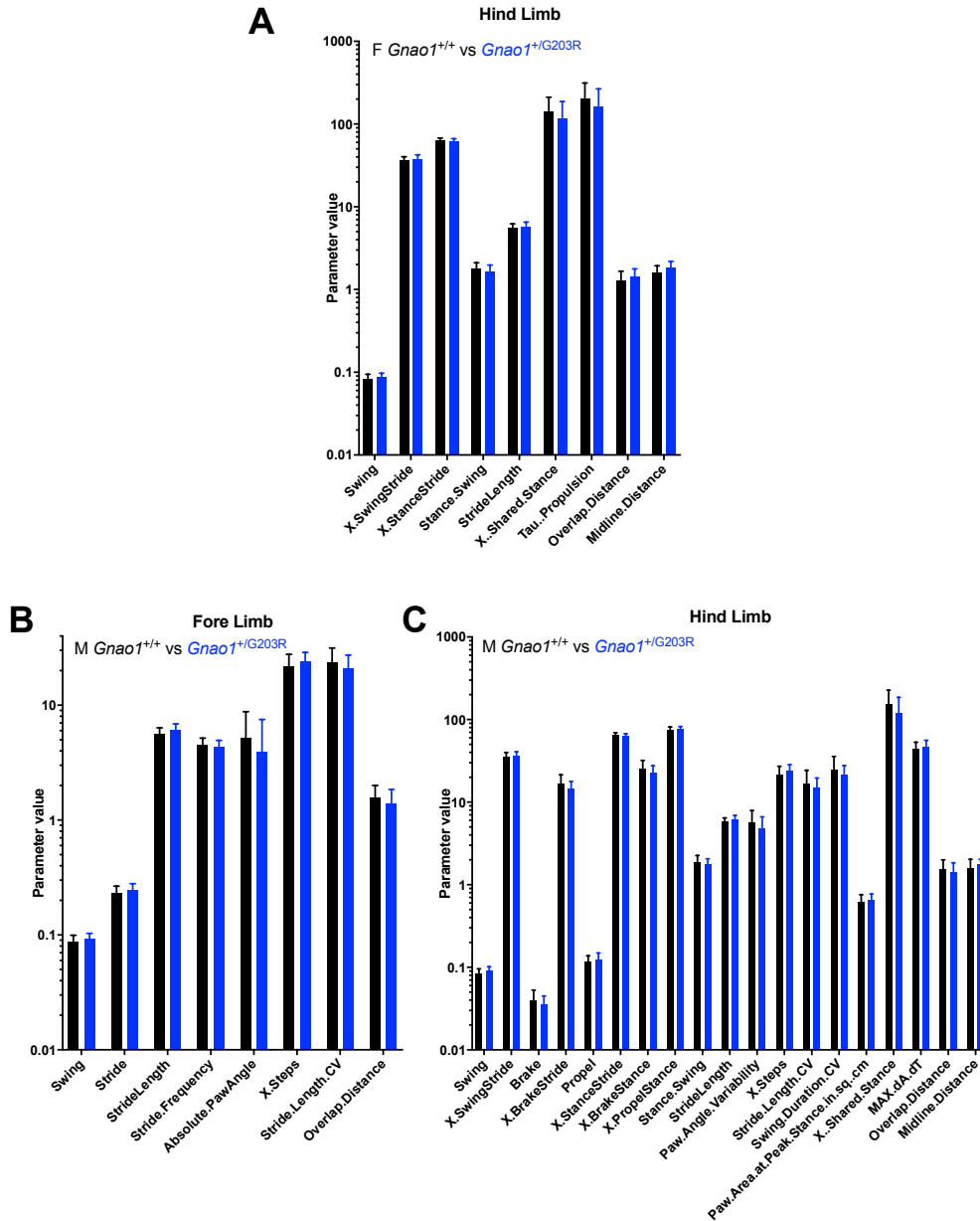


Figure S3.5 False discovery rate (FDR) calculation probed of significantly different parameters from the DigiGait data in *Gnao1*^{+/G203R} mice. All parameters that showed significance are plotted here. (A) Female *Gnao1*^{+/G203R} and their littermate controls showed 9 parameters with significance only in hind limb data detected by the FDR analysis. (B&C) Male *Gnao1*^{+/G203R} and their littermates controls exhibited 27 parameters with significance detected by the FDR analysis in fore and hind limb data combined. FDR is calculated by a two-stage step-up method of Benjamini, Krieger and Yekutieli. Significant values are defined as $q < 0.01$.

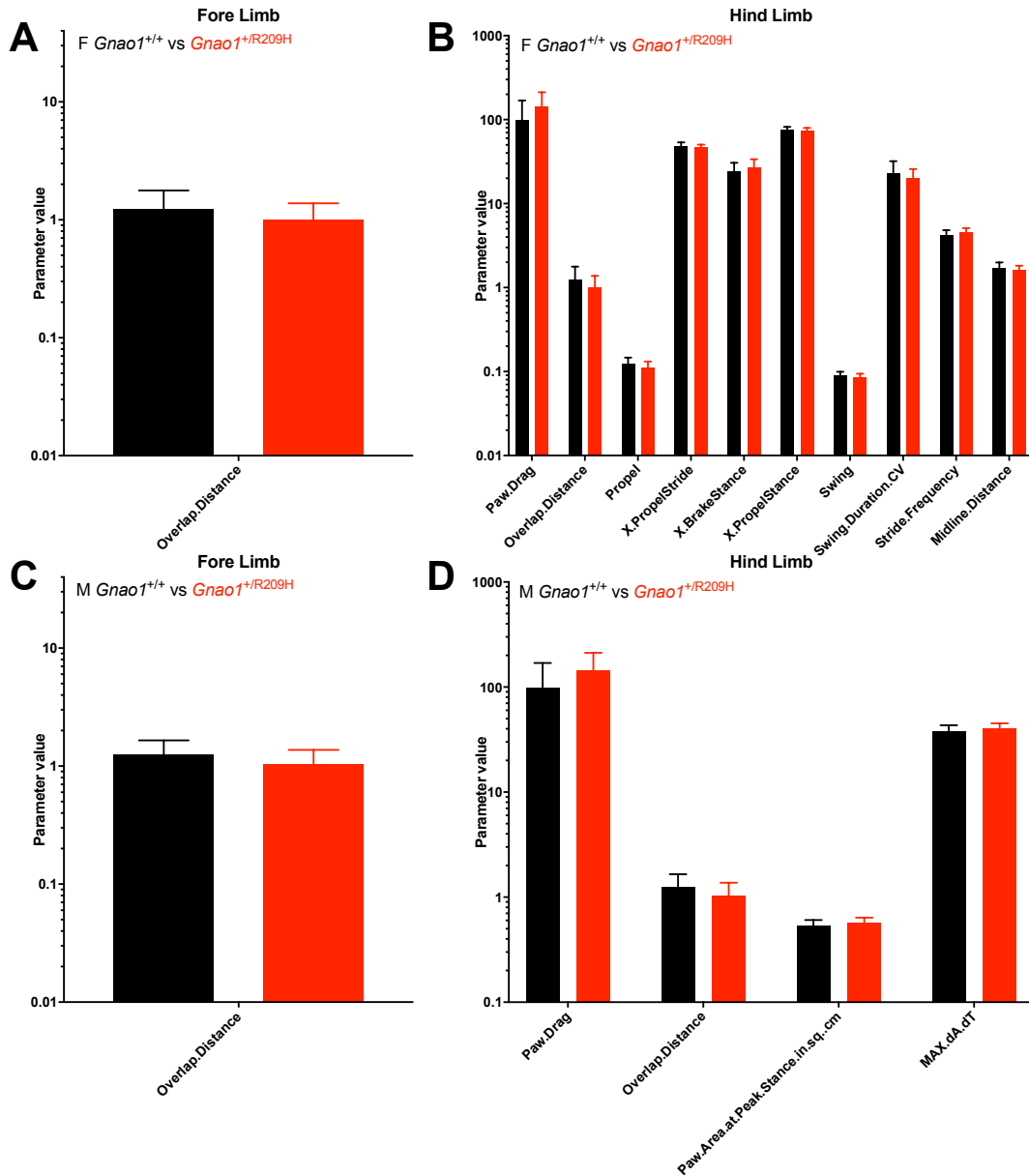


Figure S3.6 False discovery rate (FDR) calculation probed of significantly different parameters from the DigiGait data in *Gnao1*^{+/R209H} mice. All parameters that showed significance are plotted here. (A&B) Female *Gnao1*^{+/R209H} and their littermate controls showed 9 parameters with significance detected by the FDR analysis. (C&D) Male *Gnao1*^{+/R209H} and their littermates controls exhibited fewer parameters with significance comparing to female detected by the FDR analysis in fore and hind limb data combined. FDR is calculated by a two-stage step-up method of Benjamini, Krieger and Yekutieli. Significant values are defined as $q < 0.01$.

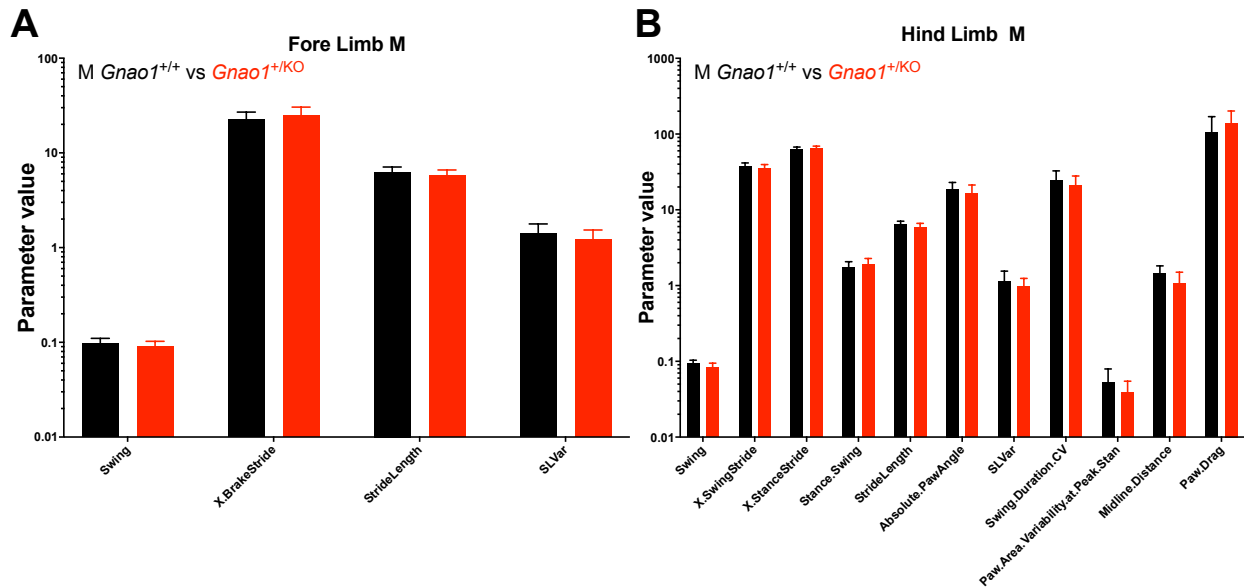


Figure S3.7 False discovery rate (FDR) calculation probed of significantly different parameters from the DigiGait data in *Gnao1*^{+/-} mice. All parameters that showed significance are plotted here. (A&B) Female *Gnao1*^{+/-} and their littermate controls did not show any significant difference in any parameters given. Male *Gnao1*^{+/-} and their littermates controls exhibited several parameters with significance comparing to female detected by the FDR analysis in fore and hind limb data combined. FDR is calculated by a two-stage step-up method of Benjamini, Krieger and Yekutieli. Significant values are defined as $q < 0.01$.

Table S3.1 Gait analysis parameters of male *Gnao1* G203R mutant mice

Measured Parameter	Fore Limb		Hind Limb		Fore Limb				Hind Limb							
	FDR	Yes	FDR	Yes	M <i>Gnao1</i> ^{+/+}	SD	n	M <i>Gnao1</i> ^{+/G203R}	SD	n	M <i>Gnao1</i> ^{+/+}	SD	n	M <i>Gnao1</i> ^{+/G203R}	SD	n
Swing	0.000086	Yes	<0.000001	Yes	0.09211667	0.0111967	180	0.08760833	0.01176783	240	0.09002222	0.01187409	180	0.08343333	0.01238566	240
X.SwingStride	0.560859	No	0.000566	Yes	38.07777778	3.54838583	180	37.85083333	4.2332119	240	36.68666667	3.98361729	180	35.24083333	4.70852526	240
Brake	0.653649	No	0.000399	Yes	0.06939444	0.016458	180	0.06865	0.01707632	240	0.03542222	0.00960271	180	0.0396125	0.01337189	240
X.BrakeStride	0.060086	No	<0.000001	Yes	28.40222222	4.89821488	180	29.43125	5.96865439	240	14.345	3.47436381	180	16.53625	4.86819351	240
Propel	0.003957	No	0.006698	Yes	0.08235556	0.01995907	180	0.076825	0.01889352	240	0.12215	0.02682225	180	0.115625	0.02219262	240
X.PropelStride	0.105634	No	0.088909	No	33.52	4.68472378	180	32.71791667	5.25089869	240	48.96611111	4.21758972	180	48.225	4.54530426	240
Stance	0.020015	No	0.413195	No	0.15173889	0.02844761	180	0.1484875	0.02613979	240	0.15758444	0.03072707	180	0.15022917	0.02615843	240
X.StanceStride	0.560859	No	0.000966	Yes	61.92222222	3.54838583	180	62.14816667	4.2332119	240	63.31333333	3.98361729	180	64.75916667	4.70852526	240
Stride	0.001621	Yes	0.010476	No	0.24383333	0.03618381	180	0.23310833	0.03278618	240	0.22762222	0.03807229	180	0.23864167	0.03329752	240
X.BrakeStance	0.073312	No	0.000004	Yes	45.82444444	7.20043157	180	47.23583333	8.50521667	240	22.61888889	5.02721964	180	25.36166667	6.5864662	240
X.PropelStance	0.073312	No	0.000004	Yes	54.17555556	7.20043157	180	52.76416667	8.50521667	240	77.38111111	5.02721964	180	74.63875	6.58555209	240
Stance.Swing	0.496204	No	0.000155	Yes	1.65222222	0.25378818	180	1.67083333	0.29341328	240	1.75555556	0.3053018	180	1.88625	0.375531	240
Stride.Length	<0.000001	Yes	<0.000001	Yes	6.09777778	0.77998392	180	5.60791667	0.74607749	240	6.17777778	0.72670955	180	5.73458333	0.71873598	240
Stride.Frequency	0.002659	Yes	0.024506	No	4.30055556	0.63908954	180	4.49708333	0.67417378	240	4.25111111	0.64785757	180	4.39541667	0.64873536	240
PawAngle	0.255886	No	0.576762	No	-2.13944444	4.87883924	180	-1.50833333	6.1258422	240	0.39222222	17.03751417	180	1.335	17.17832948	240
Absolute.PawAngle	0.000619	Yes	0.7785	No	3.90722222	3.61305873	180	5.14166667	3.64193574	240	16.34777778	4.65733584	180	16.2	5.77485245	240
Paw.Angle.Variability	0.477312	No	0.000239	Yes	8.12333333	2.56029197	180	8.31791667	2.92469857	240	4.79555556	1.82575682	180	5.57333333	2.32933748	240
Stance.Width	0.50287	No	0.718181	No	4.77777778	4.11368551	180	4.51666667	3.82128663	240	9.53888889	8.65887596	180	9.85416667	8.99741847	240
Step.Angle	0.530415	No	0.960996	No	92	97.32018227	180	86.1125	93.39500767	240	46.90555556	62.27966276	180	46.975	62.43865106	240
SLVar	0.19286	No	0.158581	No	1.24272222	0.32258674	180	1.28991667	0.34549444	240	0.89744444	0.27275979	180	0.95095833	0.45002545	240
SWVar	0.753361	No	0.324024	No	18.37222222	19.78855562	180	17.77083333	19.10096449	240	8.52777778	12.16526358	180	9.69833333	11.87042948	240
Step.Angle.Var	0.566174	No	0.422419	No	85.73888889	114.0590048	180	92.2875	116.870725	240	83.08111111	110.7694855	180	92.04583333	115.4575489	240
X.Steps	0.000053	Yes	0.000013	Yes	24.00833333	4.7819712	180	21.81975	5.87860657	240	23.67777778	4.70635557	180	21.32291667	5.88566941	240
Stride.Length.CV	0.000167	Yes	0.001176	Yes	20.82244444	6.52396481	180	23.578375	7.92635878	240	14.70616667	4.90287218	180	16.811125	7.52811028	240
Stance.Width.CV	0.957513	No	0.256205	No	82.95	94.95293012	180	83.45	95.25775208	240	128.21111111	154.5150275	180	111.12083333	150.8803385	240
Step.Angle.CV	0.205403	No	0.276243	No	81.05555556	111.6869989	180	96.21666667	127.9222556	240	99.85555556	121.4064747	180	113.77083333	135.1570046	240
Swing.Duration.CV	0.004977	No	0.001453	Yes	27.594	7.89706951	180	29.98779167	9.08822921	240	21.31672222	6.46662759	180	24.35395833	11.41084435	240
Paw.Area.at.Peak.Stance.in_sq_cm	0.111782	No	0.004248	Yes	0.30805556	0.04937709	180	0.2975	0.07788791	240	0.64966667	0.12237364	180	0.61033333	0.14866149	240
Paw.Area.Variability.at.Peak.Stance	0.534568	No	0.074908	No	0.02894444	0.01608279	180	0.02995833	0.01688003	240	0.05305556	0.033092	180	0.05908333	0.03507305	240
Hind.Limb.Shared.Stance.Time			0.286417	No	1	0	180	1	0	240	22	26.92406039	180	24.97916667	29.29988471	240
X.Shared.Stance			0.000002	Yes	1	0	180	1	0	240	118.08333333	67.80483618	180	152.34583333	74.7569858	240
StanceFactor	0.656453	No	0.927493	No	11.30555556	11.54350393	180	11.8375	12.53391424	240	13.59444444	13.27605364	180	13.475	13.52500873	240
Gait.Symmetry	0.034845	No	0.034845	No	1.01388889	0.04501259	180	1.02416667	0.05217581	240	1.01388889	0.04501259	180	1.02416667	0.05217581	240
MAX.da.dT	0.926219	No	0.001727	Yes	16.896	3.37636885	180	16.8605	4.22704441	240	46.49827778	9.49935633	180	43.518625	9.64248797	240
MIN.da.dT	0.31531	No	0.646552	No	-5.16177778	1.45335565	180	-5.31579167	1.6247547	240	-8.88277778	1.91057189	180	-8.980875	2.39585688	240
Tau.Propulsion			0.455592	No	1	0	180	1	0	240	178.93333333	101.5146521	180	186.74583333	109.3986127	240
Overlap.Distance	0.000567	Yes	0.000567	Yes	1.4025	0.4440782	180	1.55470833	0.44461341	240	1.4025	0.4440782	180	1.55470833	0.44461341	240
Paw.Placement.Positioning.PPP	0.009576	No	0.009576	No	0.47255556	0.209826	180	0.53175	0.24509639	240	0.47255556	0.209826	180	0.53175	0.24509639	240
Ataxia.Coefficient	0.065892	No	0.031149	No	0.899	0.30885281	180	0.95725	0.328734	240	0.63983333	0.24794907	180	0.7065	0.35345432	240
Midline.Distance	0.000511	Yes	0.000002	Yes	-2.22233333	0.34125483	180	-2.37679167	0.51249994	240	1.76005556	0.28026224	180	1.57204167	0.46433242	240
Axis.Distance	0.813623	No	0.774606	No	0.01011111	0.83342464	180	-0.00895833	0.80948622	240	0.02372222	1.34792041	180	-0.01433333	1.34621132	240
Paw.Drag			0.013423	No	1	0	180	1	0	240	218.82777778	112.0513066	180	190.64583333	117.356213	240

Table S3.2 Gait analysis parameters of female *Gnao1* G203R mutant mice

Measured Parameter	Fore Limb		Hind Limb		Fore Limb						Hind Limb					
	p	FDR	p	FDR	F <i>Gnao1</i> +/+	SD	n	F <i>Gnao1</i> +G203R	SD	n	F <i>Gnao1</i> +/+	SD	n	F <i>Gnao1</i> +G203R	SD	n
Swing	0.143574	No	0.000042	Yes	0.0862619	0.0112876	210	0.08465044	0.011645	226	0.08701905	0.0103341	210	0.06259735	0.011866	226
X.SwingStride	0.040102	No	0.000039	Yes	38.2376191	3.4885409	210	37.58362832	3.1433241	226	37.98428571	4.4849659	210	35.3	3.9776487	226
Brake	0.610655	No	0.239211	No	0.06979524	0.019781	210	0.07067699	0.0163127	226	0.03703333	0.0117622	210	0.03834513	0.0114719	226
X.BrakeStride	0.151434	No	0.045932	No	30.4114286	5.6522649	210	31.14867257	5.0584954	226	15.94428571	4.3353439	210	16.8199115	4.766196	226
Propel	0.962205	No	0.766869	No	0.07122857	0.0153668	210	0.07115487	0.0169889	226	0.10746667	0.0239663	210	0.10812832	0.0226036	226
X.PropelStride	0.858596	No	0.055104	No	31.35	4.8383758	210	31.26681416	4.8963937	226	46.06619048	4.7852095	210	46.88185841	4.0616338	226
Stance	0.747729	No	0.463647	No	0.14104286	0.0265394	210	0.14184071	0.0252212	226	0.14451429	0.029293	210	0.14648673	0.0268555	226
X.StanceStride	0.040102	No	0.000039	Yes	61.762381	3.4885409	210	62.41637168	3.1433241	226	62.01571429	4.4849659	210	63.70044248	3.9787156	226
Stride	0.780626	No	0.445327	No	0.22737619	0.0347068	210	0.22845575	0.0342293	226	0.23155238	0.0346545	210	0.22903982	0.0339969	226
X.BrakeStance	0.30554	No	0.327424	No	49.1166667	8.051334	210	49.8840708	7.5687729	226	25.63047619	6.3902157	210	26.23938053	6.5617814	226
X.PropelStance	0.30554	No	0.327424	No	50.8833333	8.051334	210	50.1159292	7.5687729	226	74.36952381	6.3902157	210	73.76061947	6.5617814	226
Stance.Swing	0.050429	No	0.000053	Yes	1.63809524	0.2335009	210	1.68141593	0.2274687	226	1.66857143	0.3092867	210	1.79070796	0.3146108	226
Stride.Length	0.003872	No	0.000285	Yes	5.70190476	0.7409397	210	5.50530973	0.6725528	226	5.80761905	0.7083501	210	5.5659292	0.6710776	226
Stride.Frequency	0.83429	No	0.456267	No	4.63333333	0.7236493	210	4.64778761	0.7174148	226	4.54809524	0.6820467	210	4.59734513	0.6955682	226
PawAngle	0.275233	No	0.711622	No	-2.0414286	5.1145489	210	-1.51504425	4.944406	226	0.40666667	18.071952	210	1.02699115	16.942806	226
Absolute.PawAngle	0.653751	No	0.017128	No	4.27380952	3.4631111	210	4.13274336	3.0979403	226	17.21047619	5.3965099	210	15.92699115	5.7724885	226
Paw.Angle.Variability	0.083677	No	0.459013	No	7.08	2.9170313	210	7.53495575	2.560203	226	5.24428571	2.5795276	210	5.44778761	3.1063833	226
Stance.Width	0.304131	No	0.992695	No	4.65238095	3.9041285	210	4.28318584	3.588795	226	8.97619048	8.1636612	210	8.96902655	8.1553754	226
StepAngle	0.676222	No	0.265709	No	87.4904762	95.888554	210	83.71238938	92.843532	226	46.68095238	62.270502	210	53.61946903	67.358321	226
SLVar	0.46197	No	0.160659	No	1.11104762	0.3637969	210	1.13561947	0.3330556	226	0.82042857	0.3400398	210	0.86349558	0.299672	226
SWVar	0.597496	No	0.235126	No	14.8666667	16.15035	210	15.69026549	16.365318	226	7.22380952	9.302076	210	8.37610619	10.810084	226
StepAngleVar	0.590118	No	0.742411	No	94.5571429	123.21106	210	88.42920354	114.15516	226	93.55714286	122.72527	210	89.64955752	112.67252	226
X.Steps	0.287034	No	0.176573	No	23.7642857	5.9102466	210	24.34070796	5.3805268	226	23.34761905	5.9556269	210	24.08628319	5.4387774	226
Stride.Length.CV	0.134218	No	0.029457	No	20.0334286	7.9432229	210	21.13402655	7.3727667	226	14.45657143	6.7501268	210	15.8080973	6.1679082	226
Stance.Width.CV	0.183108	No	0.787718	No	71.4761905	83.50877	210	82.69469027	91.571949	226	127.6666667	155.40339	210	123.6283186	157.26751	226
Step.Angle.CV	0.500567	No	0.496458	No	92.3857143	125.23065	210	100.6283186	129.68952	226	96.90952381	123.48735	210	105.039823	125.67239	226
Swing.Duration.CV	0.009699	No	0.012817	No	25.4634286	9.9336491	210	27.70469027	8.038455	226	20.35714286	10.045441	210	22.57513274	8.4641854	226
Paw.Area.at.Peak.Stance.in.sq.cm	0.046836	No	0.120876	No	0.31547619	0.0784235	210	0.30084071	0.0747244	226	0.624	0.138264	210	0.60482301	0.1192093	226
Paw.Area.Variability.at.Peak.Stance	0.25505	No	0.123726	No	0.03247619	0.0177047	210	0.03048673	0.0186722	226	0.06057143	0.0355498	210	0.05575221	0.029599	226
Hind.Limb.Shared.Stance.Time			0.219455	No	1	0	210	1	0	226	19.06190476	23.988055	210	21.98230088	25.48742	226
X.Shared.Stance			0.000033	Yes	1	0	210	1	0	226	116.7095238	70.404616	210	144.300885	66.869808	226
StanceFactor	0.618239	No	0.752284	No	11.6952381	12.247545	210	12.27876106	12.170536	226	13.52380952	13.510298	210	13.12389381	12.926894	226
GaitSymmetry	0.044325	No	0.044325	No	1.0192381	0.0513119	210	1.01123894	0.0292767	226	1.0192381	0.0513119	210	1.01123894	0.0292767	226
MAX.dA.dT	0.093152	No	0.528498	No	16.9396667	4.1600988	210	16.29477876	3.8423131	226	43.48771429	9.941629	210	42.92628319	8.6321179	226
MIN.dA.dT	0.001558	No	0.000411	Yes	-5.1652381	1.8030427	210	-4.63566372	1.6700964	226	-9.69980952	2.6687581	210	-8.8219469	2.4798691	226
Tau.Propulsion			0.000043	Yes	1	0	210	1	0	226	164.8380952	101.35854	210	206.1415929	106.91923	226
Overlap.Distance	0.000346	No	0.000346	Yes	1.42585714	0.3488621	210	1.30376106	0.3572146	226	1.42585714	0.3488621	210	1.30376106	0.3572146	226
PawPlacementPositioning.PPP	0.122248	No	0.122248	No	0.44066667	0.1970416	210	0.47349558	0.2414856	226	0.44066667	0.1970416	210	0.47349558	0.2414856	226
Ataxia.Coefficient	0.125326	No	0.01669	No	0.85080952	0.36314	210	0.90159292	0.3272514	226	0.62028571	0.3216493	210	0.69393805	0.3180957	226
Midline.Distance	0.844898	No	<0.000001	Yes	-1.9551905	0.4059709	210	-1.96256637	0.3777178	226	1.8667619	0.3241286	210	1.61292035	0.3222468	226
Axis.Distance	0.882318	No	0.987517	No	-0.0137143	0.794259	210	-0.00261062	0.7706896	226	-0.004	1.2942361	210	-0.00207965	1.2662788	226
Paw.Drag			0.744503	No	1	0	210	1	0	226	212.1142857	132.61357	210	215.9734513	114.3211	226

Table S3.3 Gait analysis parameters of male *Gnao1* G184S mutant mice

Measured Parameter	Fore Limb		Hind Limb		Fore Limb				Hind Limb							
	p	FDR	p	FDR	M <i>Gnao1</i> +/+	SD	n	M <i>Gnao1</i> +/G184S	SD	n	M <i>Gnao1</i> +/+	SD	n	M <i>Gnao1</i> +/G184S	SD	n
Swing	0.043466	No	0.000278	Yes	0.09253061	0.0141627	98	0.08857143	0.011722	84	0.09	0.0127724	98	0.08357143	0.0102043	84
X.SwingStride	0.726843	No	0.117241	No	37.83979592	3.1936386	98	37.6702381	3.3344055	84	36.51428571	5.1117008	98	35.3	5.2765451	84
Brake	0.826349	No	0.812719	No	0.05344898	0.0115937	98	0.05385714	0.0134703	84	0.02879592	0.0075135	98	0.02907143	0.0081415	84
X.BrakeStride	0.180502	No	0.197797	No	21.91020408	4.0355505	98	22.75119048	4.3688359	84	11.57857143	2.4412372	98	12.08333333	2.9270992	84
Propel	0.148248	No	0.66152	No	0.09986735	0.0236179	98	0.09477381	0.023563	84	0.13060204	0.029081	98	0.12857143	0.0333879	84
X.PropelStride	0.318469	No	0.336379	No	40.25714286	4.5416969	98	39.57857143	4.5858365	84	51.91632653	4.6134205	98	52.62738095	5.3388179	84
Stance	0.27969	No	0.731504	No	0.15326531	0.028498	98	0.14857143	0.0298184	84	0.15944898	0.036318	98	0.15763095	0.0377269	84
X.StanceStride	0.726843	No	0.117241	No	62.16020408	3.1936386	98	62.3297619	3.3344055	84	63.48571429	5.1117008	98	64.7	5.2765451	84
Stride	0.140428	No	0.173925	No	0.24587755	0.0396769	98	0.23721429	0.0389603	84	0.24947959	0.0391545	98	0.24122619	0.0423552	84
X.BrakeStance	0.197014	No	0.382853	No	35.25306122	6.2745798	98	36.49047619	6.6003216	84	18.21020408	3.3839064	98	18.70238095	4.2032969	84
X.PropelStance	0.197014	No	0.384084	No	64.74693878	6.2745798	98	63.50952381	6.6003216	84	81.78979592	3.3839064	98	81.29880952	4.2045728	84
Stance.Width	0.810208	No	0.579955	No	1.66326531	0.2230934	98	1.67142857	0.2341719	84	1.79183673	0.3701974	98	1.89642857	0.4203975	84
Stride.Length	0.047635	No	0.036347	No	6.17959184	0.9320147	98	5.93333333	0.693226	84	6.26122449	0.9164738	98	6.01071429	0.634551	84
Stride.Frequency	0.153098	No	0.096182	No	4.29387755	0.6895115	98	4.44761905	0.7554582	84	4.22346939	0.6697901	98	4.40238095	0.7735034	84
PawAngle	0.223604	No	0.783411	No	-0.00102041	4.7029821	98	0.91547619	5.4220321	84	-0.05204082	17.660751	98	0.675	17.87932	84
Absolute.PawAngle	0.062068	No	0.583264	No	3.73163265	2.8371467	98	4.55119048	3.046922	84	17.08877551	4.1070692	98	16.66309524	6.2551719	84
Paw.Angle.Variability	0.000004	Yes	0.007857	No	6.31938776	1.7027999	98	8.06666667	3.1549286	84	4.2877551	1.9761081	98	5.24047619	2.7850772	84
Stance.Width	0.931208	No	0.50059	No	3.83673469	3.0348283	98	3.79761905	3.0528666	84	7.12244898	6.2363506	98	7.78571429	7.0198882	84
StepAngle	0.781449	No	0.542101	No	48.89795918	51.835284	98	46.78571429	50.288342	84	25.30612245	32.434997	98	22.44047619	30.489718	84
SLVar	0.018345	No	0.480115	No	1.18122449	0.4015749	98	1.32916667	0.4444264	84	0.91683673	0.309591	98	0.9572619	0.4562322	84
SWVar	0.268206	No	0.49907	No	12.31632653	12.961161	98	14.6547619	15.444026	84	6.80612245	7.6934276	98	7.66666667	9.442704	84
StepAngleVar	0.51712	No	0.419338	No	45.3877551	58.864099	98	39.98809524	52.336606	84	42.21428571	51.158184	98	36.42857143	44.194064	84
X.Steps	0.201763	No	0.192532	No	21.35714286	4.3328046	98	22.25955238	5.1316958	84	21.0255102	4.4032395	98	21.95238095	5.1569459	84
Stride.Length.CV	0.009988	No	0.274044	No	19.70622449	7.7656016	98	22.82166667	8.3634236	84	14.93540816	5.4905719	98	16.00898095	7.6712154	84
Stance.Width.CV	0.245913	No	0.866251	No	29.3877551	33.936154	98	35.82142857	40.621426	84	57.7244898	69.576003	98	59.47619048	70.164948	84
Step.Angle.CV	0.386308	No	0.314724	No	33.97959184	48.807634	98	40.55952381	53.357704	84	48.95918367	59.29655	98	58.16666667	63.81578	84
Swing.Duration.CV	0.495053	No	0.13408	No	25.39285714	8.1613281	98	26.30416667	9.8202879	84	21.32826531	7.197867	98	23.49071429	11.914931	84
Paw.Area.at.Peak.Stance.in.sq.cm	<0.000001	Yes	0.000001	Yes	0.32091837	0.0605148	98	0.26928571	0.0702111	84	0.70244898	0.1316122	98	0.60595238	0.1286643	84
Paw.Area.Variability.at.Peak.Stance	0.002006	No	0.082786	No	0.01877551	0.0098719	98	0.02559524	0.0187148	84	0.04530612	0.030127	98	0.05357143	0.0337833	84
Hind.Limb.Shared.Stance.Time			0.669308	No	1	0	98	1	0	84	14.24489796	17.100709	98	15.35714286	17.924637	84
X.Shared.Stance			0.051594	No	1	0	98	1	0	84	74.91836735	45.56058	98	87.82142857	42.745862	84
StanceFactor	0.396136	No	0.831523	No	8.70408163	9.4859736	98	7.57142857	8.2932484	84	9.25510204	9.6744016	98	9.55952381	9.5328869	84
Gait.Symmetry	0.688994	No	0.688994	No	1.01755102	0.0511529	98	1.01452381	0.0503579	84	1.01755102	0.0511529	98	1.01452381	0.0503579	84
MAX.dA.dT	<0.000001	Yes	0.000008	Yes	19.58153061	3.7431478	98	16.61440476	3.9087463	84	51.415	10.373366	98	44.32047619	10.399373	84
MIN.dA.dT	0.891498	No	0.000429	Yes	-4.68867347	0.9273804	98	-4.71535714	1.6546185	84	-8.24183673	2.1764496	98	-9.5402381	2.7031744	84
Tau.Propulsion			0.000017	Yes	1	0	98	1	0	84	103.755102	45.984547	98	72.35714286	49.842316	84
Overlap.Distance	0.001809	No	0.001809	Yes	1.40122449	0.3999259	98	1.61261905	0.5000846	84	1.40122449	0.3999259	98	1.61261905	0.5000846	84
Paw.Placement.Positioning.PPP	0.00764	No	0.00764	No	0.43704082	0.1825829	98	0.51178571	0.1905993	84	0.43704082	0.1825829	98	0.51178571	0.1905993	84
Ataxia.Coefficient	0.055735	No	0.187315	No	0.81897959	0.3422138	98	0.91821429	0.3516473	84	0.61469388	0.248655	98	0.6727381	0.3411474	84
Midline.Distance	0.998012	No	0.035382	No	-2.76357143	0.3019703	98	-2.76369048	0.3417171	84	1.40795918	0.2798857	98	1.51952381	0.4244029	84
Axis.Distance	0.836286	No	0.951005	No	0.03887755	0.8386733	98	0.01333333	0.8200578	84	0.01989796	1.3185305	98	0.00738095	1.4239324	84
Paw.Drag			0.000004	Yes	1	0	98	1	0	84	107.2653061	45.749779	98	72.89285714	52.00487	84

Table S3.4 Gait analysis parameters of female *Gnao1* G184S mutant mice

Measured Parameter	Fore Limb		Hind Limb		Fore Limb				Hind Limb							
	p	FDR	p	FDR	F <i>Gnao1</i> ^{+/+}	SD	n	F <i>Gnao1</i> ^{+/G184S}	SD	n	F <i>Gnao1</i> ^{+/+}	SD	n	F <i>Gnao1</i> ^{+/G184S}	SD	n
Swing	0.000002	Yes	0.00019	Yes	0.08906667	0.012567	90	0.080841	0.012049	132	0.088633	0.011621	90	0.082333	0.012478	132
X.SwingStride	0.352054	No	0.571929	No	38.21333	3.504418	90	37.76212	3.562839	132	37.53889	3.24618	90	37.79697	3.394359	132
Brake	0.018172	No	0.041827	No	0.062156	0.017608	90	0.056508	0.017191	132	0.029	0.01003	90	0.026402	0.00874	132
X.BrakeStride	0.805581	No	0.827244	No	26.46	5.698922	90	26.05303	5.79599	132	12.18	3.40296	90	12.075	3.589752	132
Propel	0.073513	No	0.003264	Yes	0.083178	0.019603	90	0.078295	0.02094	132	0.119811	0.022828	90	0.110394	0.023384	132
X.PropelStride	0.303687	No	0.75231	No	35.33444	5.498685	90	36.1803	6.320866	132	50.28222	3.871491	90	50.11818	3.746567	132
Stance	0.004809	No	0.001181	Yes	0.145322	0.026527	90	0.134818	0.027276	132	0.148811	0.026549	90	0.136818	0.026794	132
X.StanceStride	0.352054	No	0.571929	No	61.78667	3.504418	90	62.23788	3.562839	132	62.46111	3.24618	90	62.20303	3.394359	132
Stride	0.000183	Yes	0.000242	Yes	0.234389	0.035201	90	0.215674	0.03649	132	0.237511	0.035089	90	0.219182	0.03649	132
X.BrakeStance	0.490318	No	0.875453	No	42.76444	8.767346	90	41.91894	9.074334	132	19.45556	5.068056	90	19.34394	5.293627	132
X.PropelStance	0.489918	No	0.875453	No	57.23556	8.767346	90	58.08182	9.073969	132	80.54444	5.068056	90	80.65606	5.293627	132
Stance.Swing	0.335195	No	0.536831	No	1.64	0.240692	90	1.672727	0.252647	132	1.687778	0.237888	90	1.667424	0.242599	132
Stride.Length	0.0007	Yes	0.000352	Yes	5.707778	0.807719	90	5.342424	0.755956	132	5.781111	0.775306	90	5.420455	0.691799	132
Stride.Frequency	0.000035	Yes	0.000096	Yes	4.468889	0.682797	90	4.908333	0.810338	132	4.415556	0.680369	90	4.823485	0.795393	132
PawAngle	0.167612	No	0.464223	No	4.784444	2.854089	90	4.209848	3.153645	132	16.32778	4.441025	90	16.82121	5.22535	132
Absolute.PawAngle	0.167612	No	0.464223	No	4.784444	2.854089	90	4.209848	3.153645	132	16.32778	4.441025	90	16.82121	5.22535	132
Paw.Angle.Variability	0.000023	Yes	0.003025	Yes	6.265556	2.252647	90	7.730303	2.613352	132	4.153333	1.479538	90	5.02197	2.460662	132
Stance.Width	0.022922	No	0.068763	No	1.684444	0.330259	90	1.536364	0.333114	132	2.566667	0.475299	90	2.410606	0.412918	132
Stance.Angle	0.998777	No	0.468437	No	64.84444	7.514911	90	64.84697	9.138359	132	56.06222	8.526091	90	54.86515	8.435848	132
SLVar	0.184572	No	0.379246	No	1.152444	0.381574	90	1.092273	0.281539	132	0.793778	0.335337	90	0.757852	0.273303	132
SWVar	0.200099	No	0.091884	No	0.349556	0.088164	90	0.375	0.104679	132	0.220667	0.097547	90	0.259242	0.129024	132
StepAngleVar	0.882892	No	0.454172	No	13.42622	4.439098	90	13.54348	3.867871	132	12.55133	3.478382	90	12.06667	3.298623	132
X.Steps	0.00456	No	0.006296	No	18.32778	5.488579	90	20.31818	4.78319	132	18.08889	5.451305	90	19.98864	4.73676	132
Stride.Length.CV	0.568182	No	0.040883	No	20.47044	6.723017	90	20.97265	6.21845	132	13.79056	5.541985	90	14.31485	5.874303	132
Stance.Width.CV	0.007756	No	0.02806	No	21.188	6.590364	90	25.38455	8.830206	132	8.748444	4.294501	90	10.9447	5.480517	132
Step.Angle.CV	0.734363	No	0.682633	No	21.42844	8.660338	90	22.01364	9.055266	132	22.82822	6.986445	90	22.30394	6.351191	132
Swing.Duration.CV	0.412289	No	0.494238	No	25.59067	8.521292	90	24.72242	7.146609	132	18.19433	6.749598	90	18.80689	6.401079	132
Paw.Area.at.Peak.Stance.in.sq.cm	0.000002	Yes	0.000015	Yes	0.398111	0.152248	90	0.311288	0.11312	132	0.818667	0.301436	90	0.660227	0.230086	132
Paw.Area.Variability.at.Peak.Stance	0.291841	No	0.294115	No	0.031556	0.019309	90	0.029091	0.015356	132	0.067	0.056299	90	0.059773	0.045725	132
Hind.Limb.Shared.Stance.Time	0.167306	No	0.112442	No			90			132	0.057378	0.021	90	0.051152	0.019511	132
X.Shared.Stance	0.25904	No	0.28745	No			90			132	37.59111	8.462962	90	36.32273	8.859942	132
StanceFactor	0.000001	Yes	0.357268	No	1.009333	0.075179	90	0.988788	0.077291	132	1.009556	0.047095	90	1.019545	0.061129	132
Gait.Symmetry	0.014025	No	0.25904	No	1.012889	0.039413	90	1.018333	0.032011	132	1.012889	0.039413	90	1.018333	0.032011	132
MAX.dA.dT	0.001549	Yes	0.000014	Yes	25.22511	9.068926	90	19.5603	6.647057	132	64.31333	24.77673	90	51.24644	18.95255	132
MIN.dA.dT	0.979063	No	0.119243	No	6.588111	2.658642	90	5.764015	2.269378	132	12.05456	5.245177	90	10.95338	5.069048	132
Tau.Propulsion	0.203884	No	0.253295	No			90			132	0.150978	0.103392	90	0.138298	0.06125	132
Overlap.Distance	0.039565	No	0.001549	Yes	1.749778	0.686131	90	1.463712	0.629242	132	1.749778	0.686131	90	1.463712	0.629242	132
Paw.Placement.Positioning.PPP	0.000293	Yes	0.979063	No	0.443222	0.221435	90	0.442424	0.222697	132	0.443222	0.221435	90	0.442424	0.222697	132
Ataxia.Coefficient	0.055735	No	0.38151	No	0.794889	0.295526	90	0.845379	0.285901	132	0.546444	0.277777	90	0.579848	0.279277	132
Midline.Distance	0.998012	No	0.000029	Yes	2.572	0.38345	90	2.450985	0.455068	132	1.539222	0.641965	90	1.190758	0.564684	132
Axis.Distance	0.836286	No	0.015682	No	0.838222	0.176753	90	0.752045	0.167454	132	1.299111	0.261708	90	1.220076	0.219397	132
Paw.Drag			0.00008	Yes	1	0	90	1	0	132	7.0439	3.321218	90	5.45697	2.551102	132

Table S3.5 Gait analysis parameters of male *Gnao1* R209H mutant mice

Measured Parameters	Fore Limb		Hind Limb		Fore Limb						Hind Limb					
	P value	FDR	P value	FDR	M WT Mean	SD	N	M R209H Mean	SD	N	M WT Mean	SD	N	M R209H Mean	SD	N
Swing	0.742713	No	0.249568	No	0.03575	0.010045	112	0.03525	0.011893	96	0.0889286	0.009719	112	0.08860417	0.012193	96
X.SwingStride	0.186611	No	0.414505	No	39.058929	3.751313	112	38.39479167	3.422753	96	36.2732143	4.576024	112	35.76979167	4.245595	96
Brake	0.07883	No	0.352804	No	0.0748482	0.018216	112	0.07973958	0.021724	96	0.03811607	0.011977	112	0.03653125	0.012519	96
X.BrakeStride	0.046818	No	0.281478	No	30.158036	5.195713	112	31.809375	6.68853	96	15.1651786	3.560158	112	14.56770833	4.418536	96
Propel	0.476735	No	0.246967	No	0.0785714	0.02064	112	0.074625	0.018382	96	0.12082143	0.021481	112	0.12441667	0.023144	96
X.PropelStride	0.224488	No	0.043317	No	30.778571	5.958209	112	29.796875	5.594329	96	48.5633929	3.628342	112	49.66354167	4.175722	96
Stance	0.459252	No	0.617997	No	0.1515089	0.02807	112	0.15432292	0.026341	96	0.15891964	0.029695	112	0.1609375	0.028273	96
X.StanceStride	0.186611	No	0.414505	No	60.941071	3.751313	112	61.60520833	3.422753	96	63.7267857	4.576024	112	64.23020833	4.245595	96
Stride	0.606739	No	0.701773	No	0.2472232	0.03416	112	0.24967708	0.034296	96	0.24777679	0.033051	112	0.2495625	0.033977	96
X.BrakeStance	0.144106	No	0.130071	No	49.605357	8.646812	112	51.459375	9.584303	96	23.6625	4.618239	112	22.54375	5.984204	96
X.PropelStance	0.143904	No	0.129692	No	50.395536	8.64638	112	48.540625	9.584303	96	76.3375	4.618239	112	77.45729167	5.983552	96
Stance.Swing	0.254797	No	0.507041	No	1.5875	0.262395	112	1.628125	0.247813	96	1.80178571	0.371018	112	1.83645833	0.379784	96
Stride.Length	0.514326	No	0.397668	No	6.2089286	0.784024	112	6.1375	0.788636	96	6.23035714	0.794104	112	6.13854167	0.76066	96
Stride.Frequency	0.599868	No	0.814209	No	4.2294643	0.586429	112	4.18645833	0.590917	96	4.21964286	0.559736	112	4.20104167	0.578291	96
PawAngle	0.409773	No	0.901338	No	-1.589286	3.516355	112	-1.11875	4.682854	96	1.14821429	17.7401	112	0.85520833	16.02805	96
Absolute.PawAngle	0.056783	No	0.005873	No	3.075	2.31787	112	3.77708333	2.962662	96	17.0785714	4.6622	112	15.265625	4.705849	96
Paw.Angle.Variability	0.708628	No	0.031802	No	6.4607143	2.427261	112	6.57083333	1.67997	96	4.3625	1.635481	112	4.95104167	2.276886	96
Stance.Width	0.384371	No	0.887767	No	3.4107143	2.559397	112	3.11458333	2.298145	96	7.05357143	6.172942	112	7.17708333	6.412151	96
Step.Angle	0.543298	No	0.524421	No	48.8125	54.21986	112	53.5625	58.20288	96	31.9732143	43.08831	112	28.34375	38.24184	96
SLVar	0.435215	No	0.15068	No	1.0917857	0.27152	112	1.13145833	0.449962	96	0.83419643	0.271292	112	0.89395833	0.326185	96
SWVar	0.920715	No	0.253516	No	12.825	12.87695	112	12.44791667	12.89053	96	5.17857143	5.429672	112	6.15625	6.875323	96
Step.Angle.Var	0.24211	No	0.878653	No	45.919643	60.59437	112	56.60416667	70.76982	96	48.75	60.6561	112	48.04166667	58.69079	96
X.Steps	0.8498	No	0.63707	No	24.424107	4.986563	112	24.5625	5.537076	96	24.3080357	4.825909	112	24.65104167	5.844336	96
Stride.Length.CV	0.286712	No	0.057982	No	17.998393	5.348469	112	19.09291667	9.18012	96	13.5108036	4.479219	112	14.95729167	6.409749	96
Stance.Width.CV	0.642162	No	0.33056	No	31.107143	36.02711	112	33.63541667	42.3313	96	65.669429	74.19895	112	76.25	82.21333	96
Step.Angle.CV	0.453618	No	0.810819	No	49.205357	63.63878	112	42.73958333	59.83877	96	52.7767857	64.92819	112	54.9375	64.68544	96
Swing.Duration.CV	0.065786	No	0.040295	No	24.166161	6.335163	112	26.689375	12.71546	96	19.8541964	5.777298	112	21.98125	8.948453	96
Paw.Area.at.Peak.Stance.in.sq.cm	0.269777	No	0.000048	Yes	0.2744643	0.031902	112	0.2796875	0.036171	96	0.57464286	0.063401	112	0.53677083	0.068032	96
Paw.Area.Variability.at.Peak.Stance	0.906173	No	0.815503	No	0.0205357	0.010209	112	0.02072917	0.013396	96	0.044375	0.019162	112	0.04375	0.019317	96
Hind.Limb.Shared.Stance.Time			0.757282	No	1	0	112	1	0	96	16.2678571	19.84035	112	17.125	19.99961	96
X.Shared.Stance			0.36289	No	1	0	112	1	0	96	82.4196429	46.81026	112	88.27083333	45.32908	96
StanceFactor	0.904653	No	0.985628	No	9.5178571	9.432532	112	9.67708333	9.675248	96	10.7142857	10.60293	112	10.6875	10.76477	96
Gait.Symmetry	0.339967	No	0.339967	No	1.0023214	0.026913	112	0.9975	0.044745	96	1.00232143	0.026913	112	0.9975	0.044745	96
MAX.dA.dT	0.337523	No	0.000739	Yes	14.877321	2.009157	112	15.17510417	2.457478	96	40.355625	4.795198	112	37.9240625	5.440301	96
MIN.dA.dT	0.043386	No	0.215019	No	-3.363571	0.813505	112	-3.645625	1.177005	96	-7.7479464	1.135325	112	-7.51552083	1.551981	96
Tau.Propulsion			0.069796	No	1	0	112	1	0	96	90.5625	46.16808	112	104.5729167	64.28223	96
Overlap.Distance	0.00004	Yes	0.00004	Yes	1.0380357	0.333044	112	1.251875	0.401419	96	1.03803571	0.333044	112	1.251875	0.401419	96
Paw.Placement.Positioning.PPP	0.072965	No	0.072965	No	0.4177679	0.151887	112	0.4609375	0.193277	96	0.41776796	0.151887	112	0.4609375	0.193277	96
Ataxia.Coefficient	0.131163	No	0.062689	No	0.7350893	0.247932	112	0.805625	0.413488	96	0.58044643	0.24559	112	0.65375	0.31857	96
Midline.Distance	0.193089	No	0.49868	No	-1.933214	0.331655	112	-1.9984375	0.388778	96	1.52928571	0.19725	112	1.506875	0.277653	96
Axis.Distance	0.734326	No	0.867511	No	0.0076786	0.789782	112	-0.02947917	0.781835	96	0.01223214	1.234583	112	-0.01677083	1.264412	96
Paw.Drag			0.141646	No	1	0	112	1	0	96	108.973214	56.80795	112	96.90625	61.0565	96

Table S3.6 Gait analysis parameters of female *Gnao1* R209H mutant mice

Measured Parameters	Fore Limb		Hind Limb		Fore Limb						Hind Limb					
	P value	FDR	P value	FDR	F WT Mean	SD	N	F R209H Mean	SD	N	F WT Mean	SD	N	F R209H Mean	SD	N
Swing	0.000862	No	0.001686	Yes	0.088759	0.011161	166	0.09418182	0.013945	88	0.0841024	0.0102	166	0.08846591	0.010834	88
X.SwingStride	0.553568	No	0.784138	No	38.269277	3.355496	166	38.53295455	3.399754	88	36.083735	4.11783	166	35.93068182	4.442386	88
Brake	0.257048	No	0.198976	No	0.0732651	0.016007	166	0.07582955	0.019054	88	0.0411506	0.013145	166	0.03895455	0.012517	88
X.BrakeStride	0.239615	No	0.003087	No	31.40241	4.642243	166	30.67613636	4.729754	88	17.425904	4.881231	166	15.58409091	4.255784	88
Propel	0.062971	No	0.000237	Yes	0.0713374	0.017694	166	0.07560227	0.016582	88	0.1098855	0.021791	166	0.12122727	0.025295	88
X.PropelStride	0.457782	No	0.000572	Yes	30.322289	4.635664	166	30.7875	4.943423	88	46.489157	3.90007	166	48.48409091	5.061345	88
Stride	0.052934	No	0.019444	No	0.1446145	0.026021	166	0.15142045	0.027503	88	0.1510843	0.028399	166	0.16014773	0.030727	88
X.StrideStride	0.553568	No	0.784138	No	61.730723	3.355496	166	61.46704545	3.399754	88	63.916265	4.11783	166	64.06931818	4.442386	88
Stride	0.009436	No	0.003393	No	0.2334036	0.033972	166	0.24563636	0.038132	88	0.2352108	0.03372	166	0.24863636	0.035716	88
X.BrakeStride	0.314746	No	0.001422	Yes	50.877108	6.954237	166	49.93863636	7.271317	88	27.063855	6.667062	166	24.28409091	6.276995	88
X.PropelStride	0.314746	No	0.001422	Yes	49.122892	6.954237	166	50.06136364	7.271317	88	72.936145	6.667062	166	75.71590909	6.276995	88
Stride.Swing	0.554245	No	0.625985	No	1.6361446	0.235657	166	1.61818182	0.218955	88	1.8054217	0.324599	166	1.82727273	0.366332	88
Stride.Length	0.920542	No	0.777101	No	5.836747	0.776261	166	5.82613636	0.859229	88	5.8759036	0.758562	166	5.9056102	0.864811	88
Stride.Frequency	0.014077	No	0.002251	Yes	4.5030121	0.657122	166	4.28636364	0.678264	88	4.4710843	0.641689	166	4.21590909	0.598059	88
PawAngle	0.094114	No	0.886736	No	-1.226506	4.09998	166	-0.36027272	3.519944	88	0.7493976	15.44145	166	0.45227273	16.46886	88
Absolute.PawAngle	0.008759	No	0.141453	No	3.673494	2.178745	166	2.94204545	1.940655	88	14.766265	4.431629	166	15.65681818	4.845256	88
Paw.Angle.Variability	0.273075	No	0.075906	No	6.5048193	1.980413	166	6.20113636	2.301149	88	4.7891566	1.885737	166	5.2431818	2.029884	88
Stride.Width	0.48535	No	0.502257	No	3.5240964	2.863991	166	3.79545455	3.093037	88	7.560241	6.89088	166	8.19318182	7.600451	88
Step.Angle	0.829913	No	0.607524	No	62.024096	67.35433	166	60.11363636	67.41746	88	34.722892	45.03798	166	37.9727273	53.14521	88
SLVar	0.178551	No	0.006484	No	1.0621687	0.280301	166	1.11465909	0.321265	88	0.8433133	0.275812	166	0.97397727	0.48285	88
SWVar	0.620186	No	0.655617	No	14.644578	15.3228	166	15.68181818	16.8117	88	6.560241	6.824598	166	6.97272727	7.549039	88
Step.Angle.Var	0.52429	No	0.895657	No	61.03012	78.19598	166	54.72727273	68.41115	88	52.662651	67.93058	166	53.84090909	68.31551	88
X.Steps	0.134323	No	0.121155	No	27.427711	6.803579	166	26.14772727	5.759629	88	27.274096	6.745719	166	25.94886364	5.887372	88
Stride.Length.CV	0.237484	No	0.006673	No	18.675843	6.063927	166	19.66806818	6.872459	88	14.471386	4.889888	166	16.61125	7.523195	88
Stride.Width.CV	0.865848	No	0.556665	No	50.23494	55.10375	166	51.48863636	58.28448	88	72.174699	94.41713	166	79.59090909	97.67394	88
Step.Angle.CV	0.162584	No	0.685476	No	51.463855	72.44272	166	65.53490909	82.82733	88	67.572289	81.02243	166	72	86.10726	88
Swing.Duration.CV	0.294853	No	0.002003	Yes	25.371325	7.757021	166	24.28715909	7.973726	88	20.003675	5.795205	166	22.93125	9.096783	88
Paw.Area.at.Peak.Stride.in.sq.cm	0.00641	No	0.66547	No	0.2454217	0.046964	166	0.2625	0.047398	88	0.5005422	0.079416	166	0.49590909	0.084386	88
Paw.Area.Variability.at.Peak.Stride	0.166619	No	0.005094	No	0.0223494	0.0077	166	0.02386364	0.009276	88	0.0453615	0.016391	166	0.05272727	0.024947	88
Hind.Limb.Shared.Stride.Time			0.537429	No	1	0	166	1	0	88	17.277108	21.25847	166	19.07954545	23.70665	88
X.Shared.Stride			0.630463	No	1	0	166	1	0	88	97.849398	53.24314	166	101.2954546	56.13001	88
StrideFactor	0.369433	No	0.629805	No	9.3192771	9.282136	166	8.26136364	8.197973	88	10.120482	9.739514	166	10.76136364	10.67169	88
Gait.Symmetry	0.140168	No	0.140168	No	1.0078313	0.026056	166	1.01545455	0.055974	88	1.0078313	0.026056	166	1.01545455	0.055974	88
MAX.dA.dT	0.013856	No	0.798156	No	12.997831	2.686344	166	13.86136364	2.557019	88	34.648434	6.534348	166	34.42875	6.45687	88
MIN.dA.dT	0.020047	No	0.170644	No	-3.557771	0.714287	166	-3.82125	1.069478	88	-7.6283133	1.321913	166	-7.84977273	1.00655	88
Tau.Propulsion			0.758007	No	1	0	166	1	0	88	112	61.46583	166	109.4545455	64.65877	88
Overlap.Distance	0.000061	Yes	0.000061	Yes	0.9884337	0.392521	166	1.23068182	0.543744	88	0.9884337	0.392521	166	1.23068182	0.543744	88
Paw.Placement.Positioning.PPP	0.110841	No	0.110841	No	0.4084337	0.147262	166	0.44352273	0.197449	88	0.4084337	0.147262	166	0.44352273	0.197449	88
Ataxia.Coefficient	0.291223	No	0.016224	No	0.7913855	0.282622	166	0.83193182	0.305505	88	0.6390964	0.254344	166	0.72954545	0.331666	88
Midline.Distance	0.495964	No	0.002418	Yes	-1.795783	0.305625	166	-1.82375	0.321102	88	1.5896988	0.233483	166	1.69352273	0.296365	88
Axis.Distance	0.755914	No	0.937074	No	0.003253	0.750176	166	-0.02784091	0.771926	88	-0.0086145	1.19335	166	-0.02136364	1.27859	88
Paw.Drag			0.000004	Yes	1	0	166	1	0	88	142.39157	69.54238	166	99.01136364	70.34978	88

Table S3.7 Gait analysis parameters of male *Gnao1* KO mutant mice

Measured Parameters	Fore Limb		Hind Limb		Fore Limb						Hind Limb					
	P value	FDR	P value	FDR	M WT Mean	SD	N	M KO Mean	SD	N	M WT Mean	SD	N	M KO Mean	SD	N
Swing	0.000054	Yes	<0.000001	Yes	0.0966143	0.013541	140	0.08936	0.013372	100	0.09272143	0.010933	140	0.08395	0.010752	100
X.SwingStride	0.024865	No	0.000566	Yes	38.773286	3.410721	140	37.65	4.330104	100	37.1207143	4.462917	140	35.062	4.550764	100
Brake	0.165567	No	0.72381	No	0.0560429	0.014514	140	0.05879	0.015854	100	0.03049286	0.008652	140	0.03093	0.010592	100
X.BrakeStride	0.000746	Yes	0.098909	No	22.397857	4.576582	140	24.677	5.745158	100	12.1007143	2.923768	140	12.858	4.159477	100
Propel	0.011982	No	0.549673	No	0.0979429	0.022044	140	0.09069	0.021648	100	0.12967857	0.029871	140	0.12735	0.029423	100
X.PropelStride	0.075845	No	0.030644	No	38.821429	4.457018	140	37.679	5.447477	100	50.775	4.326131	140	52.082	4.937619	100
Stance	0.224409	No	0.662124	No	0.1540143	0.028645	140	0.1495	0.027824	100	0.16015	0.034105	140	0.15824	0.032238	100
X.StanceStride	0.024765	No	0.000566	Yes	61.220714	3.410721	140	62.351	4.331596	100	62.8792857	4.462917	140	64.938	4.550764	100
Stride	0.017583	No	0.036704	No	0.2506429	0.03881	140	0.23888	0.035769	100	0.25293571	0.040235	140	0.24218	0.037453	100
X.BrakeStance	0.003525	No	0.430085	No	36.537143	6.893364	140	39.468	8.483339	100	19.2214286	4.247196	140	19.738	5.879957	100
X.PropelStance	0.003525	No	0.430085	No	63.462857	6.893364	140	60.532	8.483339	100	80.7785714	4.247196	140	80.262	5.879957	100
Stance.Swing	0.007551	No	0.000456	Yes	1.5964286	0.227723	140	1.689	0.304477	100	1.735	0.333269	140	1.899	0.377524	100
Stride.Length	0.000016	Yes	0.000016	Yes	6.29	0.818869	140	5.828	0.777601	100	6.33285714	0.759443	140	5.899	0.740665	100
Stride.Frequency	0.010131	No	0.029354	No	4.185	0.630966	140	4.401	0.644087	100	4.16285714	0.663579	140	4.352	0.652653	100
PawAngle	0.4019	No	0.929857	No	-0.705714	5.816768	140	-1.316	5.154065	100	0.34071429	19.33209	140	0.127	17.32487	100
Absolute.PawAngle	0.117131	No	0.000132	Yes	4.9457143	3.114537	140	4.306	3.095935	100	18.8221429	4.126107	140	16.617	4.610157	100
Paw.Angle.Variability	0.033279	No	0.975957	No	7.0635714	2.029963	140	7.682	2.431709	100	4.76857143	1.893194	140	4.761	1.949302	100
Stance.Width	0.098559	No	0.968237	No	3.45	2.661543	140	2.92	2.092217	100	7.68571429	6.825772	140	7.65	6.867248	100
StepAngle	0.582856	No	0.887753	No	61.464286	66.30954	140	56.83	61.51358	100	30.8785714	42.43293	140	31.66	41.96396	100
SLVar	0.000188	Yes	0.001399	Yes	1.4037143	0.373751	140	1.2313	0.305636	100	1.13464286	0.419421	140	0.9808	0.265626	100
SWVar	0.954784	No	0.86119	No	13.928571	14.98519	140	14.04	15.00567	100	8.29285714	10.34269	140	8.54	11.37285	100
StepAngleVar	0.90312	No	0.083955	No	58.332857	74.19071	140	59.59	73.8727	100	59.25	74.44153	140	43.77	58.11359	100
X.Steps	0.908455	No	0.970756	No	21.817857	4.385313	140	21.885	4.550977	100	21.6285714	4.351206	140	21.65	4.60758	100
Stride.Length.CV	0.229963	No	0.1875	No	22.860071	7.555922	140	21.718	6.790976	100	18.1392143	7.026218	140	17.0179	5.621839	100
Stance.Width.CV	0.57553	No	0.611842	No	46.407143	53.94267	140	50.45	56.61555	100	72.3	91.3001	140	66.41	84.49746	100
Step.Angle.CV	0.969952	No	0.668913	No	54.4	73.56002	140	54.04	72.00602	100	59.2642857	72.92655	140	63.41	75.36405	100
Swing.Duration.CV	0.041877	No	0.001224	Yes	28.250429	9.041509	140	25.9427	7.979169	100	24.3625714	8.268823	140	21.0523	6.891723	100
Paw.Area.at.Peak.Stance.in.sq.cm	0.055625	No	0.067872	No	0.2716429	0.051797	140	0.2851	0.055659	100	0.59078571	0.059483	140	0.607	0.077401	100
Paw.Area.Variability.at.P.eak.Stan	0.032442	No	0.000027	Yes	0.021	0.008591	140	0.0188	0.006557	100	0.05207143	0.027261	140	0.0391	0.015641	100
Hind.Limb.Shared.Stance.Time			0.526683	No	1	0	140	1	0	100	17.5357143	21.94513	140	19.41	23.43919	100
X..Shared.Stance			0.010604	No	1	0	140	1	0	100	87.6285714	49.65526	140	104.62	51.38344	100
StanceFactor	0.974929	No	0.843972	No	8.7571429	9.097293	140	8.72	8.903614	100	10.3857143	10.55481	140	10.12	9.93136	100
Gait.Symmetry	0.558834	No	0.558834	No	1.0077143	0.051682	140	1.011	0.025839	100	1.00771429	0.051682	140	1.011	0.025839	100
MAX.dA.dT	0.277738	No	0.036413	No	16.484857	2.680563	140	16.9022	3.247951	100	43.0139286	4.791189	140	44.5698	6.666559	100
MIN.dA.dT	0.220542	No	0.000003	Yes	-4.639	0.926215	140	-4.4848	1.002793	100	-8.8659286	1.463116	140	-7.9607	1.404932	100
Tau..Propulsion			0.111301	No	1	0	140	1	0	100	110	64.09716	140	123.91	69.66487	100
Overlap.Distance	0.282875	No	0.282875	No	1.3222857	0.336865	140	1.37	0.340982	100	1.32228571	0.336865	140	1.37	0.340982	100
PawPlacementPositioning.PPP	0.049741	No	0.049741	No	0.4799286	0.173721	140	0.5296	0.215823	100	0.47992857	0.173721	140	0.5296	0.215823	100
Ataxia.Coefficient	0.238915	No	0.394142	No	0.9550714	0.340194	140	0.9027	0.333297	100	0.77992857	0.325529	140	0.7451	0.290925	100
Midline.Distance	0.001913	No	<0.000001	Yes	-2.694786	0.350606	140	-2.8457	0.389434	100	1.45178571	0.368579	140	1.0712	0.43125	100
Axis.Distance	0.840325	No	0.817383	No	0.0115	0.801008	140	0.0323	0.768448	100	-0.0047143	1.32741	140	0.035	1.290374	100
Paw.Drag			0.000026	Yes	1	0	140	1	0	100	103.528571	66.43366	140	139.88	62.16779	100

Table S3.8 Gait analysis parameters of female *Gnao1* KO mutant mice

Measured Parameters	Fore Limb		Hind Limb		Fore Limb						Hind Limb					
	P value	FDR	P value	FDR	M WT Mean	SD	N	M KO Mean	SD	N	M WT Mean	SD	N	M KO Mean	SD	N
Swing	0.80571	No	0.820639	No	0.090881	0.015084	126	0.09034211	0.015029	76	0.08811111	0.011389	126	0.08773684	0.011287	76
X.SwingStride	0.727928	No	0.327439	No	37.835714	3.303319	126	37.99342105	2.778601	76	36.402381	4.265311	126	36.98947368	3.859001	76
Brake	0.959871	No	0.855721	No	0.0605079	0.016707	126	0.06063158	0.017212	76	0.03019841	0.009046	126	0.03043421	0.0087	76
X.BrakeStride	0.766918	No	0.604358	No	25.046825	4.950098	126	25.26184211	5.049963	76	12.4555556	3.618786	126	12.71184211	3.000665	76
Propel	0.433018	No	0.212013	No	0.0901111	0.022099	126	0.08768421	0.01981	76	0.12659524	0.030455	126	0.12134211	0.026067	76
X.PropelStride	0.611446	No	0.18154	No	37.116667	5.123838	126	36.73684211	5.16622	76	51.1444444	4.588133	126	50.30657895	3.779959	76
Stance	0.595756	No	0.287305	No	0.1505952	0.02981	126	0.14834211	0.02814	76	0.15688095	0.033709	126	0.15181579	0.030911	76
X.StanceStride	0.727928	No	0.327439	No	62.164286	3.303319	126	62.00657895	2.778601	76	63.5976191	4.265311	126	63.01052632	3.859001	76
Stride	0.63591	No	0.352323	No	0.2415397	0.041883	126	0.23867105	0.041275	76	0.24495238	0.040905	126	0.23951316	0.038918	76
X.BrakeStance	0.68239	No	0.432768	No	40.286508	7.425463	126	40.73947368	7.909034	76	19.5436508	5.338532	126	20.11447368	4.377875	76
X.PropelStance	0.68239	No	0.432118	No	59.713492	7.425463	126	59.26052632	7.909034	76	80.4571429	5.338351	126	79.88552632	4.377875	76
Stance.Swing	0.692429	No	0.26692	No	1.6603175	0.239359	126	1.64736842	0.19898	76	1.78571429	0.327344	126	1.73552632	0.279859	76
Stride.Length	0.085256	No	0.014479	No	5.3293651	0.731253	126	5.79557895	0.603678	76	6.0047619	0.663689	126	5.77763158	0.581171	76
Stride.Frequency	0.630716	No	0.365384	No	4.3777778	0.722174	126	4.42894737	0.739336	76	4.31825397	0.718285	126	4.41315789	0.723573	76
PawAngle	0.013715	No	0.462617	No	1.4746032	5.189311	126	-0.54342105	6.194951	76	-0.3563492	16.56968	126	1.41184211	16.49608	76
Absolute.PawAngle	0.044961	No	0.570224	No	4.2285714	3.331207	126	5.20657895	3.347649	76	16.1230159	3.556811	126	15.79342105	4.62412	76
Paw.Angle.Variability	0.007312	No	0.00075	No	6.8833333	1.681987	126	7.89210526	3.577812	76	4.68571429	1.67345	126	6.30394737	4.855604	76
Stance.Width	0.297271	No	0.814438	No	3.7857143	2.986924	126	3.35526316	2.564912	76	7.17460317	6.33603	126	6.96052632	6.163204	76
Step.Angle	0.489835	No	0.739738	No	54.34127	59.0929	126	48.53947368	55.40865	76	31.4126984	41.97052	126	33.48684211	44.48086	76
SLVar	0.565803	No	0.515402	No	1.3600794	0.343405	126	1.3325	0.306725	76	1.10555556	0.359134	126	1.13855263	0.330473	76
SWVar	0.444068	No	0.039537	No	14.293651	15.47285	126	16.11842105	17.7981	76	8.01587302	9.890589	126	11.75	15.73203	76
Step.Angle.Var	0.705629	No	0.904505	No	49.730159	62.78731	126	53.19736842	63.64171	76	47.5238095	61.83885	126	46.46052632	59.4231	76
X.Steps	0.139258	No	0.046748	No	23.960317	4.61762	126	24.99342105	5.068526	76	23.5277778	4.458836	126	24.89473684	5.08548	76
Stride.Length.CV	0.955387	No	0.113165	No	23.392857	6.995052	126	23.44684211	5.989497	76	18.5309524	5.962569	126	19.94105263	6.327376	76
Stance.Width.CV	0.330411	No	0.963959	No	46.468254	51.84063	126	54.17105263	58.31349	76	52.7698413	74.45967	126	52.28947368	70.78961	76
Step.Angle.CV	0.612745	No	0.622492	No	47.706349	61.74529	126	52.38157895	66.31239	76	47.9444444	60.44056	126	52.36842105	63.93452	76
Swing.Duration.CV	0.338005	No	0.430043	No	28.772381	7.820674	126	27.70763158	7.309925	76	24.2536508	6.894116	126	25.08039474	7.679944	76
Paw.Area.at.Peak.Stance.in.sq.cm	0.040811	No	0.536284	No	0.2765079	0.054792	126	0.26118421	0.04472	76	0.58753968	0.118644	126	0.57828947	0.068729	76
Paw.Area.Variability.at.Peak.Stance	0.055277	No	0.108075	No	0.0228571	0.010648	126	0.02763158	0.024214	76	0.05039683	0.021887	126	0.05644737	0.031271	76
Hind.Limb.Shared.Stance.Time			0.58501	No	1	0	126	1	0	76	18.1746032	21.7576	126	16.5	19.89874	76
X.Shared.Stance			0.138078	No	1	0	126	1	0	76	82.8174603	44.47514	126	73.63157895	38.92106	76
StanceFactor	0.175091	No	0.908552	No	10.134921	10.84019	126	8.15789474	8.423859	76	9.76984127	9.806253	126	9.60526316	9.929188	76
Gait.Symmetry	0.089351	No	0.089351	No	1.0157143	0.04399	126	1.00421053	0.050153	76	1.01571429	0.04399	126	1.00421053	0.050153	76
MAX.dA.dT	0.088329	No	0.711101	No	16.179365	3.068414	126	15.49092105	2.176046	76	42.4457143	8.392421	126	42.05407895	4.853255	76
MIN.dA.dT	0.25101	No	0.648945	No	-4.832778	1.217865	126	-4.62289474	1.315192	76	-8.7710318	2.194612	126	-8.63855263	1.626896	76
Tau.Propulsion			0.329558	No	1	0	126	1	0	76	93.0396825	54.28361	126	100.7105263	53.62383	76
Overlap.Distance	0.06535	No	0.06535	No	1.3143651	0.442389	126	1.19828947	0.412137	76	1.31436508	0.442389	126	1.19828947	0.412137	76
Paw.Placement.Positioning.PPP	0.642852	No	0.642852	No	0.3996032	0.21485	126	0.41618421	0.290181	76	0.39960317	0.21485	126	0.41618421	0.290181	76
Ataxia.Coefficient	0.406479	No	0.080856	No	1.0359524	0.359989	126	1.07894737	0.348879	76	0.82809524	0.318601	126	0.90736842	0.298098	76
Midline.Distance	0.306676	No	0.079655	No	-2.553175	0.490671	126	-2.48618421	0.372673	76	1.37214286	0.462222	126	1.26828947	0.288543	76
Axis.Distance	0.630299	No	0.878369	No	0.013254	0.758111	126	0.06552632	0.727057	76	-0.026746	1.208638	126	-0.00013158	1.614256	76
Paw.Drag			0.095768	No	1	0	126	1	0	76	96.7857143	59.58625	126	110.8289474	54.61755	76

Table S3.9 Benchling off-target list for *Gnao1* G203R gRNA

Sequence	PAM	Score	Gene	Chromosome	Mismatches
TGCAGGCTGTTTGACGTCGG	GGG	100	ENSMUSG00000031748	chr8	0
GGCAAGCTGATTGACGTCTG	TAG	0.6189		chr18	4
TGGATGGTGTGGACGTCGG	AAG	0.5200	ENSMUSG00000041390	chr6	4
TGCAGGCTGTTTGAAGTCTG	CAG	0.5076		chr3	2
GGTGGGCTGTTTGACGTGGG	AGG	0.3804		chr1	4
TTCAGGCTGAGTGACGTCAG	TGG	0.3169	ENSMUSG00000032497	chr9	4
AGCAGGCACTTTGAAGTCGG	AAG	0.2931		chr3	4
TTCAGTCTGTTAGACGTCTG	TAG	0.1953		chr1	4
TGCATGGGGTTTGACTTCGG	AGG	0.1929		chr13	4
TGCTGGCTGTTTGAGGTGGG	AAG	0.1923		chr1	3
TCCAGGCTGGTGGACGTGGG	CAG	0.1710		chr1	4
TGATGGCTGTTCCACTTCGG	GAG	0.1556	ENSMUSG00000086805	chr8	4
TACAGAATGTTTGACGTGGG	AGG	0.1543	ENSMUSG00000057614	chr5	4
TTCAGTCTGTTTGAGGTCGT	TGG	0.1515		chrX	4
AGCAGGCTGCTTGACATCGA	GAG	0.1480		chr4	4
TGCAAGCTGGTTGAGGTCAG	GGG	0.1450		chr17	4
TCCAGGATGTTTGATGCCGG	AAG	0.1403		chr18	4
TGCAGGCTGTCTGAAGTCTG	GGG	0.1343	ENSMUSG00000026413	chr1	3
GGCTGGCTGTTTGACCTCAG	AGG	0.1262		chrX	4
AGCAGCCTGTTTGAAGTCTG	TGG	0.1144		chr11	4
GGCAGGCTGTATGAAGGCGG	AGG	0.1127		chr5	4
TGGAGGCTGTTACACGTCAG	CAG	0.1127		chr1	4
TGCTGGCTATTTGAAGTCTG	AGG	0.1004		chr10	4
TGCTGGTTATTTGTCGTCGG	GAG	0.1002		chr11	4
TCCAGGCTGTCTGATGTCAG	GAG	0.0954		chrX	4
TTCAGGATGTTTGACGTATG	CAG	0.0933		chr3	4
TGCACGCTGTGAGACGTGGG	CGG	0.0930	ENSMUSG00000020015	chr10	4
TGCATGCTGTCTGAAGTCAG	AAG	0.0865		chrX	4
TGCAGGCTGTATGACCTCTG	GGG	0.0862		chr2	3
TGCAGTCTCTTTGACGACAG	TGG	0.0836		chr11	4

Table S3.9 (cont'd)

TGCATGCTGTAGGACCTCGG	AGG	0.0771		chr4	4
CGGAGGCTGTTTGACTTGGG	AGG	0.0754		chr5	4
TCCAGGCTGTTTCAGGACGG	AAG	0.0745		chr8	4
GGCAGCCTGTTTGACATCAG	GAG	0.0744		chr17	4
TGCAAGATGTTTGACCTCAG	AAG	0.0720		chr19	4
TGGAGGTTGTTTGAGGTAGG	AGG	0.0704		chr2	4
TGTGGGCTGTTTGACCTGGG	AGG	0.0693		chr19	4
GGCAGGCTGTTTGAAGCCAG	GGG	0.0669		chr9	4
TCCAGGCTGTTTGAGGGCTG	CAG	0.0647	ENSMUSG00000097637	chr8	4
TGCAGGCTGGCTGACGATGG	TGG	0.0611		chr8	4
TGCAGGATGCTTGACCTCTG	TAG	0.0604		chr2	4
TGCACTCTGTTTGAGGTTGG	AGG	0.0599		chr10	4
TCCAGGCTGTGTGAGGTGGG	AGG	0.0574		chr9	4
GGCAGGCTGTTGGAAGTAGG	GAG	0.0520		chr2	4
TGAAGGCTGTTTGAAGTGGG	GAG	0.0480		chrX	4
TGCAGGCTGATTGATGGCTG	GAG	0.0470		chr7	4
TACAGACTGTTTGACTTGGG	CAG	0.0430		chr3	4
TTCAGGCTGTTTACTTCTG	AGG	0.0422		chr15	4
AGCAGGATGTTTGTCGTGGG	GAG	0.0420		chr1	4
AGCAGGCTGTGTGACCTGGG	AGG	0.0385		chr6	4

Row 1 includes the on-target gRNA for the Gnao1 G203 site. Off-target hits are scored and ranked by an inverse likelihood of off-target binding. If an off-target is predicted to occur within a coding region of a gene, the Ensembl number of the affected locus is listed in the Gene column. Analysis was performed on the Benchling platform using reference genome GRCM38 (MM10, Mus Musculus), guide length of 20bp, and an NGG PAM.

REFERENCES

REFERENCES

- Ananth, A. L., Robichaux-Viehoever, A., Kim, Y. M., Hanson-Kahn, A., Cox, R., Enns, G. M., . . . Bernstein, J. A. (2016). Clinical Course of Six Children With GNAO1 Mutations Causing a Severe and Distinctive Movement Disorder. *Pediatr Neurol*, *59*, 81-84. doi:10.1016/j.pediatrneurol.2016.02.018
- Arya, R., Spaeth, C., Gilbert, D. L., Leach, J. L., & Holland, K. D. (2017). GNAO1-associated epileptic encephalopathy and movement disorders: c.607G>A variant represents a probable mutation hotspot with a distinct phenotype. *Epileptic Disord*, *19*(1), 67-75. doi:10.1684/epd.2017.0888
- Blumkin, L., Lerman-Sagie, T., Westenberger, A., Ben-Pazi, H., Zerem, A., Yosovich, K., & Lev, D. (2018). Multiple Causes of Pediatric Early Onset Chorea-Clinical and Genetic Approach. *Neuropediatrics*, *49*(4), 246-255. doi:10.1055/s-0038-1645884
- Bromberg, K. D., Iyengar, R., & He, J. C. (2008). Regulation of neurite outgrowth by G(i/o) signaling pathways. *Front Biosci*, *13*, 4544-4557.
- Bruun, T. U. J., DesRoches, C. L., Wilson, D., Chau, V., Nakagawa, T., Yamasaki, M., . . . Mercimek-Andrews, S. (2018). Prospective cohort study for identification of underlying genetic causes in neonatal encephalopathy using whole-exome sequencing. *Genet Med*, *20*(5), 486-494. doi:10.1038/gim.2017.129
- Danti, F. R., Galosi, S., Romani, M., Montomoli, M., Carss, K. J., Raymond, F. L., . . . Guerrini, R. (2017). GNAO1 encephalopathy: Broadening the phenotype and evaluating treatment and outcome. *Neurol Genet*, *3*(2), e143. doi:10.1212/NXG.000000000000143
- Deacon, R. M. (2013). Measuring the strength of mice. *J Vis Exp*(76). doi:10.3791/2610
- Dhamija, R., Mink, J. W., Shah, B. B., & Goodkin, H. P. (2016). GNAO1-Associated Movement Disorder. *Mov Disord Clin Pract*, *3*(6), 615-617. doi:10.1002/mdc3.12344
- Dhamija, R. M., J, W.; Shah, B, B.; Goodkin, H, P. (2016). GNAO1-Associated Movement Disorder. *Movement Disorders Clinical Practice*, *3*(6), 615-617.

doi:10.1002/mdc3.12344

- Dhir, A. (2012). Pentylentetrazol (PTZ) kindling model of epilepsy. *Curr Protoc Neurosci*, Chapter 9, Unit9.37. doi:10.1002/0471142301.ns0937s58
- DiBello, P. R., Garrison, T. R., Apanovitch, D. M., Hoffman, G., Shuey, D. J., Mason, K., . . . Dohlman, H. G. (1998). Selective uncoupling of RGS action by a single point mutation in the G protein alpha-subunit. *J Biol Chem*, 273(10), 5780-5784.
- Dietel, T. H., T. B.; Schlüter, G.; Cordes, I.; Trollmann, R.; Bast, T. (2016). Genotype and phenotype in GNAO1-Mutation – Case report of an unusual course of a childhood epilepsy. *Neuropediatrics*, 47(S 01), 1-17. doi:10.1055/s-0036-1583625
- Doench, J. G., Fusi, N., Sullender, M., Hegde, M., Vaimberg, E. W., Donovan, K. F., . . . Root, D. E. (2016). Optimized sgRNA design to maximize activity and minimize off-target effects of CRISPR-Cas9. *Nat Biotechnol*, 34(2), 184-191. doi:10.1038/nbt.3437
- Euro, E.-R. E. S. C., Epilepsy Phenome/Genome, P., & Epi, K. C. (2014). De novo mutations in synaptic transmission genes including DNMT1 cause epileptic encephalopathies. *Am J Hum Genet*, 95(4), 360-370. doi:10.1016/j.ajhg.2014.08.013
- Feng, H., Khalil, S., Neubig, R. R., & Sidiropoulos, C. (2018). A mechanistic review on GNAO1-associated movement disorder. *Neurobiol Dis*. doi:10.1016/j.nbd.2018.05.005
- Feng, H., Larrivee, C. L., Demireva, E. Y., Xie, H., Leipprandt, J. R., & Neubig, R. R. (2019). Mouse models of GNAO1-associated movement disorder: Allele- and sex-specific differences in phenotypes. *PLoS One*, 14(1), e0211066. doi:10.1371/journal.pone.0211066
- Feng, H., Sjogren, B., Karaj, B., Shaw, V., Gezer, A., & Neubig, R. R. (2017). Movement disorder in GNAO1 encephalopathy associated with gain-of-function mutations. *Neurology*, 89(8), 762-770. doi:10.1212/WNL.0000000000004262
- Franco-Pons, N., Torrente, M., Colomina, M. T., & Vilella, E. (2007). Behavioral deficits in the cuprizone-induced murine model of demyelination/remyelination. *Toxicol Lett*, 169(3), 205-213. doi:10.1016/j.toxlet.2007.01.010

- Franek, M., Pagano, A., Kaupmann, K., Bettler, B., Pin, J. P., & Blahos, J. (1999). The heteromeric GABA-B receptor recognizes G-protein alpha subunit C-termini. *Neuropharmacology*, *38*(11), 1657-1666.
- Fu, Y., Zhong, H., Nanamori, M., Mortensen, R. M., Huang, X., Lan, K., & Neubig, R. R. (2004). RGS-insensitive G-protein mutations to study the role of endogenous RGS proteins. *Methods Enzymol*, *389*, 229-243. doi:10.1016/S0076-6879(04)89014-1
- Gawlinski, P., Posmyk, R., Gambin, T., Sielicka, D., Chorazy, M., Nowakowska, B., . . . Wiszniewski, W. (2016). PEHO Syndrome May Represent Phenotypic Expansion at the Severe End of the Early-Onset Encephalopathies. *Pediatr Neurol*, *60*, 83-87. doi:10.1016/j.pediatrneurol.2016.03.011
- Gazi, L., Nickolls, S. A., & Strange, P. G. (2003). Functional coupling of the human dopamine D2 receptor with G alpha i1, G alpha i2, G alpha i3 and G alpha o G proteins: evidence for agonist regulation of G protein selectivity. *Br J Pharmacol*, *138*(5), 775-786. doi:10.1038/sj.bjp.0705116
- Gillies, G. E., Murray, H. E., Dexter, D., & McArthur, S. (2004). Sex dimorphisms in the neuroprotective effects of estrogen in an animal model of Parkinson's disease. *Pharmacol Biochem Behav*, *78*(3), 513-522. doi:10.1016/j.pbb.2004.04.022
- Goldenstein, B. L., Nelson, B. W., Xu, K., Luger, E. J., Pribula, J. A., Wald, J. M., . . . Doze, V. A. (2009). Regulator of G protein signaling protein suppression of Galphao protein-mediated alpha2A adrenergic receptor inhibition of mouse hippocampal CA3 epileptiform activity. *Mol Pharmacol*, *75*(5), 1222-1230. doi:mol.108.054296 [pii]10.1124/mol.108.054296
- Grecksch, G., Becker, A., Schroeder, H., Kraus, J., Loh, H., & Holtt, V. (2004). Accelerated kindling development in mu-opioid receptor deficient mice. *Naunyn Schmiedebergs Arch Pharmacol*, *369*(3), 287-293. doi:10.1007/s00210-004-0870-4
- Haeussler M, S. K., Eckert H, Eschstruth A, Mianné J, Renaud JB, Schneider-Maunoury S, Shkumatava A, Teboul L, Kent J, Joly JS, Concordet JP. (2016). Evaluation of off-target and on-target scoring algorithms and integration into the guide RNA selection tool CRISPOR. *Genome Biol*, *17*(1), 148. doi:https://doi.org/10.1186/s13059-016-1012-2

- Hansen, S. T., & Pulst, S. M. (2013). Response to ethanol induced ataxia between C57BL/6J and 129X1/SvJ mouse strains using a treadmill based assay. *Pharmacol Biochem Behav*, *103*(3), 582-588. doi:10.1016/j.pbb.2012.10.010
- Hirata, H., Takahashi, A., Shimoda, Y., & Koide, T. (2016). Caspr3-Deficient Mice Exhibit Low Motor Learning during the Early Phase of the Accelerated Rotarod Task. *PLoS One*, *11*(1), e0147887. doi:10.1371/journal.pone.0147887
- Honey, C. M., Malhotra, A. K., Tarailo-Graovac, M., van Karnebeek, C. D. M., Horvath, G., & Sulistyanto, A. (2018). GNAO1 Mutation-Induced Pediatric Dystonic Storm Rescue With Pallidal Deep Brain Stimulation. *J Child Neurol*, *33*(6), 413-416. doi:10.1177/0883073818756134
- Hsu, P. D., Scott, D. A., Weinstein, J. A., Ran, F. A., Konermann, S., Agarwala, V., . . . Zhang, F. (2013). DNA targeting specificity of RNA-guided Cas9 nucleases. *Nat Biotechnol*, *31*(9), 827-832. doi:10.1038/nbt.2647
- Iyer, V., Boroviak, K., Thomas, M., Doe, B., Riva, L., Ryder, E., & Adams, D. J. (2018). No unexpected CRISPR-Cas9 off-target activity revealed by trio sequencing of gene-edited mice. *PLoS Genet*, *14*(7), e1007503. doi:10.1371/journal.pgen.1007503
- Jiang, M., & Bajpayee, N. S. (2009). Molecular mechanisms of go signaling. *Neurosignals*, *17*(1), 23-41. doi:10.1159/000186688
- Jiang, M., Gold, M. S., Boulay, G., Spicher, K., Peyton, M., Brabet, P., . . . Birnbaumer, L. (1998). Multiple neurological abnormalities in mice deficient in the G protein Go. *Proc Natl Acad Sci U S A*, *95*(6), 3269-3274. doi:10.1073/pnas.95.6.3269
- Kehrl, J. M., Sahaya, K., Dalton, H. M., Charbeneau, R. A., Kohut, K. T., Gilbert, K., . . . Neubig, R. R. (2014). Gain-of-function mutation in Gnao1: a murine model of epileptiform encephalopathy (EIEE17)? *Mamm Genome*, *25*(5-6), 202-210. doi:10.1007/s00335-014-9509-z
- Kelly, M., Park, M., Mihalek, I., Roctus, A., Gramm, M., Perez-Palma, E., . . . Poduri, A. (2019). Spectrum of neurodevelopmental disease associated with the GNAO1 guanosine triphosphate-binding region. *Epilepsia*, *60*(3), 406-418. doi:10.1111/epi.14653
- Kompoliti, K. (1999). Estrogen and movement disorders. *Clin Neuropharmacol*, *22*(6),

318-326.

- Kulkarni, N., Tang, S., Bhardwaj, R., Bernes, S., & Grebe, T. A. (2016). Progressive Movement Disorder in Brothers Carrying a GNAO1 Mutation Responsive to Deep Brain Stimulation. *J Child Neurol*, 31(2), 211-214. doi:10.1177/0883073815587945
- Lan, K. L., Sarvazyan, N. A., Taussig, R., Mackenzie, R. G., DiBello, P. R., Dohlman, H. G., & Neubig, R. R. (1998). A point mutation in Galphao and Galphai1 blocks interaction with regulator of G protein signaling proteins. *J Biol Chem*, 273(21), 12794-12797.
- Larrivee, C. L., Feng, H., Leipprandt, J. R., Demireva, E. Y., Xie, H., & Neubig, R. R. (2019). Mice with *GNAO1* R209H Movement Disorder Variant Display Hyperlocomotion Alleviated by Risperidone. *bioRxiv*.
- Law, C. Y., Chang, S. T., Cho, S. Y., Yau, E. K., Ng, G. S., Fong, N. C., & Lam, C. W. (2015). Clinical whole-exome sequencing reveals a novel missense pathogenic variant of GNAO1 in a patient with infantile-onset epilepsy. *Clin Chim Acta*, 451(Pt B), 292-296. doi:10.1016/j.cca.2015.10.011
- Li, Q., Lau, A., Morris, T. J., Guo, L., Fordyce, C. B., & Stanley, E. F. (2004). A syntaxin 1, Galpha(o), and N-type calcium channel complex at a presynaptic nerve terminal: analysis by quantitative immunocolocalization. *J Neurosci*, 24(16), 4070-4081. doi:10.1523/JNEUROSCI.0346-04.2004
- Lorenzen, A., Lang, H., & Schwabe, U. (1998). Activation of various subtypes of G-protein alpha subunits by partial agonists of the adenosine A1 receptor. *Biochem Pharmacol*, 56(10), 1287-1293.
- Madalan, A., Yang, X., Ferris, J., Zhang, S., & Roman, G. (2012). G(o) activation is required for both appetitive and aversive memory acquisition in Drosophila. *Learn Mem*, 19(1), 26-34. doi:10.1101/lm.024802.111
- Marce-Grau, A., Dalton, J., Lopez-Pison, J., Garcia-Jimenez, M. C., Monge-Galindo, L., Cuenca-Leon, E., . . . Macaya, A. (2016). GNAO1 encephalopathy: further delineation of a severe neurodevelopmental syndrome affecting females. *Orphanet J Rare Dis*, 11, 38. doi:10.1186/s13023-016-0416-0
- Marecos, C., Duarte, S., Alonso, I., Calado, E., & Moreira, A. (2018). [GNAO1: a new

- gene to consider on early-onset childhood dystonia]. *Rev Neurol*, 66(9), 321-322.
- Menke, L. A., Engelen, M., Alders, M., Odekerken, V. J., Baas, F., & Cobben, J. M. (2016). Recurrent GNAO1 Mutations Associated With Developmental Delay and a Movement Disorder. *J Child Neurol*, 31(14), 1598-1601. doi:10.1177/0883073816666474
- Nakamura, K., Kodera, H., Akita, T., Shiina, M., Kato, M., Hoshino, H., . . . Saitsu, H. (2013). De Novo mutations in GNAO1, encoding a Gα subunit of heterotrimeric G proteins, cause epileptic encephalopathy. *Am J Hum Genet*, 93(3), 496-505. doi:10.1016/j.ajhg.2013.07.014
- Oleas, J., Yokoi, F., DeAndrade, M. P., Pisani, A., & Li, Y. (2013). Engineering animal models of dystonia. *Mov Disord*, 28(7), 990-1000. doi:10.1002/mds.25583
- Parr, T., & Friston, K. J. (2017). Working memory, attention, and salience in active inference. *Sci Rep*, 7(1), 14678. doi:10.1038/s41598-017-15249-0
- Qin, W., Dion, S. L., Kutny, P. M., Zhang, Y., Cheng, A. W., Jillette, N. L., . . . Wang, H. (2015). Efficient CRISPR/Cas9-Mediated Genome Editing in Mice by Zygote Electroporation of Nuclease. *Genetics*, 200(2), 423-430. doi:10.1534/genetics.115.176594
- Revankar, C. M., Cimino, D. F., Sklar, L. A., Arterburn, J. B., & Prossnitz, E. R. (2005). A transmembrane intracellular estrogen receptor mediates rapid cell signaling. *Science*, 307(5715), 1625-1630. doi:10.1126/science.1106943
- Saitsu, H., Fukai, R., Ben-Zeev, B., Sakai, Y., Mimaki, M., Okamoto, N., . . . Matsumoto, N. (2016). Phenotypic spectrum of GNAO1 variants: epileptic encephalopathy to involuntary movements with severe developmental delay. *Eur J Hum Genet*, 24(1), 129-134. doi:10.1038/ejhg.2015.92
- Schirinzi, T., Garone, G., Travaglini, L., Vasco, G., Galosi, S., Rios, L., . . . Leuzzi, V. (2019). Phenomenology and clinical course of movement disorder in GNAO1 variants: Results from an analytical review. *Parkinsonism Relat Disord*, 61, 19-25. doi:10.1016/j.parkreldis.2018.11.019
- Schorling, D. C., Dietel, T., Evers, C., Hinderhofer, K., Korinthenberg, R., Ezzo, D., . . . Kirschner, J. (2017). Expanding Phenotype of De Novo Mutations in GNAO1: Four New Cases and Review of Literature. *Neuropediatrics*, 48(5), 371-377.

doi:10.1055/s-0037-1603977

- Schutsky, K., Ouyang, M., & Thomas, S. A. (2011). Xamoterol impairs hippocampus-dependent emotional memory retrieval via Gi/o-coupled beta2-adrenergic signaling. *Learn Mem*, 18(9), 598-604. doi:10.1101/lm.2302811
- Smith, K. M., & Dahodwala, N. (2014). Sex differences in Parkinson's disease and other movement disorders. *Exp Neurol*, 259, 44-56. doi:10.1016/j.expneurol.2014.03.010
- Solis, G. P., & Katanaev, V. L. (2018). Galphao (GNAO1) encephalopathies: plasma membrane vs. Golgi functions. *Oncotarget*, 9(35), 23846-23847. doi:10.18632/oncotarget.22067
- Song, C. H., Fan, X., Exeter, C. J., Hess, E. J., & Jinnah, H. A. (2012). Functional analysis of dopaminergic systems in a DYT1 knock-in mouse model of dystonia. *Neurobiol Dis*, 48(1), 66-78. doi:10.1016/j.nbd.2012.05.009
- Strittmatter, S. M., Fishman, M. C., & Zhu, X. P. (1994). Activated mutants of the alpha subunit of G(o) promote an increased number of neurites per cell. *J Neurosci*, 14(4), 2327-2338.
- Stroobants, S., Gantois, I., Pooters, T., & D'Hooge, R. (2013). Increased gait variability in mice with small cerebellar cortex lesions and normal rotarod performance. *Behav Brain Res*, 241, 32-37. doi:10.1016/j.bbr.2012.11.034
- Tatem, K. S., Quinn, J. L., Phadke, A., Yu, Q., Gordish-Dressman, H., & Nagaraju, K. (2014). Behavioral and locomotor measurements using an open field activity monitoring system for skeletal muscle diseases. *J Vis Exp*(91), 51785. doi:10.3791/51785
- Tian, W. N., Duzic, E., Lanier, S. M., & Deth, R. C. (1994). Determinants of alpha 2-adrenergic receptor activation of G proteins: evidence for a precoupled receptor/G protein state. *Mol Pharmacol*, 45(3), 524-531.
- Truett, G. E., Heeger, P., Mynatt, R. L., Truett, A. A., Walker, J. A., & Warman, M. L. (2000). Preparation of PCR-quality mouse genomic DNA with hot sodium hydroxide and tris (HotSHOT). *Biotechniques*, 29(1), 52, 54.

- Valenzuela, D., Han, X., Mende, U., Fankhauser, C., Mashimo, H., Huang, P., . . . Fishman, M. C. (1997). G alpha(o) is necessary for muscarinic regulation of Ca²⁺ channels in mouse heart. *Proc Natl Acad Sci U S A*, *94*(5), 1727-1732. doi:10.1073/pnas.94.5.1727
- Waak, M., Mohammad, S. S., Coman, D., Sinclair, K., Copeland, L., Silburn, P., . . . Malone, S. (2018). GNAO1-related movement disorder with life-threatening exacerbations: movement phenomenology and response to DBS. *J Neurol Neurosurg Psychiatry*, *89*(2), 221-222. doi:10.1136/jnnp-2017-315653
- Wettschureck, N., & Offermanns, S. (2005). Mammalian G proteins and their cell type specific functions. *Physiol Rev*, *85*(4), 1159-1204. doi:10.1152/physrev.00003.2005
- Wilczynski, G. M., Konopacki, F. A., Wilczek, E., Lasiecka, Z., Gorlewicz, A., Michaluk, P., . . . Kaczmarek, L. (2008). Important role of matrix metalloproteinase 9 in epileptogenesis. *J Cell Biol*, *180*(5), 1021-1035. doi:10.1083/jcb.200708213
- Wilmshurst, P. T., Byrne, J. C., & Webb-Peploe, M. M. (1989). Relation between interatrial shunts and decompression sickness in divers. *Lancet*, *2*(8675), 1302-1306.
- Wilson, B. K., & Hess, E. J. (2013). Animal models for dystonia. *Mov Disord*, *28*(7), 982-989. doi:10.1002/mds.25526
- Wooten, G. F., Currie, L. J., Bovbjerg, V. E., Lee, J. K., & Patrie, J. (2004). Are men at greater risk for Parkinson's disease than women? *J Neurol Neurosurg Psychiatry*, *75*(4), 637-639.
- Xiong, J., Peng, J., Duan, H. L., Chen, C., Wang, X. L., Chen, S. M., & Yin, F. (2018). [Recurrent convulsion and pulmonary infection complicated by psychomotor retardation in an infant]. *Zhongguo Dang Dai Er Ke Za Zhi*, *20*(2), 154-157.
- Yilmaz, S., Turhan, T., Ceylaner, S., Gokben, S., Tekgul, H., & Serdaroglu, G. (2016). Excellent response to deep brain stimulation in a young girl with GNAO1-related progressive choreoathetosis. *Childs Nerv Syst*, *32*(9), 1567-1568. doi:10.1007/s00381-016-3139-6
- Zhang, Q., Pacheco, M. A., & Doupnik, C. A. (2002). Gating properties of GIRK channels activated by Galpha(o)- and Galpha(i)-coupled muscarinic m2 receptors in

Xenopus oocytes: the role of receptor precoupling in RGS modulation. *J Physiol*, 545(Pt 2), 355-373.

Zhu, X., Petrovski, S., Xie, P., Ruzzo, E. K., Lu, Y. F., McSweeney, K. M., . . . Goldstein, D. B. (2015). Whole-exome sequencing in undiagnosed genetic diseases: interpreting 119 trios. *Genet Med*, 17(10), 774-781. doi:10.1038/gim.2014.191

**CHAPTER 4: MICE WITH *GNAO1*-ASSOCIATED MOVEMENT DISORDER EXHIBIT
REDUCED INHIBITORY SYNAPTIC INPUT TO CEREBELLAR PURKINJE CELLS**

Yukun, Y. did the recording for Figure S4.4 A-H.

4.1 Abstract

GNAO1 encodes a heterotrimeric G protein subunit, $G\alpha_o$, which belongs to the $G_{i/o}$ family. Mutations in *GNAO1* are associated with both early infantile epileptic encephalopathy 17 (EIEE17) and neurodevelopmental disorder with involuntary movement (NEDIM). Our previous finding showed that gain-of-function (GOF) or normal-function (NF) *GNAO1* mutations, characterized by their inhibition of cAMP production, are associated with movement disorder patients (Chapter 2) (Feng et al., 2017). The majority of these patients present early onset dystonia or chorea/athetosis, hypotonia, and developmental delay. Although NEDIM patients have been treated with numerous available drugs, few proved to be effective. The pathological mechanisms of this disorder also remain unclear. In this chapter, I provide the first data elucidating neural mechanisms of a human *GNAO1* mutant by investigating electrophysiological effects in *Gnao1*^{+/*G203R*} mice, a *Gnao1*-associated movement disorder mouse model. These mice carry one of the most prevalent *GNAO1* GOF mutations, G203R.

Patch clamp studies of cerebellar Purkinje cells showed significantly lower frequencies of both action potential (AP) related (sIPSCs) and non AP-related (mIPSCs) GABAergic responses in G203R mice. Amplitudes were not affected. $G\alpha_o$ inhibitors reversed this reduction in inhibition significantly, and eliminated the difference between WT and G203R mice. Furthermore, $G\alpha_o$ -coupled α_{2A} adrenergic receptors played a critical role in reducing the sIPSCs while mIPSCs events were regulated by $GABA_B$

receptors. The results prove G203R to be a *bona fide* GOF mutation in an *in vivo* context, supporting our proposed mechanistic genotype-phenotype correlation of *GNAO1*-associated neurological disorders. Also, the identification of receptors that regulate both mIPSCs and sIPSCs should facilitate the discovery of new drugs or drug repurposing for *GNAO1*-associated disorders.

4.2 Introduction

GNAO1 encodes the α subunit of a heterotrimeric G protein, G_{α_o} , which is the most abundant membrane protein in mammalian central nervous system. It participates in multiple neural signaling pathways (Jiang & Bajpayee, 2009). Mutations in *GNAO1* were first found in early onset epileptic encephalopathy (EIEE17). However, since 2016, there have been a growing number of reports on *GNAO1* mutation-associated movement disorders with/without seizures. This disorder was officially categorized by OMIM (Online Mendelian Inheritance in Man) in 2017 as neurodevelopmental disorder with involuntary movements (NEDIM). *GNAO1*-associated NEDIM is a rare neurogenetic disorder, characterized by early onset of hypotonia, movement disorder and developmental delay. Although numerous available drug treatments were tested on NEDIM patients, few proved to be effective (Feng, Khalil, Neubig, & Sidiropoulos, 2018). The pathological mechanisms of this disorder also remained unclear.

The G_{α_o} protein functions as a messenger for a broad range of signaling pathways. They include inhibition of cAMP (Levitt, Purington, & Traynor, 2011; Sunahara & Taussig,

2002), inhibition of high-voltage-gated calcium channels (N- and P/Q-type calcium channels) (Ikeda, 1996), and activation of G-protein regulated inward rectifying potassium (GIRK) channels (Zhang, Dickson, & Doupnik, 2004). Our lab has previously established a genotype-phenotype correlation of *GNAO1*-associated neurological disorders based on $G\alpha_o$'s canonical pathway of inhibiting cAMP production (Feng et al., 2017). We proposed that loss-of-function (LOF) and partial-loss-of-function (PLOF) *GNAO1* mutations are found in epilepsy patients, while the gain-of-function (GOF) and normal-function (NF) mutations are generally found in movement disorder patients (Feng et al., 2017). We have also generated a novel animal model with a knock-in GOF mutation G203R (Feng et al., 2019). Similar to human patients with *GNAO1* G203R mutation, this animal model exhibited movement abnormalities in a battery of behavioral assessment including RotaRod, grip strength, and DigiGait (Chapter 3) (Feng et al., 2019). Unlike most GOF *GNAO1* mutations, patients with the G203R mutant allele also exhibit early-onset epilepsy (Arya, Spaeth, Gilbert, Leach, & Holland, 2017; Feng et al., 2019; Kelly et al., 2019; Nakamura et al., 2013; Saitsu et al., 2016; Schorling et al., 2017; Xiong et al., 2018), validating the relevance of this animal model, which also showed an increased sensitivity to pentylentetrazole (PTZ) kindling.

Although the G203R animal model mimics the symptoms of human G203R patients, the mechanisms by which these mice develop their movement disorder are still unclear. Also, the GOF nature of the G203R mutation in a physiological environment has only

been demonstrated for cAMP regulation in HEK293T cells. It is critical to know if $G\alpha_o$ G203R also has GOF behavior in neurons. To answer these questions, I performed patch clamp studies of Purkinje cells in cerebellar slices of WT and *Gnao1*^{+G203R} mutant mice. The cerebellum has long been known for its critical regulation of motor coordination. The evidence for a role in dystonia has begun to emerge. Deficiency in cerebellar motor control may manifest as inaccuracies of visual guided movement, speeded complex movement, loss of muscle tone, abnormal timing, and loss of prediction and coordination (Gowen & Miall, 2007). Clinically, these features are characterized as dysmetria (inaccurate movement), dysdiadochokinesis (inability to execute rapidly alternating movements), hypotonia (reduced muscle tone), and dyscoordination or ataxia (inability to perform smoothly coordinated voluntary movement) (Gowen & Miall, 2007). Structural and/or functional abnormalities of the cerebellum are also associated with dystonia (Bologna & Berardelli, 2018) and chorea (Walker, 2016). Several reports elucidated the role of cerebellum in DYT1 hereditary dystonia (Fremont, Tewari, Angueyra, & Khodakhah, 2017; Song, Bernhard, Hess, & Jinnah, 2014; Vanni et al., 2015). Interestingly, dystonia and chorea/athetosis are the most commonly seen involuntary movements in patients with the G203R mutation (Arya et al., 2017; Kelly et al., 2019; Nakamura et al., 2013; Saitsu et al., 2016; Schorling et al., 2017). Structurally, a core cerebellar circuit mediates all of its function (Eccles, 1967; Reeber, Otis, & Sillitoe, 2013). This circuit centers on Purkinje cells, which are the sole output of the cerebellar

cortex (Brown et al., 2019). Purkinje cells receive input from several classes of interneurons. Granule cells project parallel fibers that send excitatory signals to Purkinje cells (Barbour, 1993; Eccles, Llinas, & Sasaki, 1966a, 1966b; Konnerth, Llano, & Armstrong, 1990), while basket cells and stellate cells send inhibitory input to Purkinje cell (Cesana et al., 2013; Hull & Regehr, 2012).

In this chapter, I report data on patch clamp recordings of the Purkinje cells in cerebellar slices. I found a decreased frequency in both sIPSC and mIPSC events in G203R mutant mice. A likely mechanism underlying this reduction in frequency is enhanced signaling by the mutant $G\alpha_o$ to mediate presynaptic inhibition of GABA release. Different receptors serve as the driving force for this inhibition. $GABA_B$ receptor-activated $G\alpha_o$ mediates non-AP related mIPSCs while α_{2A} adrenergic receptors stimulate AP mediated sIPSCs. Although $G\alpha_o$ -mediated inhibition of high-voltage activated (N, P/Q-type) calcium channels is well-studied (Ikeda, 1996), only α_{2A} adrenergic receptor-mediated sIPSCs function through the activation of membrane-located, voltage-gated calcium channels. $GABA_B$ receptor mediated inhibition of mIPSCs is likely to involve $G\beta\gamma$ -mediated direct inhibition of synaptic vesicle release (Feng et al., 2018; Zurawski et al., 2017; Zurawski, Rodriguez, Hyde, Alford, & Hamm, 2016).

4.3 Materials and Methods

4.3.1 Tissue preparation and solutions

All animal procedures complied with the National Institutes of Health of the USA

guidelines on animal care and were approved by Michigan State University Institutional Animal Use and Care Committee. Animal used for this chapter were between 5 to 10 weeks old. Only male animals were used due to the sex difference we have observed in our previous study (Chapter 3) (Feng et al., 2019). Mice were sacrificed by direct cervical dislocation and cerebellums were dissected and quickly mounted on a Vibrotome™ 1000 machine (Leica, Wetzlar, Germany). Sagittal cerebellar slices (250 µm) were prepared according to methods previously described by Yuan Y et al (Yuan & Atchison, 1999, 2003, 2007, 2016). Briefly, the cerebellums were transferred into a chilled oxygenated sucrose-based slicing solution and parasagittal cerebellar slices (250 µm thick) were cut using the Vibrotome™ 1000 machine (Leica, Wetzlar, Germany). The slicing solution contains (in mM): 125, NaCl; 2.5, KCl; 4, MgCl₂; 1.25, KH₂PO₄; 26, NaHCO₃; 0.5, CaCl₂ and 25, D-glucose (pH 7.35–7.4 when saturated with 95% O₂ /5% CO₂ at room temperature of 22–25°C). Slices were incubated in the pre-chilled and oxygenated slicing solution for 15 min, and then transferred into standard artificial cerebrospinal fluid (ACSF) solution at room temperature for 30 min. The standard ACSF contains: 125, NaCl; 2.5, KCl; 1, MgCl₂; 1.25, KH₂PO₄; 26, NaHCO₃; 2, CaCl₂ and 20, D-glucose (pH 7.35–7.4 saturated with 95% O₂/5% CO₂ at room temperature).

4.3.2 Electrophysiological recording

Whole-cell patch clamp recording methods were detailed in previous publications (Yuan & Atchison, 1999, 2003, 2007, 2016). Slices were placed in a recording chamber

and perfused with standard ACSF bubbled with 95% O₂/5% CO₂. Individual neurons were visualized with a Nomarski 40X water immersion lens with infrared differential interference contrast optics using a Nikon E600FN upright microscope. Recording electrodes were fire polished and had a resistance of 3–7 MΩ when filled with pipette solution. For recording sIPSCs and mIPSCs, the pipette solution consisted of (in mM) 140, CsCl; 0.4, GTP; 2, Mg-ATP; 0.5, CaCl₂; 5, Phosphocreatine Na₂; 5, EGTA-CsOH; 10, HEPES (pH 7.3 adjusted with CsOH). For recording sEPSCs and mEPSCs, the pipette solution consisted of (in mM) 140, K-Gluconate; 0.4, GTP; 2, Mg-ATP; 0.5, CaCl₂; 5, Phosphocreatine Na₂; 5, EGTA-CsOH; 10, HEPES (pH 7.3 adjusted with KOH). The holding potential was –70 mV for recording of both IPSCs and EPSCs. For recording inhibitory currents, 6-Cyano-7-nitroquinoxaline-2,3-dione (CNQX, 10 μM) and amino-5-phosphonopentanoic acid (APV, 100 μM) were added to the external solution to block glutamate receptor-mediated sEPSCs. For recordings of miniature IPSCs (mIPSCs), 0.5 μM tetrodotoxin (TTX) was added to the external solution in addition to CNQX and APV. For recording sEPSCs, bicuculline (10 μM) was added to the external solution to block GABAergic receptor-mediated sIPSCs. For recording of miniature EPSCs (mEPSCs), the external solution was supplemented with 0.5 μM TTX in addition to bicuculline. Whole cell currents were filtered at 2–5 kHz with an 8-pole low-pass Bessel filter and digitized at 10–20 kHz for later off-line analysis using the pClamp 9.0

program (Molecular Devices, Inc., Sunnyvale, CA). All experiments were carried out at room temperature of 22–25°C.

4.3.3 Pharmacology

The following agents were used: CNQX disodium salts (Sigma-Aldrich, St. Louis, MO), DL-2-Amino-5-phosphono-pentanoic (APV) acid solid (Sigma-Aldrich, St. Louis, MO), tetrodotoxin (TTX) (Tocris, Bristol, UK), pertussis toxin (PTX) (List Biological Laboratories, Campbell, CA), baclofen (Sigma-Aldrich, St. Louis, MO), N-ethylmaleimide (NEM) (Sigma-Aldrich, St. Louis, MO), UK14,304 (Sigma-Aldrich, St. Louis, MO), CGP36216 (hydrochloride) (Cayman Chemical, Ann Arbor, MI), BRL44408 (Sigma-Aldrich, St. Louis, MO), cadmium chloride (Sigma-Aldrich, St. Louis, MO). All drugs were made up as 1000 x concentrated stock solutions in distilled water, aliquoted and stored at ~20°C. Aliquots were thawed and dissolved in oxygenated ACSF immediately prior to use.

4.3.4 SDS Page and Western Blots

Male mice (6-8 weeks old) were sacrificed and their brains were dissected into different regions and flash-frozen in liquid nitrogen. For Western Blot analysis, tissues were thawed on ice and homogenized for 5 min with 0.5 mm zirconium beads in a Bullet Blender (Next Advance; Troy, NY) in RIPA buffer (20mM Tris-HCl, pH7.4, 150mM NaCl, 1mM EDTA, 1mM β -glycerophosphate, 1% Triton X-100 and 0.1% SDS) with a protease inhibitor cocktail (Roche/1 tablet in 10 mL RIPA). Homogenates were centrifuged for 5

min at 4°C at 13,000 G. Supernatants were collected and protein concentrations determined using the bicinchoninic acid method (BCA method; Pierce; Rockford, IL). Protein concentration was normalized for all tissues with RIPA buffer and 2x SDS sample buffer containing β -mercaptoethanol (Sigma-Aldrich, St. Louis, MO) was added. Thirty μ g of protein was loaded onto a 12% Bis-Tris gel (homemade), and samples were separated for 1.5 hrs at 160V. Proteins were then transferred to an Immobilon-FL PVDF membrane (Millipore, Billerica, MA) on ice either for 2 h at 100 V, 400 mA or overnight at 30 V, 50 mA. Immediately after transfer, PDVF membranes were washed and blocked in Odyssey PBS blocking buffer (Li-Cor, Lincoln, NE) for 40 min at RT. The membranes were then incubated with anti-G α_o (rabbit; 1:1,000; sc-387; Santa Cruz biotechnologies, Santa Cruz, CA) or anti-G β (recommended for detection of G β_1 , G β_2 , G β_3 and G β_4 ; mouse; 1:1000; sc-378; Santa Cruz biotechnologies, Santa Cruz, CA) and anti-actin (goat; 1:1,000; sc-1615; Santa Cruz) antibodies diluted in Odyssey blocking buffer with 0.1% Tween-20 overnight at 4°C. Following four 5-min washes in phosphate-buffered saline with 0.1 % Tween-20 (PBS-T), the membrane was incubated for 1 hr at room temperature with secondary antibodies (1:10,000; IRDye® 800CW Donkey anti-rabbit; IRDye® 800CW Donkey anti-mouse; IRDye® 680RD Donkey anti-goat; LI-COR Biosciences) diluted in Odyssey blocking buffer with 0.1 % Tween-20. The membrane was subjected to four 5-min washes in PBS-T and a final rinse in PBS for 5 minutes. The membrane was kept in the dark and the infrared signals at 680 and 800nm were

detected with an Odyssey Fc image system (LI-COR Biosciences). The $G\alpha_o$ polyclonal antibody recognizes an epitope located between positions 90-140 of the $G\alpha_o$ protein (Santa Cruz, personal communication).

4.3.5 Statistical Analysis

Electrophysiological data analysis was performed as described previously (Yuan & Atchison, 1999, 2003, 2007, 2016). The individual performing the analysis was blinded to the genotype of the sample until all results were recorded. In brief, spontaneous synaptic currents were first screened automatically using MiniAnalysis software (Synaptosoft Inc., Decatur, GA) with a set of pre-specified parameters. They were accepted or rejected manually with an event detection amplitude threshold at 5 pA for sIPSCs/mIPSCs and 3pA for sEPSCs/mEPSCs as well as the kinetic properties (fast rising phase and slow decay phase) of the spontaneous events. Unless otherwise specified, synaptic events per cell collected over a 2-min period were averaged to calculate the frequency and amplitude of spontaneous synaptic currents. Amplitudes of currents were measured after subtraction of the baseline noise. MiniAnalysis-derived results were plotted in GraphPad Prism (GraphPad; LaJolla, CA). Results from more than one neuron from a single animal were averaged prior to statistical analysis. Some graphs, when indicated, do show points for each individual neuron while bar graphs and error bars are calculated from the per animal data. Data are presented as mean value \pm SEM, where n=number of animals.

Statistical significance was determined using unpaired Student's t-test unless stated otherwise. A p value < 0.05 was deemed as significant.

Quantification of infrared (IR) Western blot signals was performed using Image Studio Lite (LI-COR Biosciences). Individual bands were normalized to the corresponding actin signals, and WT $G\alpha_o$ was set as control for each blot. All data were analyzed using GraphPad Prism 7.0 (GraphPad; LaJolla, CA).

4.4 Results

Purkinje cells mediate the entire output of the cerebellar cortex; therefore any mechanisms able to modulate the firing pattern of Purkinje cells will influence cerebellar function. Purkinje cells fire spontaneously, even in the absence of glutamate input, and the pattern of firing is strongly influenced by GABAergic input. At least under experiment conditions, two types of inhibitory interneurons, the basket cells and the stellate cells largely convey this inhibitory input onto the Purkinje cells (Donato et al., 2008). Presynaptic neurotransmitter release is strongly regulated by G-protein-coupled receptors (GPCRs). Many GPCRs in the central nervous system are coupled to the $G\alpha_o$ protein, which belongs to the $G\alpha_{i/o}$ family. The activation of $G\alpha_o$ protein by GPCRs leads to the inhibition of voltage-gated calcium channels, inhibition of cAMP production, activation of G-protein coupled inward rectifying potassium channels (GIRKs) and also inhibition of synaptic vesicle release, all of which can be possible mechanisms of GPCRs-mediated inhibition of GABA release.

4.4.1 Presynaptic GABA release is suppressed in the cerebellar Purkinje cells of *Gnao1*^{+/-G203R} mice

Baseline recording of sIPSCs, which are due to AP-dependent GABA release, was isolated by adding 10 μ M CNQX and 100 μ M AP-V in standard ACSF. Interestingly, CNQX and AP-V significantly increased IPSC events in Purkinje cells (data not shown), which is consistent with previous observations (Brickley, Farrant, Swanson, & Cull-Candy, 2001). There is a significant decrease in sIPSC frequency in G203R mice comparing to that of their WT sibling (WT: 21.0 ± 1.7 Hz; G203R: 12.7 ± 2.5 Hz; Figure 4.1C & 4.1D), but no difference is detected in sIPSC amplitude (WT: 41.8 ± 8.5 pA; G203R: 36.7 ± 7.4 pA; Figure 4.1E & 4.1F). Data were recorded from 25 cells of 13 mice for WT and 21 cells from 9 mice for G203R.

mIPSCs, which are due to AP-independent GABA release in the Purkinje cells were investigated by the additional application of 0.5 μ M TTX. As reported previously in cerebellar Purkinje cells, TTX reduced mean IPSC frequency and amplitude to isolate mIPSCs (Bardo, Robertson, & Stephens, 2002; Boxall, 2000; Harvey & Stephens, 2004; Yuan & Atchison, 2003). Slices from G203R mice exhibited a marked reduction in mIPSC frequency compared to that of WT mice (Figure 4.1G - 4.1L). The effect on mIPSC frequency was greater than that on sIPSCs (75% vs 40% decrease). Data were recorded from 25 cells of 13 mice for WT and 21 cells from 9 mice for G203R.

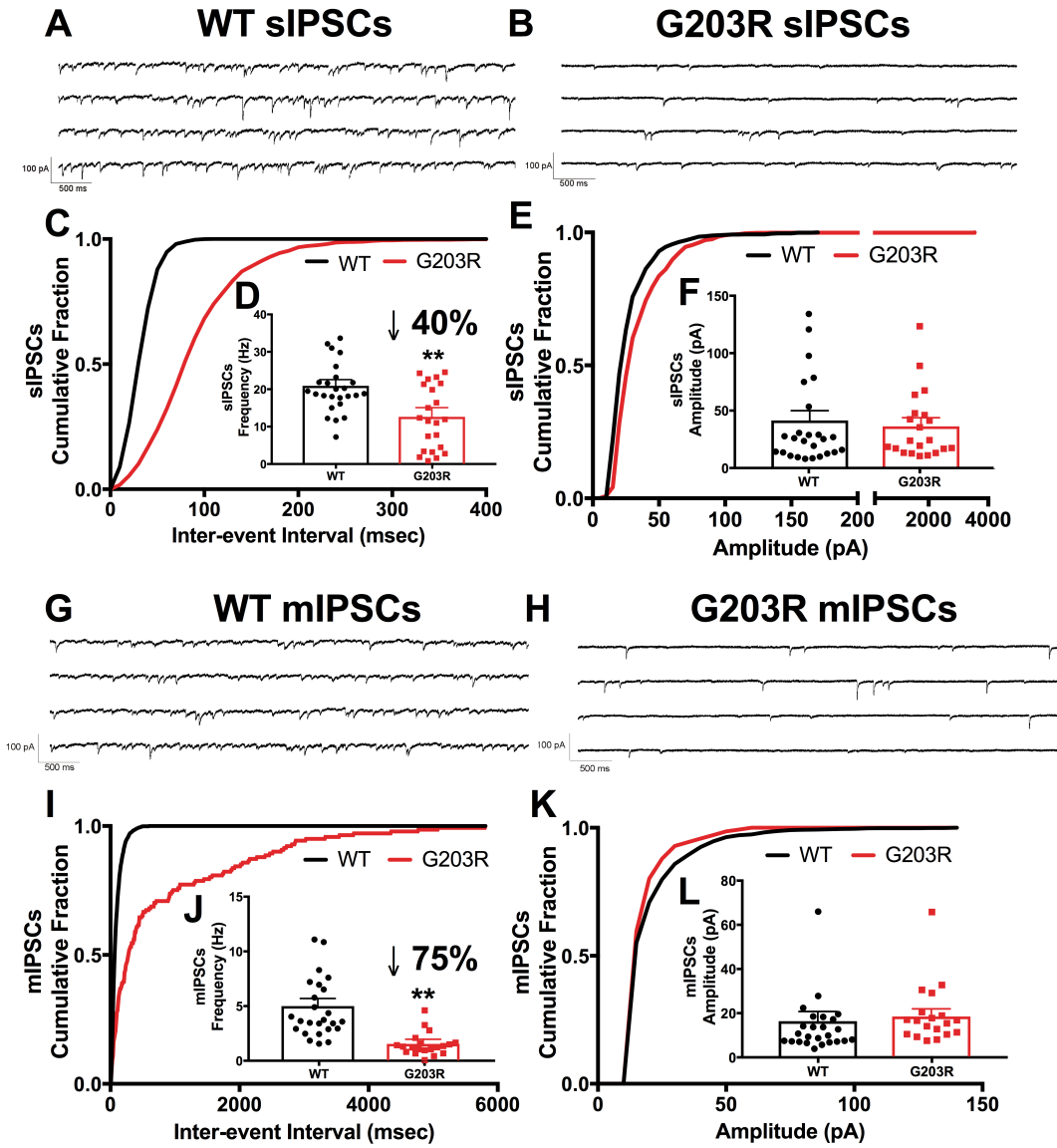


Figure 4.1 Cerebellar Purkinje cells in brain slices from 4-6 week-old G203R mice display reduced GABAergic spontaneous synaptic currents (sIPSCs) and reduced miniature synaptic currents (mIPSCs). (A, B) Representative recording of spontaneous inhibitory postsynaptic currents in a cerebellar Purkinje cell from a 4 week-old mouse in the presence of 10 μ M of CNQX and 100 μ M of AP-V at a holding potential of -70 mV. (C, D) G203R mice showed a decrease in the frequency of sIPSCs. (E, F) No significant difference is observed in the amplitude of sIPSCs between WT and G203R mice. Unpaired Student's t-test; **p=0.0086 WT (n=13 mice), G203R (n=9 mice). (G, H) Representative recording of spontaneous miniature inhibitory postsynaptic currents in a cerebellar Purkinje cell from a 4 week-old mouse in the presence of 10 μ M

Figure 4.1 (cont'd) of CNQX, 100 μ M of AP-V and 0.5 μ M TTX at a holding potential of -70mV. (I, J) G203R mice showed a decrease in the frequency of mIPSCs. (K, L) No significant difference is observed in the amplitude of mIPSCs between WT and G203R mice. Unpaired Student's t-test; **p=0.0011; WT (n=13 mice), G203R (n=9 mice). Recordings from each cell are shown as a data point but the bar graph, error bars, and statistical analysis was averaged data per animal.

4.4.2 $G\alpha_o$ blockers can reverse the enhanced inhibition of mIPSC frequency in G203R mice

To investigate whether the reduced frequency of sIPSCs and mIPSCs is due to an enhanced signaling by the G203R mutant $G\alpha_o$, we examined the effect of sulphydryl alkylating agent NEM, which uncouples pertussis toxin-sensitive $G\alpha_{i/o}$ subunits from receptors by modifying cysteine residues (Aktories, Schultz, & Jakobs, 1982). Similar to the effects of NEM on GABAergic mIPSCs in other brain slice preparations, 50 μ M NEM significantly increased the frequency of mIPSCs in both WT and G203R cerebellar slices (WT: from 4.19 ± 0.57 Hz to 22.3 ± 0.4 Hz; G203R: from 1.52 ± 0.35 Hz to 20.8 ± 1.4 Hz; Figure 4.2D & 4.2G) but did not affect the amplitude (WT: 11.1 ± 1.7 pA to 19.1 ± 3.1 pA; G203R: 16.0 ± 1.9 pA to 30.8 ± 5.5 pA; Figure 4.2F & 4.2H). Also, NEM eliminated the difference in the mIPSC frequency between WT and G203R mice (WT: 22.3 ± 0.4 Hz; G203R: 20.8 ± 1.4 Hz; Figure 4.2D & 4.2F).

Considering that NEM is not a selective $G\alpha_o$ protein blocker, we also examined the effects of PTX incubation on the AP-dependent and AP-independent IPSCs in cerebellar

Purkinje cells. PTX catalyzes the ADP-ribosylation of the α subunit of the heterotrimeric $G_{i/o}$ family, thereby preventing the G proteins from interacting with GPCRs (Mangmool & Kurose, 2011). All slices in this study were subject to incubation in 1 μ g/mL PTX for more than 6 hours before recording. To maintain comparable conditions to compare data with and without PTX, separate slices were used as control so that both groups underwent the 6-hour incubation. PTX incubation significantly increased the mIPSC frequency in slices from G203R mice but had no effects on WT mice (WT: 4.10 ± 0.70 Hz to 3.40 ± 0.68 Hz; G203R: 1.31 ± 0.16 Hz to 2.29 ± 0.30 Hz; Figure 4.3C & 4.3G). The amplitude of mIPSCs was not changed in either WT or G203R mice after PTX incubation (WT: 12.1 ± 1.6 pA to 9.7 ± 1.4 pA, G203R: 19.6 ± 1.6 pA to 15.8 ± 2.9 pA; Figure 4.3D & 4.3H). In contrast to mIPSCs, sIPSC frequency was not significantly affected by PTX in either WT or G203R mice (Frequency: WT: 13.8 ± 1.7 Hz to 10.9 ± 3.6 Hz; G203R: 9.1 ± 1.4 Hz to 12.5 ± 2.3 Hz; Amplitude: WT: 18.9 ± 3.4 pA to 19.2 ± 8.9 pA; G203R: 29.2 ± 4.1 pA to 24.4 ± 4.5 pA; Figure 4.3E-4.3F, 4.3I-4.3J).

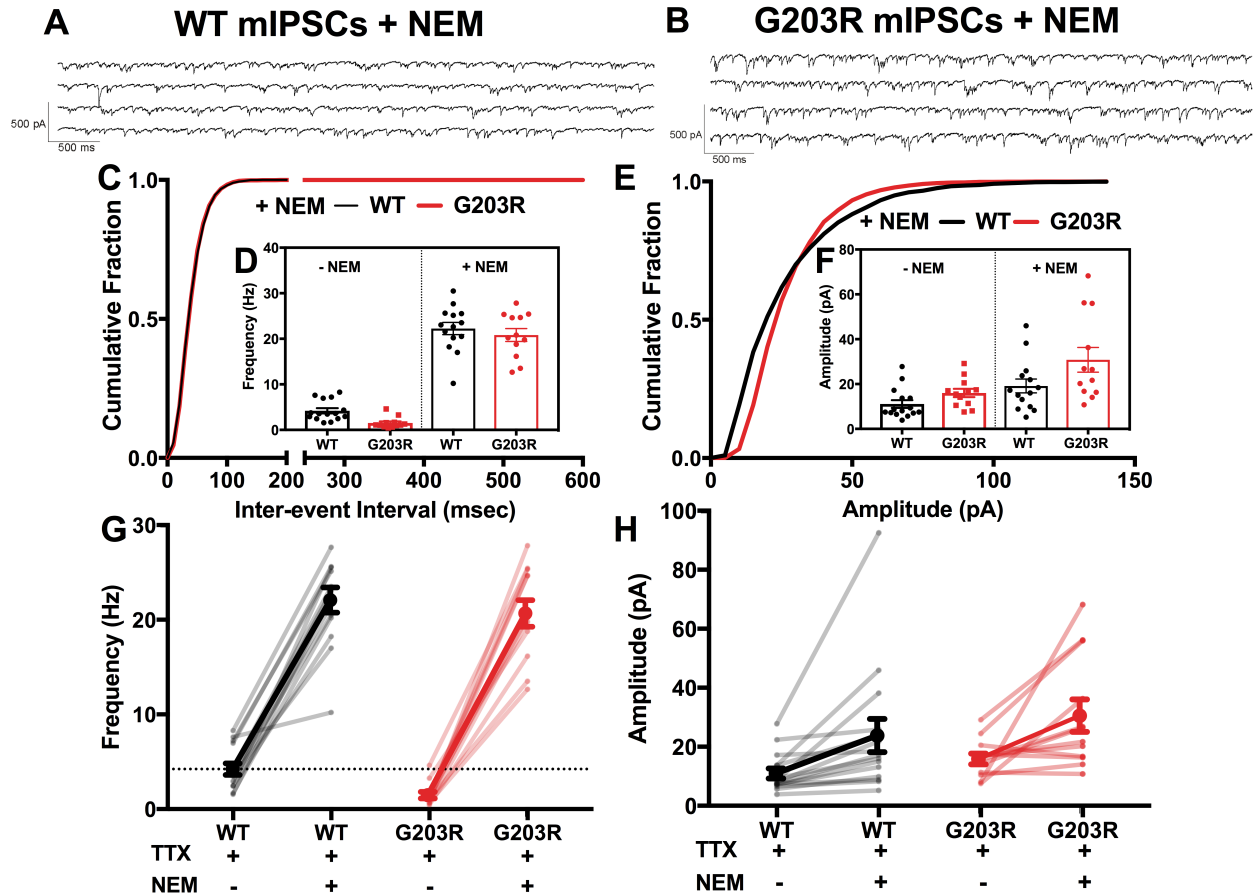


Figure 4.2 The frequencies of mIPSCs were sensitive to NEM, an inhibitor of $G\alpha_{i/o}$ proteins. (A, B) Representative recordings showing mIPSCs traces in (A) WT and (B) G203R mice with the presence of 50 μ M NEM. (C, D) NEM eliminated the difference in mIPSC frequency between WT and G203R. (E, F) No significant difference was observed in amplitude of mIPSCs after adding NEM. (G) NEM significantly increased the frequency of mIPSCs, (H) but with minor influence in the amplitude of mIPSCs. Unpaired Student's t-test; WT (n=8 mice), G203R (n=7 mice).

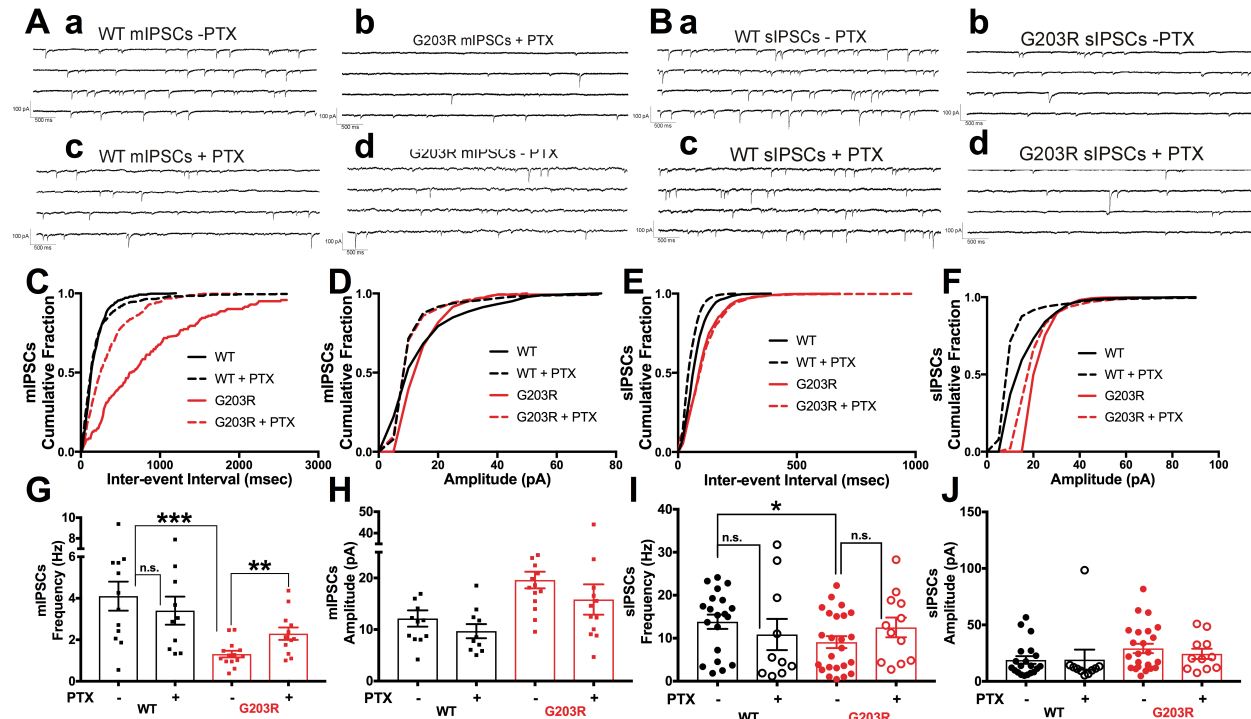


Figure 4.3 A selective inhibitor of $G_{i/o}$, pertussis toxin (PTX), increased the frequency of mIPSCs in G203R but not WT mice. Slices were incubated in 1 μ M/ml of PTX for >6 hrs pre-recording. Representative traces showed the example recordings of (A) mIPSCs and (B) sIPSCs in WT and G203R mice before and after PTX incubation. (C, G) PTX incubation significantly relieved the G_0 mediated inhibition of mIPSC frequency in G203R mice, but not WT mice. Unpaired Student's t-test; WT (n=5 mice), G203R (N=6 mice); **p=0.006. (D, H) PTX did not change the mIPSC amplitude of either G203R or WT mice. Neither frequency (E, I) nor amplitude (F, J) of sIPSCs was affected by PTX incubation. Unpaired Student's t-test; WT (n=5 mice), G203R (n=6 mice); *p=0.03 between WT vs. G203R mice without PTX incubation. Results between WT and G203R were not significant.

4.4.3 Presynaptic glutamate release is not affected by the G203R mutation in $G\alpha_o$ protein

Purkinje cells receive glutamatergic inputs at their extremely elaborated dendrites from parallel fibers at the molecular layer of the cerebellar cortex and send GABA outputs to the deep nuclei (Tian & Zhu, 2018). To investigate whether the GOF mutation G203R also affects excitatory inputs on Purkinje cells, we recorded sEPSCs and mEPSCs from Purkinje cells. The AP-dependent excitatory postsynaptic currents (sEPSCs) were isolated with 10 μ M bicuculline and AP-independent mEPSCs were recorded with the addition of 0.5 μ M TTX. Although the GOF $G\alpha_o$ protein significantly decreased sIPSCs and mIPSCs frequency, EPSCs are not seemingly affected by the G203R mutation in $G\alpha_o$. Neither frequency nor amplitude of sEPSCs and mEPSCs showed significant differences between WT and G203R slices (Figure 4.4; sEPSC frequency: WT: 1.50 ± 0.20 Hz vs. G203R: 1.36 ± 0.43 Hz; sEPSC amplitude: WT: 7.52 ± 0.92 pA vs. G203R: 6.42 ± 0.50 pA; mEPSC frequency: WT: 1.05 ± 0.16 Hz vs. G203R: 0.99 ± 0.46 Hz; mEPSC amplitude: WT: 6.39 ± 0.91 pA; G203R: 6.24 ± 0.60 pA).

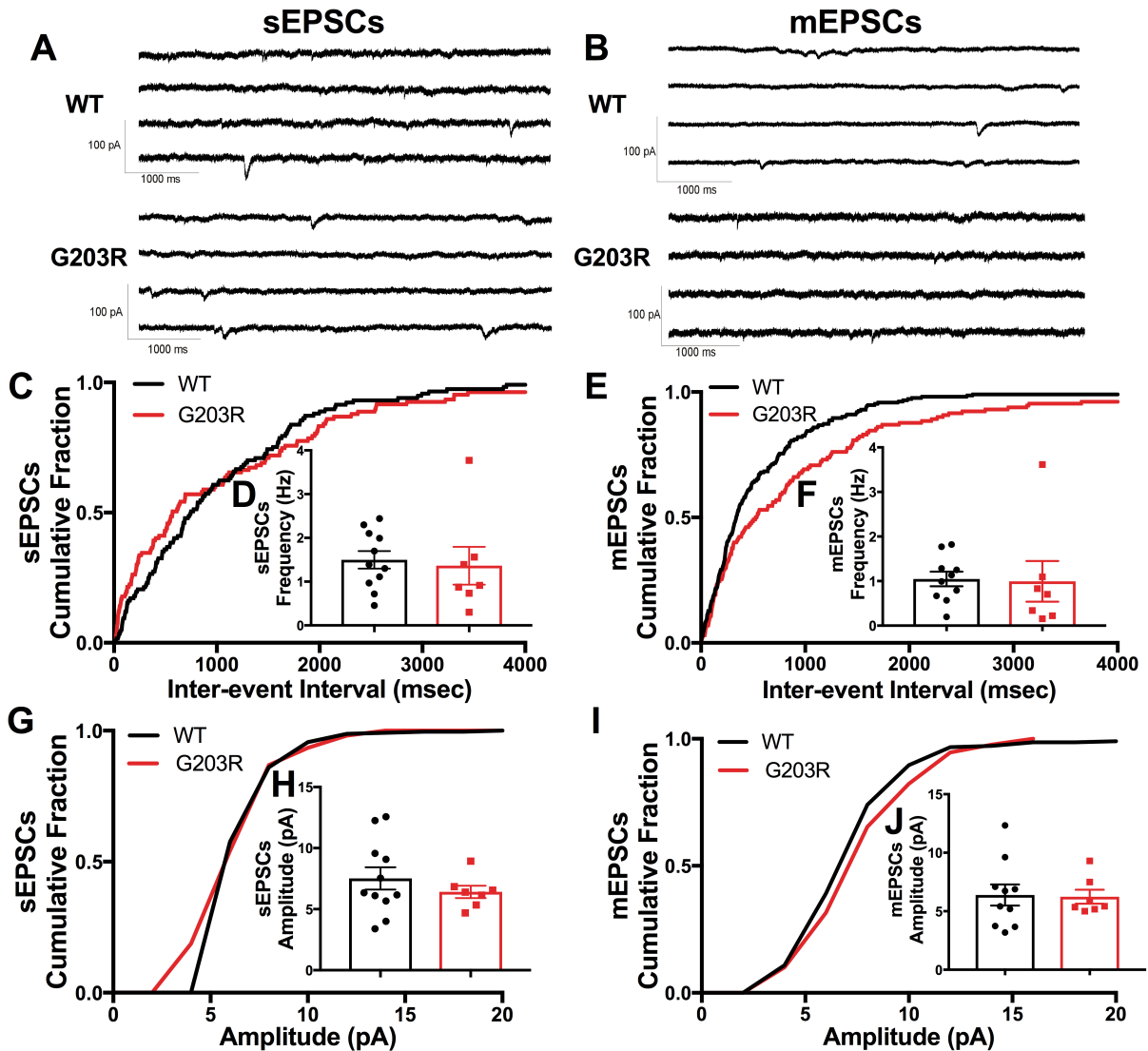


Figure 4.4 G203R mutant slices show no difference in either spontaneous excitatory postsynaptic currents (sEPSCs) or miniature excitatory postsynaptic currents (mEPSCs). (A) sEPSCs were recorded from Purkinje cells at a holding potential of -70mV in the presence of 10 μ M bicuculline. (B) 0.5 μ M TTX was then added to the bath in order to record mEPSCs. (C, D & G, H) No significant difference in either frequency or amplitude was observed between WT and G203R. (E, F & I, J) No significant difference between WT and G203R was observed in mEPSCs either. Unpaired Student's t-test; WT (n=5), G203R (n=5).

4.4.4 Effects of G-protein coupled GABA_B receptors on AP-independent GABA release onto Purkinje cells

The effects of baclofen on AP-independent mIPSCs, isolated by the application of 0.5 μ M TTX, were investigated. After recording baseline mIPSCs, baclofen (10 μ M) was applied to the bath. Baclofen caused a clear reduction in mean mIPSC frequency in slices from both WT (from 5.47 ± 0.80 Hz to 1.19 ± 0.25 Hz, 78% inhibition) and G203R mice (from 1.24 ± 0.20 Hz to 0.65 ± 0.11 Hz, 48% inhibition). Baclofen was typically applied for 4 to 8 min in this and subsequent experiments. After baclofen application, the difference in mIPSC frequency still remains between WT (1.19 ± 0.25 Hz) and G203R (0.65 ± 0.11 Hz) mice (Figure 4.5C & 4.5E). This suggests a role of GABA_B receptors in regulating AP-independent GABA release. Mean mIPSC amplitude was unchanged by baclofen (Figure 4.5F; WT: 12.8 ± 2.3 pA to 13.6 ± 4.3 pA; G203R: 17.8 ± 1.9 pA to 17.3 ± 1.6 pA) (Figure 4.5D). Interestingly, the application baclofen did not affect either frequency or amplitude of sIPSCs (Figure S4.2), suggesting that GABA_B receptors do not regulate the AP-dependent inhibitory neurotransmitter release.

To confirm that G α_o causes the baclofen-induced inhibition of mIPSC frequency as previously reported (Harvey & Stephens, 2004), PTX was used to block G α_o protein. The G α_o antagonist, 1 μ g/mL PTX eliminated baclofen-induced inhibition of mIPSC frequency (Figure 4.5I & 4.5K & 4.5M), while exhibiting no effects on mIPSC amplitude (Figure 4.5J, 4.5L, 4.5N). PTX increased mean mIPSC frequency from 1.31 ± 0.16 Hz to 2.29 ± 0.30

Hz in G203R mice but did not change that of the WT mice (non-PTX: 4.10 ± 0.70 Hz; PTX: 3.40 ± 0.68 Hz). These data are consistent with a presynaptic role of $G_{i/o}$ subunit in baclofen-induced inhibition of AP-independent GABA release onto Purkinje cells.

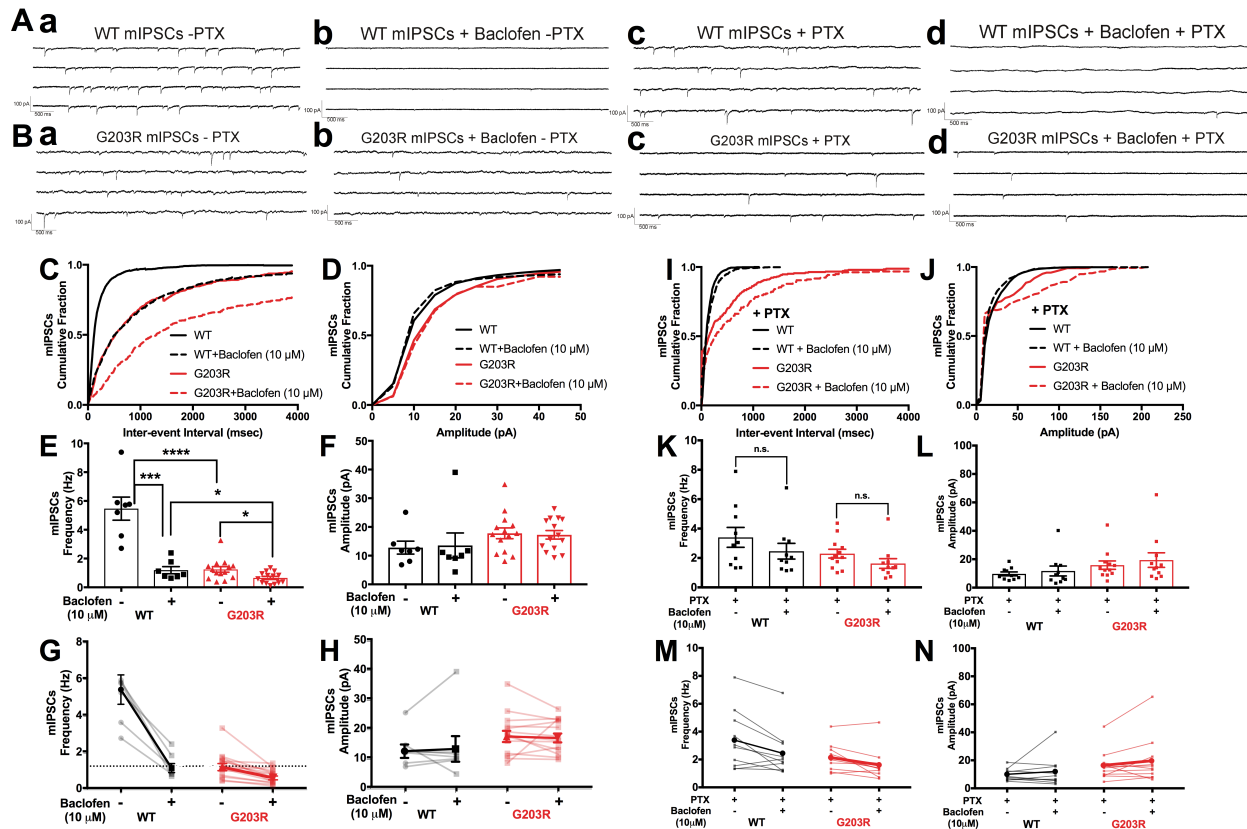


Figure 4.5 Activating $GABA_B$ receptor with baclofen reduces mIPSC frequency but not amplitude. PTX incubation eliminates baclofen-induced inhibition of mIPSC frequency in WT and G203R mice. Representative traces showing the reduced mIPSC responses before and after adding baclofen ($10 \mu\text{M}$) in WT (A) and G203R (B) mice w/o PTX or baclofen. (C, E, G) Baclofen significantly decreased the frequency of mIPSC and the difference between WT and G203R remains though baclofen was present. Unpaired Student's t-test; WT ($n=6$), G203R ($n=6$); **** $p<0.001$, *** $p=0.003$, * $p=0.029$ (WT vs. G203R), * $p=0.014$ (G203R w/o baclofen). (D, F, H) Amplitude remained unchanged regardless of the existence of baclofen. No significant change was observed in the (I, K,

Figure 4.5 (cont'd) M) frequency or the (J, L, N) amplitude of mIPSCs after adding baclofen in both WT and G203R mice. Unpaired Student's t-test; WT (n=5), G203R (n=6).

4.4.5 Effects of G-protein coupled α_{2A} adrenergic receptors on AP-dependent GABA release onto Purkinje cells

Adrenoceptors are divided into three subtypes, α_1 , α_2 , and β receptors, which are coupled to $G_{q/11}$, $G_{i/o}$ - and G_s -proteins respectively (Kobilka et al., 1987; O'Rourke, Iversen, Lomasney, & Bylund, 1994). Previous publications reported the dual regulation of AP-dependent GABA release modulated by both $G_{i/o}$ -coupled α_2 receptors and G_q -coupled α_1 receptors (Hirono & Obata, 2006). Here, we investigated whether $G_{i/o}$ -coupled α_2 receptors plays a role in regulating AP-dependent GABA release. We used a selective α_2 receptor agonist UK14,304 to confirm whether α_2 receptors drives the decrease in sIPSC frequency and whether G203R mutant enhanced this reduction in sIPSC frequency. We applied 10 μ M UK14,304 in bath perfusion. UK14,304 greatly inhibited AP-dependent GABAergic IPSC (sIPSC) frequencies of both WT (from 10.7 ± 2.6 Hz to 4.48 ± 1.65 Hz) and G203R (from 3.38 ± 0.99 Hz to 1.03 ± 0.14 Hz) mice (Figure 4.6C & 4.6E & 4.6G). Interestingly, a significant difference remained between WT and G203R mice in mIPSC frequency after the application of UK14,304 (Figure 4.6E; WT: 4.48 ± 1.65 Hz vs. G203R: 1.03 ± 0.14 Hz). Like baclofen, the amplitude of mIPSC was not affected by the application of UK14, 304 (Figure 4.6D & 4.6F & 4.6H).

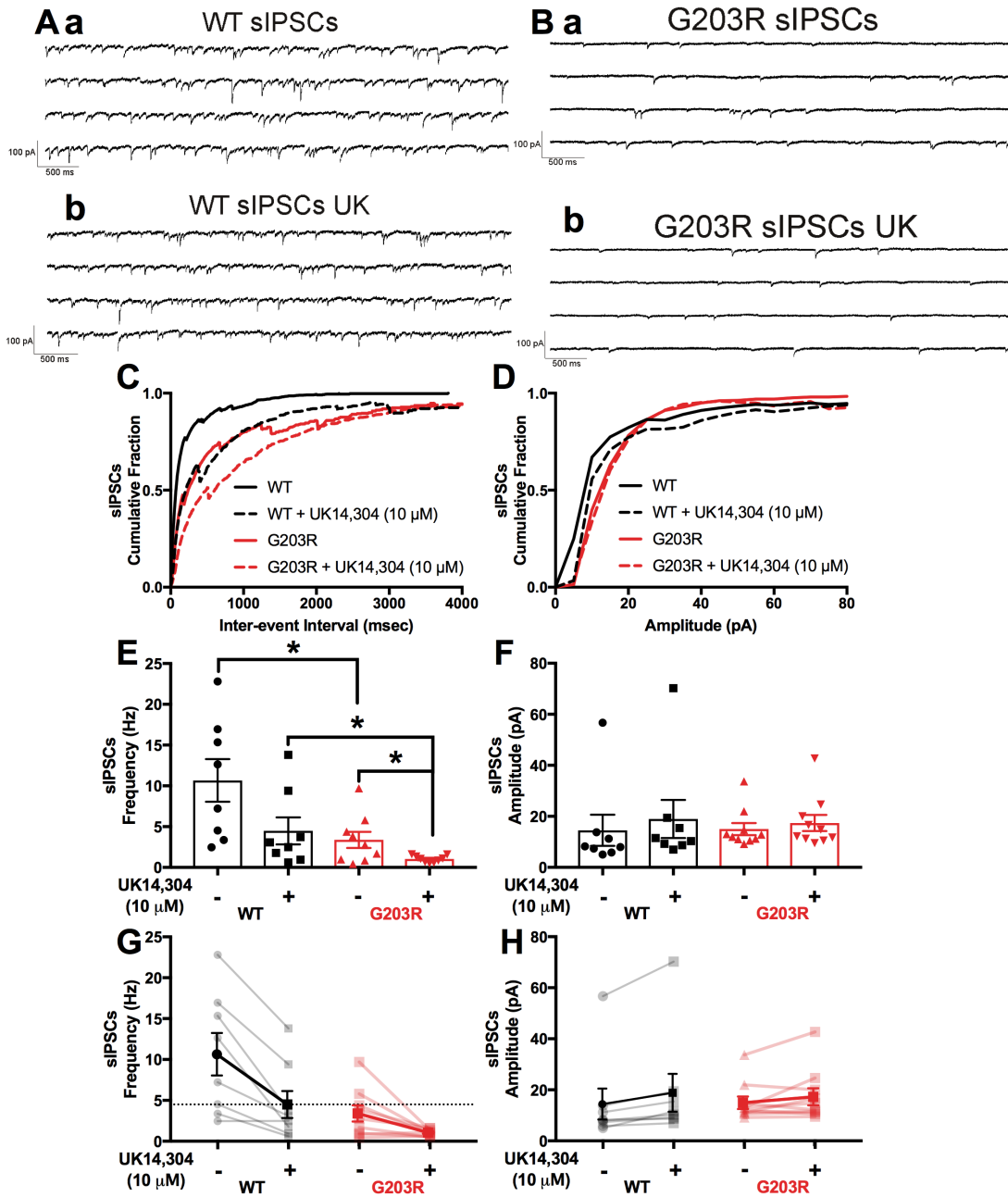


Figure 4.6 The frequency of sIPSCs is modulated by α_2 AR receptors. Representative recordings showing the sIPSCs of (A) WT and (B) G203R mice before and after adding the selective α_2 AR receptor agonist UK14,304 (10 μ M). (C, E, G) UK14,304 significantly reduced the frequency of sIPSCs in both WT and G203R mice, and the frequency of sIPSCs remained lower in G203R mice after UK14,304 treatment comparing to WT. (D, F, H) The amplitude of sIPSCs was unaffected with UK14,304 treatment. Unpaired Student's t test; WT (n=8 mice), G203R (n=9 mice); *p<0.05

4.4.6 α_{2A} adrenergic receptor-induced inhibition of sIPSC frequency depends on activation of voltage-gated calcium channels

It has been established that G $\beta\gamma$ subunits can act on multiple types of voltage-gated calcium channels to inhibit calcium influx from the extracellular space and decrease neurotransmitter release (Currie, 2010; Zamponi & Currie, 2013). For AP-dependent GABA release, high voltage activated calcium channels (N-type and P/Q-type calcium channels) are first activated by depolarization from AP-stimulated influx of sodium ions. Following the activation of calcium channels, GPCRs stimulate G $_o$, which releases the G $\beta\gamma$ subunit. Since the neurotransmitter release is directly proportional to the extent of calcium influx from the extracellular space and the resultant changes in the intra-terminal calcium concentration (Wu & Saggau, 1997), we examined whether the UK14,304-induced inhibition of GABAergic IPSCs is dependent on the extracellular calcium concentration. To verify effects of low extracellular calcium on the UK14,304-induced inhibition of GABAergic IPSCs, we recorded baseline sIPSCs and UK14,304-induced inhibition of sIPSCs in the presence of 100 μ M cadmium chloride (CdCl $_2$). Cd $^{2+}$ greatly decreased sIPSC frequency in both WT (from 17.3 \pm 1.6 Hz to 1.01 \pm 0.22 Hz) and G203R (from 10.9 \pm 2.3 Hz to 1.46 \pm 0.27 Hz) mice (Figure 4.7Aa-b, 4.7Ba-b & 4.7C & 4.7E). It also eliminated the inhibition of sIPSC frequency induced by application of 10 μ M UK14,304 (Figure 4.7Ab-c, 4.7Bb-c & 4.7C & 4.7E). The amplitude of sIPSCs showed a trend toward a decrease with application of Cd $^{2+}$ but the change

was not significant (Figure 4.7D & 4.7F). Interestingly, UK14,304 did not affect the frequency of mIPSCs in either WT or G203R mice (Figure S4.2).

However, since mIPSCs do not depend on the activation of extracellular calcium channels, Cd^{2+} does not affect the frequency and amplitudes of mIPSCs in either WT or G203R mice (Figure 4.8). Moreover, baclofen induced decrease of mIPSC frequency was not affected by the inhibition of membrane calcium channels either (Figure 4.8). Although the difference between mIPSC frequency of WT and G203R is not significant in this figure, it is understandable since there is fewer n numbers for this experiment shown in Figure 4.8 comparing to experiment in Figure 4.5.

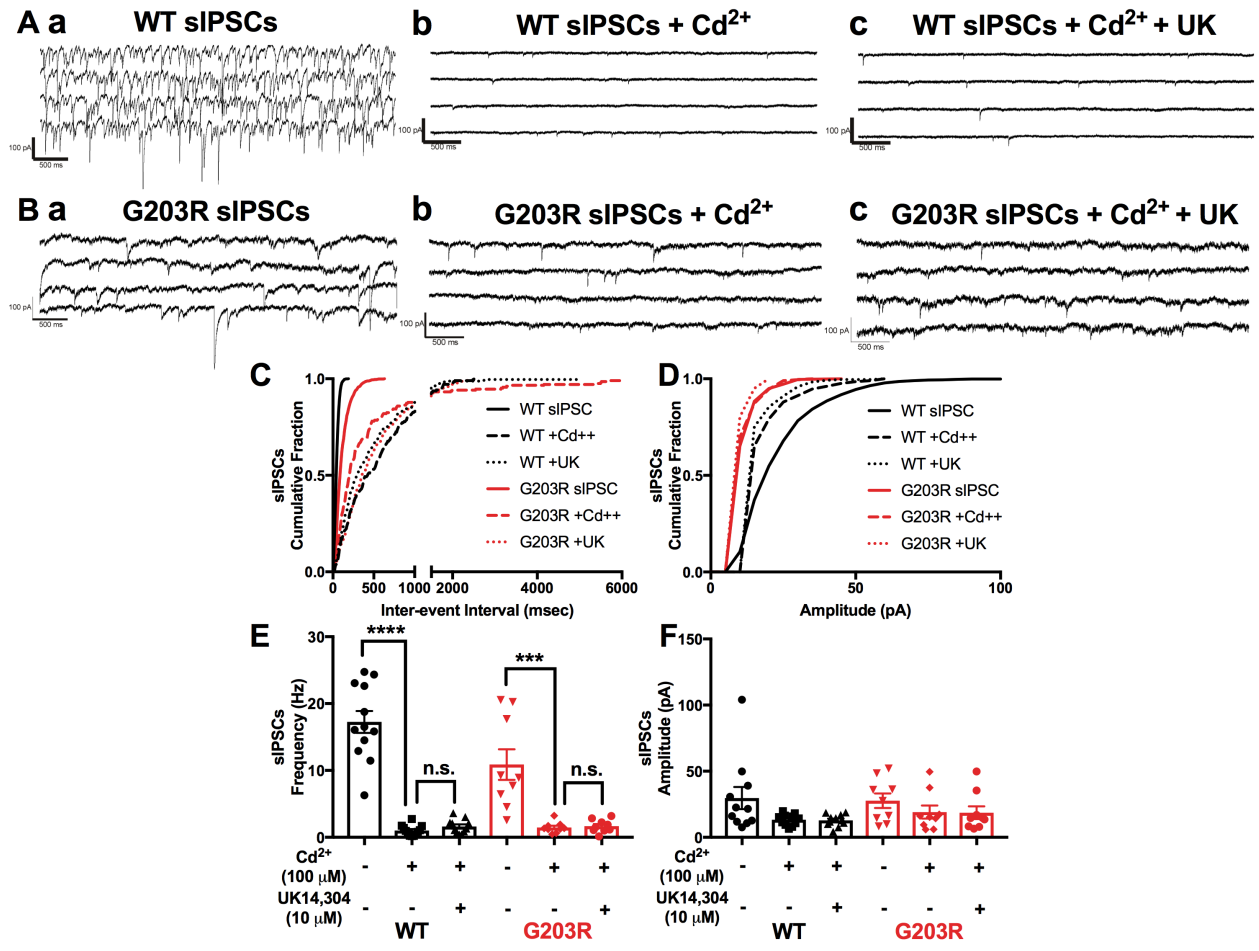


Figure 4.7 Cadmium-block of extracellular calcium influx suppresses the frequency of sIPSCs in both WT and G203R mice. Representative recordings showing the sIPSCs of (A) WT and (B) G203R in (a) ASCF with 100 μM AP-V and 10 μM CNQX, (b) Cd²⁺ (100 μM)-ASCF with AP-V and CNQX, (c) Cd²⁺ (100 μM)-ASCF with AP-V, CNQX and 10 μM UK14,304. (C, E) 100 μM Cd²⁺ significantly reduced sIPSC frequency in both WT and G203R mice and blocks inhibition of sIPSC frequency induced by UK14,304. (D, F) 100 μM Cd²⁺ did not affect amplitudes of sIPSCs. Unpaired Student's t-test; WT (n=5 mice), G203R (n=5 mice); ****p<0.0001, ***p<0.001.

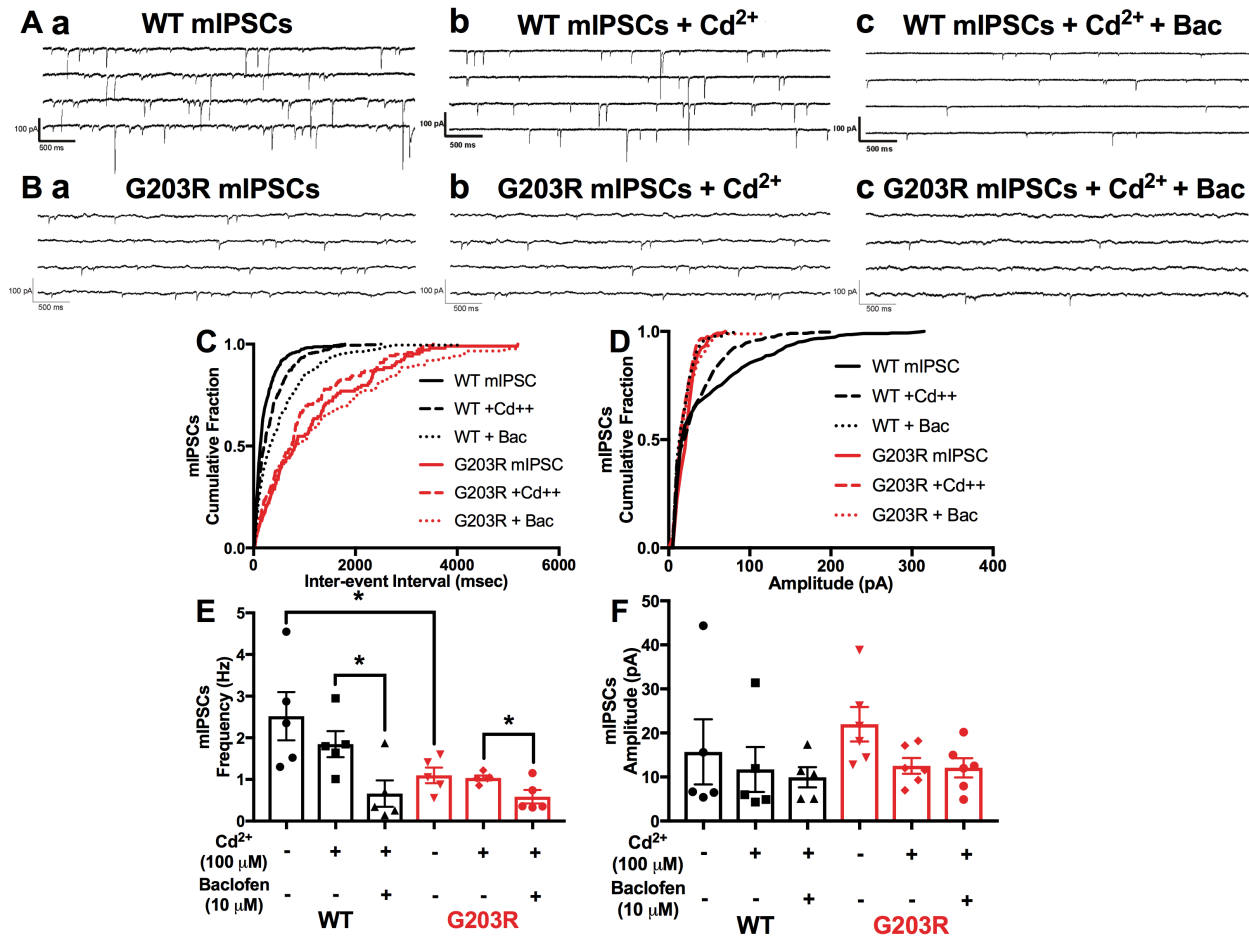


Figure 4.8 Cadmium-block of extracellular calcium influx does not affect the frequency and the amplitude of mIPSCs in both WT and G203R mice. Representative recordings showing the sIPSCs of (A) WT and (B) G203R in (a) ASCF with 100 μM AP-V, 10 μM CNQX and 0.5 μM TTX; (b) Cd²⁺(100 μM)-ASCF with AP-V, CNQX and TTX; (c) Cd²⁺ (100 μM)-ASCF with AP-V, CNQX, TTX and 10 μM baclofen. (C, E) 100 μM Cd²⁺ did not reduce the frequency of mIPSCs in either WT or G203R mice. Baclofen (10 μM) reduced the frequency of mIPSC with the presence of 100 μM Cd²⁺. (D, F) Similarly, 100 μM Cd²⁺ does not affect amplitudes of sIPSCs. Unpaired Student's t-test; WT (n=5 mice), G203R (n=5 mice); *p<0.05.

4.4.7 G203R mice exhibit decreased $G\alpha_o$ protein expression but no change in $G\beta$ levels

$G\alpha_o$ G203R mutation led to a reduction in $G\alpha_o$ protein expression in transiently transfected HEK293T cells (Feng et al., 2017). To see if this still stands *in vivo*, we tested $G\alpha_o$ protein expression in whole brain and also selected brain regions WT and G203R mice. Results showed a significant reduction in $G\alpha_o$ protein expression (50% of WT) in the whole brain (Figure 4.9A, 4.9C). The decrease in $G\alpha_o$ protein expression was significant in cerebellum, cortex, hippocampus and striatum of the G203R mice (Figure 4.9B, 4.9D). No significant change was observed in the brain stem and the olfactory bulb between the WT and G203R mice.

The $G\beta\gamma$ subunits not only support the role of GPCR- $G\alpha$ interaction, but also act directly and independently to regulate downstream signaling. The number of identified effectors of $G\beta\gamma$ has grown in recently years. They include some important targets like the GIRK channel, P/Q and N-type calcium channels, and the SNARE protein complex (Blackmer et al., 2005; Herlitze et al., 1996; Qin, Platano, Olcese, Stefani, & Birnbaumer, 1997; Wells et al., 2012; Zhang et al., 2004; Zurawski et al., 2017). The current model of heterotrimeric G protein function hypothesizes that the conformational changes in $G\alpha$ lead to its dissociation from $G\beta\gamma$ to expose effector interaction surfaces on $G\beta\gamma$. In fact, many of the GPCR-dependent physiological process inhibited by PTX ($G_{o/i}$ family) are mediated by the $G\beta\gamma$ subunits rather than the $G\alpha$ subunits (Ikeda, 1996; Logothetis,

Kurachi, Galper, Neer, & Clapham, 1987; Stephens et al., 1994; Welch et al., 2002). Thus, the gain-of-function mutation G203R in $G\alpha_o$ may function through $G\beta\gamma$ subunits to regulate the neurotransmitter release. The expression level of $G\beta$ did not change in G203R mutant mice (Figure 4.10). However, G203R is a GOF mutation with a decreased $G\alpha_o$ protein expression level and a normal $G\beta$ protein level. This could lead to a constitutive increase in $G\beta\gamma$ protein function in G203R mice.

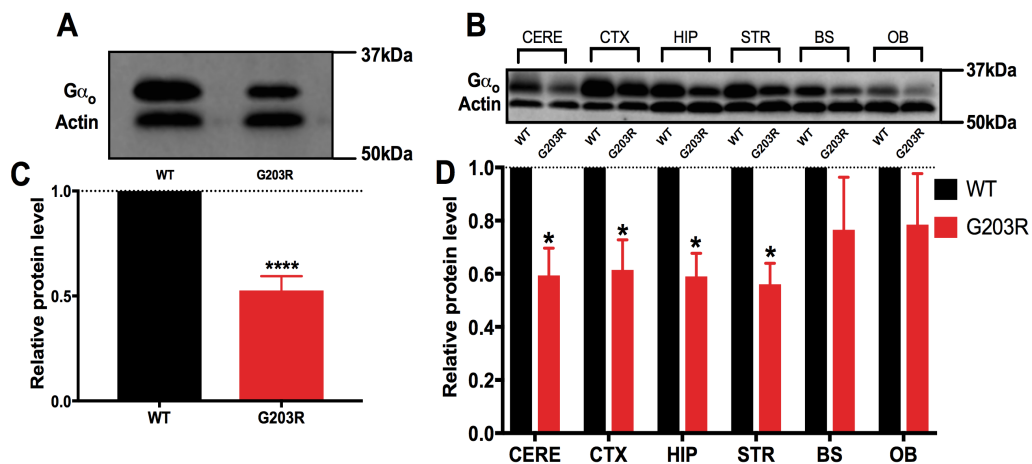


Figure 4.9 G203R mice showed a significant decrease in $G\alpha_o$ protein expression.

(A, C) Whole brain $G\alpha_o$ expression level decreased to about 50% in G203R mice's brain lysates. (B, D) This reduction in expression was most significant in specific regions like cerebellum (CERE), cortex (CTX), hippocampus (HIP) and striatum (STR), while remained unaffected in brain stem (BS) and olfactory bulb (OB). All expression levels were normalized to that of WT accordingly. Unpaired Student's t-test; WT (n=8), G203R (n=8); ****p<0.0001, *p<0.05.

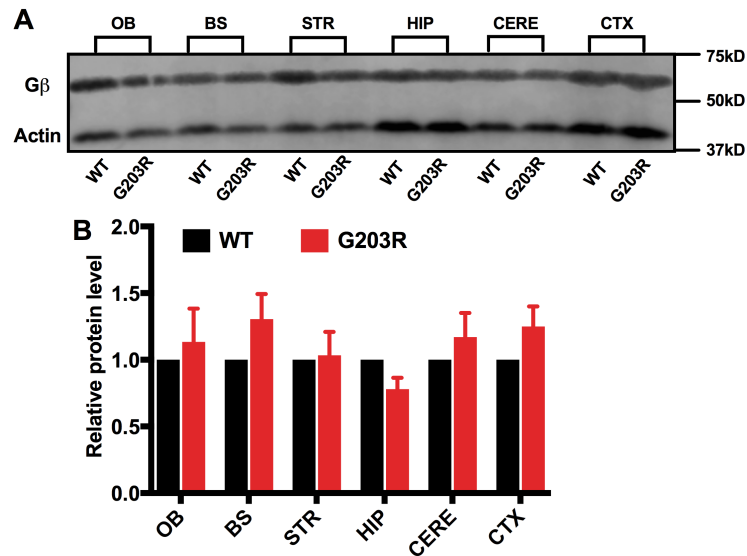


Figure 4.10 G203R mice did not show any significant changes in Gβ expression in the brain. (A) A representative gel shows the Gβ protein expression patterns in each individual brain region, including olfactory bulb (OB), brain stem (BS), striatum (STR), hippocampus (HIP), cerebellum (CERE) and cortex (CTX). (B) Quantification of the protein expression levels is unchanged in G203R mice brain lysates comparing to those of their WT siblings. Unpaired Student's t-test; WT (n=4), G203R (n=4).

4.5 Discussion

G203R was deemed a gain-of-function mutation in our previous report, where it showed an enhanced ability to support α_{2A} adrenergic receptor mediated inhibition of cAMP production (Feng et al., 2017). Patients with G203R all develop severe movement disorders and seizures at an early age (Arya et al., 2017; Kelly et al., 2019; Nakamura et al., 2013; Saitsu et al., 2016; Schirinzi et al., 2019; Schorling et al., 2017; Xiong et al., 2018). Previously, we reported that G203R mice, especially male mice, exhibit abnormalities in a battery of motor and behavioral tests (Feng et al., 2019). In this

chapter, we explore possible physiological mechanisms of *GNAO1*-related movement disorders.

Purkinje cells function as the sole output of cerebellar neural signaling transduction. They synapse onto the deep nuclei of the cerebellum and release inhibitory neurotransmitter to control their interaction with the thalamus. Therefore, the altered excitatory/inhibitory regulation received by Purkinje cells can reflect possible abnormalities in the cerebellum. The cerebellum is well-known for playing a role in motor coordination and control of movement. Recent research has also linked disturbed cerebellar function to ataxia and dystonia (Bologna & Berardelli, 2018; Garcia et al., 2017; Marsden, 2018). Consequently, I started my investigation by examining neural control of cerebellar Purkinje cells.

I discovered that the *Gnao1* G203R mutation decreased both AP-dependent sIPSC frequency and AP-independent mIPSC frequency. Amplitudes were unaffected. Inhibition of G_o signaling with NEM or PTX increased the frequency of mIPSCs. This finding suggests that the G203R mutation enhanced inhibition of GABA release through a pre-synaptic mechanism (Figure 4.11). Since PTX only increased the IPSC frequency in G203R but not WT slices, this suggests that G203R is a *bona fide* gain-of-function mutation. As such, the mutant $G\alpha_o$ protein has enhanced inhibition compared to a normal-functioning WT protein. Moreover, we have also confirmed that mIPSCs and sIPSCs are likely mediated by different receptors through different mechanisms.

AP-independent mIPSCs are mainly mediated by GABA_B receptors (Figure 4.11C & 4.11D). However, GABA_B receptors likely modulate spontaneous GABA release by inhibition of synaptic vesicle fusion through actions of Gβγ rather than inhibition of membrane calcium channels (Figure 4.11C & 4.11D). In contrast, AP-dependent sIPSCs are regulated by α_{2A} adrenergic receptors through inhibition of voltage-gated calcium channels (Figure 4.11A & 4.11B). The identification of the relevant GPCRs provides a possible direction for new drug discovery and drug repurposing. Antagonists with combined effects on GABA_B receptors and α_{2A} adrenergic receptors may be an effective strategy for suppressing *GNAO1*-associated movement disorders.

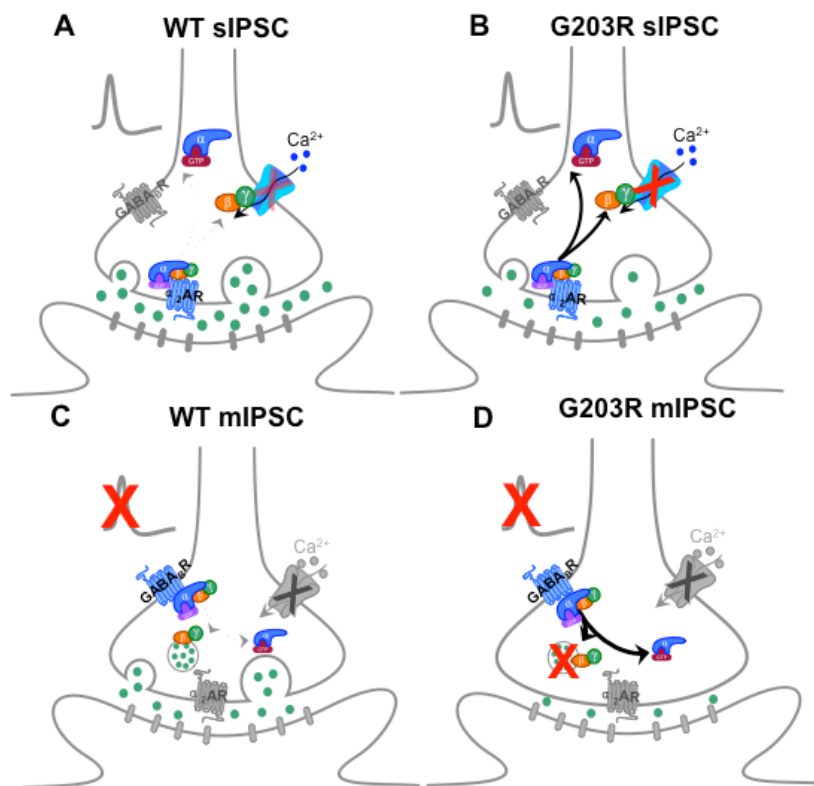


Figure 4.11 Models of GABA_BR and α_{2A}R mediated inhibition of GABA release. (A) α_{2A}R agonist activates α_{2A}R, which results in the separation of Gα_o and Gβγ. Gβγ inhibits

Figure 4.11 (cont'd) calcium influx from membrane calcium channels activated by AP. (B) G203R mutant $G\alpha_o$ protein enhances the suppression of calcium influx, which lead to a reduction in GABA release. (C) Spontaneous GABA release without AP stimulation is regulated by the activation of $GABA_B$ R, which inhibits synaptic vesicle fusion. (D) G203R mutant $G\alpha_o$ further inhibits the synaptic vesicle release.

However, it is not clear whether the G203R mutant G_o heterotrimer inhibits the neurotransmitter release via the mutated $G\alpha_o$ subunit or by the released free $G\beta\gamma$ protein. Activated $G\alpha_o$ protein can expose the surface on $G\beta\gamma$ to form a core site for effector binding and effector activation (Smrcka, 2008). The G203R mutant mice exhibited a reduced mIPSC frequency in cerebellar Purkinje cells in the absence of any external GPCR agonists. This suggests three possibilities. First, endogenous agonists in the cerebellar slices may activate G_o -coupled GPCRs. Second, sufficient free $G\beta\gamma$ subunits may exist, due to the reduced amount of mutant $G\alpha_o$, and may cause pre-synaptic inhibition of GABA release. This is plausible considering that G203R mutant mice did not show any reduction in $G\beta$ protein (Figure 4.10) but had a significant decrease in $G\alpha_o$ protein expression (Figure 4.9). Third, the G203R mutation may consecutively activate $G\alpha_o$ signaling pathways. This could activate both $G\alpha_o$ and also release free $G\beta\gamma$ subunits to mediate $G\beta\gamma$ signaling. There has been reported *GNAO1* mutation that is consecutively active: Q205L (Ram, Horvath, & Iyengar, 2000). Structurally, G203 and Q205 are located close together; therefore it is reasonable to suspect that G203R may be a constitutively active *GNAO1* mutation that does not require the activation by a

GPCR. Moreover, the $G\alpha_o$ G203R mutant showed a more rapid GDP release than the WT - as measured by the binding of a fluorescent GTP analog (personal communication). That suggests that the GOF effect of G203R may provide free $G\beta\gamma$ subunits more quickly than the WT $G\alpha$.

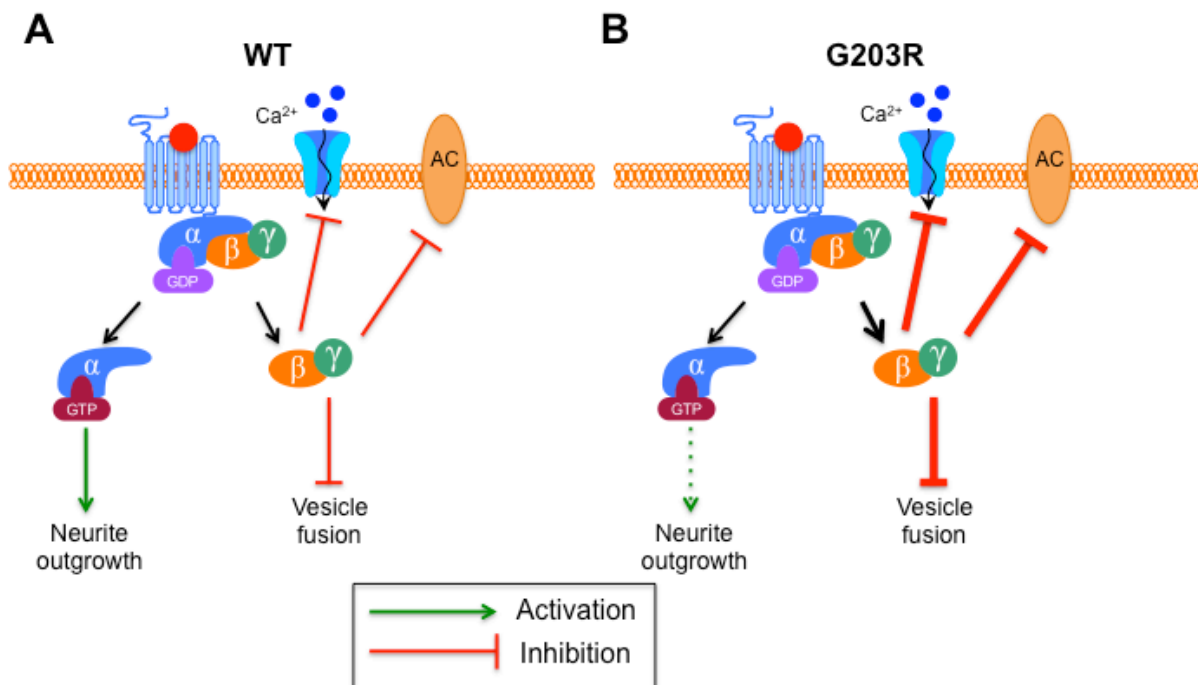


Figure 4.12 $G\beta\gamma$ may play a major role in the regulation of IPSCs. (A) Activation of GPCRs leads to the separation of $G\alpha$ -GTP and $G\beta\gamma$. They may carry on content dependent activation or inhibition of the downstream signaling targets. (B) G203R mutant $G\alpha_o$ protein may contribute to an enhanced function of $G\beta\gamma$, which leads to an increased inhibition of $G\beta\gamma$ -mediated inhibition of N- and P/Q-type calcium channels, AC, and synaptic vesicle fusion. But G203R may tamper the signaling pathway mediated by $G\alpha_o$ -GTP, like $G\alpha_o$ -activated neurite outgrowth.

A confusing aspect of the GOF *GNAO1* mutations in children and in our mouse models has been that these mutants causing the dual phenotypes of MD and epilepsy. One potential explanation for this could be that *GNAO1* G203R mutant mice may have context-dependent GOF and LOF in for different signal outputs (Figure 4.12) or in different brain regions (Figure 4.13). Despite the preliminary biochemical data showing G203R mutant $G\alpha_o$ protein's rapid GDP release, we also found that protein expression of the G203R mutant is significantly lower than normal in cerebellum, striatum, cortex, and hippocampus (Figure 4.9). If one signal (e.g. neural migration) was mediated by $G\alpha$ and the other (e.g. VGCC inhibitor) was mediated by $G\beta\gamma$, the signal mediated by $G\alpha_o$ could be reduced (i.e. $G\alpha_o$ mediated activation of neurite outgrowth), while there is more free $G\beta\gamma$ causing GOF for the inhibition of AC, VGCC or vesicle release (Figure 4.12). There is one precedent for this with a human $G\alpha_s$ mutant that causes increased signaling in the testis but reduced signaling in the pituitary (Turan & Bastepe, 2015). In a similar aspect, the reason why G203R and R209H mutant mice showed different behavioral results can be attributed to that the different *Gnao1* mutations tilt the balance between excitatory and inhibitory effects in different brain regions (Figure 4.13). If the G203R GOF mutant has a stronger influence on neurotransmitter release in brain regions that are closely related to epileptogenesis (i.e. cortex and hippocampus), while the R209H mutant with NF behavior does not, then it is more likely for G203R mutant mice to develop a higher susceptibility to seizures.

More research needs to be done to assess whether the G203R mutation could lead to different signaling outcomes in different brain regions. Future directions should focus on identifying the link between the cell-types and signal outputs that can test this model we proposed.

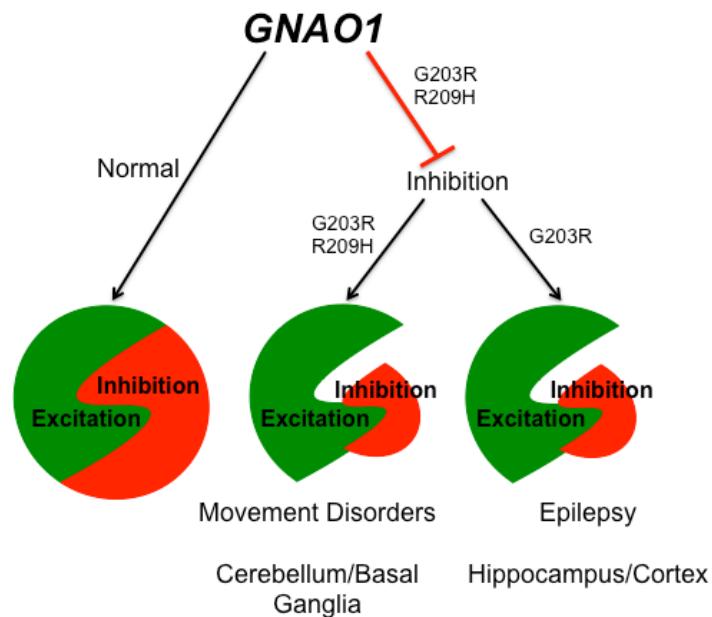


Figure 4.13 *GNAO1* mutations may have region specific effects, which cause an imbalance between excitatory and inhibitory neurotransmitters. Under normal condition, G_o mainly inhibits the inhibitory neurotransmitter release to keep a fine-tuned balance between inhibitory and excitatory effects. However, G203R mutant and R209H mutant may reduce the inhibitory effects, hence overexcite the brain. Considering the difference in the presence of human symptoms, it is likely that G203R and R209H mutants affects brain regions that control movements like cerebellum or basal ganglia, but G203R mutant can further affect hippocampus and cortex therefore lead to the onset of epilepsy in both animals and humans.

APPENDIX

APPENDIX

SUPPLEMENTAL DATA

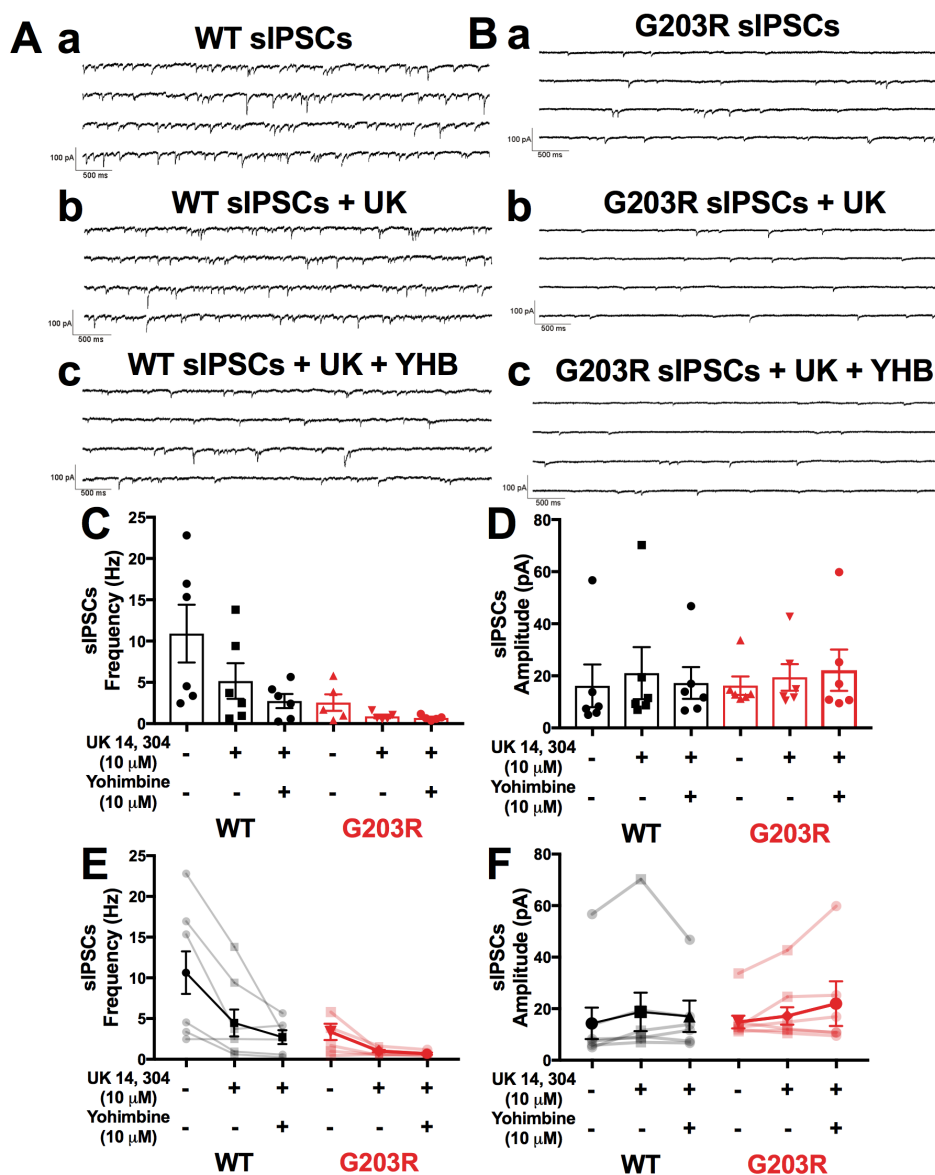


Figure S4.1 Despite the hypothesis that α_{2A} receptor antagonist yohimbine (10 μ M) could reverse the inhibition of sIPSC frequency induced by UK14, 304, the application of yohimbine further reduced the sIPSC frequency with the application of UK14, 304. Representative traces are shown here with WT (A) and G203R (B) mice in the recording of baseline level sIPSCs (a), sIPSCs with the application of UK14, 304 (b),

Figure S4.1 (cont'd) and sIPSCs with the application of both UK14, 304 and yohimbine (c). (C, E) Although not significant, yohimbine seems further reduced the sIPSC frequency that has already been decreased by the application of UK14, 304. It is highly possible since yohimbine is not a highly selective α_{2A} receptor antagonist. It also antagonizes multiple serotonin receptors (Papeschi, Sourkes, & Youdim, 1971; Winter & Rabin, 1992), which also plays a role in regulating cerebellar GABA release and development (Nichols, 2011; Oostland & van Hooft, 2013). (D, F) Neither UK14, 304 nor yohimbine has any effects on the amplitudes of sIPSCs in WT and G203R mice. Unpaired Student's t-test; WT (n=5), G203R (n=5).

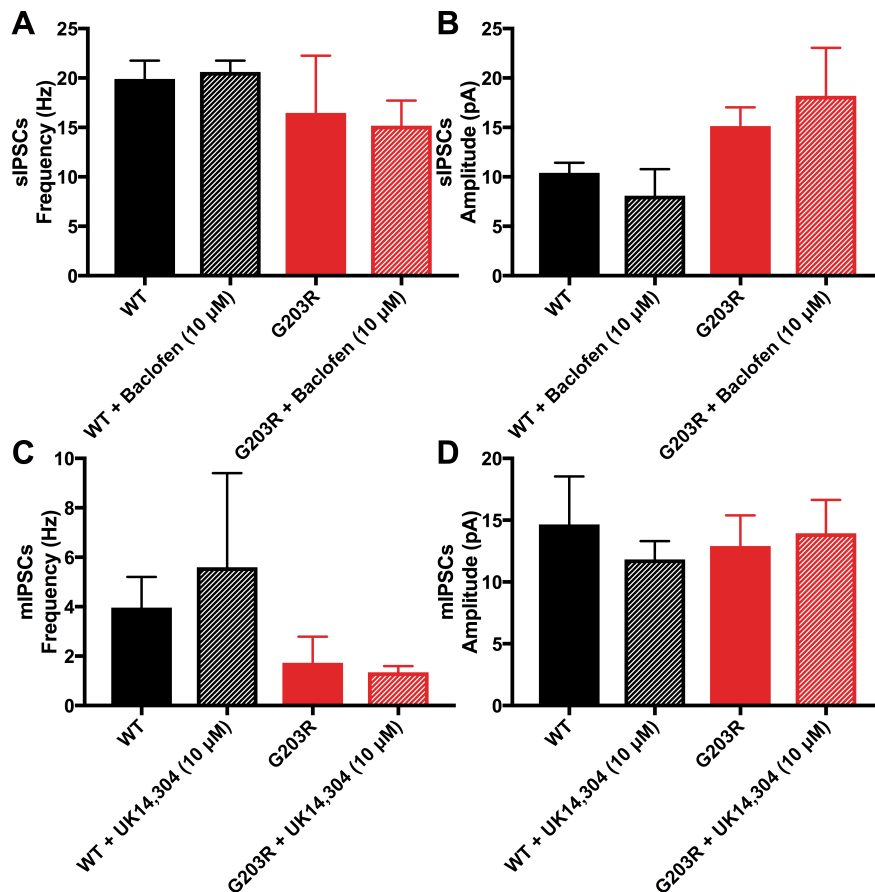


Figure S4.2 Baclofen does not affect either frequency or amplitude of sIPSCs, and UK14,304 does not affect mIPSC frequency or amplitude. Recording of sIPSCs are not affected by baclofen (10 μ M) in either frequency (A) or amplitude (B). (WT: n=2 mice;

Figure S4.2 (cont'd) G203R: n=2 mice). Amplitudes (C) or frequency (D) of mIPSCs are not decreased by UK14, 304 (10 μ M) either. (WT: n=2 mice; G203R: n=2 mice).

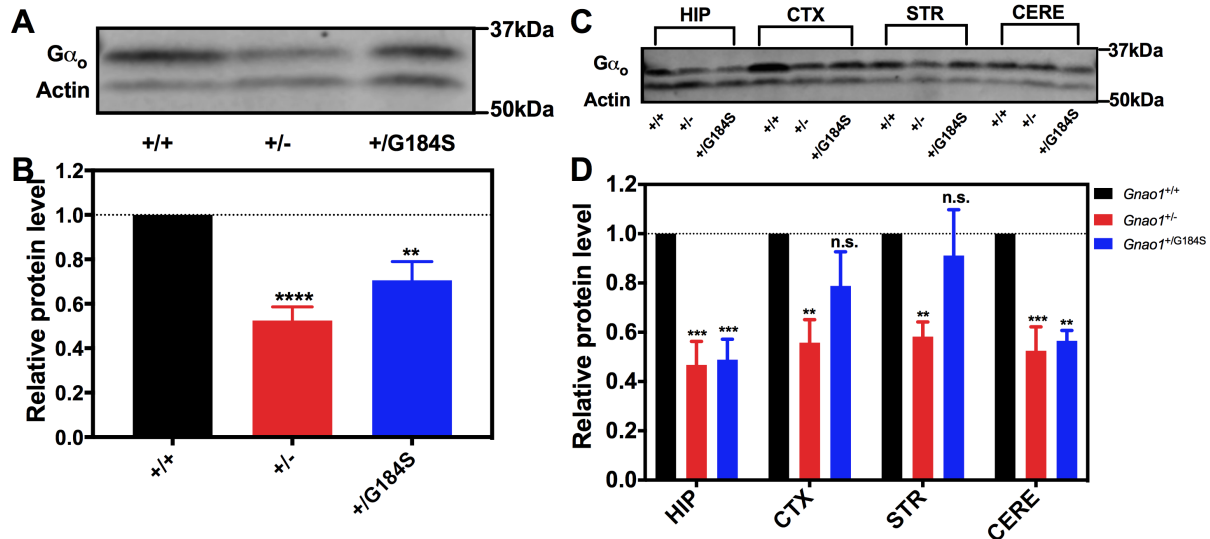


Figure S4.3 Heterozygous G184S (GOF) mice also showed a low $G\alpha_o$ protein expression level. In whole brain lysates, (A) representative gel and (B) quantification of the relative protein level both showed that G184S mice had a reduced $G\alpha_o$ protein expression level (80% expression) comparing to WT (100%) and heterozygous KO mice (50%). Similar to the protein expression pattern seen in G203R mice, the $G\alpha_o$ protein levels were different in different brain regions. Onw-way ANOVA; +/+ (n=9), +/- (n=9), +/G184S (n=9); ****p<0.001, **p<0.01. (C, D) Heterozygous KO mice exhibited a reduced $G\alpha_o$ protein level in all brain regions tested: hippocampus (HIP), cortex (CTX), striatum (STR) and cerebellum (CERE). However, heterozygous G184S mice showed selective $G\alpha_o$ protein reduction in hippocampus and cerebellum but not in cortex or striatum. Two-way ANOVA; +/+ (n=6), +/- (n=6), +/G184S (n=6); ***p<0.001, **p<0.01.

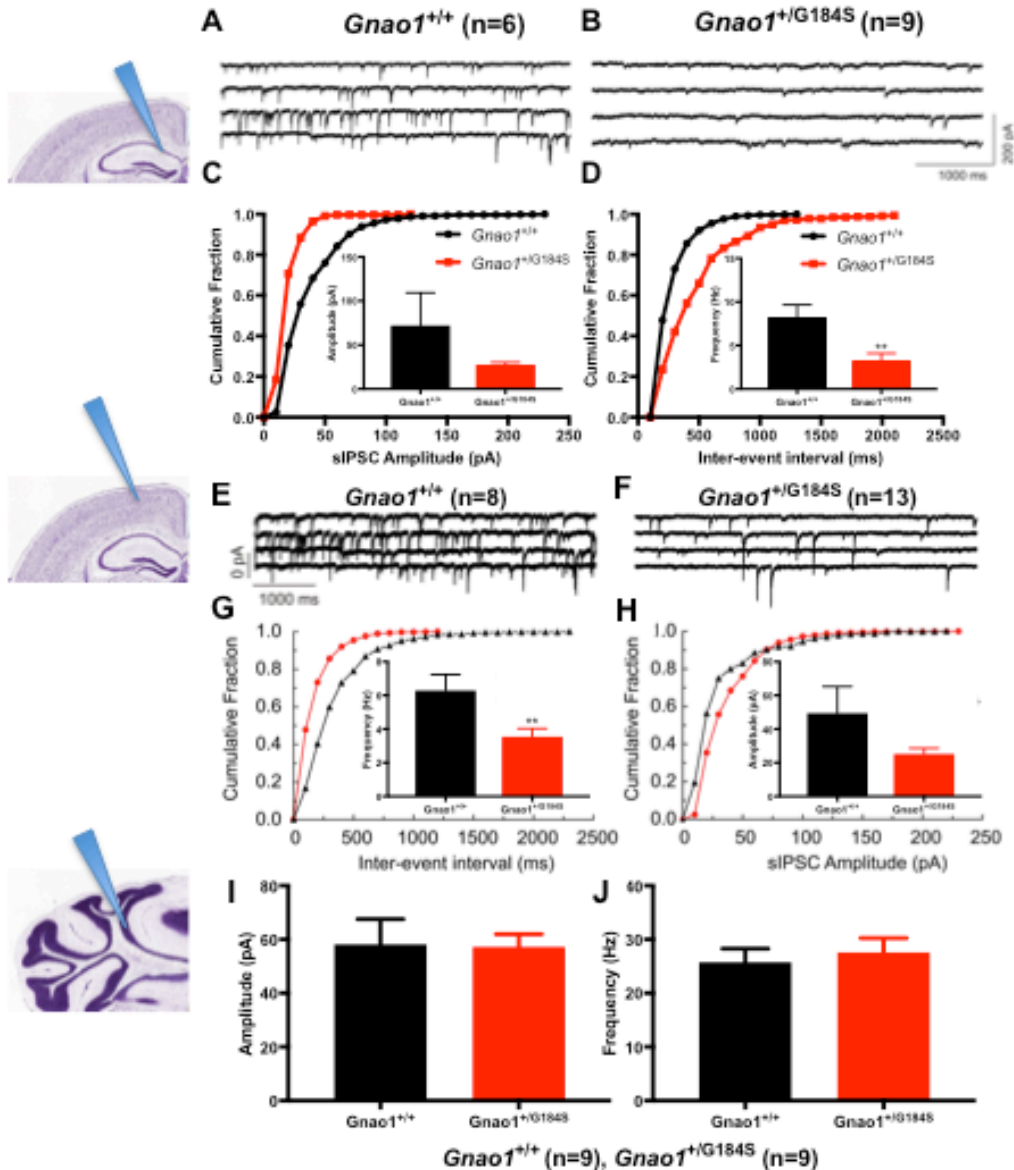


Figure S4.4 Female *Gnao1*^{+/G184S} mice showed reduced sIPSC frequency in hippocampal pyramidal cells, cortical layer II/IV pyramidal cells but not in cerebellar Purkinje cells. (A-D) Frequency of sIPSCs was significantly different in *Gnao1*^{+/G184S} mice in the hippocampal CA1 pyramidal neurons (B, D), but amplitude showed no difference between WT and G184S mice (A, C). Unpaired Student's t-test; WT (n=6), G184S (n=9); **p<0.01. (E-H) The same trend of a reduced sIPSC frequency was also seen in the cortical layer II/IV pyramidal neurons in the G184S mice (E, G), and the amplitudes of those two groups were not significantly different, although a trend of decreased amplitude can be seen in the G184S mice (F, H). Unpaired t-test; WT (n=8),

Figure S4.4 (cont'd) G184S (n=13); **p<0.01. (I, J) There is no significant difference in either frequency or amplitude in sIPSCs between WT and G184S mice's cerebellar Purkinje cell. Unpaired Student's t-test; WT (n=9), G184S (n=9).

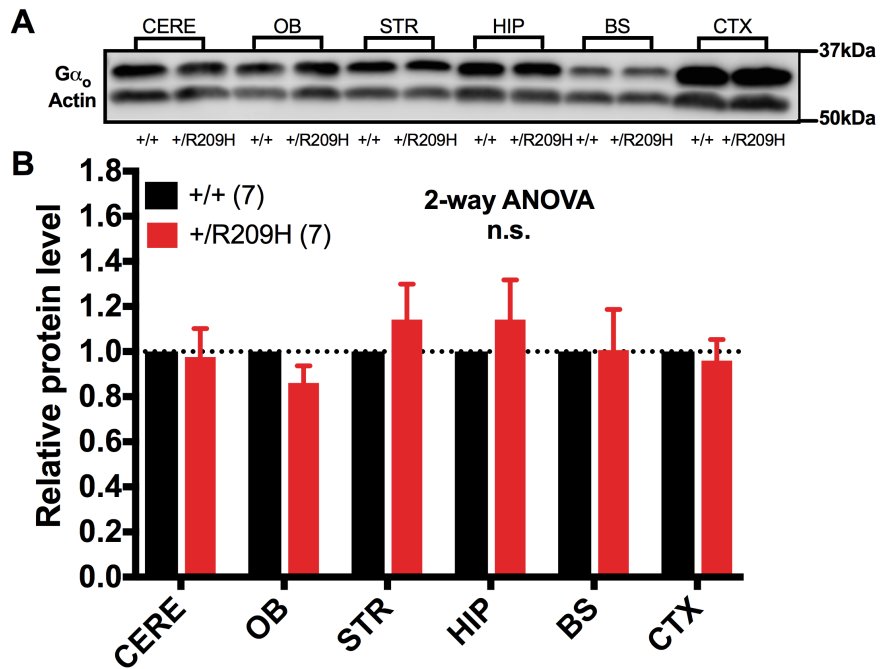


Figure S4.5 Brain $G\alpha_0$ expression does not change in R209H mice's brain lysates. (A) Representative gel showing the $G\alpha_0$ protein expression in different brain regions of both WT (+/+) and R209H (+/R209H) mice. (B) Quantification of $G\alpha_0$ protein expression shows that there is no significant difference in all 6 brain regions tested between WT and R209H mice. CERE: cerebellum; OB: olfactory bulb; STR: striatum; HIP: hippocampus; BS: brain stem; CTX: cortex; Unpaired Student's t-test; WT (n=7), R209H (n=7).

REFERENCES

REFERENCES

- Aktories, K., Schultz, G., & Jakobs, K. H. (1982). Inactivation of the guanine nucleotide regulatory site mediating inhibition of the adenylate cyclase in hamster adipocytes. *Naunyn Schmiedebergs Arch Pharmacol*, 321(4), 247-252.
- Arya, R., Spaeth, C., Gilbert, D. L., Leach, J. L., & Holland, K. D. (2017). GNAO1-associated epileptic encephalopathy and movement disorders: c.607G>A variant represents a probable mutation hotspot with a distinct phenotype. *Epileptic Disord*, 19(1), 67-75. doi:10.1684/epd.2017.0888
- Barbour, B. (1993). Synaptic currents evoked in Purkinje cells by stimulating individual granule cells. *Neuron*, 11(4), 759-769.
- Bardo, S., Robertson, B., & Stephens, G. J. (2002). Presynaptic internal Ca²⁺ stores contribute to inhibitory neurotransmitter release onto mouse cerebellar Purkinje cells. *Br J Pharmacol*, 137(4), 529-537. doi:10.1038/sj.bjp.0704901
- Blackmer, T., Larsen, E. C., Bartleson, C., Kowalchuk, J. A., Yoon, E. J., Preininger, A. M., . . . Martin, T. F. (2005). G protein betagamma directly regulates SNARE protein fusion machinery for secretory granule exocytosis. *Nat Neurosci*, 8(4), 421-425. doi:10.1038/nn1423
- Bologna, M., & Berardelli, A. (2018). The cerebellum and dystonia. *Handb Clin Neurol*, 155, 259-272. doi:10.1016/B978-0-444-64189-2.00017-2
- Boxall, A. R. (2000). GABAergic mIPSCs in rat cerebellar Purkinje cells are modulated by TrkB and mGluR1-mediated stimulation of Src. *J Physiol*, 524 Pt 3, 677-684. doi:10.1111/j.1469-7793.2000.00677.x
- Brickley, S. G., Farrant, M., Swanson, G. T., & Cull-Candy, S. G. (2001). CNQX increases GABA-mediated synaptic transmission in the cerebellum by an AMPA/kainate receptor-independent mechanism. *Neuropharmacology*, 41(6), 730-736.
- Brown, A. M., Arancillo, M., Lin, T., Catt, D. R., Zhou, J., Lackey, E. P., . . . Sillitoe, R. V. (2019). Molecular layer interneurons shape the spike activity of cerebellar

Purkinje cells. *Sci Rep*, 9(1), 1742. doi:10.1038/s41598-018-38264-1

Cesana, E., Pietrajtis, K., Bidoret, C., Isope, P., D'Angelo, E., Dieudonne, S., & Forti, L. (2013). Granule cell ascending axon excitatory synapses onto Golgi cells implement a potent feedback circuit in the cerebellar granular layer. *J Neurosci*, 33(30), 12430-12446. doi:10.1523/JNEUROSCI.4897-11.2013

Currie, K. P. (2010). G protein modulation of CaV2 voltage-gated calcium channels. *Channels (Austin)*, 4(6), 497-509. doi:10.4161/chan.4.6.12871

Donato, R., Rodrigues, R. J., Takahashi, M., Tsai, M. C., Soto, D., Miyagi, K., . . . Edwards, F. A. (2008). GABA release by basket cells onto Purkinje cells, in rat cerebellar slices, is directly controlled by presynaptic purinergic receptors, modulating Ca²⁺ influx. *Cell Calcium*, 44(6), 521-532. doi:10.1016/j.ceca.2008.03.006

Eccles, J. C. (1967). Circuits in the cerebellar control of movement. *Proc Natl Acad Sci U S A*, 58(1), 336-343. doi:10.1073/pnas.58.1.336

Eccles, J. C., Llinas, R., & Sasaki, K. (1966a). The mossy fibre-granule cell relay of the cerebellum and its inhibitory control by Golgi cells. *Exp Brain Res*, 1(1), 82-101.

Eccles, J. C., Llinas, R., & Sasaki, K. (1966b). Parallel fibre stimulation and the responses induced thereby in the Purkinje cells of the cerebellum. *Exp Brain Res*, 1(1), 17-39.

Feng, H., Khalil, S., Neubig, R. R., & Sidiropoulos, C. (2018). A mechanistic review on GNAO1-associated movement disorder. *Neurobiol Dis*. doi:10.1016/j.nbd.2018.05.005

Feng, H., Larrivee, C. L., Demireva, E. Y., Xie, H., Leipprandt, J. R., & Neubig, R. R. (2019). Mouse models of GNAO1-associated movement disorder: Allele- and sex-specific differences in phenotypes. *PLoS One*, 14(1), e0211066. doi:10.1371/journal.pone.0211066

Feng, H., Sjogren, B., Karaj, B., Shaw, V., Gezer, A., & Neubig, R. R. (2017). Movement disorder in GNAO1 encephalopathy associated with gain-of-function mutations. *Neurology*, 89(8), 762-770. doi:10.1212/WNL.0000000000004262

- Fremont, R., Tewari, A., Angueyra, C., & Khodakhah, K. (2017). A role for cerebellum in the hereditary dystonia DYT1. *Elife*, 6. doi:10.7554/eLife.22775
- Garcia, A. M., Abrevaya, S., Kozono, G., Cordero, I. G., Cordoba, M., Kauffman, M. A., . . . Ibanez, A. (2017). The cerebellum and embodied semantics: evidence from a case of genetic ataxia due to STUB1 mutations. *J Med Genet*, 54(2), 114-124. doi:10.1136/jmedgenet-2016-104148
- Gowen, E., & Miall, R. C. (2007). The cerebellum and motor dysfunction in neuropsychiatric disorders. *Cerebellum*, 6(3), 268-279. doi:10.1080/14734220601184821
- Harvey, V. L., & Stephens, G. J. (2004). Mechanism of GABA receptor-mediated inhibition of spontaneous GABA release onto cerebellar Purkinje cells. *Eur J Neurosci*, 20(3), 684-700. doi:10.1111/j.1460-9568.2004.03505.x
- Herlitze, S., Garcia, D. E., Mackie, K., Hille, B., Scheuer, T., & Catterall, W. A. (1996). Modulation of Ca²⁺ channels by G-protein beta gamma subunits. *Nature*, 380(6571), 258-262. doi:10.1038/380258a0
- Hirono, M., & Obata, K. (2006). Alpha-adrenoceptive dual modulation of inhibitory GABAergic inputs to Purkinje cells in the mouse cerebellum. *J Neurophysiol*, 95(2), 700-708. doi:10.1152/jn.00711.2005
- Hull, C., & Regehr, W. G. (2012). Identification of an inhibitory circuit that regulates cerebellar Golgi cell activity. *Neuron*, 73(1), 149-158. doi:10.1016/j.neuron.2011.10.030
- Ikeda, S. R. (1996). Voltage-dependent modulation of N-type calcium channels by G-protein beta gamma subunits. *Nature*, 380(6571), 255-258. doi:10.1038/380255a0
- Jiang, M., & Bajpayee, N. S. (2009). Molecular mechanisms of go signaling. *Neurosignals*, 17(1), 23-41. doi:10.1159/000186688
- Kelly, M., Park, M., Mihalek, I., Rochtus, A., Gramm, M., Perez-Palma, E., . . . Poduri, A. (2019). Spectrum of neurodevelopmental disease associated with the GNAO1 guanosine triphosphate-binding region. *Epilepsia*, 60(3), 406-418. doi:10.1111/epi.14653

- Kobilka, B. K., Matsui, H., Kobilka, T. S., Yang-Feng, T. L., Francke, U., Caron, M. G., . . . Regan, J. W. (1987). Cloning, sequencing, and expression of the gene coding for the human platelet alpha 2-adrenergic receptor. *Science*, 238(4827), 650-656.
- Konnerth, A., Llano, I., & Armstrong, C. M. (1990). Synaptic currents in cerebellar Purkinje cells. *Proc Natl Acad Sci U S A*, 87(7), 2662-2665. doi:10.1073/pnas.87.7.2662
- Levitt, E. S., Purington, L. C., & Traynor, J. R. (2011). Gi/o-coupled receptors compete for signaling to adenylyl cyclase in SH-SY5Y cells and reduce opioid-mediated cAMP overshoot. *Mol Pharmacol*, 79(3), 461-471. doi:10.1124/mol.110.064816
- Logothetis, D. E., Kurachi, Y., Galper, J., Neer, E. J., & Clapham, D. E. (1987). The beta gamma subunits of GTP-binding proteins activate the muscarinic K⁺ channel in heart. *Nature*, 325(6102), 321-326. doi:10.1038/325321a0
- Mangmool, S., & Kurose, H. (2011). G(i/o) protein-dependent and -independent actions of Pertussis Toxin (PTX). *Toxins (Basel)*, 3(7), 884-899. doi:10.3390/toxins3070884
- Marsden, J. F. (2018). Cerebellar ataxia. *Handb Clin Neurol*, 159, 261-281. doi:10.1016/B978-0-444-63916-5.00017-3
- Nakamura, K., Kodera, H., Akita, T., Shiina, M., Kato, M., Hoshino, H., . . . Saitsu, H. (2013). De Novo mutations in GNAO1, encoding a Galphao subunit of heterotrimeric G proteins, cause epileptic encephalopathy. *Am J Hum Genet*, 93(3), 496-505. doi:10.1016/j.ajhg.2013.07.014
- Nichols, R. A. (2011). Serotonin, presynaptic 5-HT(3) receptors and synaptic plasticity in the developing cerebellum. *J Physiol*, 589(Pt 21), 5019-5020. doi:10.1113/jphysiol.2011.219782
- O'Rourke, M. F., Iversen, L. J., Lomasney, J. W., & Bylund, D. B. (1994). Species orthologs of the alpha-2A adrenergic receptor: the pharmacological properties of the bovine and rat receptors differ from the human and porcine receptors. *J Pharmacol Exp Ther*, 271(2), 735-740.
- Oostland, M., & van Hooff, J. A. (2013). The role of serotonin in cerebellar development. *Neuroscience*, 248, 201-212. doi:10.1016/j.neuroscience.2013.05.029

- Papeschi, R., Sourkes, T. L., & Youdim, M. B. (1971). The effect of yohimbine on brain serotonin metabolism, motor behavior and body temperature of the rat. *Eur J Pharmacol*, 15(3), 318-326. doi:10.1016/0014-2999(71)90098-7
- Qin, N., Platano, D., Olcese, R., Stefani, E., & Birnbaumer, L. (1997). Direct interaction of gbetagamma with a C-terminal gbetagamma-binding domain of the Ca²⁺ channel alpha1 subunit is responsible for channel inhibition by G protein-coupled receptors. *Proc Natl Acad Sci U S A*, 94(16), 8866-8871. doi:10.1073/pnas.94.16.8866
- Ram, P. T., Horvath, C. M., & Iyengar, R. (2000). Stat3-mediated transformation of NIH-3T3 cells by the constitutively active Q205L Galphao protein. *Science*, 287(5450), 142-144.
- Reeber, S. L., Otis, T. S., & Sillitoe, R. V. (2013). New roles for the cerebellum in health and disease. *Front Syst Neurosci*, 7, 83. doi:10.3389/fnsys.2013.00083
- Saitsu, H., Fukai, R., Ben-Zeev, B., Sakai, Y., Mimaki, M., Okamoto, N., . . . Matsumoto, N. (2016). Phenotypic spectrum of GNAO1 variants: epileptic encephalopathy to involuntary movements with severe developmental delay. *Eur J Hum Genet*, 24(1), 129-134. doi:10.1038/ejhg.2015.92
- Schirinzi, T., Garone, G., Travaglini, L., Vasco, G., Galosi, S., Rios, L., . . . Leuzzi, V. (2019). Phenomenology and clinical course of movement disorder in GNAO1 variants: Results from an analytical review. *Parkinsonism Relat Disord*, 61, 19-25. doi:10.1016/j.parkreldis.2018.11.019
- Schorling, D. C., Dietel, T., Evers, C., Hinderhofer, K., Korinthenberg, R., Ezzo, D., . . . Kirschner, J. (2017). Expanding Phenotype of De Novo Mutations in GNAO1: Four New Cases and Review of Literature. *Neuropediatrics*, 48(5), 371-377. doi:10.1055/s-0037-1603977
- Smrcka, A. V. (2008). G protein betagamma subunits: central mediators of G protein-coupled receptor signaling. *Cell Mol Life Sci*, 65(14), 2191-2214. doi:10.1007/s00018-008-8006-5
- Song, C. H., Bernhard, D., Hess, E. J., & Jinnah, H. A. (2014). Subtle microstructural changes of the cerebellum in a knock-in mouse model of DYT1 dystonia. *Neurobiol Dis*, 62, 372-380. doi:10.1016/j.nbd.2013.10.003

- Stephens, L., Smrcka, A., Cooke, F. T., Jackson, T. R., Sternweis, P. C., & Hawkins, P. T. (1994). A novel phosphoinositide 3 kinase activity in myeloid-derived cells is activated by G protein beta gamma subunits. *Cell*, *77*(1), 83-93.
- Sunahara, R. K., & Taussig, R. (2002). Isoforms of mammalian adenylyl cyclase: multiplicities of signaling. *Mol Interv*, *2*(3), 168-184. doi:10.1124/mi.2.3.168
- Tian, J., & Zhu, M. X. (2018). GABAB Receptors Augment TRPC3-Mediated Slow Excitatory Postsynaptic Current to Regulate Cerebellar Purkinje Neuron Response to Type-1 Metabotropic Glutamate Receptor Activation. *Cells*, *7*(8). doi:10.3390/cells7080090
- Turan, S., & Bastepe, M. (2015). GNAS Spectrum of Disorders. *Curr Osteoporos Rep*, *13*(3), 146-158. doi:10.1007/s11914-015-0268-x
- Vanni, V., Puglisi, F., Bonsi, P., Ponterio, G., Maltese, M., Pisani, A., & Mandolesi, G. (2015). Cerebellar synaptogenesis is compromised in mouse models of DYT1 dystonia. *Exp Neurol*, *271*, 457-467. doi:10.1016/j.expneurol.2015.07.005
- Walker, R. H. (2016). The non-Huntington disease choreas: Five new things. *Neurol Clin Pract*, *6*(2), 150-156. doi:10.1212/CPJ.0000000000000236
- Welch, H. C., Coadwell, W. J., Ellson, C. D., Ferguson, G. J., Andrews, S. R., Erdjument-Bromage, H., . . . Stephens, L. R. (2002). P-Rex1, a PtdIns(3,4,5)P3- and Gbetagamma-regulated guanine-nucleotide exchange factor for Rac. *Cell*, *108*(6), 809-821.
- Wells, C. A., Zurawski, Z., Betke, K. M., Yim, Y. Y., Hyde, K., Rodriguez, S., . . . Hamm, H. E. (2012). Gbetagamma inhibits exocytosis via interaction with critical residues on soluble N-ethylmaleimide-sensitive factor attachment protein-25. *Mol Pharmacol*, *82*(6), 1136-1149. doi:10.1124/mol.112.080507
- Winter, J. C., & Rabin, R. A. (1992). Yohimbine as a serotonergic agent: evidence from receptor binding and drug discrimination. *J Pharmacol Exp Ther*, *263*(2), 682-689.
- Wu, L. G., & Saggau, P. (1997). Presynaptic inhibition of elicited neurotransmitter release. *Trends Neurosci*, *20*(5), 204-212.
- Xiong, J., Peng, J., Duan, H. L., Chen, C., Wang, X. L., Chen, S. M., & Yin, F. (2018).

[Recurrent convulsion and pulmonary infection complicated by psychomotor retardation in an infant]. *Zhongguo Dang Dai Er Ke Za Zhi*, 20(2), 154-157.

Yuan, Y., & Atchison, W. D. (1999). Comparative effects of methylmercury on parallel-fiber and climbing-fiber responses of rat cerebellar slices. *J Pharmacol Exp Ther*, 288(3), 1015-1025.

Yuan, Y., & Atchison, W. D. (2003). Methylmercury differentially affects GABA(A) receptor-mediated spontaneous IPSCs in Purkinje and granule cells of rat cerebellar slices. *J Physiol*, 550(Pt 1), 191-204. doi:10.1113/jphysiol.2003.040543

Yuan, Y., & Atchison, W. D. (2007). Methylmercury-induced increase of intracellular Ca²⁺ increases spontaneous synaptic current frequency in rat cerebellar slices. *Mol Pharmacol*, 71(4), 1109-1121. doi:10.1124/mol.106.031286

Yuan, Y., & Atchison, W. D. (2016). Multiple Sources of Ca²⁺ Contribute to Methylmercury-Induced Increased Frequency of Spontaneous Inhibitory Synaptic Responses in Cerebellar Slices of Rat. *Toxicol Sci*, 150(1), 117-130. doi:10.1093/toxsci/kfv314

Zamponi, G. W., & Currie, K. P. (2013). Regulation of Ca(V)₂ calcium channels by G protein coupled receptors. *Biochim Biophys Acta*, 1828(7), 1629-1643. doi:10.1016/j.bbamem.2012.10.004

Zhang, Q., Dickson, A., & Doupnik, C. A. (2004). Gbetagamma-activated inwardly rectifying K(+) (GIRK) channel activation kinetics via Galphai and Galphao-coupled receptors are determined by Galpha-specific interdomain interactions that affect GDP release rates. *J Biol Chem*, 279(28), 29787-29796. doi:10.1074/jbc.M403359200

Zurawski, Z., Page, B., Chicka, M. C., Brindley, R. L., Wells, C. A., Preininger, A. M., . . . Hamm, H. E. (2017). Gbetagamma directly modulates vesicle fusion by competing with synaptotagmin for binding to neuronal SNARE proteins embedded in membranes. *J Biol Chem*, 292(29), 12165-12177. doi:10.1074/jbc.M116.773523

Zurawski, Z., Rodriguez, S., Hyde, K., Alford, S., & Hamm, H. E. (2016). Gbetagamma Binds to the Extreme C Terminus of SNAP25 to Mediate the Action of Gi/o-Coupled G Protein-Coupled Receptors. *Mol Pharmacol*, 89(1), 75-83. doi:10.1124/mol.115.101600

CHAPTER 5: CONCLUSION AND FUTURE DIRECTIONS

5.1 General conclusion

It has been six years since the first reported cases of the *GNAO1* mutation-associated neurological disorders in 2013 (Nakamura et al., 2013). There is a rapid increase in the number of *GNAO1* mutations reported. Advances in neurological genetics and the growing interest in genetic counseling have pushed the increased interest in *GNAO1* mutation-related movement disorders and/or epilepsy. Recently, The Bow Foundation (www.gnao1.org) has been founded in support of research for understanding *GNAO1*-associated neurological disorders.

We are one of the first labs that took an interest in *GNAO1*-related neurological disorders. Through five years of research on my dissertation, I identified a genotype-phenotype correlation between the *in vitro* function of *GNAO1* mutations and the nature of patients' neurological symptoms (Chapter 2). Our lab has also established three animal models that phenocopy human *GNAO1* patients and I have, in collaboration with Cassie Larrivee and Jeffrey Leipprandt, characterized their movement abnormalities and seizure propensity (Chapter 3). Furthermore, I have obtained electrophysiological data establishing altered cerebellar signaling in mice with the *Gnao1* G203R mutation which causes a movement disorder and verified that G203R is a *bona fide* GOF mutation in the neural context (Chapter 4).

Although I established that all functioning *GNAO1* mutations (GOF and NF mutations) are associated with movement disorder patients, and all non-functioning mutations (LOF

and PLOF mutations) are related to epilepsy patients (Feng et al., 2017), this genotype-phenotype correlation was created based on a human engineered system with transiently transfected Ga_o mutants and the $\alpha_{2A}R$ in HEK293T cells. To test this correlation in a physiological background, we have selected mutations that are either the most prevalent (GOF: G203R and NF: R209H) or related to the most severe epilepsy (LOF; $\Delta T191F197$) to verify our genotype-phenotype correlation model. Interestingly, mice with the LOF mutation $\Delta T191F197$ were abnormally small and developed severe behavioral seizure at around day 7 of life (P7). All mice with the $\Delta T191F197$ mutation died before P16 and the strain was lost. Like human patients with G203R mutations, mice heterozygous for the G203R mutations ($Gnao1^{+/G203R}$ or G203R mice) behaved abnormally in our behavioral tests of movement and also showed heightened sensitivity to seizures, which was assessed by a PTZ kindling study (Feng et al., 2019). Comparably, the NF mutation R209H is only associated with movement disorders in both humans and mice (Larrivee et al., 2019); they do not show an epilepsy pattern. These behavioral tests established that our genotype-phenotype correlation stands in a physiological context across both mice and humans. However, there is an obvious sex difference in our animal models that has not been consistently observed in patients, perhaps due to the relatively small size of human *GNAO1* patient population. Also in humans, the *GNAO1* mutations could cause prenatal death of male embryos. G203R mice showed a male-dominant movement abnormality, while R209H mice have

symptoms that are equally severe in both male and female mice. Since our animal models exhibit symptoms similar to human *GNAO1* patients, they make it possible to use those animal models to study the mechanisms of how *GNAO1* mutations could lead to the onset of neurological disorders. Specifically, I used the patch clamp technique to measure both the excitatory and inhibitory neurotransmitter release in cerebellar slices of G203R mice and discovered that G203R mice exhibited decreased GABA release while glutamate release was unaffected. Also, it is possible to use the animal models to test new compounds or to repurpose drugs that are specifically effective for *GNAO1* mutation-related disorders.

While my work has covered preliminary aspects of *GNAO1* mutation-associated neurological disorders, more research needs to be done to address unanswered questions that are beyond the scope of this dissertation. First, we have not tested the functions of mutant $G\alpha_o$ in any neuronal cell line or used different canonical pathways (such as Ca^{++} or K^+ channel regulation) for characterization. Second, we have not explained why NF mutations also cause neurological disorders. It is possible that NF *GNAO1* mutations could lead to other disturbed downstream signaling pathways but do not affect inhibition of cAMP. Third, since the majority of patients with *GNAO1* mutations present with developmental delay and hypotonia at birth, it is yet to be established that *GNAO1* mouse models (G203R and R209H) also present developmental issues. One other interesting question on development is how this disorder will progress when our

mutant mice become older. There haven't been any reported human *GNAO1* patients over 45 years old; therefore understanding the progression of this disorder could potentially prepare patients for any future complications. Last but not least, the sex difference in expression of neurological disorders, as mentioned before, needs to be verified as larger patient populations are reported. In our animal model, there is an obvious sex difference in the movement disorders or epilepsy but it differs among genotypes.

In this chapter, I will discuss some major directions this project could take and provide some analysis for the development of each direction. Many of these ideas are based on preliminary data that I collected but did not have time to develop into a complete story. Those results are presented as an Appendix to this chapter

5.2 Testing the functional changes of a growing variety of *GNAO1* mutations

Our previous model of genotype-phenotype correlation was established on $G\alpha_o$ -mediated inhibition of cAMP production in HEK293 cells. However, the $G\alpha_o$ protein, either functioning by itself or through interaction with the $G\beta\gamma$ protein, regulates multiple essential intracellular effectors in its functional signaling pathways. Therefore, cAMP cannot be the sole evaluation upon which the *GNAO1* mutations are examined.

5.2.1 Do *GNAO1* mutations affect G_o 's inhibition of high-voltage gated calcium channels (N- type & P/Q- type calcium channels)?

G_o 's inhibition of Ca^{2+} channels has received extensive scrutiny. Intracellular calcium

levels are important for neuronal signal transduction and neuronal development. Numerous hormones or neurotransmitters suppress Ca^{2+} channel currents (Dunlap & Fischbach, 1978). Later, Dunlap and colleagues showed that treating dorsal root ganglion with PTX blocks noradrenaline and GABA-mediated inhibition of Ca^{2+} channels (Holz, Rane, & Dunlap, 1986). Moreover, GTP γ S, a non-hydrolysable GTP analog that binds to and activates G proteins, irreversibly potentiates agonist-mediated inhibition of Ca^{2+} channels (Holz et al., 1986; Scott & Dolphin, 1986) while GDP β S, a stable form of GDP, blocks it. Specifically, opioids activate their receptors in dorsal root ganglion neurons to suppress N-type Ca^{2+} channels (Jiang et al., 1998). Neurons lacking G_o protein lose the opioid inhibitory effect (Jiang et al., 1998). As mentioned in Chapter 1, LOF mutations in *CACNA1A* (which encodes the P/Q type Ca^{2+} channel subunit) and *CACNA1B* (which encodes the N-type Ca^{2+} subunit) and *GNAO1* GOF mutations lead to similar neurological symptoms.

There are several ways to test how mutations in *GNAO1* affect G_o 's inhibition of calcium channels. The most traditional way is to measure the Ca^{2+} currents with the patch clamp technique. This was also used in the first published *GNAO1* mutation case report in 2013 (Nakamura et al., 2013). In preliminary data, I transfected a previously established HEK293 cell line stably expressing the three subunits of N-type Ca^{2+} channels (G1A1 cell line with $\alpha 1B-1$, $\alpha 2B\delta$, $\beta 1B$ subunits) with plasmids for the $\alpha_{2A}R$ and WT $G\alpha_o$. In this system, I found that norepinephrine could inhibit calcium currents (Figure

S5.1) (Bleakman et al., 1995; McCool, Pin, Brust, Harpold, & Lovinger, 1996). Using this approach, it should be possible to transiently transfect these cells with all of the *GNAO1* mutants and test their ability to inhibit the calcium currents with the patch clamp technique.

However, with the ever-growing number of the *GNAO1* mutations, patch clamp methods may be a time-consuming procedure for this aim. An alternative to patch clamp studies is to use the high-throughput calcium mobilization assay. There have been multiple reports describing high-throughput assays with multiple available calcium dyes to screen for N-type calcium channel blockers (Lubin et al., 2006; Zamponi, Striessnig, Koschak, & Dolphin, 2015; Zhang, Kauffman, Yagel, & Codd, 2006). Using this strategy, we could use either the N-type channel expressing G1A1 cell line or a neuronal cell line to screen the *GNAO1* mutants' effects on calcium currents in a relatively short time. A preliminary study with the Fluo-4 NW dye and the Hamamatsu's FDSS μ Cell imaging system in the MSU Assay Core confirmed that G1A1 cell line does express N-type calcium channels (Figure S5.2A). Also the SH-SY5Y human neuroblastoma cell line is a good candidate for this screening (Figure S5.3B). Evaluation of whether *GNAO1* mutations alter membrane calcium channel function is extremely important. The findings would not only broaden our understanding of the genotype-phenotype correlation of the *GNAO1* mutation-related neurological disorders, but also could determine the most predictive functional assay for drug repurposing or development.

5.2.2 Do *GNAO1* mutations affect G_o 's activation of G protein-regulated inward rectifying potassium (GIRK) channels?

Potassium channels on the plasma membrane are another intracellular effector of G_o -mediated signaling. Not only have multiple studies documented the importance of this pathway, mutations in potassium channels were also reported to cause movement disorders as discussed in Chapter 1 (Luscher & Slesinger, 2010). In hippocampal pyramidal cells, serotonin and the selective $GABA_B$ R agonist baclofen hyperpolarize cells by increasing K^+ channel conductance. The serotonin and baclofen responses are also ablated in PTX-treated cells (Andrade, Malenka, & Nicoll, 1986). Addition of $GDP\beta S$ reduces the cell's response to serotonin and baclofen, while $GTP\gamma S$ mimics the action of serotonin and baclofen (Andrade et al., 1986). Moreover, both purified bovine brain G_o proteins as well as a recombinant form of $G\alpha_o$ proteins activate K^+ channels in membranes from hippocampal pyramidal cells (Jiang & Bajpayee, 2009; Peleg, Varon, Ivanina, Dessauer, & Dascal, 2002; VanDongen et al., 1988). However, studies later focused on the role of $G\beta\gamma$ complex's ability to activate the K^+ channels while the $G\alpha$ subunit mostly modulates the channel kinetics (Corey & Clapham, 2001; Huang, Jan, & Jan, 1997; Lei et al., 2000; Logothetis, Kurachi, Galper, Neer, & Clapham, 1987; Reuveny et al., 1994). Mutations in the $G\alpha_o$ protein may affect its role as a chaperone to release the $G\beta\gamma$ complex.

Apart from traditionally used patch clamp techniques, using high-throughput screening with thallium ions as a surrogate for potassium ions was also developed for screening potassium ion channel blockers (Beacham, Blackmer, M, & Hanson, 2010). Cell lines stably expressing GIRK channels (Lei et al., 2000) or primary hippocampal neurons are both available and good candidates for screening the effects of *GNAO1* mutation on G_o -mediated activation of GIRK channels (for both $G\alpha_o$ and $G\beta\gamma$ mechanisms).

5.2.3 How do *GNAO1* mutations affect G protein-regulated neurite outgrowth?

The initial formation of neurites during neuronal differentiation is commonly referred to as “neurite outgrowth”. This is the beginning point for neurogenesis, which is a crucial but long and winding journey in the development process. The $G\alpha_o$ protein is not only the most abundant membrane protein in the mammalian central nervous system, but is also highly enriched in neuronal growth cones. Elucidation of the effects of *GNAO1* mutations’ on regulation of neurite outgrowth can be an essential step towards understanding *GNAO1* mutation-associated developmental delay. Recent studies showed that the $G\alpha_o$ protein might directly stimulate neurite outgrowth. First, both $G\alpha_o$ and one of its interactors GRIN (G protein-regulated inducer of neurite outgrowth) are largely enriched in the growth cones, and activation of both can induce neurite outgrowth (Chen, Gilman, & Kozasa, 1999; Hwangpo et al., 2012; Strittmatter, Fishman, & Zhu, 1994; Strittmatter, Valenzuela, Kennedy, Neer, & Fishman, 1990). Second, dopamine-activated D_2

receptors, which couple to the $G\alpha_o$ protein, induce neurite outgrowth in cortical neurons (Reinoso, Undie, & Levitt, 1996). Also, activation of CB1 receptors leads to the activation of downstream signaling converging on STAT3, which induces neurite outgrowth in Neuro2A cells (He et al., 2005; Jordan et al., 2005). Additionally, collapse of growth cones, induced by contact between neurites and a variety of molecules, can be inhibited by pertussis toxin (Igarashi, Strittmatter, Vartanian, & Fishman, 1993). Moreover, $G\beta\gamma$ is also involved in regulating neurite outgrowth. Research showed that Nerve Growth Factor (NGF) promoted $G\beta\gamma$'s interaction with microtubules and stimulated microtubule assembly (Sierra-Fonseca et al., 2014). Also, GRK2i, which sequesters $G\beta\gamma$, inhibited neurite formation, disrupted microtubules and led to neurite damage, while the $G\beta\gamma$ activator mSIRK stimulated neurite outgrowth (Sierra-Fonseca et al., 2014).

A neurite outgrowth assay has been performed with PC12 cells (Figure S5.3) (Strittmatter, Fishman, et al., 1994; Traina, Petrucci, Gargini, & Bagnoli, 1998), Neuro2A cells (Georganta, Tsoutsi, Gaitanou, & Georgoussi, 2013; He et al., 2005), SH-SY5Y cells (Figure S5.4) (Paik, Somvanshi, & Kumar, 2019) and with primary isolated neurons (Lotto, Upton, Price, & Gaspar, 1999; Reinoso et al., 1996). A high-throughput neurite outgrowth assay kit has also been developed to reduce the labor of neurite staining and counting (Yeyeodu, Witherspoon, Gilyazova, & Ibeanu, 2010). Whether mutations in *GNAO1* would affect its role in neurite outgrowth remains unanswered.

Additionally, for neurite outgrowth, one inevitable question is how activation of the α_0 protein (Strittmatter, Fishman, et al., 1994) and increases in cAMP levels (Aglah, Gordon, & Posse de Chaves, 2008) both lead to neurite outgrowth. These two competitive pathways may take control during different stages during neurite extension. It would be interesting to see how GOF *GNAO1* mutations, which lead to enhanced suppression of cAMP production, regulate neurite outgrowth *in vitro*.

Table 5.1 Comparison of clinical patterns of G203R and R209H patients

Case No.	G203R									R209H							
	1	2	3	4	5	6	7	8	9	1	2	3	4	5	6	7	8
Sex	F	F	F	M	F	F	F	F	M	M	M	M	M	M	F	M	F
Age of onset	7 mo	7 d	9 d	1 mo	3 mo	birth	birth (deceased at 12 mo)	birth	12 d	1 y	18 mo	2 y	10 mo	3 y	6 mo	6 mo	6 mo
Seizures	+	+	+	+	+	+	+	+	+	+	+	+	+	+	+	+	+
Hypotonia						+		+	+	+	+		+	+	+	+	+
Developmental Delay																	
Chorea/athetosis	+	+		+	+	+		+	+	+	+	+	+	+	+	+	+
Dystonia			impressive movement disorder but not characterized														
Severe EEG	++	++	+	++	+	++	++	+	+	+			+		+	+	+
EEG	diffuse irregular spike-and-slow-wave complex at 5 yr	slow-wave bursts, migrating focal epileptiform discharges	delta and theta activity and rare multi-regional, bi-hemispheric epileptic activity	multifocal and diffuse discharges, along with generalized -onset seizures	background slowing	multifocal sharp waves, left temporal seizure pattern	hypsarrhythmia	multifocal paroxysmal activities in both temporal hemispheres	NA	normal	no irregularities other than diffuse slowing	no irregularities other than diffuse slowing	NA	NA	normal	NA	normal
Severe MRI	++	++	+	++	++	+	+	+	+					++	++	NA	normal
MRI	delayed myelination at 1 yr, 3 mo, reduced cerebral white matter, thin corpus callosum at 4 yr, 8 mo	progressive cerebral atrophy with delayed myelination at 14 mo	mild atrophy	progressive diffuse cerebral atrophy and volume loss in cerebellum	atrophy, thin corpus callosum (2 y)	mild atrophy (10 mo)	normal	thin corpus callosum	hypomyelination and atrophy	normal	normal	normal	normal	global atrophy at 15 yr	13 mo: frontal lobe volume loss	normal	frontal lobe volume loss (13 mo)
Reference	Nakamura et al 2013	Saito et al 2015	Dietel et al 2016	Arya et al 2017	Schorling et al 2017	Schorling et al 2017	Xiong et al. 2018	Schirzini et al 2018	Schirzini et al 2018	Menke et al 2016	Kulkarni et al 2015	Kulkarni et al 2015	Dhamija et al 2016	Ananth et al 2016	Kelly et al 2019	Blumkin et al 2018	Kelly et al 2018

5.3 Comparison between R209H and G203R mouse models

We have studied behavioral abnormalities using our mouse models with the R209H and G203R *Gnao1* mutations (Chapter 3) and also explored electrophysiological characteristics of cerebellar Purkinje cells in the G203R mouse model (Chapter 4). Needless to say, the two models exhibit some differences and similarities that may help

us understand the differences between patients with NF *GNAO1* mutations (i.e. R209) and patients with GOF mutations (i.e. G203R). A comparison between patients with R209H and G203R mutations is shown in Table 5.1. All patients present with developmental delay from an early age. However, the G203R patients all exhibited seizure episodes while R209H patients very seldom developed seizure events. In addition, G203R patients are more likely to develop severe brain malformations, which can be seen from their MRI results. It is hard to say, however, if those malformations were caused by or contributed to epileptogenesis in those patients. In this section, I will discuss some ideas for future directions generated from the similarities and differences between R209H and G203R human patients and animal models.

5.3.1 Do G203R and R209H mouse models exhibit delayed development?

Among reported cases with *GNAO1*-associated neurological disorders, all G203R patients (Arya, Spaeth, Gilbert, Leach, & Holland, 2017; Dietel, 2016; Nakamura et al., 2013; Saito et al., 2016; Schorling et al., 2017; Xiong et al., 2018) and R209H patients (Ananth et al., 2016; Dhamija, 2016; Kulkarni, Tang, Bhardwaj, Bernes, & Grebe, 2016; Menke et al., 2016) exhibit developmental delay. Although we have assessed movement abnormalities of adult mice, we are still unclear about whether our mouse models replicate this seemingly universal symptom for human G203R and R209H patients. Heyser (Heyser, 2004) published a very detailed milestone assessment for rodents that can be adopted by this project. Understanding the role of $G\alpha_o$ role in neural development

is crucial for understanding *GNAO1*-associated disorders, since developmental delay seems to be unrelated to the genotype-phenotype correlation that we established between epilepsy and movement disorders. Patients with both GOF/NF and LOF *GNAO1* mutations exhibit developmental delay. So far, apart from $G\alpha_o$'s regulation of neurite outgrowth (Strittmatter, Fishman, et al., 1994) and growth cone collapse (Igarashi et al., 1993) *in vitro*, there has been little research done on the role of $G\alpha_o$ in mammalian neuronal development (Tanaka, Treloar, Kalb, Greer, & Strittmatter, 1999).

In addition to confirming whether G203R and R209H mice have developmental delay, how $G\alpha_o$ might play a role in regulating neuronal development should also be addressed. At the *in vitro* level, primary neurons from brains of G203R and R209H mutant mice can be isolated for assessing neurite outgrowth, axonal elongation, and growth cone development. Mechanistically, one interesting question is how G203R and R209H mutations in $G\alpha_o$ affect its interaction with GAP-43. GAP-43 (also called neuromodulin or B57) is a “growth” or “plasticity” related presynaptic protein that plays a key role in modulating growth cone signal transduction (Strittmatter, Valenzuela, Vartanian, et al., 1991), axonal growth and guidance (Goslin, Schreyer, Skene, & Banker, 1988), and synapse formation (Holahan, 2017). Homozygous mice lacking GAP-43 die in the early postnatal period (Strittmatter, Fankhauser, Huang, Mashimo, & Fishman, 1995) and heterozygous GAP-43 deficient mice survived but suffered from neuronal developmental defects that last through adulthood (Latchney et al., 2014). The amino-terminal domain

of GAP-43 promotes release of GDP from and binding of GTP to $G\alpha_o$ (Strittmatter, Igarashi, & Fishman, 1994; Strittmatter et al., 1990; Strittmatter, Valenzuela, Sudo, Linder, & Fishman, 1991). Co-expression of $G\alpha_o$ and GAP-43 can also be seen throughout mouse embryo development stages (Schmidt, Zubiaur, Valenzuela, Neer, & Drager, 1994). GAP-43 increases the GTP γ S binding activity of $G\alpha_o$ (Jiang & Bajpayee, 2009; Yang, Wan, Song, Wang, & Huang, 2009). It is possible that *GNAO1* mutants affect the $G\alpha_o$ and GAP-43 interaction by changing the guanine nucleotide exchange rate.

Another interactor of $G\alpha_o$ protein that may be of interest here is GRIN1 (G protein-regulated inducer of neurite outgrowth 1) encoded by the *GPRIN1* gene. GRIN1 binds to both $G\alpha_i$ and $G\alpha_o$ protein through the GRIN1 carboxyl-terminal region (Chen et al., 1999). Co-expression of GRIN1 and constitutively active $G\alpha_o$ protein (Q205L) induces neurite extensions in Neuro2A cells through the activation of Cdc42 (Nakata & Kozasa, 2005). Like GAP-43, GRIN1 also co-localizes with $G\alpha_o$ protein expression at neuronal dendrites and axons in different regions of adult mouse brains (Masuho et al., 2008).

There are other possibilities for how $G\alpha_o$ protein may play a role in mouse development. Understanding the mechanisms of *GNAO1*-related neurodevelopmental disorders might provide unique insights into mechanisms of *GNAO1*-related movement disorder and epilepsy after birth.

5.3.2 How does the G203R mutation in $G\alpha_o$ lead to epileptogenesis?

One puzzle between the patients with R209H and G203R mutations is why R209H patients very seldom exhibit epilepsy, while all of the G203R patients present with both epilepsy and movement disorders (Table 5.1) (Feng, Khalil, Neubig, & Sidiropoulos, 2018). This difference was also confirmed in our animal models with the PTZ kindling study (Chapter 3) where male G203R mutants have enhanced kindling responses to PTZ. We did not observe spontaneous seizures by G203R mice but we have not done EEG recordings so spontaneous seizures are not entirely ruled out. Three of the *Gnao1*^{+G203R} mutant mice did die in adulthood (Figure 3.1C) - similar to the G184S mutant mice that do have rare spontaneous seizures (Kehrl et al., 2014).

The mechanisms of epileptogenesis in the G203R mutant are unclear. Since $G\alpha_o$ and $G\beta\gamma$ are involved in multiple aspects of neurobiology, possible mechanisms of G203R mutation-induced epileptogenesis includes: 1) altered neurotransmitter release; 2) a loss of subset of neurons; 3) altered neurite density and/or synaptogenesis; 4) changed membrane properties (lower threshold for activation); 5) altered cell morphology; and/or 6) malformation of cortical/hippocampal development.

Activation of $G\alpha_o$ and $G\beta\gamma$ is well-studied for regulation of neurotransmitter release pre-synaptically (Stephens, 2009) and membrane potential post-synaptically (Beckstead & Williams, 2007; Newberry & Nicoll, 1985). It would not be surprising if the G203R GOF mutant has a stronger influence on neurotransmitter release in brain regions that are

closely related to epileptogenesis, while the R209H mutant with NF behavior does not. In addition, due to the role of $G\alpha_o$ and $G\beta\gamma$ in regulating neuronal development, it is possible that the $G\alpha_o$ protein with the G203R mutation leads to malformation during one or more neural developmental stages. This hypothesis can be tested by carefully monitoring the developmental states of G203R mice at the behavioral, morphological and cellular levels. Malformations of cerebral cortical development are common causes of neurodevelopmental delay and epilepsy (Barkovich, Guerrini, Kuzniecky, Jackson, & Dobyns, 2012). The alteration of one or several developmental steps, including proliferation of neural progenitors, migration of neuroblasts, layer organization, or neuronal maturation may all lead to cortical malformation (Pang, Atefy, & Sheen, 2008). Previously, I have stained and observed the cerebellum region of adult *Gnao1*^{+/*G184S*} mice, which exhibited similar behavioral abnormalities with *Gnao1*^{+/*G203R*} mice (Chapter 3). There were no major abnormalities in the morphology of the cerebellum in the G184S mice except for a slight decrease in lobule number (Figure S5.7). No staining for the G203R mutant mouse brain was done for the purpose of observing the gross morphology.

Activated $G\alpha_o$ and $G\beta\gamma$ both play a role in regulating these developmental steps. The literature shows that stimulation of $G\alpha_o$ inhibited neuronal migration of the EP cells, which are a set of ~300 gut neurons begin to express $G\alpha_o$ at the time coincident with their migration along the stereotyped pathways (Copenhaver & Taghert, 1989; Horgan &

Copenhaver, 1998; Horgan, Lagrange, & Copenhaver, 1994). Also, G β 1 knockout mouse embryos developed neural tube defects, abnormal actin organization, and microcephaly and then died at P2 (Okoe & Iwakura, 2010). In the G203R mice or human patients, the G203R mutant may trigger an abnormal formation at one or multiple embryonic stages in cortex or hippocampus, resulting in susceptibility to epilepsy. For example, mutant G α_o may cause the failure of GABAergic neurons to migrate toward the cortex thus altering the excitatory/inhibitory balance. This could result in network hyperactivity (Wonders & Anderson, 2006). Or mutant G α_o may cause abnormal SNAP-25 function (Zurawski, Rodriguez, Hyde, Alford, & Hamm, 2016), which could lead to derangements of synaptic transmission in the hippocampus.

5.3.3 How do G203R and R209H mice differ in movement disorder phenotypes?

Although dystonia and chorea/athetosis are both seen in G203R and R209H patients, G203R mice and R209H mice exhibit a striking difference in their movement disorder phenotypes. G203R mice were less able to remain on the RotaRod, had decreased capability of lifting up heavy weights, and had more abnormal gait characteristics like human patients with G203R mutation. They did not exhibit abnormalities in the open field test. In contrast, R209H mice mainly exhibited increased locomotor activity in the open field arena, which has not been seen in any previous *Gnao1* mouse model. While it is understandable that mouse models will not precisely reflect human symptoms, it is still an interesting question on how mutations in the same gene cause different movement

phenotypes in rodents. One hypothesis is that R209H and G203R mutations affect different brain regions.

$G\alpha_o$ expression seems to be ubiquitous in mammalian brains, however, due to the complex and diverse neural networking system in different regions, it is possible that G203R and R209H mutations have effects distinct from each other. $G\alpha_o$ staining is enriched in the cerebral cortex (particularly the molecular layer), the neuropil of the hippocampal formation, and in the striatum, substantia nigra pars reticulata, and in the molecular layer of the cerebellum (Worley, Baraban, Van Dop, Neer, & Snyder, 1986). Coincidentally, dystonia is commonly linked with injury to the basal ganglia, thalamus, brainstem, and the cerebellum. Chorea is associated with disorders of the cerebral cortex, basal ganglia, cerebellum and thalamus (Sanger et al., 2010). Both disorders are seemingly associated with brain areas with significant $G\alpha_o$ protein expression levels.

In chapter 4, I showed that the G203R mutation causes a reduced frequency of GABA release in cerebellar slices from G203R mice. However, we have not yet tested changes due to the G203R mutation in other brain regions, so we are not sure whether signaling in the striatum is also affected. The brain regions affected by the R209H mutation are not yet known. To quickly locate the brain regions related to the movement phenotype, we can do regional injection of oxotremorine (Pelosi, Menardy, Popa, Girault, & Herve, 2017) or pertussis toxin (PTX) to help exclude the irrelevant brain regions. This will be a crucial finding to help guide follow-up research on more detailed mechanisms of

the movement disorder and to find more targeted therapeutic methods for *GNAO1*-associated movement disorders.

5.3.4 How is sex involved in abnormalities of the *Gnao1* mutants?

GNAO1-associated neurological disorders are more prevalent in females than males overall according to currently published reports (Chapter 1), but it may also only be due to relatively small patient numbers. Alternatively, a more severe male phenotype would cause a premature death of the fetus. However, in animal models we have observed striking sex-related phenotypes. In G184S GOF mouse models, female mice are more prone to both abnormal movements and seizures; while in G203R mouse models, male mice developed more a significant phenotype compared to female for both movement disorders and epilepsy. Interestingly, R209H mice do not seem to differ much in sex-related phenotypes. Although sex differences in human *GNAO1* patients remains unclear, it is still interesting to consider the sex differences of the *Gnao1* mutant animals in terms of their behavioral abnormalities.

Biological differences between the male and female sexes contribute to many sex-specific illness and disorders. These differences are not only due to gonadal hormone secretion-related events, such as differences in neuroanatomy, synaptic patterns, and neuronal density, but also due to non-hormonal related aspects, particularly direct gene products mediated by genes located on the X- and Y-chromosomes (Ngun, Ghahramani, Sanchez, Bocklandt, & Vilain, 2011).

Most researchers attribute the sex differences in neurological disorders to the actions of estrogens, progestins, and androgens. After all, those hormones regulate early neurodevelopment to program the brain to be sexually bimorphic, and later activate circuitries that trigger adult behaviors after puberty (Kight & McCarthy, 2014). The actions of gonadal hormones lead to differences in brain structure (Farrell, Gruene, & Shansky, 2015; Phan et al., 2012), connectivity (Ingalhalikar et al., 2014), signaling (Harte-Hargrove, Varga-Wesson, Duffy, Milner, & Scharfman, 2015; Skucas et al., 2013), responsivity (Garrett & Wellman, 2009), plasticity (Gould, Woolley, Frankfurt, & McEwen, 1990; Greenough, Carter, Steerman, & DeVoogd, 1977; Parducz et al., 2006), and even adult neurogenesis (Galea, Spritzer, Barker, & Pawluski, 2006; Livneh & Mizrahi, 2011; Vivar, Peterson, & van Praag, 2016). This makes hormone levels and functions an important aspect to consider for the mechanisms of sex differences in our *Gnao1* mutant mouse models. $G\alpha_o$ may directly play a role in this hormonal regulation. Estrogen attenuates the reuptake of both endogenous and exogenous dopamine in the striatum and nucleus accumbens by altering the D_2 receptor responsiveness (Thompson & Certain, 2005). Estrogen also destabilizes $GABA_B$, $5-HT_{1a}$, $5-HT_{1b}$ and CB1 receptors after a short exposure (Mize & Alper, 2000). Progesterone activates progestin membrane receptors to down-regulate adenylyl cyclase activities, which can be blocked by PTX (Thomas et al., 2007). Nuclear localization of androgen receptors is also controlled by G_i -specific RGS proteins (Rimler, Jockers, Lupowitz, & Zisapel, 2007).

Emerging research has also shown that sex differences are mediated by mechanisms other than action of the hormone secretions. If hormones do not explain the sex differences, then we should consider the different effects of XX versus XY sex chromosome complement. After all, every neuron, glia, or other cell type carries either the male chromosomes (XY) or female chromosomes (XX), but not both (Arnold & Burgoyne, 2004). Although the traditional view attributes sex differences in neuronal development to different hormonal exposure, recent research shows that some non-gonadal tissues, including the brain, are sexually dimorphic even when they develop in a similar endocrine environment (Arnold & Burgoyne, 2004). For example, primary cell cultures harvested from the XX and XY mesencephalon and diencephalon before the differentiating actions of gonadal hormones are present can develop into different numbers of dopamine neurons or prolactin neurons, respectively (Beyer, Kolbinger, Froehlich, Pilgrim, & Reisert, 1992; Beyer, Pilgrim, & Reisert, 1991). Another example is the fact that male and female mammalian embryos develop at different rates at ages before the onset of gonadal differentiation. There is evidence supporting that genes on the Y chromosome enhance the rate of embryonic development (Burgoyne, 1993; Burgoyne et al., 1995); while X chromosome genes slow down development (Thornhill & Burgoyne, 1993). Another aspect is the presence of the *SRY* gene on the Y-chromosome. Research shows that animals with *Sry gene* are associated with a higher number of tyrosine hydroxylase (TH⁺) cells compared to those without *Sry* (Ngun

et al., 2011). In humans, SRY expression is seen in both adult and fetal brains (Clepet et al., 1993; Mayer, Lahr, Swaab, Pilgrim, & Reisert, 1998). Also *Sry* has a direct effect on the expression of TH in the substantia nigra in the rat (Dewing et al., 2006). Effects of the *SRY* gene are suspected to contribute to the susceptibility of men to Parkinson's disease (PD).

Previous research has not yet established the interconnection between functions of $G\alpha_o$ and other embryonic developmental events in mammals; therefore it is hard to determine whether $G\alpha_o$ plays a role in the embryonic development before or after gonadal hormones are present, or both. Besides, two different GOF mutations, G184S and G203R, seem to affect a different sex in terms of the severity of the motor behavior and seizures in mice (Chapter 3). This observation provides additional evidence of a pathophysiological mechanism more complex than just $G\alpha_o$ -regulated inhibition of cAMP. The sex differences in the G184S and G203R mice should each be established as a separate project with a deeper understanding of the differences between the G184S and G203R mutant mice. Here, I will mainly focus on the discussion of the male-dominant phenotype in the G203R mutant mice.

From a hormonal secretion aspect, it is possible that estrogen exerts a neuroprotective effect in the female mice (Brann, Dhandapani, Wakade, Mahesh, & Khan, 2007; Green & Simpkins, 2000); therefore the male G203R mice have a more severe genotype. Research showed that estrogen reduced dopamine D_2 receptors by 20%

to 25% (Chavez et al., 2010), which could counterbalance the GOF mechanisms induced by the G203R mutant in female mice, and leave the male mice affected. Another possibility would be that $G\alpha_o$ with the GOF G203R mutation affects the nuclear localization of androgen receptors in the hippocampus (Rimler et al., 2007), which reduces the serum androgen level, and consequently lead to reduction of the GABAergic inhibition (Frye, 2006; Reddy & Jian, 2010). This would expose the male G203R mice to the risk of disease such as temporal lobe epilepsy (Harden & MacLusky, 2004, 2005; Herzog, 1991).

From a non-hormonal perspective, we should look into the embryonic developmental stages of the G203R mutant mice to see if it correlated with the Y-chromosome regulated increase in rate of development. Otherwise, we should also consider the *SRY* gene's modulation of dopamine biosynthesis and motor function. *SRY*, as a transcription factor, can directly activate the TH promoter, which enhances expression of tyrosine hydroxylase, the rate-limiting enzyme of dopamine synthesis (Czech et al., 2012). Although it is yet to be established whether the G203R mutation could affect dopamine transmission or the survival of dopamine neurons in the brain, the presence of the *SRY* gene on the Y-chromosome in the male G203R mutant mice could potentially exacerbate the effect of increased dopamine in causing abnormal movements (Cepeda, Murphy, Parent, & Levine, 2014).

While we are not yet sure of the effect of the R209H mutation on $G\alpha_o$'s functional pathways, R209H mutants may not exhibit as extensive an effect as G203R mutants do. This may be why we do not see a significant sex difference in the R209H mutant mice.

5.4 Development of a high-throughput assay for drug repurposing or drug development

Calcium ions participate in a variety of physiological and pathological mechanisms. In presynaptic neurons, calcium levels regulate neurotransmitter release. Detectable calcium signaling results from a complicated interaction between activation and inactivation of both intracellular and extracellular calcium channels. This interaction can be observed with calcium-sensing probes such as Fura-2 or Fluo-4. Neural calcium signaling often results in sequential regenerative discharges of stored calcium, a process referred to as calcium oscillation (Dupont, Combettes, Bird, & Putney, 2011). Calcium oscillations can be categorized into two classes based on the involvement of intracellular calcium storage. The intracellular release of calcium most commonly derives from the endoplasmic reticulum (ER) driven by inositol 1,4,5-trisphosphate (IP_3) (Streb, Irvine, Berridge, & Schulz, 1983). However, in excitable cells like neurons, the increase of intracellular calcium levels can also be initiated by activation of membrane channels that lead to the influx of calcium ions from the extracellular space (Tsien et al., 1986). This may further facilitate intracellular calcium release from the endoplasmic reticulum (ER) into the cytoplasm (Fabiato, 1983).

Dissociated mouse cortical neurons can re-associate *in vitro* to form connected synaptic networks. This method provides an assay to reduce the expense and labor of testing drugs *in vivo* and provides a potential approach for high-throughout screening. Previous research has shown that neural calcium oscillations involve the activation of NMDA, AMPA/kainate receptors, and mGluR (Dravid & Murray, 2004; Nash et al., 2002; Robinson, Kawahara, et al., 1993). Also, the rising phase of each calcium spike is usually coincident with a brief burst of action potentials (Murphy, Blatter, Wier, & Baraban, 1992). Additionally, calcium oscillations measured from dissociated rat cortical neurons are dependent on the influx of extracellular calcium rather than mobilization from intracellular stores (Wang & Gruenstein, 1997). Oscillating calcium activity in dissociated neurons is also temporally correlated with the maturity of neurons and the time in culture to allow connections between neurons. Generally, synchronized calcium oscillations occur in around DIV7-DIV10 after plating and they plateau at DIV13 (Pacico & Mingorance-Le Meur, 2014). This is coincident with a burst of synapse formation that happens around DIV14 (Ichikawa, Muramoto, Kobayashi, Kawahara, & Kuroda, 1993). Thus, the synchronized calcium-spiking events seem to be an emergent property due to the formation of a large number of glutamatergic synapses. In agreement with earlier studies (Robinson, Kawahara, et al., 1993; Robinson, Torimitsu, Jimbo, Kuroda, & Kawana, 1993; Wang & Gruenstein, 1997), my preliminary data showed that removal of extracellular Mg^{2+} induces cultured mouse neurons to undergo synchronized calcium

oscillations (Figure S5.5). Calcium oscillation activities are also dependent on extracellular calcium concentrations (Figure S5.5). Although previous studies showed that inhibition of voltage-gated K^+ channels induces calcium oscillation (Wang & Gruenstein, 1997), we found that high levels of extracellular K^+ also suppress calcium oscillation activity (Figure S5.5). Since the calcium oscillations shown here are uniform and stationary, the analysis can be accomplished by Fast Fourier Transform (FFT) that will identify both the frequency and the amplitude of these oscillations (Barhoumi, Qian, Burghardt, & Tiffany-Castiglioni, 2010; Vajda, Donnan, Phillips, & Bladin, 1981).

Here, we intend to use this technique to explore whether there is any difference between WT and G203R mice in the calcium oscillatory activity. As discussed previously, the $G\alpha_o$ protein mainly functions to inhibit synaptic neurotransmitter release. However, since $G\alpha_o$ is present at both excitatory and inhibitory synapses, it is hard to predict the end result of abnormalities in $G\alpha_o$ regulation. Based on what we observed in Chapter 4, the G203R GOF $G\alpha_o$ protein mainly enhanced presynaptic inhibition of GABA release but has less to no inhibitory effect on glutamate release. Therefore, we hypothesize that the GOF G203R mutant enhances suppression of GABA release thereby increasing excitability of the neural network, which leads to increased calcium spiking events. Our preliminary study confirmed our hypothesis that G203R mutant animal cortical cell cultures (both $Gnao1^{+/G203R}$ and $Gnao1^{G203R/G203R}$) have more calcium spikes (Figure S5.6). However, it has been challenging to optimize this technique for high-throughput

screening. The data generated between experiments are highly variable; therefore comparison between plates in multiple experiments done at different times requires a standard control for each plate. Another issue is the variability between animals, which is hard to avoid but can be minimized by increasing the n number for experiments. With further optimization, calcium oscillation can utilize primary neurons from different brain regions to address the different oscillatory activities between WT and mutant mice. Ultimately, this may be used in high throughput methods to identify candidate drugs or receptor targets for drug repurposing or new drug development.

5.5 Impact of work in this thesis on the field

This thesis is the summary of the first project to explore the *GNAO1*-related rare but serious neurologic disorders in children. I defined the biochemical correlation between the functional changes of the human *GNAO1* mutants and the patients' neurological symptoms. In addition, our work also provided the first human avatar *Gnao1* mutant mice and verified their value in studying the neurophysiological mechanisms of *GNAO1* mutations. Subsequent mechanistic and intervention studies should greatly enhance the development of potential therapeutic strategies for these devastating childhood neurologic disorders. In a broader aspect, due to the ubiquitous expression of $G\alpha_o$ (encoded by *GNAO1*) and its multiple effectors, our study may enhance understanding of neurological disorders that involve the same pathways shared by the $G\alpha_o$ protein. Similar pharmacological interventions may also be valuable for genetic conditions

involving *GNB1*, *ADCY5*, *PDE10A* and *GNAL*. Furthermore, our study may serve as a prototype for other correlations between reported monogenic mutations and human neurological disorders.

APPENDIX

APPENDIX

SUPPLEMENTAL DATA

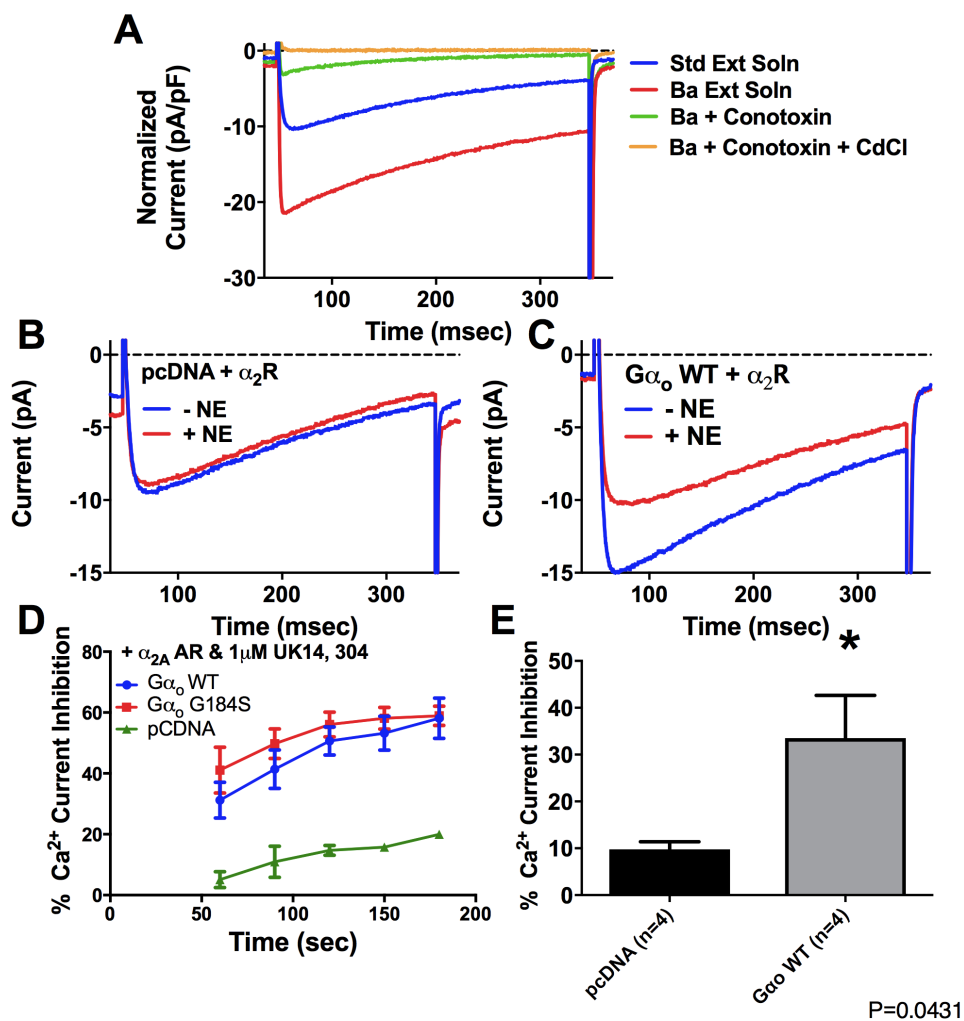


Figure S5.1 α_2A R activates $G\alpha_o$, which inhibits N-type calcium channels in G1A1 cells. GOF mutation G184S enhance the inhibition of calcium currents. (A) G1A1 cells stably express N-type calcium channels, which can be blocked by MVIIa but not entirely. Previous report showed G1A1 cells have endogenous L-type calcium channels. All membrane calcium channels can be blocked by Cd^{2+} ions and enhanced by Ba^{2+} ions. (B) G1A1 cells have negligible amount of $G\alpha_{i/o}$ proteins, therefore activating α_2A R alone cannot inhibit the calcium currents. (C) G1A1 cells with transiently transfected $G\alpha_o$

Figure S5.1 (cont'd) protein and $\alpha_{2A}R$ can lead to the inhibition of calcium current when $\alpha_{2A}R$ is activated by norepinephrine (NE). (D) GOF *GNAO1* mutation G184S causes a slight enhanced inhibition of calcium current immediately after adding selective $\alpha_{2A}R$ agonist UK14, 304, however, the maximum inhibition between WT and G184S is not significant. WT (n=6), G184S (n=7), pcDNA (n=3). (E) G184S (n=4) significantly enhanced inhibition of N-type calcium channels comparing to WT (n=4). Unpaired Student's t-test; p=0.0431.

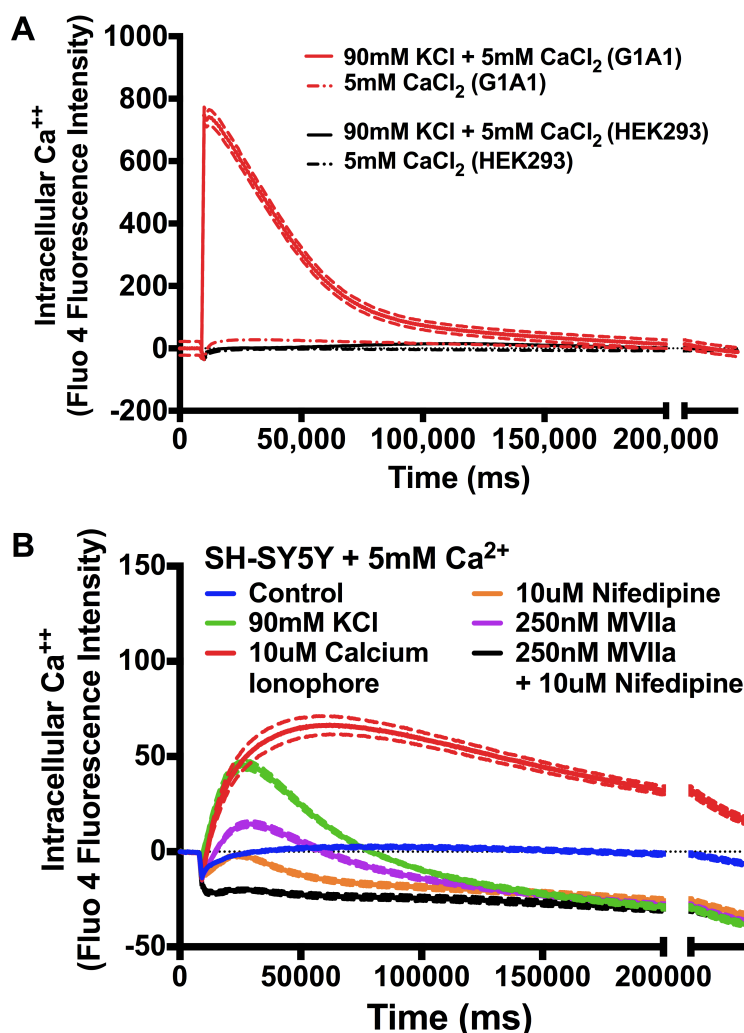


Figure S5.2 Both G1A1 and SH-SY5Y cells are good candidates to study mutant $G\alpha_o$'s effects on N-type calcium channels with Fluo 4-NW dye in a Hamamatsu μ CELL plate reader. (A) N-type calcium channels in G1A1 cells are activated by 90 mM

Figure S5.2 (cont'd) KCl with the presence of 5 mM CaCl₂. (B) SH-SY5Y cells have more types of endogenous calcium channels. All calcium currents can be induced by 90 mM KCl. N-type calcium channels can be blocked by 250 nM MVIIa, and L-type calcium channels can be inhibited by 10 μM Nifedipine.

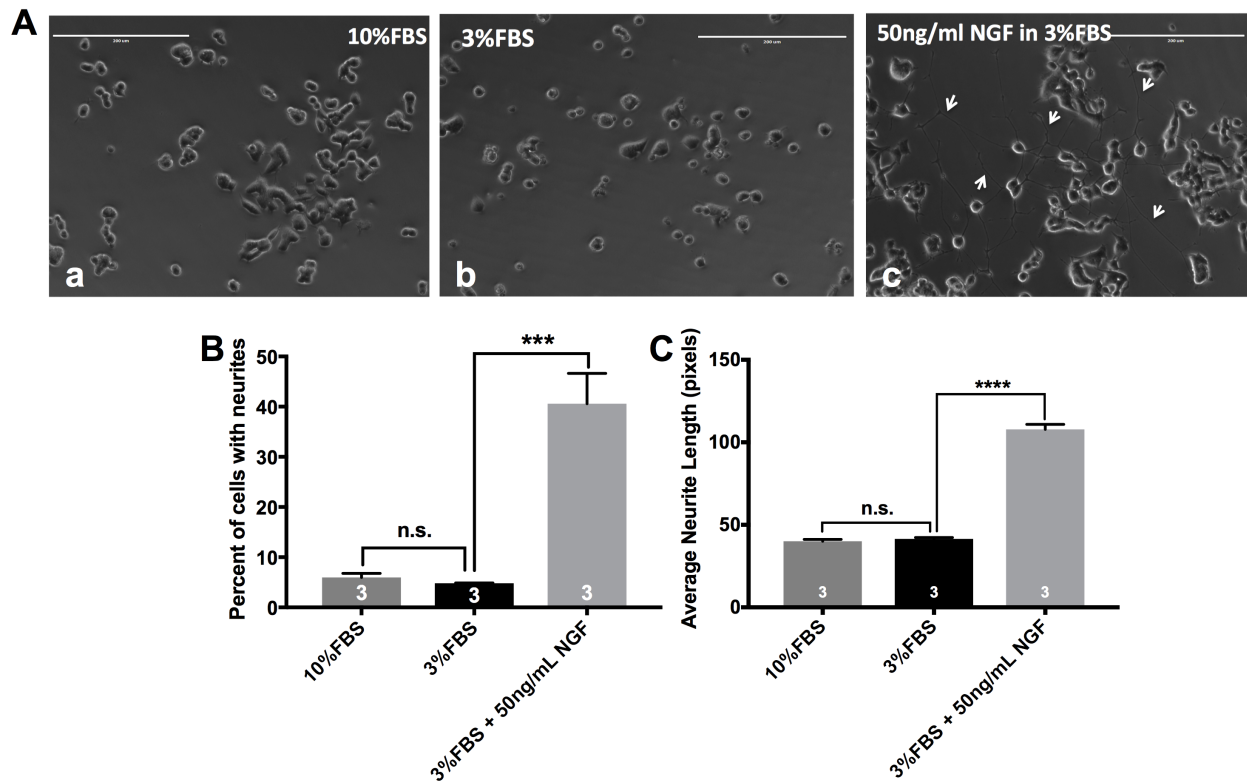


Figure S5.3 Neurite outgrowth in rat pheochromocytoma cells (PC12) can be induced by 50 ng/mL Nerve Growth Factor (NGF) in normal growth medium with reduced serum. (A) Representative pictures showing PC12 cells growth after 48 hrs in (a) normal growth medium, (b) normal growth medium with reduced FBS (3% FBS), and (c) 50 ng/mL NGF in normal growth medium with 3% FBS. (B) NGF significantly promotes the percent of cells with visible neurites (n=3; Unpaired Student's t-test; p<0.001). Spontaneous neurite outgrowth does occur without any NGF. (C) NGF also significantly increases the neurite length from PC12 cells (n=3; Unpaired Student t-test; p<0.0001).

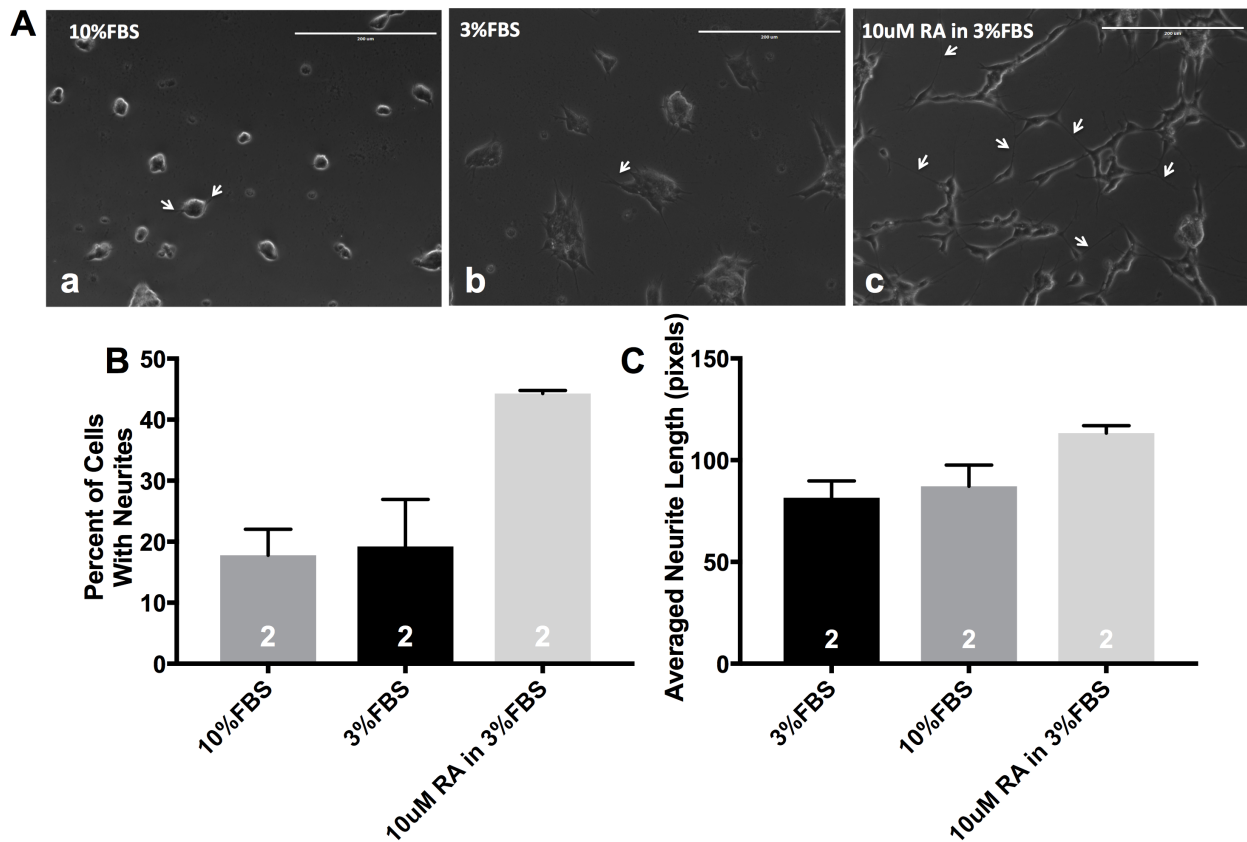


Figure S5.4 Neurite outgrowth can be induced by 10 μM retinoid acid (RA) in normal growth medium with reduced serum (30% FBS) in human neuroblastoma cells (SH-SY5Y). (A) SH-SY5Y cells are largely non-differentiated in normal growth medium with 10% FBS (a); reduced serum induces morphological changes and neurite outgrowth in SH-SY5Y cells (b); 10 μM RA in 3% FBS medium induces the majority of cells to differentiated (c). (B) Preliminary studies show that RA increases the percent of cells with neurites, (C) but does not seemingly affect the average neurite length. Since the n number is small, there is no significance in comparison but the trend of change is obvious.

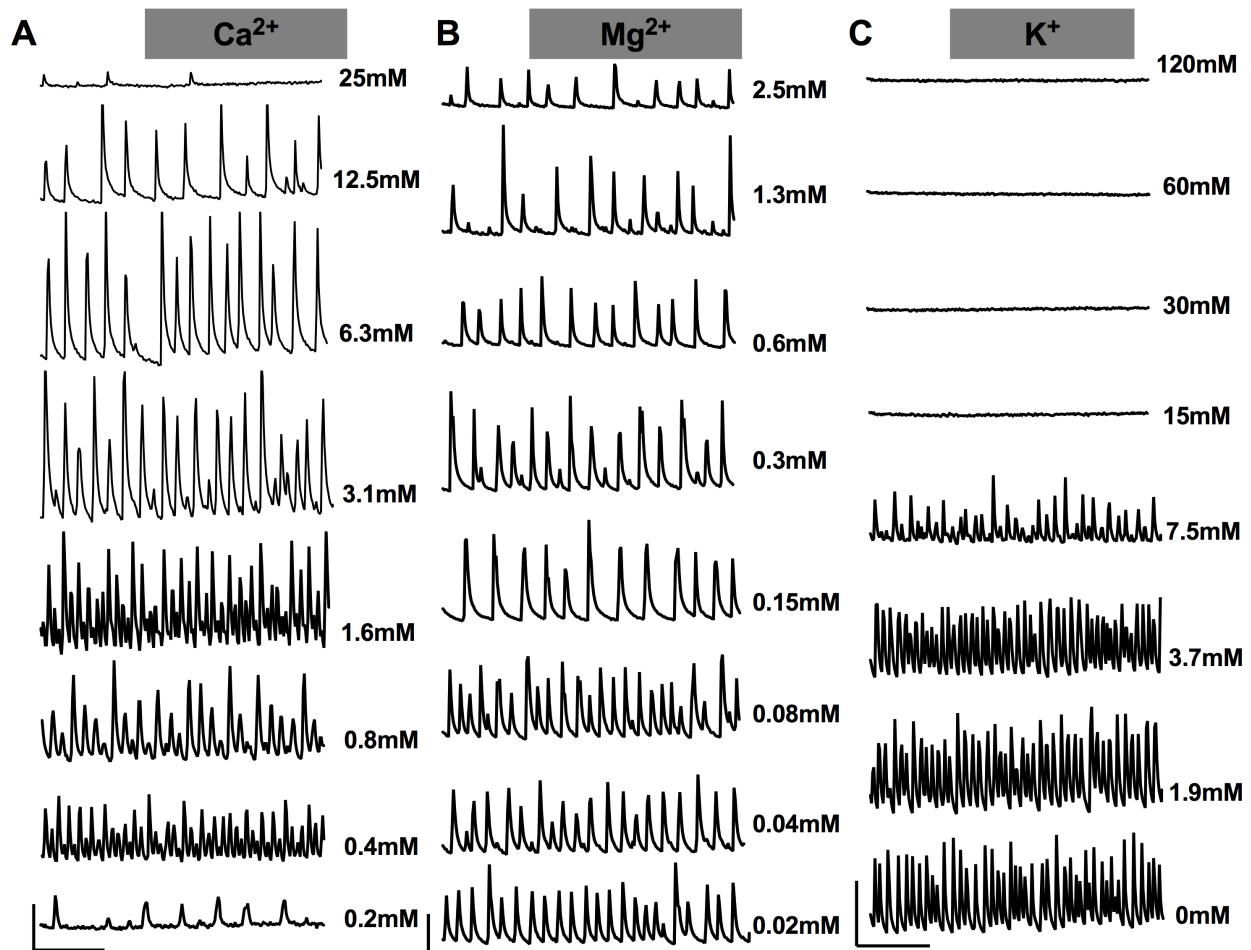


Figure S5.5 Representative traces of modulations in calcium oscillations with different ion concentration in mixed cortical cultures from a WT mouse. (A) Extracellular calcium concentration is crucial for calcium spiking events. The frequency of calcium oscillation increases with lower calcium concentrations but the amplitudes of calcium spikes peaks with a calcium concentration between 6.3 mM and 3.1 mM. (B) Higher concentrations of magnesium inhibit calcium oscillatory activities and lower magnesium concentrations induce them. All magnesium concentration responses were done with 5 mM calcium present. (C) When potassium concentration is above 15 mM, calcium oscillatory activities are completely quiescent. Lower concentrations of potassium facilitate calcium oscillation. All potassium concentration responses were done with 5 mM calcium present.

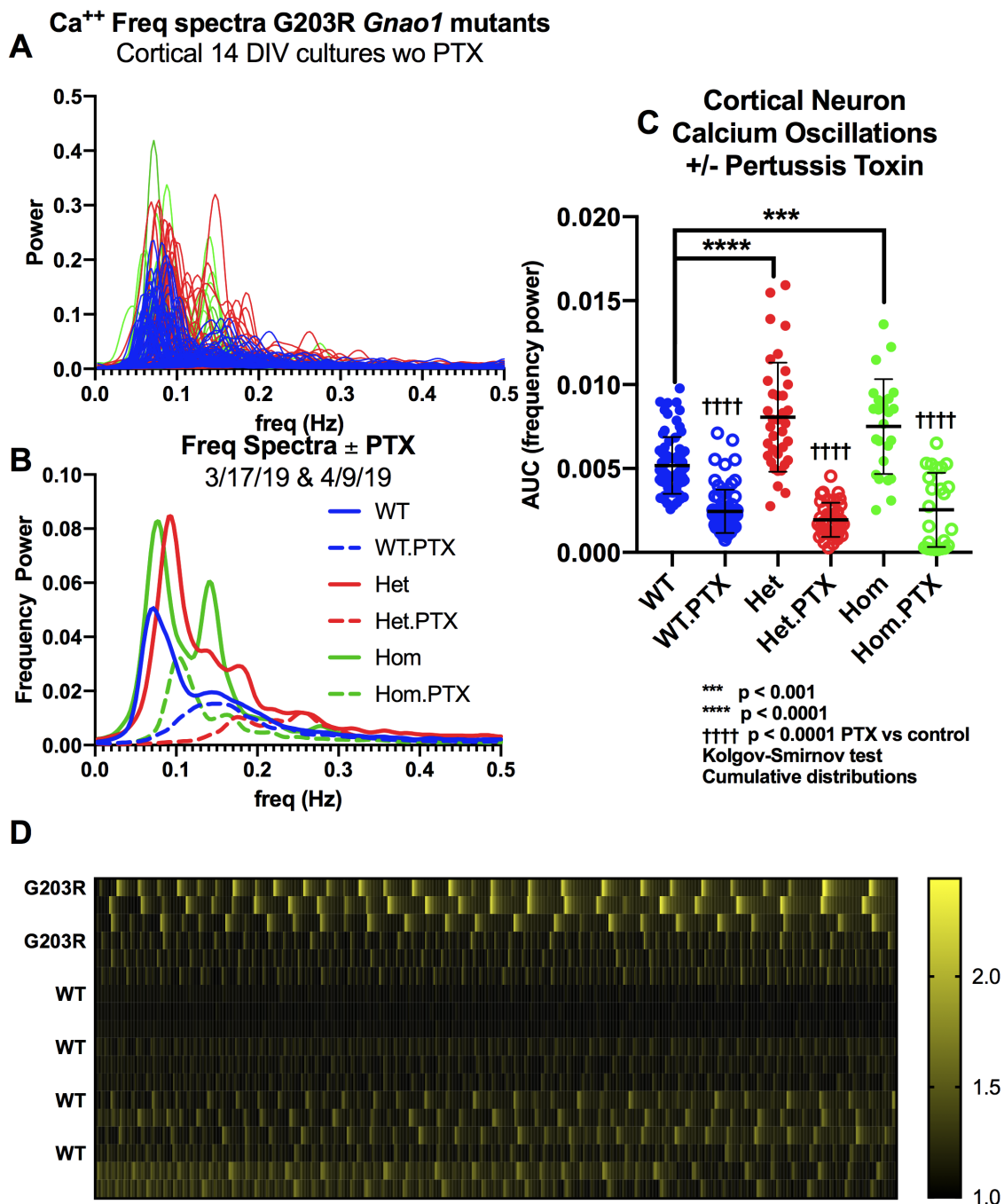


Figure S5.6 High-throughput assessment of neural excitability in cortical cultures. Cortical cultures (neurons and glia) from P0 *Gnao1*^{+G203R} mutant mice and WT littermates (triplicate wells shown) were prepared in 96-well plates, allowed to form

Figure S5.6 (cont'd) connections (14 DIV), labeled with Fluo-4-NW calcium indicator, then read in a Hamamatsu Cell reader for 10 minutes. Power spectra - (A) (all) & (B) (mean \pm SD) of 10 WT (96 wells), 10 heterozygous (Het 66 wells), and 2 homozygous (Homo 24 wells) pups under conditions showing differences in epilepsy studies (CaCl₂ 5 mM and KCl 7.5 mM), (C) AUC of Ca²⁺ power spectra for all wells. Due to the non-normal distribution, statistical analysis used the non-parametric Kolgov-Smirnov test of cumulative distributions (GraphPad Prism 8.1). (D) Heat map of Ca²⁺ levels - 3 wells per mouse (4 WT & 2 Het) at CaCl₂ 5 mM and MgCl₂ 7.5 mM.

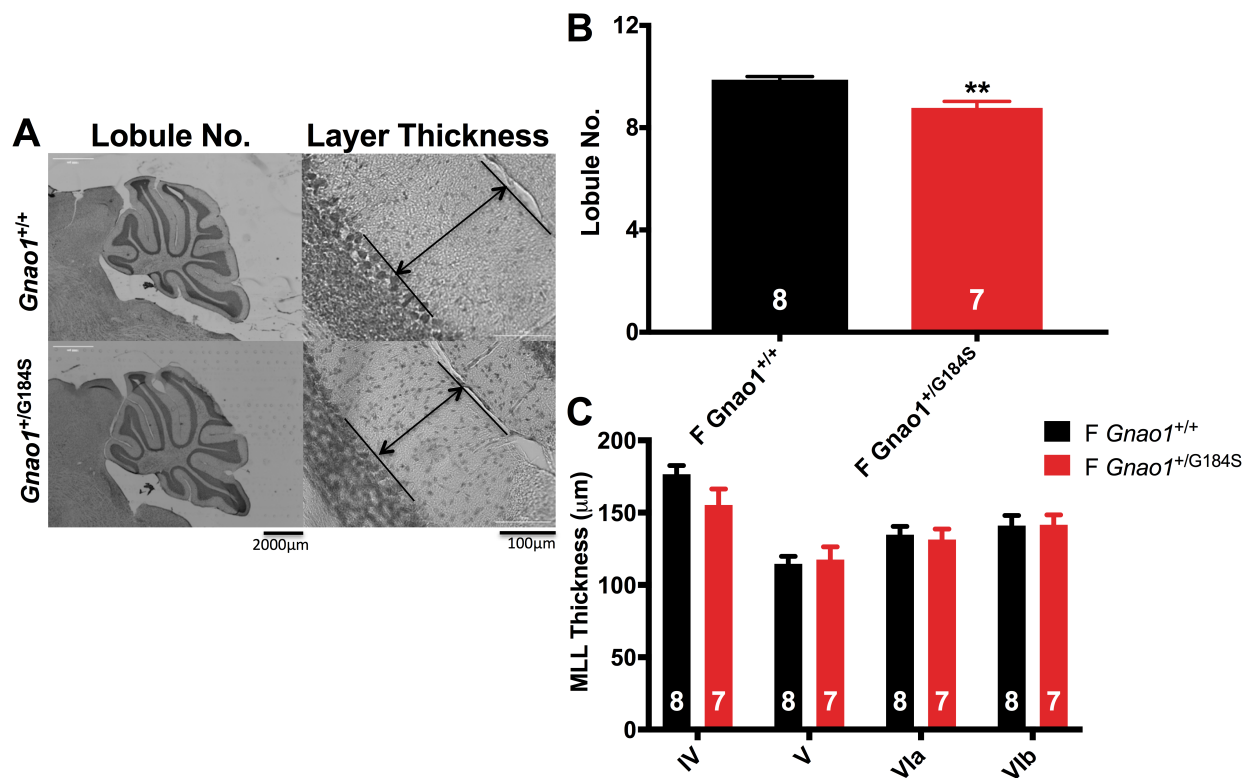


Figure S5.7 Nissl staining compares gross morphological changes in cerebellum from *Gnao1*^{+/G184S} and *Gnao1*^{+/+} mice at age 8 weeks old. (A) No obvious gross difference in cerebellum region of *Gnao1*^{+/G184S} and *Gnao1*^{+/+} mice. (B) Lobule number is slightly lower in *Gnao1*^{+/G184S} mice (4 slices were measured from each mice; *Gnao1*^{+/+}: n=8, *Gnao1*^{+/G184S}: n=7). (C) Molecular layer thickness of IV, V, VIa and VIb in the cerebellar region of *Gnao1*^{+/G184S} and *Gnao1*^{+/+} mice does not show significant difference

Figure S5.7 (cont'd) (12 repeated measurements were obtained from 4 slices for each region per mouse; *Gnao1*^{+/+}: n=8, *Gnao1*^{+/G184S}: n=7).

REFERENCES

REFERENCES

- Aglah, C., Gordon, T., & Posse de Chaves, E. I. (2008). cAMP promotes neurite outgrowth and extension through protein kinase A but independently of Erk activation in cultured rat motoneurons. *Neuropharmacology*, *55*(1), 8-17. doi:10.1016/j.neuropharm.2008.04.005
- Ananth, A. L., Robichaux-Viehoever, A., Kim, Y. M., Hanson-Kahn, A., Cox, R., Enns, G. M., . . . Bernstein, J. A. (2016). Clinical Course of Six Children With GNAO1 Mutations Causing a Severe and Distinctive Movement Disorder. *Pediatr Neurol*, *59*, 81-84. doi:10.1016/j.pediatrneurol.2016.02.018
- Andrade, R., Malenka, R. C., & Nicoll, R. A. (1986). A G protein couples serotonin and GABAB receptors to the same channels in hippocampus. *Science*, *234*(4781), 1261-1265.
- Arnold, A. P., & Burgoyne, P. S. (2004). Are XX and XY brain cells intrinsically different? *Trends Endocrinol Metab*, *15*(1), 6-11.
- Arya, R., Spaeth, C., Gilbert, D. L., Leach, J. L., & Holland, K. D. (2017). GNAO1-associated epileptic encephalopathy and movement disorders: c.607G>A variant represents a probable mutation hotspot with a distinct phenotype. *Epileptic Disord*, *19*(1), 67-75. doi:10.1684/epd.2017.0888
- Barhoumi, R., Qian, Y., Burghardt, R. C., & Tiffany-Castiglioni, E. (2010). Image analysis of Ca²⁺ signals as a basis for neurotoxicity assays: promises and challenges. *Neurotoxicol Teratol*, *32*(1), 16-24. doi:10.1016/j.ntt.2009.06.002
- Barkovich, A. J., Guerrini, R., Kuzniecky, R. I., Jackson, G. D., & Dobyns, W. B. (2012). A developmental and genetic classification for malformations of cortical development: update 2012. *Brain*, *135*(Pt 5), 1348-1369. doi:10.1093/brain/aws019
- Beacham, D. W., Blackmer, T., M, O. G., & Hanson, G. T. (2010). Cell-based potassium ion channel screening using the FluxOR assay. *J Biomol Screen*, *15*(4), 441-446. doi:10.1177/1087057109359807

- Beckstead, M. J., & Williams, J. T. (2007). Long-term depression of a dopamine IPSC. *J Neurosci*, 27(8), 2074-2080. doi:10.1523/JNEUROSCI.3251-06.2007
- Beyer, C., Kolbinger, W., Froehlich, U., Pilgrim, C., & Reisert, I. (1992). Sex differences of hypothalamic prolactin cells develop independently of the presence of sex steroids. *Brain Res*, 593(2), 253-256. doi:10.1016/0006-8993(92)91315-6
- Beyer, C., Pilgrim, C., & Reisert, I. (1991). Dopamine content and metabolism in mesencephalic and diencephalic cell cultures: sex differences and effects of sex steroids. *J Neurosci*, 11(5), 1325-1333.
- Bleakman, D., Bowman, D., Bath, C. P., Brust, P. F., Johnson, E. C., Deal, C. R., . . . et al. (1995). Characteristics of a human N-type calcium channel expressed in HEK293 cells. *Neuropharmacology*, 34(7), 753-765.
- Brann, D. W., Dhandapani, K., Wakade, C., Mahesh, V. B., & Khan, M. M. (2007). Neurotrophic and neuroprotective actions of estrogen: basic mechanisms and clinical implications. *Steroids*, 72(5), 381-405. doi:10.1016/j.steroids.2007.02.003
- Burgoyne, P. S. (1993). A Y-chromosomal effect on blastocyst cell number in mice. *Development*, 117(1), 341-345.
- Burgoyne, P. S., Thornhill, A. R., Boudrean, S. K., Darling, S. M., Bishop, C. E., & Evans, E. P. (1995). The genetic basis of XX-XY differences present before gonadal sex differentiation in the mouse. *Philos Trans R Soc Lond B Biol Sci*, 350(1333), 253-260 discussion 260-251. doi:10.1098/rstb.1995.0159
- Cepeda, C., Murphy, K. P., Parent, M., & Levine, M. S. (2014). The role of dopamine in Huntington's disease. *Prog Brain Res*, 211, 235-254. doi:10.1016/B978-0-444-63425-2.00010-6
- Chavez, C., Hollaus, M., Scarr, E., Pavey, G., Gogos, A., & van den Buuse, M. (2010). The effect of estrogen on dopamine and serotonin receptor and transporter levels in the brain: an autoradiography study. *Brain Res*, 1321, 51-59. doi:10.1016/j.brainres.2009.12.093
- Chen, L. T., Gilman, A. G., & Kozasa, T. (1999). A candidate target for G protein action in brain. *J Biol Chem*, 274(38), 26931-26938. doi:10.1074/jbc.274.38.26931

- Clepet, C., Schafer, A. J., Sinclair, A. H., Palmer, M. S., Lovell-Badge, R., & Goodfellow, P. N. (1993). The human SRY transcript. *Hum Mol Genet*, 2(12), 2007-2012. doi:10.1093/hmg/2.12.2007
- Copenhaver, P. F., & Taghert, P. H. (1989). Development of the enteric nervous system in the moth. I. Diversity of cell types and the embryonic expression of FMRFamide-related neuropeptides. *Dev Biol*, 131(1), 70-84.
- Corey, S., & Clapham, D. E. (2001). The Stoichiometry of Gbeta gamma binding to G-protein-regulated inwardly rectifying K⁺ channels (GIRKs). *J Biol Chem*, 276(14), 11409-11413. doi:10.1074/jbc.M100058200
- Czech, D. P., Lee, J., Sim, H., Parish, C. L., Vilain, E., & Harley, V. R. (2012). The human testis-determining factor SRY localizes in midbrain dopamine neurons and regulates multiple components of catecholamine synthesis and metabolism. *J Neurochem*, 122(2), 260-271. doi:10.1111/j.1471-4159.2012.07782.x
- Dewing, P., Chiang, C. W., Sinchak, K., Sim, H., Fernagut, P. O., Kelly, S., . . . Vilain, E. (2006). Direct regulation of adult brain function by the male-specific factor SRY. *Curr Biol*, 16(4), 415-420. doi:10.1016/j.cub.2006.01.017
- Dhamija, R. M., J, W.; Shah, B, B.; Goodkin, H, P. (2016). GNAO1-Associated Movement Disorder. *Movement Disorders Clinical Practice*, 3(6), 615-617. doi:10.1002/mdc3.12344
- Dietel, T. H., T. B.; Schlüter, G.; Cordes, I.; Trollmann, R.; Bast, T. (2016). Genotype and phenotype in GNAO1-Mutation – Case report of an unusual course of a childhood epilepsy. *Neuropediatrics*, 47(S 01), 1-17. doi:10.1055/s-0036-1583625
- Dravid, S. M., & Murray, T. F. (2004). Spontaneous synchronized calcium oscillations in neocortical neurons in the presence of physiological [Mg(2+)]: involvement of AMPA/kainate and metabotropic glutamate receptors. *Brain Res*, 1006(1), 8-17. doi:10.1016/j.brainres.2004.01.059
- Dunlap, K., & Fischbach, G. D. (1978). Neurotransmitters decrease the calcium component of sensory neurone action potentials. *Nature*, 276(5690), 837-839.
- Dupont, G., Combettes, L., Bird, G. S., & Putney, J. W. (2011). Calcium oscillations. *Cold Spring Harb Perspect Biol*, 3(3). doi:10.1101/cshperspect.a004226

- Fabiato, A. (1983). Calcium-induced release of calcium from the cardiac sarcoplasmic reticulum. *Am J Physiol*, 245(1), C1-14. doi:10.1152/ajpcell.1983.245.1.C1
- Farrell, M. R., Gruene, T. M., & Shansky, R. M. (2015). The influence of stress and gonadal hormones on neuronal structure and function. *Horm Behav*, 76, 118-124. doi:10.1016/j.yhbeh.2015.03.003
- Feng, H., Khalil, S., Neubig, R. R., & Sidiropoulos, C. (2018). A mechanistic review on GNAO1-associated movement disorder. *Neurobiol Dis*. doi:10.1016/j.nbd.2018.05.005
- Feng, H., Larrivee, C. L., Demireva, E. Y., Xie, H., Leipprandt, J. R., & Neubig, R. R. (2019). Mouse models of GNAO1-associated movement disorder: Allele- and sex-specific differences in phenotypes. *PLoS One*, 14(1), e0211066. doi:10.1371/journal.pone.0211066
- Feng, H., Sjogren, B., Karaj, B., Shaw, V., Gezer, A., & Neubig, R. R. (2017). Movement disorder in GNAO1 encephalopathy associated with gain-of-function mutations. *Neurology*, 89(8), 762-770. doi:10.1212/WNL.0000000000004262
- Frye, C. A. (2006). Role of androgens in epilepsy. *Expert Rev Neurother*, 6(7), 1061-1075. doi:10.1586/14737175.6.7.1061
- Galea, L. A., Spritzer, M. D., Barker, J. M., & Pawluski, J. L. (2006). Gonadal hormone modulation of hippocampal neurogenesis in the adult. *Hippocampus*, 16(3), 225-232. doi:10.1002/hipo.20154
- Garrett, J. E., & Wellman, C. L. (2009). Chronic stress effects on dendritic morphology in medial prefrontal cortex: sex differences and estrogen dependence. *Neuroscience*, 162(1), 195-207. doi:10.1016/j.neuroscience.2009.04.057
- Georganta, E. M., Tsoutsis, L., Gaitanou, M., & Georgoussi, Z. (2013). delta-opioid receptor activation leads to neurite outgrowth and neuronal differentiation via a STAT5B-Galphai/o pathway. *J Neurochem*, 127(3), 329-341. doi:10.1111/jnc.12386
- Goslin, K., Schreyer, D. J., Skene, J. H., & Banker, G. (1988). Development of neuronal polarity: GAP-43 distinguishes axonal from dendritic growth cones. *Nature*, 336(6200), 672-674. doi:10.1038/336672a0

- Gould, E., Woolley, C. S., Frankfurt, M., & McEwen, B. S. (1990). Gonadal steroids regulate dendritic spine density in hippocampal pyramidal cells in adulthood. *J Neurosci*, *10*(4), 1286-1291.
- Green, P. S., & Simpkins, J. W. (2000). Neuroprotective effects of estrogens: potential mechanisms of action. *Int J Dev Neurosci*, *18*(4-5), 347-358.
- Greenough, W. T., Carter, C. S., Steerman, C., & DeVogd, T. J. (1977). Sex differences in dentritic patterns in hamster preoptic area. *Brain Res*, *126*(1), 63-72. doi:10.1016/0006-8993(77)90215-3
- Harden, C., & MacLusky, N. J. (2004). Aromatase inhibition, testosterone, and seizures. *Epilepsy Behav*, *5*(2), 260-263. doi:10.1016/j.yebeh.2003.12.001
- Harden, C., & MacLusky, N. J. (2005). Aromatase inhibitors as add-on treatment for men with epilepsy. *Expert Rev Neurother*, *5*(1), 123-127. doi:10.1586/14737175.5.1.123
- Harte-Hargrove, L. C., Varga-Wesson, A., Duffy, A. M., Milner, T. A., & Scharfman, H. E. (2015). Opioid receptor-dependent sex differences in synaptic plasticity in the hippocampal mossy fiber pathway of the adult rat. *J Neurosci*, *35*(4), 1723-1738. doi:10.1523/JNEUROSCI.0820-14.2015
- He, J. C., Gomes, I., Nguyen, T., Jayaram, G., Ram, P. T., Devi, L. A., & Iyengar, R. (2005). The G alpha(o/i)-coupled cannabinoid receptor-mediated neurite outgrowth involves Rap regulation of Src and Stat3. *J Biol Chem*, *280*(39), 33426-33434. doi:10.1074/jbc.M502812200
- Herzog, A. G. (1991). Reproductive endocrine considerations and hormonal therapy for men with epilepsy. *Epilepsia*, *32 Suppl 6*, S34-37.
- Heyser, C. J. (2004). Assessment of developmental milestones in rodents. *Curr Protoc Neurosci*, *Chapter 8*, Unit 8 18. doi:10.1002/0471142301.ns0818s25
- Holahan, M. R. (2017). A Shift from a Pivotal to Supporting Role for the Growth-Associated Protein (GAP-43) in the Coordination of Axonal Structural and Functional Plasticity. *Front Cell Neurosci*, *11*, 266. doi:10.3389/fncel.2017.00266
- Holz, G. G. t., Rane, S. G., & Dunlap, K. (1986). GTP-binding proteins mediate

- transmitter inhibition of voltage-dependent calcium channels. *Nature*, 319(6055), 670-672. doi:10.1038/319670a0
- Horgan, A. M., & Copenhaver, P. F. (1998). G protein-mediated inhibition of neuronal migration requires calcium influx. *J Neurosci*, 18(11), 4189-4200.
- Horgan, A. M., Lagrange, M. T., & Copenhaver, P. F. (1994). Developmental expression of G proteins in a migratory population of embryonic neurons. *Development*, 120(4), 729-742.
- Huang, C. L., Jan, Y. N., & Jan, L. Y. (1997). Binding of the G protein betagamma subunit to multiple regions of G protein-gated inward-rectifying K⁺ channels. *FEBS Lett*, 405(3), 291-298.
- Hwangpo, T. A., Jordan, J. D., Premsrirut, P. K., Jayamaran, G., Licht, J. D., Iyengar, R., & Neves, S. R. (2012). G Protein-regulated inducer of neurite outgrowth (GRIN) modulates Sprouty protein repression of mitogen-activated protein kinase (MAPK) activation by growth factor stimulation. *J Biol Chem*, 287(17), 13674-13685. doi:10.1074/jbc.M111.320705
- Ichikawa, M., Muramoto, K., Kobayashi, K., Kawahara, M., & Kuroda, Y. (1993). Formation and maturation of synapses in primary cultures of rat cerebral cortical cells: an electron microscopic study. *Neurosci Res*, 16(2), 95-103.
- Igarashi, M., Strittmatter, S. M., Vartanian, T., & Fishman, M. C. (1993). Mediation by G proteins of signals that cause collapse of growth cones. *Science*, 259(5091), 77-79.
- Ingalhalikar, M., Smith, A., Parker, D., Satterthwaite, T. D., Elliott, M. A., Ruparel, K., . . . Verma, R. (2014). Sex differences in the structural connectome of the human brain. *Proc Natl Acad Sci U S A*, 111(2), 823-828. doi:10.1073/pnas.1316909110
- Jiang, M., & Bajpayee, N. S. (2009). Molecular mechanisms of go signaling. *Neurosignals*, 17(1), 23-41. doi:10.1159/000186688
- Jiang, M., Gold, M. S., Boulay, G., Spicher, K., Peyton, M., Brabet, P., . . . Birnbaumer, L. (1998). Multiple neurological abnormalities in mice deficient in the G protein Go. *Proc Natl Acad Sci U S A*, 95(6), 3269-3274. doi:10.1073/pnas.95.6.3269

- Jordan, J. D., He, J. C., Eungdamrong, N. J., Gomes, I., Ali, W., Nguyen, T., . . . Iyengar, R. (2005). Cannabinoid receptor-induced neurite outgrowth is mediated by Rap1 activation through G(alpha)o/i-triggered proteasomal degradation of Rap1GAPII. *J Biol Chem*, 280(12), 11413-11421. doi:10.1074/jbc.M411521200
- Kehrl, J. M., Sahaya, K., Dalton, H. M., Charbeneau, R. A., Kohut, K. T., Gilbert, K., . . . Neubig, R. R. (2014). Gain-of-function mutation in Gnao1: a murine model of epileptiform encephalopathy (EIEE17)? *Mamm Genome*, 25(5-6), 202-210. doi:10.1007/s00335-014-9509-z
- Kight, K. E., & McCarthy, M. M. (2014). Using sex differences in the developing brain to identify nodes of influence for seizure susceptibility and epileptogenesis. *Neurobiol Dis*, 72 Pt B, 136-143. doi:10.1016/j.nbd.2014.05.027
- Kulkarni, N., Tang, S., Bhardwaj, R., Bernes, S., & Grebe, T. A. (2016). Progressive Movement Disorder in Brothers Carrying a GNAO1 Mutation Responsive to Deep Brain Stimulation. *J Child Neurol*, 31(2), 211-214. doi:10.1177/0883073815587945
- Larrivee, C. L., Feng, H., Leipprandt, J. R., Demireva, E. Y., Xie, H., & Neubig, R. R. (2019). Mice with *GNAO1* R209H Movement Disorder Variant Display Hyperlocomotion Alleviated by Risperidone. *bioRxiv*.
- Latchney, S. E., Masiulis, I., Zaccaria, K. J., Lagace, D. C., Powell, C. M., McCasland, J. S., & Eisch, A. J. (2014). Developmental and adult GAP-43 deficiency in mice dynamically alters hippocampal neurogenesis and mossy fiber volume. *Dev Neurosci*, 36(1), 44-63. doi:10.1159/000357840
- Lei, Q., Jones, M. B., Talley, E. M., Schrier, A. D., McIntire, W. E., Garrison, J. C., & Bayliss, D. A. (2000). Activation and inhibition of G protein-coupled inwardly rectifying potassium (Kir3) channels by G protein beta gamma subunits. *Proc Natl Acad Sci U S A*, 97(17), 9771-9776. doi:10.1073/pnas.97.17.9771
- Livneh, Y., & Mizrahi, A. (2011). Experience-dependent plasticity of mature adult-born neurons. *Nat Neurosci*, 15(1), 26-28. doi:10.1038/nn.2980
- Logothetis, D. E., Kurachi, Y., Galper, J., Neer, E. J., & Clapham, D. E. (1987). The beta gamma subunits of GTP-binding proteins activate the muscarinic K⁺ channel in heart. *Nature*, 325(6102), 321-326. doi:10.1038/325321a0

- Lotto, B., Upton, L., Price, D. J., & Gaspar, P. (1999). Serotonin receptor activation enhances neurite outgrowth of thalamic neurones in rodents. *Neurosci Lett*, 269(2), 87-90.
- Lubin, M. L., Reitz, T. L., Todd, M. J., Flores, C. M., Qin, N., & Xin, H. (2006). A nonadherent cell-based HTS assay for N-type calcium channel using calcium 3 dye. *Assay Drug Dev Technol*, 4(6), 689-694. doi:10.1089/adt.2006.4.689
- Luscher, C., & Slesinger, P. A. (2010). Emerging roles for G protein-gated inwardly rectifying potassium (GIRK) channels in health and disease. *Nat Rev Neurosci*, 11(5), 301-315. doi:10.1038/nrn2834
- Masuhō, I., Mototani, Y., Sahara, Y., Asami, J., Nakamura, S., Kozasa, T., & Inoue, T. (2008). Dynamic expression patterns of G protein-regulated inducer of neurite outgrowth 1 (GRIN1) and its colocalization with Galphao implicate significant roles of Galphao-GRIN1 signaling in nervous system. *Dev Dyn*, 237(9), 2415-2429. doi:10.1002/dvdy.21686
- Mayer, A., Lahr, G., Swaab, D. F., Pilgrim, C., & Reisert, I. (1998). The Y-chromosomal genes SRY and ZFY are transcribed in adult human brain. *Neurogenetics*, 1(4), 281-288.
- McCool, B. A., Pin, J. P., Brust, P. F., Harpold, M. M., & Lovinger, D. M. (1996). Functional coupling of rat group II metabotropic glutamate receptors to an omega-conotoxin GVIA-sensitive calcium channel in human embryonic kidney 293 cells. *Mol Pharmacol*, 50(4), 912-922.
- Menke, L. A., Engelen, M., Alders, M., Odekerken, V. J., Baas, F., & Cobben, J. M. (2016). Recurrent GNAO1 Mutations Associated With Developmental Delay and a Movement Disorder. *J Child Neurol*, 31(14), 1598-1601. doi:10.1177/0883073816666474
- Mize, A. L., & Alper, R. H. (2000). Acute and long-term effects of 17beta-estradiol on G(i/o) coupled neurotransmitter receptor function in the female rat brain as assessed by agonist-stimulated [35S]GTPgammaS binding. *Brain Res*, 859(2), 326-333. doi:10.1016/s0006-8993(00)01998-3
- Murphy, T. H., Blatter, L. A., Wier, W. G., & Baraban, J. M. (1992). Spontaneous synchronous synaptic calcium transients in cultured cortical neurons. *J Neurosci*, 12(12), 4834-4845.

- Nakamura, K., Kodera, H., Akita, T., Shiina, M., Kato, M., Hoshino, H., . . . Saitsu, H. (2013). De Novo mutations in GNAO1, encoding a G α subunit of heterotrimeric G proteins, cause epileptic encephalopathy. *Am J Hum Genet*, 93(3), 496-505. doi:10.1016/j.ajhg.2013.07.014
- Nakata, H., & Kozasa, T. (2005). Functional characterization of G α signaling through G protein-regulated inducer of neurite outgrowth 1. *Mol Pharmacol*, 67(3), 695-702. doi:10.1124/mol.104.003913
- Nash, M. S., Schell, M. J., Atkinson, P. J., Johnston, N. R., Nahorski, S. R., & Challiss, R. A. (2002). Determinants of metabotropic glutamate receptor-5-mediated Ca²⁺ and inositol 1,4,5-trisphosphate oscillation frequency. Receptor density versus agonist concentration. *J Biol Chem*, 277(39), 35947-35960. doi:10.1074/jbc.M205622200
- Newberry, N. R., & Nicoll, R. A. (1985). Comparison of the action of baclofen with gamma-aminobutyric acid on rat hippocampal pyramidal cells in vitro. *J Physiol*, 360, 161-185. doi:10.1113/jphysiol.1985.sp015610
- Ngun, T. C., Ghahramani, N., Sanchez, F. J., Bocklandt, S., & Vilain, E. (2011). The genetics of sex differences in brain and behavior. *Front Neuroendocrinol*, 32(2), 227-246. doi:10.1016/j.yfrne.2010.10.001
- Okae, H., & Iwakura, Y. (2010). Neural tube defects and impaired neural progenitor cell proliferation in Gbeta1-deficient mice. *Dev Dyn*, 239(4), 1089-1101. doi:10.1002/dvdy.22256
- Pacico, N., & Mingorance-Le Meur, A. (2014). New in vitro phenotypic assay for epilepsy: fluorescent measurement of synchronized neuronal calcium oscillations. *PLoS One*, 9(1), e84755. doi:10.1371/journal.pone.0084755
- Paik, S., Somvanshi, R. K., & Kumar, U. (2019). Somatostatin-Mediated Changes in Microtubule-Associated Proteins and Retinoic Acid-Induced Neurite Outgrowth in SH-SY5Y Cells. *J Mol Neurosci*, 68(1), 120-134. doi:10.1007/s12031-019-01291-2
- Pang, T., Atefy, R., & Sheen, V. (2008). Malformations of cortical development. *Neurologist*, 14(3), 181-191. doi:10.1097/NRL.0b013e31816606b9
- Parducz, A., Hajszan, T., Maclusky, N. J., Hoyk, Z., Csakvari, E., Kurunczi, A., . . .

- Leranth, C. (2006). Synaptic remodeling induced by gonadal hormones: neuronal plasticity as a mediator of neuroendocrine and behavioral responses to steroids. *Neuroscience*, *138*(3), 977-985. doi:10.1016/j.neuroscience.2005.07.008
- Peleg, S., Varon, D., Ivanina, T., Dessauer, C. W., & Dascal, N. (2002). G(alpha)i controls the gating of the G protein-activated K(+) channel, GIRK. *Neuron*, *33*(1), 87-99.
- Pelosi, A., Menardy, F., Popa, D., Girault, J. A., & Herve, D. (2017). Heterozygous Gnal Mice Are a Novel Animal Model with Which to Study Dystonia Pathophysiology. *J Neurosci*, *37*(26), 6253-6267. doi:10.1523/JNEUROSCI.1529-16.2017
- Phan, A., Gabor, C. S., Favaro, K. J., Kaschack, S., Armstrong, J. N., MacLusky, N. J., & Choleris, E. (2012). Low doses of 17beta-estradiol rapidly improve learning and increase hippocampal dendritic spines. *Neuropsychopharmacology*, *37*(10), 2299-2309. doi:10.1038/npp.2012.82
- Reddy, D. S., & Jian, K. (2010). The testosterone-derived neurosteroid androstanediol is a positive allosteric modulator of GABAA receptors. *J Pharmacol Exp Ther*, *334*(3), 1031-1041. doi:10.1124/jpet.110.169854
- Reinoso, B. S., Undie, A. S., & Levitt, P. (1996). Dopamine receptors mediate differential morphological effects on cerebral cortical neurons in vitro. *J Neurosci Res*, *43*(4), 439-453.
doi:10.1002/(SICI)1097-4547(19960215)43:4<439::AID-JNR5>3.0.CO;2-G
- Reuveny, E., Slesinger, P. A., Inglese, J., Morales, J. M., Iniguez-Lluhi, J. A., Lefkowitz, R. J., . . . Jan, L. Y. (1994). Activation of the cloned muscarinic potassium channel by G protein beta gamma subunits. *Nature*, *370*(6485), 143-146. doi:10.1038/370143a0
- Rimler, A., Jockers, R., Lupowitz, Z., & Zisapel, N. (2007). Gi and RGS proteins provide biochemical control of androgen receptor nuclear exclusion. *J Mol Neurosci*, *31*(1), 1-12.
- Robinson, H. P., Kawahara, M., Jimbo, Y., Torimitsu, K., Kuroda, Y., & Kawana, A. (1993). Periodic synchronized bursting and intracellular calcium transients elicited by low magnesium in cultured cortical neurons. *J Neurophysiol*, *70*(4), 1606-1616. doi:10.1152/jn.1993.70.4.1606

- Robinson, H. P., Torimitsu, K., Jimbo, Y., Kuroda, Y., & Kawana, A. (1993). Periodic bursting of cultured cortical neurons in low magnesium: cellular and network mechanisms. *Jpn J Physiol*, *43 Suppl 1*, S125-130.
- Saitou, H., Fukai, R., Ben-Zeev, B., Sakai, Y., Mimaki, M., Okamoto, N., . . . Matsumoto, N. (2016). Phenotypic spectrum of GNAO1 variants: epileptic encephalopathy to involuntary movements with severe developmental delay. *Eur J Hum Genet*, *24*(1), 129-134. doi:10.1038/ejhg.2015.92
- Sanger, T. D., Chen, D., Fehlings, D. L., Hallett, M., Lang, A. E., Mink, J. W., . . . Valero-Cuevas, F. (2010). Definition and classification of hyperkinetic movements in childhood. *Mov Disord*, *25*(11), 1538-1549. doi:10.1002/mds.23088
- Schmidt, C. J., Zubiaur, M., Valenzuela, D., Neer, E. J., & Drager, U. C. (1994). G(O), a guanine nucleotide binding protein, is expressed during neurite extension in the embryonic mouse. *J Neurosci Res*, *38*(2), 182-187. doi:10.1002/jnr.490380208
- Schorling, D. C., Dietel, T., Evers, C., Hinderhofer, K., Korinthenberg, R., Ezzo, D., . . . Kirschner, J. (2017). Expanding Phenotype of De Novo Mutations in GNAO1: Four New Cases and Review of Literature. *Neuropediatrics*, *48*(5), 371-377. doi:10.1055/s-0037-1603977
- Scott, R. H., & Dolphin, A. C. (1986). Regulation of calcium currents by a GTP analogue: potentiation of (-)-baclofen-mediated inhibition. *Neurosci Lett*, *69*(1), 59-64.
- Sierra-Fonseca, J. A., Najera, O., Martinez-Jurado, J., Walker, E. M., Varela-Ramirez, A., Khan, A. M., . . . Roychowdhury, S. (2014). Nerve growth factor induces neurite outgrowth of PC12 cells by promoting Gbetagamma-microtubule interaction. *BMC Neurosci*, *15*, 132. doi:10.1186/s12868-014-0132-4
- Skucas, V. A., Duffy, A. M., Harte-Hargrove, L. C., Magagna-Poveda, A., Radman, T., Chakraborty, G., . . . Scharfman, H. E. (2013). Testosterone depletion in adult male rats increases mossy fiber transmission, LTP, and sprouting in area CA3 of hippocampus. *J Neurosci*, *33*(6), 2338-2355. doi:10.1523/JNEUROSCI.3857-12.2013
- Stephens, G. J. (2009). G-protein-coupled-receptor-mediated presynaptic inhibition in the cerebellum. *Trends Pharmacol Sci*, *30*(8), 421-430. doi:10.1016/j.tips.2009.05.008

- Streb, H., Irvine, R. F., Berridge, M. J., & Schulz, I. (1983). Release of Ca²⁺ from a nonmitochondrial intracellular store in pancreatic acinar cells by inositol-1,4,5-trisphosphate. *Nature*, *306*(5938), 67-69.
- Strittmatter, S. M., Fankhauser, C., Huang, P. L., Mashimo, H., & Fishman, M. C. (1995). Neuronal pathfinding is abnormal in mice lacking the neuronal growth cone protein GAP-43. *Cell*, *80*(3), 445-452.
- Strittmatter, S. M., Fishman, M. C., & Zhu, X. P. (1994). Activated mutants of the alpha subunit of G(o) promote an increased number of neurites per cell. *J Neurosci*, *14*(4), 2327-2338.
- Strittmatter, S. M., Igarashi, M., & Fishman, M. C. (1994). GAP-43 amino terminal peptides modulate growth cone morphology and neurite outgrowth. *J Neurosci*, *14*(9), 5503-5513.
- Strittmatter, S. M., Valenzuela, D., Kennedy, T. E., Neer, E. J., & Fishman, M. C. (1990). G0 is a major growth cone protein subject to regulation by GAP-43. *Nature*, *344*(6269), 836-841. doi:10.1038/344836a0
- Strittmatter, S. M., Valenzuela, D., Sudo, Y., Linder, M. E., & Fishman, M. C. (1991). An intracellular guanine nucleotide release protein for G0. GAP-43 stimulates isolated alpha subunits by a novel mechanism. *J Biol Chem*, *266*(33), 22465-22471.
- Strittmatter, S. M., Valenzuela, D., Vartanian, T., Sudo, Y., Zuber, M. X., & Fishman, M. C. (1991). Growth cone transduction: Go and GAP-43. *J Cell Sci Suppl*, *15*, 27-33.
- Tanaka, M., Treloar, H., Kalb, R. G., Greer, C. A., & Strittmatter, S. M. (1999). G(o) protein-dependent survival of primary accessory olfactory neurons. *Proc Natl Acad Sci U S A*, *96*(24), 14106-14111. doi:10.1073/pnas.96.24.14106
- Thomas, P., Pang, Y., Dong, J., Groenen, P., Kelder, J., de Vlieg, J., . . . Tubbs, C. (2007). Steroid and G protein binding characteristics of the seatrout and human progestin membrane receptor alpha subtypes and their evolutionary origins. *Endocrinology*, *148*(2), 705-718. doi:10.1210/en.2006-0974
- Thompson, T. L., & Certain, M. E. (2005). Estrogen mediated inhibition of dopamine transport in the striatum: regulation by G alpha i/o. *Eur J Pharmacol*, *511*(2-3),

121-126. doi:10.1016/j.ejphar.2005.02.005

- Thornhill, A. R., & Burgoyne, P. S. (1993). A paternally imprinted X chromosome retards the development of the early mouse embryo. *Development*, *118*(1), 171-174.
- Traina, G., Petrucci, C., Gargini, C., & Bagnoli, P. (1998). Somatostatin enhances neurite outgrowth in PC12 cells. *Brain Res Dev Brain Res*, *111*(2), 223-230.
- Tsien, R. W., Bean, B. P., Hess, P., Lansman, J. B., Nilius, B., & Nowycky, M. C. (1986). Mechanisms of calcium channel modulation by beta-adrenergic agents and dihydropyridine calcium agonists. *J Mol Cell Cardiol*, *18*(7), 691-710.
- Vajda, F. J., Donnan, G. A., Phillips, J., & Bladin, P. F. (1981). Human brain, plasma, and cerebrospinal fluid concentration of sodium valproate after 72 hours of therapy. *Neurology*, *31*(4), 486-487. doi:10.1212/wnl.31.4.486
- VanDongen, A. M., Codina, J., Olate, J., Mattera, R., Joho, R., Birnbaumer, L., & Brown, A. M. (1988). Newly identified brain potassium channels gated by the guanine nucleotide binding protein Go. *Science*, *242*(4884), 1433-1437.
- Vivar, C., Peterson, B. D., & van Praag, H. (2016). Running rewires the neuronal network of adult-born dentate granule cells. *Neuroimage*, *131*, 29-41. doi:10.1016/j.neuroimage.2015.11.031
- Wang, X., & Gruenstein, E. I. (1997). Mechanism of synchronized Ca²⁺ oscillations in cortical neurons. *Brain Res*, *767*(2), 239-249. doi:10.1016/s0006-8993(97)00585-4
- Wonders, C. P., & Anderson, S. A. (2006). The origin and specification of cortical interneurons. *Nat Rev Neurosci*, *7*(9), 687-696. doi:10.1038/nrn1954
- Worley, P. F., Baraban, J. M., Van Dop, C., Neer, E. J., & Snyder, S. H. (1986). Go, a guanine nucleotide-binding protein: immunohistochemical localization in rat brain resembles distribution of second messenger systems. *Proc Natl Acad Sci U S A*, *83*(12), 4561-4565. doi:10.1073/pnas.83.12.4561
- Xiong, J., Peng, J., Duan, H. L., Chen, C., Wang, X. L., Chen, S. M., & Yin, F. (2018). [Recurrent convulsion and pulmonary infection complicated by psychomotor retardation in an infant]. *Zhongguo Dang Dai Er Ke Za Zhi*, *20*(2), 154-157.

- Yang, H., Wan, L., Song, F., Wang, M., & Huang, Y. (2009). Palmitoylation modification of Galpha(o) depresses its susceptibility to GAP-43 activation. *Int J Biochem Cell Biol*, 41(7), 1495-1501. doi:10.1016/j.biocel.2008.12.011
- Yeyeodu, S. T., Witherspoon, S. M., Gilyazova, N., & Ibeanu, G. C. (2010). A rapid, inexpensive high throughput screen method for neurite outgrowth. *Curr Chem Genomics*, 4, 74-83. doi:10.2174/1875397301004010074
- Zamponi, G. W., Striessnig, J., Koschak, A., & Dolphin, A. C. (2015). The Physiology, Pathology, and Pharmacology of Voltage-Gated Calcium Channels and Their Future Therapeutic Potential. *Pharmacol Rev*, 67(4), 821-870. doi:10.1124/pr.114.009654
- Zhang, S. P., Kauffman, J., Yagel, S. K., & Codd, E. E. (2006). High-throughput screening for N-type calcium channel blockers using a scintillation proximity assay. *J Biomol Screen*, 11(6), 672-677. doi:10.1177/1087057106289210
- Zurawski, Z., Rodriguez, S., Hyde, K., Alford, S., & Hamm, H. E. (2016). Gbetagamma Binds to the Extreme C Terminus of SNAP25 to Mediate the Action of Gi/o-Coupled G Protein-Coupled Receptors. *Mol Pharmacol*, 89(1), 75-83. doi:10.1124/mol.115.101600